Friedrich-Alexander-Universität
Erlangen-Nürnberg

Spatio-temporal correlations of ensembles of multi-level atoms

Der Naturwissenschaftlichen Fakultät

der Friedrich-Alexander-Universität Erlangen-Nürnberg

zur Erlangung des Doktorgrades Dr. rer. nat.

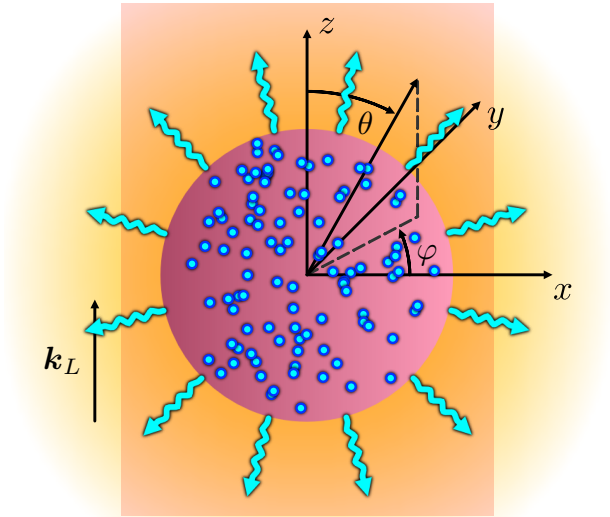

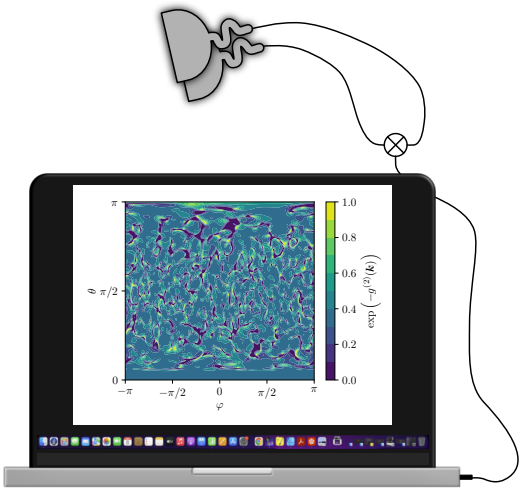

vorgelegt von

Manuel Dietmar Bojer

aus Lichtenfels

Spatio-temporal correlations of ensembles of multi-level atoms

Räumlich-zeitliche Korrelationen von Ensembles von Mehr-Zustands-Atomen

Der Naturwissenschaftlichen Fakultät
der Friedrich-Alexander-Universität Erlangen-Nürnberg
zur Erlangung des Doktorgrades Dr. rer. nat.

vorgelegt von

Manuel Dietmar Bojer

aus Lichtenfels

Als Dissertation genehmigt
von der Naturwissenschaftlichen Fakultät
der Friedrich-Alexander-Universität Erlangen-Nürnberg

Tag der mündlichen Prüfung:	23.09.2024
Gutachter:	Prof. Dr. Joachim von Zanthier
	Dr. Claudiu Genes

Zusammenfassung

Bis 1963 beschränkte sich das Konzept der Kohärenz optischer Felder auf das, was man heute Kohärenz erster Ordnung nennt. 1963 verallgemeinerte Roy J. Glauber den Begriff der Kohärenz, indem er Korrelationsfunktionen höherer Ordnung der Feldvariablen einführte und darauf basierend geeignete Bedingungen definierte. Eine besondere Klasse von Korrelationsfunktionen sind die sogenannten Photonenkorrelationsfunktionen, die mit einfachen Photonendetektoren gemessen werden können. Einerseits können diese Korrelationsmessungen zur Charakterisierung des zugrunde liegenden optischen Systems verwendet werden, andererseits können die Korrelationsmessungen als bedingte Photonenmessungen angesehen werden. Dabei entstehen durch die Messung der ersten einfallenden Photonen korrelierte Zustände, deren Eigenschaften dann über die später gemessenen Photonen erfasst werden. Auf diese Weise können messinduzierte Quantenkorrelationen einem Quantensystem aufgeprägt werden. Eine weitere Methode, Quantenkorrelationen zu erzeugen, besteht in einer Interaktion mit dem System. Dabei können sich Quantenkorrelationen über die Dynamik des Systems aufbauen.

In dieser Arbeit untersuchen wir die räumlich-zeitlichen Korrelationen mehrerer Ensembles von Atomen, wobei Quantenkorrelationen über Dipol-Dipol-Wechselwirkungen im Verlauf der Dynamik der Atome sowie über bedingte Photonenmessungen erzeugt werden. Als erstes System betrachten wir drei Atome, wobei zwei Atome miteinander interagieren, das verbleibende Atom jedoch weit vom Zwei-Atom-Subsystem entfernt ist, sodass es nicht mit den anderen beiden Atomen wechselwirkt. Wir zeigen, dass das spontane Emissionsverhalten dieses Systems durch bedingte Photonenmessungen so eingestellt werden kann, dass abhängig von der Beobachtungsrichtung gleichzeitig eine starke subradiante sowie superradiante Strahlung von Photonen beobachtet werden kann. Darüber hinaus zeigen wir, dass wir durch die Einführung des entfernten Atoms in das System Informationen extrahieren können, beispielsweise über den Abstand und den Anfangszustand der beiden benachbarten Atome, die im Zwei-Atom-System allein nicht zugänglich sind. Auf diese Weise demonstrieren wir eine mögliche Perspektive für die Quantensensorik, nämlich das Hinzufügen eines Hilfssystems und die Verwendung bedingter Photonenmessungen zur Verschränkung dieses Hilfssystems mit dem eigentlichen System. Wir wechseln dann zu einem Atomensemble aus N weit voneinander entfernten Atomen, sodass Wechselwirkungen zwischen den Atomen vernachlässigt werden können. Auch hier zeigen wir, dass durch bedingte Photonenmessungen, die zur Erzeugung von Quantenkorrelationen zwischen den verschiedenen Atomen verwendet werden, ein zeitlich Dicke-ähnliches superradiantes Emissionsverhalten der nacheinander gemessenen Photonen in einer bestimmten Richtung beobachtet werden kann. Dieses Emissionsverhalten, bekannt als Dicke-Superradianz, ist normalerweise auf Atome beschränkt, die näher zusammen sind als die Wellenlänge des Lichts, sodass sie über Dipol-Dipol-Wechselwirkungen miteinander interagieren und im Verlauf der Photonenemission Korrelationen aufbauen. Anschließend untersuchen wir, unter welchen Bedingungen ein unabhängiges Atomensemble im Hinblick auf Photonenkorrelationsfunktionen höherer Ordnung ähnlich einer thermischen Quelle emittiert. Wir definieren zwei Bedingungen, die einerseits die Einzelatomkohärenzen in Bezug auf die Population der Atome und andererseits die Korrelationsordnung in Bezug auf die Anzahl der Atome einschränken. Wir demonstrieren die Gültigkeit der beiden Bedingungen und die Ähnlichkeit der Lichtstatistik zu der von thermischen Quellen anhand mehrerer Beispiele. Eines davon ist eine dünne Atomwolke, die von einem ebenen Wellen-Laserfeld im starken Antriebsbereich getrieben wird. Abschließend analysieren wir die Photonenemission desselben Atomensembles, jedoch schwach getrieben. Dabei lässt sich die Dynamik der Atome im Wesentlichen durch ein klassisches oszillierendes Dipolmodell beschreiben. Da

die Atome jedoch jeweils nur ein Photon emittieren können, unterscheidet sich die Statistik des abgestrahlten Lichts drastisch von der klassischer Dipole. Insbesondere finden wir Beobachtungsrichtungen, in denen die Atome Quantenlicht emittieren, das durch einen Wert der normierten Autokorrelationsfunktion zweiter Ordnung kleiner als 1 gekennzeichnet ist.

Abstract

Until 1963, the concept of coherence of optical fields was limited to what is nowadays called first-order coherence. In 1963, Roy J. Glauber generalised the notion of coherence by introducing higher-order correlation functions of the field variables and defining appropriate conditions based on them. A particular class of correlation functions are the so-called photon correlation functions, which can be measured with simple photon detectors. On the one hand, these correlation measurements can be used to characterise the underlying optical system, on the other hand the correlation measurements can be viewed as conditional photon measurements. Thereby, the measurement of the first incoming photons create correlated states whose properties are then detected via the later measured photons. In that way, measurement-induced quantum correlations can be imprinted on a quantum system. Another method to create quantum correlations is via an interaction with the system, such that quantum correlations can build up via the dynamics of the system.

In this thesis, we investigate the spatio-temporal correlations of several ensembles of atoms, with quantum correlations generated via dipole-dipole interactions in the course of the dynamics of the atoms as well as via conditional photon measurements. As a first setup, we consider three atoms, where two atoms interact with each other, but the remaining atom is far distant from the two-atom subsystem, such that it does not interact with the other two atoms. We demonstrate that the spontaneous emission behaviour of this system can be engineered via conditional photon measurements allowing to observe strong subradiant and superradiant radiation of photons simultaneously depending solely on the direction of observation. Further, we show that by introducing the remote atom into the system, we can extract information, for instance, the separation and the initial state of the two close-by atoms, which is not accessible in the two-atom system alone. In this way, we demonstrate a potential prospect for quantum sensing, i.e., adding an auxiliary system and using conditional photon measurements to entangle it with the system of interest. We then switch to an atomic ensemble of N mutually far separated atoms, such that interactions between the atoms can be neglected. Again, by conditional photon measurements, used to create quantum correlations between the different atoms, we demonstrate that a temporal Dicke-like superradiant emission behaviour of the consecutively measured photons can be observed in a particular direction. Such an emission behaviour, known as Dicke superradiance, is usually restricted to atoms, which are closer separated than the wavelength of the light, such that they interact with each other via dipole-dipole interactions and become correlated in the course of photon emission. Afterwards, we investigate under which conditions an independent atomic ensemble emits similar to a thermal source in terms of higher-order photon correlation functions. We define two conditions restricting on the one hand the single-atom coherences with respect to the population of the atoms, and on the other hand the correlation order with respect to the number of atoms. We demonstrate the validity of the two conditions and the similarity of the light statistics to the one of thermal sources via several examples, one of them being a dilute atomic cloud driven by a plane wave laser field in the strong driving regime. Finally, we analyse the photon emission of the same atomic ensemble, but weakly driven. Here, the dynamics of the atoms can be essentially described by a classical oscillating dipole model. However, since the atoms can only emit one photon at a time, the radiated light statistics differs drastically from that of classical dipoles. In particular, we find observation directions in which the atoms emit quantum light characterised by a value of the normalised second-order autocorrelation function less than 1.

Note

Parts of this thesis have been published or will be published in the near future in the form of journal articles; see the list of publications at the end of this thesis.

Acknowledgment

I would like to thank the *International Max Planck Research School - Physics of Light* and the *Deutsche Forschungsgemeinschaft (DFG, German Research Foundation), Project-ID No. 429529648, TRR 306 QuCoLiMa ("Quantum Cooperativity of Light and Matter")* for granting me a PhD scholarship. Further, I would like to thank the *Bavarian Academic Center for Latin America (BAYLAT)*. Their academic and financial support has made this thesis possible.

Contents

1 Introduction

> *The possibility of detecting individual quanta raises interesting questions concerning their statistical distributions, distributions that should in principle be quite accessible to measurement. We might imagine, for example, putting a quantum counter in a given light beam and asking for the distribution of time intervals between successive counts. Statistical problems of that sort were never, to my knowledge, addressed until the importance of quantum correlations began to become clear in the 1950's. Until that time virtually all optical experiments measured only average intensities or quantum counting rates, and the correlation function $G^{(1)}$ was all we needed to describe them. It was in that decade, however, that several new sorts of experiments requiring a more general approach were begun. That period seemed to mark the beginning of quantum optics as a relatively new or rejuvenated field.*
>
> – Roy J. Glauber

Nowadays, the notion of optical coherence is a well-established concept describing correlations of fluctuations of optical fields, i.e., it addresses the study of higher-order moments of statistical distributions of light. Probably the most prominent manifestation of coherence is Young's double-slit experiment [1], in which a light beam is separated into two parts and later recombined allowing the observation of interference fringes. Thereby, the appearance of interference fringes is directly related to the coherence properties of the light beam. In fact, Young's double-slit experiment only demonstrates the existence of so-called first-order coherence. Historically, the concept of optical coherence goes back until the mid of the 19th century and was studied and developed further in the century thereafter [2]. However, basically all studies at this time investigated the possibility of two interfering fields, which is nowadays referred to as first-order coherence.
Then, in 1956, a remarkable and controversially discussed experiment was conducted by R. Hanbury Brown and R. Q. Twiss [3]. Their goal was to measure the angular size of several thermal sources, i.e., stars in the radio frequency domain using two antennas. Mathematically, this measurement involves not only a correlation of two, but four optical field amplitudes going beyond the usual first-order coherence theory. They demonstrated that, even though the observed thermal sources have not possessed any coherence properties in first-order accessible by measuring the intensity, they show coherence in second-order accessible by measuring

intensity-intensity correlations, which allows one to extract spatial information about the light sources. The interpretation of the experiment remained, however, unclear, in particular since the occurring interference term in the intensity-intensity correlation measurement involves the interference of pairs of photons, which according to Dirac is inhibited. Dirac states in his famous textbook *The principles of quantum mechanics* [4] that "each photon then interferes only with itself. Interference between two different photons never occurs." However, strictly speaking the term interference refers to the summation of probability amplitudes instead of a physical interference of photons and probability amplitudes are not restricted to a certain number of photons [5]. Inspired by the experiments by Hanbury Brown and Twiss, Robert J. Glauber developed a fully quantum-mechanical description of higher-order correlations and redefined the notion of coherence by a class of conditions in 1963 [6].

One important subject area of the concept of optical coherence is the study of the emitted light of atomic systems. Thereby, the most famous phenomenon is probably so-called *Dicke superradiance*, where an ensemble of independent two-level atoms is concentrated in a small volume compared to the transition wavelength of the atoms (ideally a single space point). In this case, the atoms, which are all prepared in the excited state, develop dipole-dipole correlations in the course of light emission leading to a coherent emission of spontaneous radiation [7]. The emitted intensity of this atomic system does then not follow a usual exponential decay, as would be the case for a single atom, but shows a short burst. Multiple theoretical [7–39] and experimental [40–51] investigations of superradiance, but also so-called subradiance [28, 31, 34, 52–56], have been carried out since then, with a renewed interest in the recent years.

In this thesis, we combine the system of dipole-dipole interacting atoms and the concept of optical coherence in terms of higher-order correlation functions to enhance effects like super- and subradiant emission of light or to extract information about the atomic system utilising measurement-induced entanglement. In addition, we present new investigations on the statistical moments of the emitted light of independent atoms.

Therefore, in a first part consisting of the Chapters 2 and 3 we give an introduction to light-matter interactions leading to the aforementioned photon-induced dipole-dipole interactions between atoms, which are closely separated with respect to the transition wavelength. At the end of Chapter 2, we will arrive at a Markovian quantum master equation describing the dynamics of the atomic system, where the dissipation into the free field comes across via tracing out the electromagnetic field degrees of freedom. In Chapter 3, we then link the measurable photonic higher-order correlation functions to multi-time expectation values of atomic observables. Applying the so-called quantum regression theorem, these multi-time expectation values can be calculated using the quantum master equation derived in the previous chapter.

In a second part, we apply the introduced concepts to three different systems investigated in the Chapters 4-6. We start in Chapter 4 by considering a rather small system consisting

of three atoms, where two atoms are close to each other, such that they interact via the dipole-dipole interaction leading to modified decay rates and energy levels. However, the remaining third atom is placed remotely, i.e., several wavelengths away from the two-atom subsystem, such that no interaction is present. By entangling all three atoms with each other using higher-order photon correlation measurements, we demonstrate that this system shows an enhanced super- and subradiant decay beyond the canonical two-atom case. In particular, the interplay of dipole-dipole interactions and measurement-induced entanglement allows for engineering the spontaneous emission behaviour in space and time. Afterwards, we investigate the possibility of using the remote atom as an auxiliary system to extract information, which is inaccessible without the additional atom. Via the interference of quantum paths associated with the two-atom subsystem and the third atom we are able to determine the distance of the subwavelength separated atoms with sub-Abbe resolution. Thereafter, we extend the level scheme of the atoms to four levels with three excited states corresponding to angular momentum $J = 1$ and one ground state corresponding to $J = 0$. Assuming that the two close-by atoms are initially in an arbitrary superposition of the three excited states, we are able to deduce the coefficients of this state via a third-order photon correlation measurement using again the interference with the third non-interacting atom.

In Chapter 5, we then consider a system of an arbitrary number of two-level atoms N and recapitulate first the phenomenon of Dicke superradiance. In this context, we split the emitted intensity in different terms accounting, in particular, for the contributions of single-atom coherences and dipole-dipole correlations. In the case of Dicke superradiance, we demonstrate that the resulting coherent emission of spontaneous radiation can be traced back to the evolving dipole-dipole correlations rather than a macroscopic dipole moment. Afterwards, we use this understanding to mimic a Dicke-like superradiant burst with non-interacting far distant atoms via higher-order photon measurements. Instead of the necessary dipole-dipole correlations being evolved via the dynamics, here the dipole-dipole correlations are created by consecutive photon measurements. This allows us to model a temporal Dicke-like emission behaviour in a particular observation direction. We interpret the resulting photon emission within a quantum path interference formalism and support our findings with entanglement and quantum correlation calculations, which we discuss in more detail in the last section of this chapter.

Finally, in Chapter 6, we consider again N non-interacting atoms in a tensor product state and investigate under which conditions this atomic ensemble shows thermal statistics in terms of higher-order photon correlation measurements. We explicitly derive two conditions, one for the number of atoms in comparison to the correlation order and one for the strength of the coherences in comparison to the population of the atoms. Afterwards, we demonstrate the conditions by applying them to several simple examples, one of them being a dilute atomic cloud driven by a plane wave laser field. In the last section of this chapter, we then analyse the dilute atom cloud system in more detail in the small driving regime, in which

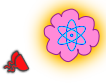

the dynamics can be essentially described by a classical dipole model. However, in contrast to classical oscillating dipoles the emitted radiation is neither purely coherent nor classical. Instead, this system of weakly driven atoms emits, depending on the observation direction, a plethora of different light statistics reaching from superbunching over thermal and coherent light to even quantum light, based on antibunching indicated by a value of the normalised second-order autocorrelation function less than 1. We identify conditions, for which these different emission characteristics can be observed and show, in particular, that the height of the superbunching peaks and the depth of the antibunching dips can be controlled via the so-called saturation parameter. We thus clearly demonstrate the important difference between classical oscillating dipoles and weakly driven two-level atoms.
Lastly, in Chapter 7, we summarise our results and give a short outlook of possible investigations in the future.

2 Light-matter coupling and quantum master equation approach

> *[T]he usual theories become exceedingly involved as the number of atoms taking part in spontaneous emission increases [...]. Quantum statistical theories [...] are especially well suited to such cases and naturally predict results identical to those predicted by the usual theories. [...] Quantum statistical theories are interesting in their own right as they are based on techniques of nonequilibrium statistical mechanics [...].*
>
> – Girish S. Agarwal

In the above quote, by "usual theories" Girish S. Agarwal refers to the methods developed by Weisskopf and Wigner [57], later reformulated by Heitler and Ma [58, 59], and by Goldberger and Watson [60] for treating the dynamics of spontaneous emission from atoms. Atoms usually do not follow a unitary dynamics, but are coupled to some environment, e.g., the vacuum of the electromagnetic field. In the case of a single excited atom, this coupling leads to the disexcitation of the atom via the radiation of a photon, a random process called spontaneous emission. Considering not only a single atom, but many atoms, the coupling to the electromagnetic field gives rise to collective effects, i.e., photon-mediated dipole-dipole interactions between the atoms, which can be split into a coherent and an incoherent part. The coherent part causes level shifts and splittings, whereas the incoherent part modifies the spontaneous decay rates. Instead of following the "usual theories" to describe these processes, we will introduce a powerful quantum statistical method, namely the general reservoir theory, which leads us to a quantum master equation that covers the dynamics of the atoms in the presence of the electromagnetic field. The following sections are based on Refs. [61–63].

2.1 Light-matter Hamiltonian

We consider a system of N identical atoms coupled to the electromagnetic field. The Hamiltonian in this situation, obtained from the Hamiltonian in Coulomb gauge via the so-called Power-Zienau-Woolley transformation and long-wavelength approximation derived in Ap-

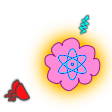

pendix A, reads

$$\hat{H} = \sum_{\mu=1}^{N} \sum_{\alpha} \frac{[\hat{\boldsymbol{p}}_{\alpha}^{(\mu)}]^2}{2m_{\alpha}^{(\mu)}} + \frac{1}{2\varepsilon_0} \int d^3r \, |\hat{\boldsymbol{P}}^{(\mu)}(\boldsymbol{r})|^2 - \frac{\hat{\boldsymbol{d}}^{(\mu)} \hat{\boldsymbol{D}}_{\perp}(\boldsymbol{R}_{\mu})}{\varepsilon_0} + \frac{1}{\varepsilon_0} \sum_{\substack{\mu,\nu=1 \\ \mu \neq \nu}}^{N} \int d^3r \, \hat{\boldsymbol{P}}^{(\mu)}(\boldsymbol{r}) \hat{\boldsymbol{P}}^{(\nu)}(\boldsymbol{r}) + \int d^3k \sum_{\boldsymbol{\varepsilon}} \hbar\omega_k \left[\hat{a}_{\varepsilon}^{\dagger}(\boldsymbol{k}) \hat{a}_{\varepsilon}(\boldsymbol{k}) + \frac{1}{2} \right] . \tag{2.1}$$

Thereby, $\hat{\boldsymbol{p}}_{\alpha}^{(\mu)}$ and $m_{\alpha}^{(\mu)}$ are the momentum and mass of the αth charge of atom μ, and $\hat{\boldsymbol{P}}^{(\mu)}(\boldsymbol{r})$ and $\hat{\boldsymbol{d}}^{(\mu)}$ are the polarisation density and the dipole moment of the μth atom. Further,

$$\hat{\boldsymbol{D}}_{\perp}(\boldsymbol{R}_{\mu}) = i\varepsilon_0 \int d^3k \sum_{\boldsymbol{\varepsilon}} \sqrt{\frac{\hbar\omega_k}{2\varepsilon_0 (2\pi)^3}} \left[\boldsymbol{\varepsilon} \hat{a}_{\varepsilon}(\boldsymbol{k}) e^{i\boldsymbol{k}\boldsymbol{R}_{\mu}} - \boldsymbol{\varepsilon}^* \hat{a}_{\varepsilon}^{\dagger}(\boldsymbol{k}) e^{-i\boldsymbol{k}\boldsymbol{R}_{\mu}} \right] \tag{2.2}$$

represents the transverse displacement field at the position of the μth atom $\boldsymbol{R}_{\mu}$. Finally, $\hat{a}_{\varepsilon}(\boldsymbol{k})$ and $\hat{a}_{\varepsilon}^{\dagger}(\boldsymbol{k})$ are the annihilation and creation operators of the field mode characterised by the polarisation $\boldsymbol{\varepsilon}$ and the wave vector $\boldsymbol{k}$, with ω_k being the corresponding frequency. We split the polarisation term of the individual atoms as

$$\frac{1}{2\varepsilon_0} \int d^3r \, |\hat{\boldsymbol{P}}^{(\mu)}(\boldsymbol{r})|^2 = \frac{1}{2\varepsilon_0} \int d^3r \, |\hat{\boldsymbol{P}}_{\perp}^{(\mu)}(\boldsymbol{r})|^2 + \frac{1}{2\varepsilon_0} \int d^3r \, |\hat{\boldsymbol{P}}_{\parallel}^{(\mu)}(\boldsymbol{r})|^2 , \tag{2.3}$$

where the first term describes a self-energy contributing to the Lamb shift, which can not be correctly captured in the following description, such that we omit this term. The second term is exactly the Coulomb energy of atom μ. For the following derivations, we subtract the vacuum energy and do the replacement

$$\int d^3k \sum_{\boldsymbol{\varepsilon}} \hbar\omega_k \left[\hat{a}_{\varepsilon}^{\dagger}(\boldsymbol{k}) \hat{a}_{\varepsilon}(\boldsymbol{k}) + \frac{1}{2} \right] \to \int d^3k \sum_{\boldsymbol{\varepsilon}} \hbar\omega_k \hat{a}_{\varepsilon}^{\dagger}(\boldsymbol{k}) \hat{a}_{\varepsilon}(\boldsymbol{k}) \tag{2.4}$$

for the energy of the electromagnetic field. Further, we assume that the mutual separations of the atoms are larger than the extend of the individual atoms, such that

$$\int d^3r \, \hat{\boldsymbol{P}}^{(\mu)}(\boldsymbol{r}) \hat{\boldsymbol{P}}^{(\nu)}(\boldsymbol{r}) = 0 \tag{2.5}$$

for $\mu \neq \nu$. Then, the Hamiltonian reduces to

$$\hat{H} = \sum_{\mu=1}^{N} \sum_{\alpha} \frac{[\hat{\boldsymbol{p}}_{\alpha}^{(\mu)}]^2}{2m_{\alpha}^{(\mu)}} + V_{\text{coul}}^{(\mu)} - \frac{\hat{\boldsymbol{d}}^{(\mu)} \hat{\boldsymbol{D}}_{\perp}(\boldsymbol{R}_{\mu})}{\varepsilon_0} + \int d^3k \sum_{\boldsymbol{\varepsilon}} \hbar\omega_k \hat{a}_{\varepsilon}^{\dagger}(\boldsymbol{k}) \hat{a}_{\varepsilon}(\boldsymbol{k}) . \tag{2.6}$$

The sum of the kinetic and potential energies of the individual atoms gives rise to a characteristic level structure with eigenenergies E_l and eigenstates $|l_{\mu}\rangle$. Assuming that only L

atomic states are relevant, we do the replacement

$$\sum_{\alpha} \frac{[\hat{\boldsymbol{p}}_{\alpha}^{(\mu)}]^2}{2m_{\alpha}^{(\mu)}} + V_{\text{coul}}^{(\mu)} \to \sum_{l=1}^{L} E_l \, |l_\mu\rangle\langle l_\mu| \tag{2.7}$$

and arrive at the final Hamiltonian

$$\hat{H} = \hat{H}_A + \hat{H}_R + \hat{H}_I \,, \tag{2.8}$$

where

$$\hat{H}_A = \sum_{\mu=1}^{N} \sum_{l=1}^{L} E_l \, |l_\mu\rangle\langle l_\mu| \tag{2.9}$$

describes the Hamiltonian of the atoms,

$$\hat{H}_R = \int d^3k \sum_{\boldsymbol{\varepsilon}} \hbar\omega_k \hat{a}_{\varepsilon}^{\dagger}(\boldsymbol{k}) \hat{a}_{\varepsilon}(\boldsymbol{k}) \tag{2.10}$$

is the Hamiltonian of the free radiation field, and

$$\hat{H}_I = -\sum_{\mu=1}^{N} \frac{\hat{\boldsymbol{d}}^{(\mu)} \hat{\boldsymbol{D}}_{\perp}(\boldsymbol{R}_\mu)}{\varepsilon_0} \tag{2.11}$$

represents the interaction in the long-wavelength approximation (or also called electric dipole approximation).

2.2 Reservoir theory

Usually, the system of interest, e.g., the collection of atoms is coupled to a large environment, e.g., the infinite number of modes of the electromagnetic field. The general idea of a reservoir theory is then to trace out the environment degrees of freedom, which we are not interested in to find an equation of motion for the system alone. We start with the Liouville-von Neumann equation in the interaction picture with respect to the uncoupled Hamiltonian $\hat{H}_0 = \hat{H}_A + \hat{H}_R$

$$\frac{\partial}{\partial t}\hat{\tilde{\rho}}(t) = -\frac{i}{\hbar}[\hat{H}_I(t), \hat{\tilde{\rho}}(t)] = -\frac{i}{\hbar}\mathscr{L}(t)\hat{\tilde{\rho}}(t) \,, \tag{2.12}$$

where $\hat{\tilde{\rho}}(t) = \hat{U}_0^{\dagger}(t)\hat{\rho}\hat{U}_0(t)$, $\hat{H}_I(t) = \hat{U}_0^{\dagger}(t)\hat{H}_I\hat{U}_0(t)$, $\hat{U}_0(t) = e^{-\frac{i}{\hbar}\hat{H}_0 t}$, and we set the reference time to $t_0 = 0$. Further, we defined the Liouville superoperator $\mathscr{L}(t)\ldots \coloneqq [\hat{H}_I(t), \ldots]$. We now proceed with a projection operator technique [62, 64], which amounts to obtain an equation of motion for the relevant part of the density operator. Therefore, we define the

projection operator $\mathscr{P}$ by

$$\mathscr{P}\hat{\tilde{\rho}}(t) = \mathrm{Tr}_R[\hat{\tilde{\rho}}(t)] \otimes \hat{\tilde{\rho}}_R(0) = \hat{\tilde{\rho}}_A(t) \otimes \hat{\tilde{\rho}}_R(0)\,. \tag{2.13}$$

The complementary operator projecting onto the irrelevant part of $\hat{\tilde{\rho}}$ is then $\mathscr{Q} = \mathbb{1} - \mathscr{P}$. Indeed, the two operators are projection operators, since they fulfil $\mathscr{P}^2 = \mathscr{P}$ and $\mathscr{Q}^2 = \mathscr{Q}$. Further, they add up to the identity by construction and the successive application of $\mathscr{P}$ and $\mathscr{Q}$ gives zero, i.e., $\mathscr{P}\mathscr{Q} = \mathscr{Q}\mathscr{P} = 0$. Applying the two projection operators onto Eq. (2.12) and using $\mathscr{P} + \mathscr{Q} = \mathbb{1}$, we find

$$\frac{\partial}{\partial t}\mathscr{P}\hat{\tilde{\rho}}(t) = -\frac{i}{\hbar}\mathscr{P}\mathscr{L}(t)\mathscr{P}\hat{\tilde{\rho}}(t) - \frac{i}{\hbar}\mathscr{P}\mathscr{L}(t)\mathscr{Q}\hat{\tilde{\rho}}(t)\,, \tag{2.14}$$

$$\frac{\partial}{\partial t}\mathscr{Q}\hat{\tilde{\rho}}(t) = -\frac{i}{\hbar}\mathscr{Q}\mathscr{L}(t)\mathscr{P}\hat{\tilde{\rho}}(t) - \frac{i}{\hbar}\mathscr{Q}\mathscr{L}(t)\mathscr{Q}\hat{\tilde{\rho}}(t)\,. \tag{2.15}$$

We can formally solve the second equation via Duhamel's principle leading to

$$\mathscr{Q}\hat{\tilde{\rho}}(t) = \mathscr{G}(t,0)\mathscr{Q}\hat{\tilde{\rho}}(0) - \frac{i}{\hbar}\int_0^t ds\,\mathscr{G}(t,s)\mathscr{Q}\mathscr{L}(s)\mathscr{P}\hat{\tilde{\rho}}(s)\,, \tag{2.16}$$

where

$$\mathscr{G}(t,s) = \mathscr{T}\exp\left[-\frac{i}{\hbar}\int_s^t ds'\,\mathscr{Q}\mathscr{L}(s')\right] \tag{2.17}$$

and $\mathscr{T}$ being the time-ordering operator. Plugging the solution into the first equation we finally arrive at the so-called Nakajima-Zwanzig equation

$$\frac{\partial}{\partial t}\mathscr{P}\hat{\tilde{\rho}}(t) = -\frac{i}{\hbar}\mathscr{P}\mathscr{L}(t)\mathscr{P}\hat{\tilde{\rho}}(t) - \frac{i}{\hbar}\mathscr{P}\mathscr{L}(t)\left[\mathscr{G}(t,0)\mathscr{Q}\hat{\tilde{\rho}}(0) - \frac{i}{\hbar}\int_0^t ds\,\mathscr{G}(t,s)\mathscr{Q}\mathscr{L}(s)\mathscr{P}\hat{\tilde{\rho}}(s)\right]\,, \tag{2.18}$$

which is an exact equation of motion for the relevant part of the density operator $\mathscr{P}\hat{\tilde{\rho}}(t)$. To simplify the equation, we assume that the initial state is factorisable, i.e., $\hat{\tilde{\rho}}(0) = \hat{\tilde{\rho}}_A(0) \otimes \hat{\tilde{\rho}}_R(0)$. Then, $\mathscr{Q}\hat{\tilde{\rho}}(0) = 0$ and the second term on the right side of Eq. (2.18) vanishes. A further assumption, which is often met by environmental states, is that the expectation value of the interaction Hamiltonian $\hat{H}_I(t)$ with respect to the radiation state $\hat{\tilde{\rho}}_R(0)$ vanishes, i.e., $\mathrm{Tr}_R[\hat{H}_I(t)\hat{\tilde{\rho}}_R(0)] = 0$. This implies that $\mathscr{P}\mathscr{L}(t)\mathscr{P} = 0$ and thus that the first term on the right side is zero. An exception will be discussed later. With the two assumptions just described, Eq. (2.18) reduces to

$$\frac{\partial}{\partial t}\mathscr{P}\hat{\tilde{\rho}}(t) = -\frac{1}{\hbar^2}\mathscr{P}\mathscr{L}(t)\int_0^t ds\,\mathscr{G}(t,s)\mathscr{Q}\mathscr{L}(s)\mathscr{P}\hat{\tilde{\rho}}(s)\,. \tag{2.19}$$

2.3 Quantum master equation

Considering the right side of Eq. (2.19), we see that due to the appearance of $\mathscr{L}$ it is at least of second order in the interaction $\hat{H}_I$. However, since

$$\mathscr{G}(t,s) = \sum_{n=0}^{\infty} \left(-\frac{i}{\hbar}\right)^n \frac{\mathscr{Q}}{n!} \int_s^t dt_1 \ldots \int_s^{t_{n-1}} dt_n \, \mathscr{T}\left[\mathscr{L}(t_1)\ldots\mathscr{L}(t_n)\right] \tag{2.20}$$

contains the operator $\mathscr{L}$, we additionally obtain all higher-order contributions. We now do our first approximation, the so-called *Born approximation*, which assumes that the coupling between the system of interest and the environment is weak. This justifies to expand the right side of Eq. (2.19) up to the leading order in the interaction $\hat{H}_I$, which is obtained by approximating $\mathscr{G}(t,s) \approx \mathbb{1}$. By using

$$\mathscr{P}\mathscr{L}(t)\mathscr{Q}\mathscr{L}(s)\mathscr{P}\hat{\tilde{\rho}}(s) = \mathscr{P}\mathscr{L}(t)\mathscr{L}(s)\mathscr{P}\hat{\tilde{\rho}}(s) - \underbrace{\mathscr{P}\mathscr{L}(t)\mathscr{P}}_{=0}\mathscr{L}(s)\mathscr{P}\hat{\tilde{\rho}}(s) \tag{2.21}$$

$$= \mathscr{P}\mathscr{L}(t)\mathscr{L}(s)\mathscr{P}\hat{\tilde{\rho}}(s) = \mathrm{Tr}_R\left\{[\hat{H}_I(t),[\hat{H}_I(s),\hat{\tilde{\rho}}_A(s)\otimes\hat{\tilde{\rho}}_R(0)]]\right\}\otimes\hat{\tilde{\rho}}_R(0)\,, \tag{2.22}$$

we can then find an equation for the reduced density matrix $\hat{\tilde{\rho}}_A(t)$ given by

$$\begin{aligned}\frac{\partial}{\partial t}\hat{\tilde{\rho}}_A(t) &= -\frac{1}{\hbar^2}\int_0^t ds\ \mathrm{Tr}_R\left\{[\hat{H}_I(t),[\hat{H}_I(s),\hat{\tilde{\rho}}_A(s)\otimes\hat{\tilde{\rho}}_R(0)]]\right\}\\ &= -\frac{1}{\hbar^2}\int_0^t ds\ \mathrm{Tr}_R\left\{[\hat{H}_I(t),\hat{H}_I(s)\hat{\tilde{\rho}}_A(s)\otimes\hat{\tilde{\rho}}_R(0)] + H.c.\right\}\\ &= \frac{1}{\hbar^2}\int_0^t ds\ \mathrm{Tr}_R\left\{[\hat{H}_I(t-s)\hat{\tilde{\rho}}_A(t-s)\otimes\hat{\tilde{\rho}}_R(0),\hat{H}_I(t)] + H.c.\right\}\,,\end{aligned} \tag{2.23}$$

where $H.c.$ denotes the Hermitian conjugate. In what follows, we consider the explicit form of the light-matter interaction Hamiltonian. If we assume that there are D dipole-allowed transitions, we can write the dipole operator of the μth atom as

$$\hat{\boldsymbol{d}}^{(\mu)} = \sum_{m=1}^{D}[\boldsymbol{d}_m\hat{S}_{m+}^{(\mu)} + H.c.] \tag{2.24}$$

with $\hat{S}_{m+}^{(\mu)} = |h_\mu\rangle\langle l_\mu|$ the raising operator of the mth transition. Thereby, $|h_\mu\rangle$ is the excited and $|l_\mu\rangle$ the ground state of the mth transition and $\boldsymbol{d}_m = \langle h_\mu|\hat{\boldsymbol{d}}^{(\mu)}|l_\mu\rangle$ is the corresponding matrix element. By using Eq. (2.11) and $\hat{U}_0^\dagger(t)\hat{S}_{m+}^{(\mu)}\hat{U}_0(t) = \hat{S}_{m+}^{(\mu)}e^{i\omega_m t}$ with $\omega_m = \frac{1}{\hbar}(E_h - E_l)$ the transition frequency of the mth transition, a straightforward calculation leads to

$$\frac{\partial}{\partial t}\hat{\tilde{\rho}}_A(t) = \sum_{\mu,\nu=1}^{N}\sum_{m,n=1}^{D}\left\{\left[\hat{S}_{n+}^{(\nu)}\boldsymbol{d}_m K_-^{\mu\nu,n}(t)\boldsymbol{d}_n,\hat{S}_{m+}^{(\nu)}\right]e^{i(\omega_m+\omega_n)t}\right.$$

$$+\left[\hat{S}^{(\nu)}_{n+}\boldsymbol{d}^*_m K^{\mu\nu,n}_-(t)\boldsymbol{d}_n, \hat{S}^{(\mu)}_{m-}\right] e^{-i(\omega_m-\omega_n)t} + \left[\hat{S}^{(\nu)}_{n-}\boldsymbol{d}_m K^{\mu\nu,n}_+(t)\boldsymbol{d}^*_n, \hat{S}^{(\mu)}_{m+}\right] e^{i(\omega_m-\omega_n)t}$$
$$+\left[\hat{S}^{(\nu)}_{n-}\boldsymbol{d}^*_m K^{\mu\nu,n}_+(t)\boldsymbol{d}^*_n, \hat{S}^{(\mu)}_{m-}\right] e^{-i(\omega_m+\omega_n)t} + H.c.\Big\}\,, \tag{2.25}$$

where we defined auxiliary matrices with operators as matrix elements given by

$$\hat{K}^{\mu\nu,n}_{pq\pm}(t) = \frac{1}{\hbar^2}\int_0^t ds\, G^{\mu\nu}_{pq}(t,s) e^{\pm i\omega_n s}\hat{\tilde{\rho}}_A(t-s) \tag{2.26}$$

with

$$G^{\mu\nu}_{pq}(t,s) = \frac{1}{\varepsilon_0^2}\,\mathrm{Tr}_R\left\{[\boldsymbol{e}_p\hat{\boldsymbol{D}}_\perp(\boldsymbol{R}_\mu,t)][\boldsymbol{e}_q\hat{\boldsymbol{D}}_\perp(\boldsymbol{R}_\nu,t-s)]\hat{\tilde{\rho}}_R(0)\right\} \tag{2.27}$$

the reservoir correlation function and $\boldsymbol{e}_{p/q}$ being Cartesian unit vectors. Usually, there are two different time scales, on which the atoms and the reservoir evolve. The reservoir correlation function $G^{\mu\nu}_{pq}(t,s)$ is zero for times t much larger than a typical correlation time τ_c. Therefore, we can replace the integral in Eq. (2.26) by $\int_0^{\tau_c} ds$. The atoms instead evolve on a time scale on the order of the radiation life time $\tau_\gamma \gg \tau_c$. Since $\tau_\gamma \gg \tau_c$, the state of the atoms does not change much within times on the order of the correlation time τ_c. We can then approximate $\hat{\tilde{\rho}}_A(t-s) \approx \hat{\tilde{\rho}}_A(t)$ in the integral. On the other hand, since the correlation function is zero for times much larger than the correlation time, we can also expand the upper limit of the integral to infinity and replace it by $\int_0^\infty ds$. This is the so-called *Markov approximation*. Further, if we assume a stationary reservoir with respect to the radiation field Hamiltonian, i.e., $[\hat{H}_R, \hat{\tilde{\rho}}_R(0)] = 0$, we can simplify the correlation function as

$$G^{\mu\nu}_{pq}(t,s) = G^{\mu\nu}_{pq}(s,s) \equiv G^{\mu\nu}_{pq}(s) = \frac{1}{\varepsilon_0^2}\,\mathrm{Tr}_R\left\{[\boldsymbol{e}_p\hat{\boldsymbol{D}}_\perp(\boldsymbol{R}_\mu,s)][\boldsymbol{e}_q\hat{\boldsymbol{D}}_\perp(\boldsymbol{R}_\nu,0)]\hat{\tilde{\rho}}_R(0)\right\}\,, \tag{2.28}$$

i.e., it depends only on the time difference s. The operator of Eq. (2.26) can thus be approximated by

$$\hat{K}^{\mu\nu,n}_{pq\pm}(t) \approx \hat{\tilde{\rho}}_A(t)\underbrace{\frac{1}{\hbar^2}\int_0^\infty ds\, G^{\mu\nu}_{pq}(s)e^{\pm i\omega_n s}}_{=:K^{\mu\nu,n}_{pq\pm}}\,. \tag{2.29}$$

Before we proceed, we have to assure that the remaining equation of motion is consistent with the aforementioned approximation. The obtained equation in Markov approximation captures only processes on a "coarse-grained" time axis [65], i.e., processes that happen on time scales smaller than the correlation time τ_c are not resolved. This means, we have to eliminate all terms in the equation of motion, which might cause a dynamics faster than τ_c. This can be achieved by averaging the equation over a time interval Δt with $\tau_c \ll \Delta t \ll \tau_\gamma$. This will average out the fast oscillating terms $e^{\pm i(\omega_m+\omega_n)t}$, which is usually referred to as *rotating wave approximation*. However, note that this neglection of the fast oscillating terms

is mandatory to be consistent with the Markov approximation. In contrast, for the difference terms we assume that $|\omega_m - \omega_n|\Delta t \ll 1$, such that we keep these terms.
Now, we turn back to the calculation of the correlation function $G_{pq}^{\mu\nu}(s)$. By plugging Eq. (2.2) in Eq. (2.28), we obtain the following four expectation values

$$\mathrm{Tr}_R[\hat{a}_\varepsilon(\boldsymbol{k})\hat{a}_{\varepsilon'}(\boldsymbol{k}')\hat{\tilde{\rho}}_R(0)]\,, \tag{2.30}$$

$$\mathrm{Tr}_R[\hat{a}_\varepsilon^\dagger(\boldsymbol{k})\hat{a}_{\varepsilon'}(\boldsymbol{k}')\hat{\tilde{\rho}}_R(0)]\,, \tag{2.31}$$

$$\mathrm{Tr}_R[\hat{a}_\varepsilon^\dagger(\boldsymbol{k})\hat{a}_{\varepsilon'}^\dagger(\boldsymbol{k}')\hat{\tilde{\rho}}_R(0)]\,, \tag{2.32}$$

$$\mathrm{Tr}_R[\hat{a}_\varepsilon(\boldsymbol{k})\hat{a}_{\varepsilon'}^\dagger(\boldsymbol{k}')\hat{\tilde{\rho}}_R(0)]\,. \tag{2.33}$$

In the following, we consider the radiation field to be in the vacuum state, i.e., $\hat{\tilde{\rho}}_R(0) = |0\rangle\langle 0|$ with $\hat{a}_\varepsilon(\boldsymbol{k})\,|0\rangle = 0$. Therefore, the expectation values of Eqs. (2.30)-(2.32) become zero and the last expectation value is $\mathrm{Tr}_R[\hat{a}_\varepsilon(\boldsymbol{k})\hat{a}_{\varepsilon'}^\dagger(\boldsymbol{k}')\hat{\tilde{\rho}}_R(0)] = \delta_{\varepsilon,\varepsilon'}\delta(\boldsymbol{k}-\boldsymbol{k}')$. The correlation function then simplifies to

$$\begin{aligned} G_{pq}^{\mu\nu}(s) &= \frac{\hbar}{2\varepsilon_0(2\pi)^3}\int d^3k\,\sum_{\boldsymbol{\varepsilon}}\omega_k e^{i\boldsymbol{k}(\boldsymbol{R}_\mu-\boldsymbol{R}_\nu)}[\boldsymbol{e}_p\boldsymbol{\varepsilon}][\boldsymbol{e}_q\boldsymbol{\varepsilon}^*]e^{-i\omega_k s} \\ &= \frac{\hbar}{2\varepsilon_0(2\pi c)^3}\int_0^{\omega_c} d\omega_k\,\omega_k^3\int d\Omega_k\,\sum_{\boldsymbol{\varepsilon}} e^{i\boldsymbol{k}(\boldsymbol{R}_\mu-\boldsymbol{R}_\nu)}[\boldsymbol{e}_p\boldsymbol{\varepsilon}][\boldsymbol{e}_q\boldsymbol{\varepsilon}^*]e^{-i\omega_k s}\,, \end{aligned} \tag{2.34}$$

where we plugged the expectation values in Eq. (2.28), used $\hat{U}_0^\dagger(t)\hat{a}_\varepsilon(\boldsymbol{k})\hat{U}_0(t) = \hat{a}_\varepsilon(\boldsymbol{k})e^{-i\omega_k t}$, and transformed to polar coordinates. For the latter step, we used $\omega_k = kc$ with $k = |\boldsymbol{k}|$ and Ω_k denotes the solid angle. Note that we also introduced a cutoff frequency ω_c according to the long-wavelength approximation, which the initial Hamiltonian is based on. Plugging the correlation function in Eq. (2.29), we find

$$\begin{aligned} K_{pq\pm}^{\mu\nu,n} \approx K_{pq\pm}^{\mu\nu} =& \frac{1}{2\varepsilon_0\hbar(2\pi c)^3}\times \\ & \int_0^{\omega_c} d\omega_k\,\omega_k^3 \underbrace{\int d\Omega_k\,\sum_{\boldsymbol{\varepsilon}} e^{i\boldsymbol{k}(\boldsymbol{R}_\mu-\boldsymbol{R}_\nu)}[\boldsymbol{e}_p\boldsymbol{\varepsilon}][\boldsymbol{e}_q\boldsymbol{\varepsilon}^*]}_{=:F_{pq}(k,\boldsymbol{R}_{\mu\nu})}\int_0^\infty ds\,e^{i(\pm\omega_0-\omega_k)s}\,. \end{aligned} \tag{2.35}$$

Here, we defined $\boldsymbol{R}_{\mu\nu} \coloneqq \boldsymbol{R}_\mu - \boldsymbol{R}_\nu$ and we assumed that the differences between the transition frequencies $|\omega_m - \omega_n|$ are much smaller than the mean transition frequency $\omega_0 = \frac{1}{D}\sum_{m=1}^D \omega_m$, i.e., $\frac{|\omega_m-\omega_n|}{\omega_0} \ll 1$, such that we can approximate $\omega_n \approx \omega_0$. The matrix elements $F_{pq}(k, \boldsymbol{R}_{\mu\nu})$ read (see Appendix B)

$$\begin{aligned} F_{pq}(k,\boldsymbol{R}_{\mu\nu}) = 4\pi\Bigg\{&\delta_{p,q}\left[\left(\frac{1}{\eta_{\mu\nu}}-\frac{1}{\eta_{\mu\nu}^3}\right)\sin\eta_{\mu\nu}+\frac{1}{\eta_{\mu\nu}^2}\cos\eta_{\mu\nu}\right] \\ &-\frac{[\boldsymbol{e}_p\boldsymbol{R}_{\mu\nu}][\boldsymbol{e}_q\boldsymbol{R}_{\mu\nu}]}{R_{\mu\nu}^2}\left[\left(\frac{1}{\eta_{\mu\nu}}-\frac{3}{\eta_{\mu\nu}^3}\right)\sin\eta_{\mu\nu}+\frac{3}{\eta_{\mu\nu}^2}\cos\eta_{\mu\nu}\right]\Bigg\} \end{aligned} \tag{2.36}$$

with $\eta_{\mu\nu} = kR_{\mu\nu}$ and $R_{\mu\nu} = |\boldsymbol{R}_{\mu\nu}|$. Now, let us consider the time integral. In terms of distributions, it evaluates to

$$\int_0^\infty ds\, e^{i(\pm\omega_0-\omega_k)s} = \pi\delta(\pm\omega_0-\omega_k) + i\,\text{p.v.}\left(\frac{1}{\pm\omega_0-\omega_k}\right), \tag{2.37}$$

where p.v. denotes the Cauchy principal value. With this at hand, we define the matrices

$$\Gamma_\pm^{\mu\nu} \coloneqq \frac{\pi}{2\varepsilon_0\hbar(2\pi c)^3}\int_0^{\omega_c} d\omega_k\,\omega_k^3 F(k,\boldsymbol{R}_{\mu\nu})\delta(\pm\omega_0-\omega_k)\,, \tag{2.38}$$

$$\Delta_\pm^{\mu\nu} \coloneqq \frac{1}{2\varepsilon_0\hbar(2\pi c)^3}\text{p.v.}\left(\int_0^{\omega_c} d\omega_k\,\omega_k^3 F(k,\boldsymbol{R}_{\mu\nu})\frac{1}{\pm\omega_0-\omega_k}\right), \tag{2.39}$$

and write

$$K_{pq\pm}^{\mu\nu} = \Gamma_{pq\pm}^{\mu\nu} + i\Delta_{pq\pm}^{\mu\nu}\,. \tag{2.40}$$

We note that since $\omega_0 > 0$ and $\omega_k \geq 0$, $\Gamma_-^{\mu\nu} = 0$. Now, we come back to Eq. (2.25). Using the previous equation, a lengthy but straightforward calculation leads to the following differential equation

$$\begin{aligned}\frac{\partial}{\partial t}\hat\rho_A(t) =& -\frac{i}{\hbar}[\hat H_A,\hat\rho_A(t)]\\ &-\sum_{\mu,\nu=1}^{N}\sum_{m,n=1}^{D}\Gamma_{mn}^{\mu\nu}\left(\hat S_{m+}^{(\mu)}\hat S_{n-}^{(\nu)}\hat\rho_A(t)+\hat\rho_A(t)\hat S_{m+}^{(\mu)}\hat S_{n-}^{(\nu)}-2\hat S_{n-}^{(\nu)}\hat\rho_A(t)\hat S_{m+}^{(\mu)}\right)\\ &-i\sum_{\mu,\nu=1}^{N}\sum_{m,n=1}^{D}\left\{\Delta_{mn+}^{\mu\nu}\left[\hat S_{m+}^{(\mu)}\hat S_{n-}^{(\nu)},\hat\rho_A(t)\right]+\left(\Delta_{mn-}^{\mu\nu}\right)^*\left[\hat S_{m-}^{(\mu)}\hat S_{n+}^{(\nu)},\hat\rho_A(t)\right]\right\},\end{aligned} \tag{2.41}$$

where we transformed back to the Schrödinger picture and defined

$$\Gamma_{mn}^{\mu\nu} \coloneqq \boldsymbol{d}_m\Gamma_+^{\mu\nu}\boldsymbol{d}_n^*\,, \tag{2.42}$$

$$\Delta_{mn+}^{\mu\nu} \coloneqq \boldsymbol{d}_m\Delta_+^{\mu\nu}\boldsymbol{d}_n^*\,, \tag{2.43}$$

$$\Delta_{mn-}^{\mu\nu} \coloneqq \boldsymbol{d}_m\Delta_-^{\mu\nu}\boldsymbol{d}_n^*\,. \tag{2.44}$$

Since $F_{pq}(k,\boldsymbol{R}_{\mu\nu})$ is a real-valued function and invariant under a change of μ and ν, we have $\left(\Delta_{mn-}^{\mu\nu}\right)^* = \left(\Delta_{nm-}^{\nu\mu}\right)$. Using this property and defining $\Omega_{mn}^{\mu\nu} \coloneqq -\left(\Delta_{mn+}^{\mu\nu}+\Delta_{mn-}^{\mu\nu}\right)$, Eq. (2.41) can be rewritten as

$$\frac{\partial}{\partial t}\hat\rho_A(t) = -\frac{i}{\hbar}[\hat H_A,\hat\rho_A(t)] + i\sum_{\substack{\mu,\nu=1\\ \mu\neq\nu}}^{N}\sum_{m,n=1}^{D}\Omega_{mn}^{\mu\nu}\left[\hat S_{m+}^{(\mu)}\hat S_{n-}^{(\nu)},\hat\rho_A(t)\right]$$

$$- \sum_{\mu,\nu=1}^{N} \sum_{m,n=1}^{D} \Gamma_{mn}^{\mu\nu} \left(\hat{S}_{m+}^{(\mu)} \hat{S}_{n-}^{(\nu)} \hat{\rho}_A(t) + \hat{\rho}_A(t) \hat{S}_{m+}^{(\mu)} \hat{S}_{n-}^{(\nu)} - 2 \hat{S}_{n-}^{(\nu)} \hat{\rho}_A(t) \hat{S}_{m+}^{(\mu)} \right)$$
$$- i \sum_{\mu=1}^{N} \sum_{m,n=1}^{D} \left\{ \Delta_{mn+}^{\mu\mu} \left[\hat{S}_{m+}^{(\mu)} \hat{S}_{n-}^{(\mu)}, \hat{\rho}_A(t) \right] - \left(\Delta_{mn-}^{\mu\mu} \right)^* \left[\hat{S}_{m-}^{(\mu)} \hat{S}_{n+}^{(\mu)}, \hat{\rho}_A(t) \right] \right\} . \quad (2.45)$$

We recognise that the last line only depends on the individual atoms separately. In particular, the terms with $m = n$ lead to level shifts, which are related to the Lamb shift. However, a correct treatment of the Lamb shift needs to include relativistic effects and normalisation procedures. Therefore, we omit these terms and assume that they are already correctly included in the energies E_l. Further, terms with $m \neq n$ correspond to a coherent coupling between dipole transitions, but are only nonzero if the corresponding dipole moments are not perpendicular and either the operator $\hat{S}_{m+}^{(\mu)} \hat{S}_{n-}^{(\mu)}$ or the operator $\hat{S}_{m-}^{(\mu)} \hat{S}_{n+}^{(\mu)}$ does not vanish. However, for transitions between atomic angular momentum multiplets, these two conditions can not be fulfilled simultaneously [63], which justifies to neglect these terms in the following. In summary, we thus omit the entire last line. The final master equation for an ensemble of identical multi-level atoms coupled to the vacuum of the electromagnetic field then reads

$$\frac{\partial}{\partial t} \hat{\rho}_A(t) = - \frac{i}{\hbar} [\hat{H}_A, \hat{\rho}_A(t)] + i \sum_{\substack{\mu,\nu=1 \\ \mu \neq \nu}}^{N} \sum_{m,n=1}^{D} \Omega_{mn}^{\mu\nu} \left[\hat{S}_{m+}^{(\mu)} \hat{S}_{n-}^{(\nu)}, \hat{\rho}_A(t) \right]$$
$$- \sum_{\mu,\nu=1}^{N} \sum_{m,n=1}^{D} \Gamma_{mn}^{\mu\nu} \left(\hat{S}_{m+}^{(\mu)} \hat{S}_{n-}^{(\nu)} \hat{\rho}_A(t) + \hat{\rho}_A(t) \hat{S}_{m+}^{(\mu)} \hat{S}_{n-}^{(\nu)} - 2 \hat{S}_{n-}^{(\nu)} \hat{\rho}_A(t) \hat{S}_{m+}^{(\mu)} \right) , \quad (2.46)$$

where the coupling parameters are given by (see Appendix B)

$$\Omega_{mn}^{\mu\nu} = \frac{\omega_0^3}{4\pi\varepsilon_0 \hbar c^3} \left\{ \boldsymbol{d}_m \boldsymbol{d}_n^* \left[\left(\frac{1}{\eta_{0\mu\nu}} - \frac{1}{\eta_{0\mu\nu}^3} \right) \cos \eta_{0\mu\nu} - \frac{1}{\eta_{0\mu\nu}^2} \sin \eta_{0\mu\nu} \right] \right.$$
$$\left. - \frac{[\boldsymbol{d}_m \boldsymbol{R}_{\mu\nu}] [\boldsymbol{d}_n^* \boldsymbol{R}_{\mu\nu}]}{R_{\mu\nu}^2} \left[\left(\frac{1}{\eta_{0\mu\nu}} - \frac{3}{\eta_{0\mu\nu}^3} \right) \cos \eta_{0\mu\nu} - \frac{3}{\eta_{0\mu\nu}^2} \sin \eta_{0\mu\nu} \right] \right\} , \quad (2.47)$$
$$\Gamma_{mn}^{\mu\nu} = \frac{\omega_0^3}{4\pi\varepsilon_0 \hbar c^3} \left\{ \boldsymbol{d}_m \boldsymbol{d}_n^* \left[\left(\frac{1}{\eta_{0\mu\nu}} - \frac{1}{\eta_{0\mu\nu}^3} \right) \sin \eta_{0\mu\nu} + \frac{1}{\eta_{0\mu\nu}^2} \cos \eta_{0\mu\nu} \right] \right.$$
$$\left. - \frac{[\boldsymbol{d}_m \boldsymbol{R}_{\mu\nu}] [\boldsymbol{d}_n^* \boldsymbol{R}_{\mu\nu}]}{R_{\mu\nu}^2} \left[\left(\frac{1}{\eta_{0\mu\nu}} - \frac{3}{\eta_{0\mu\nu}^3} \right) \sin \eta_{0\mu\nu} + \frac{3}{\eta_{0\mu\nu}^2} \cos \eta_{0\mu\nu} \right] \right\} , \quad (2.48)$$

with $\eta_{0\mu\nu} = k_0 R_{\mu\nu}$ and $k_0 = \frac{\omega_0}{c}$. We want to end this section by adding two more comments. The first comment we want to make is that we can also write the coherent and dissipative coupling parameters as the real and imaginary parts of

$$\Sigma_{mn}^{\mu\nu} := i \boldsymbol{d}_m (K_+^{\mu\nu} + K_-^{\mu\nu}) \boldsymbol{d}_n^* , \quad (2.49)$$

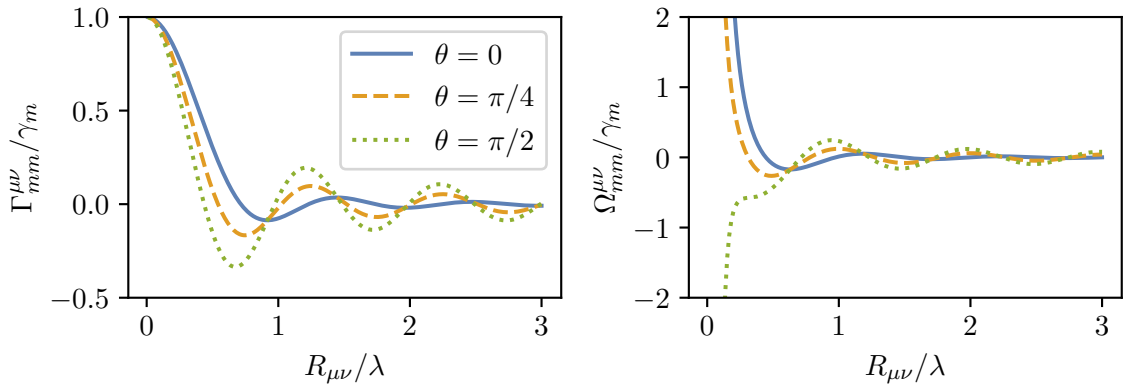

Figure 2.1: Dissipative and coherent coupling parameters of atoms μ and ν for the same dipole transition m against the separation $R_{\mu\nu}$ of the two corresponding atoms in units of the transition wavelength λ. The parameters are normalised by the so-called half-decay rate γ_m of the mth transition and plotted for three different orientations of the dipole moment $\boldsymbol{d}_m$ with respect to the separation vector $\boldsymbol{R}_{\mu\nu}$. Here, θ denotes the angle between these two vectors.

i.e., $\Omega^{\mu\nu}_{mn} = \mathrm{Re}(\Sigma^{\mu\nu}_{mn})$ and $\Gamma^{\mu\nu}_{mn} = \mathrm{Im}(\Sigma^{\mu\nu}_{mn})$. Thereby, Σ has the meaning of a self-energy, which is essentially given by the sum of the one-sided Fourier transforms of the reservoir correlation function at frequencies $\pm\omega_0$ [see Eq. (2.29)]. The second comment we want to make is that the coupling of the atoms to the reservoir leads, by tracing out the reservoir degrees of freedom, to an effective dipole-dipole interaction between the atoms, which we discuss in more detail in the next section. However, beforehand we want to stress that this effective dipole-dipole interaction strongly depends on the separation of the corresponding atoms as we show in Fig. 2.1. Here, we plot the parameters $\Gamma^{\mu\nu}_{mm}$ and $\Omega^{\mu\nu}_{mm}$ coupling atoms μ and ν for the same dipole transition m against the separation $R_{\mu\nu}$ of the two atoms in units of the transition wavelength $\lambda = \frac{2\pi}{k_0}$. Further, we normalised the parameters by the so-called half-decay rate of the mth transition $\gamma_m \coloneqq \gamma_{mm}$ with $\gamma_{mn} \coloneqq \Gamma^{\mu\mu}_{mn}$ and plotted them for different orientations of the dipole moment $\boldsymbol{d}_m$ with respect to the separation vector $\boldsymbol{R}_{\mu\nu}$. In the figure, θ denotes the angle between these two vectors, where we assumed a real dipole moment. It is worth noting that the strength as well as the sign depend on the dipole orientation with respect to the separation vector. In this context, we already note that the sign of the coherent coupling parameter leads to an either appropriate attractive or repulsive interaction of the two dipoles constituting the symmetric or antisymmetric superposition of the two atoms, which we introduce in a later chapter. More important for us is, however, the behaviour as a function of the distance of the atoms. In particular, we find that if the atoms are far apart from each other, i.e., $R_{\mu\nu}/\lambda \gg 1$, the coupling can be essentially neglected, whereas for $R_{\mu\nu}/\lambda \ll 1$ a significant coupling can be achieved.

2.4 Dipole-dipole interaction - Dyadic Green's function

In this section, we give a physical meaning to the effective dipole-dipole interaction derived in the last section. For this, we need to introduce the so-called *dyadic* Green's function for the electric field. We start by finding a *scalar* Green's function to the wave equation of, for instance, the scalar potential, i.e., we search for a Green's function $G(\boldsymbol{r}, \boldsymbol{r}', t, t')$ [66], which solves the equation

$$\left(\nabla^2 - \frac{1}{c^2}\frac{\partial^2}{\partial t^2}\right) G(\boldsymbol{r}, \boldsymbol{r}', t, t') = \delta(\boldsymbol{r} - \boldsymbol{r}')\delta(t - t')\,. \tag{2.50}$$

Since the operator $\nabla^2 - \frac{1}{c^2}\frac{\partial^2}{\partial t^2}$ is invariant under spatial and temporal translations, the Green's functions only depend on the differences of the positions and times, i.e., $G(\boldsymbol{r}, \boldsymbol{r}', t, t') = G(\boldsymbol{r} - \boldsymbol{r}', t - t')$. A solution can be obtained by Fourier transforming the equation to frequency space. With $\boldsymbol{r}'' = \boldsymbol{r} - \boldsymbol{r}'$ and $t'' = t - t'$ we obtain

$$\left(\nabla^2 + \frac{\omega^2}{c^2}\right) \mathscr{G}(\boldsymbol{r}'', \omega) = \delta(\boldsymbol{r}'')\,, \tag{2.51}$$

where

$$\mathscr{G}(\boldsymbol{r}'', \omega) = \int dt''\, G(\boldsymbol{r}'', t'') e^{i\omega t''} \tag{2.52}$$

is the Fourier transform of the Green's function $G(\boldsymbol{r}'', t'')$. Note that, for convenience, we defined the Fourier transform asymmetrically in this section. Outside of $\boldsymbol{r}'' = \boldsymbol{0}$, Eq. (2.51) is the homogeneous Helmholtz equation. Thus, accounting also for the limit $\boldsymbol{r}'' \to \boldsymbol{0}$, the Green's function in Fourier space is a spherical wave with proper normalisation, i.e.,

$$\mathscr{G}(\boldsymbol{r}'', \omega) = -\frac{e^{\pm i\omega|\boldsymbol{r}''|/c}}{4\pi|\boldsymbol{r}''|}\,, \tag{2.53}$$

where the plus sign in the exponent denotes an outgoing spherical wave, whereas the minus sign describes an incoming spherical wave. Before we come to the dyadic Green's function, let us first find a Green's function solving Eq. (2.50), since we need it in the next chapter. The solution can be obtained by Fourier transforming back, i.e.,

$$G(\boldsymbol{r}'', t'') = \frac{1}{2\pi}\int d\omega\, \mathscr{G}(\boldsymbol{r}'', \omega) e^{-i\omega t''} = -\frac{c}{4\pi|\boldsymbol{r}''|}\delta(|\boldsymbol{r}''| \pm ct'')\,. \tag{2.54}$$

If one demands for the Green's function that it exhibits the effect of a wave disturbance at the point $\boldsymbol{r}$ and time t originated at an earlier time t' at the point $\boldsymbol{r}'$, only the minus sign is relevant. We can then include the Heaviside step function $\theta(t'')$ to arrive at the so-called

retarded Green's function

$$G_R(\boldsymbol{r}-\boldsymbol{r}',t-t') = -\frac{c}{4\pi|\boldsymbol{r}-\boldsymbol{r}'|}\theta(t-t')\delta(|\boldsymbol{r}-\boldsymbol{r}'|-c(t-t'))\,. \tag{2.55}$$

Now, let us motivate the introduction of the dyadic Green's function. Coming from Maxwell's equations, we obtain the following wave equation for the electric field

$$\nabla\times\nabla\times\boldsymbol{E}(\boldsymbol{r},t)+\frac{1}{c^2}\frac{\partial^2}{\partial t^2}\boldsymbol{E}(\boldsymbol{r},t) = -\frac{1}{\varepsilon_0 c^2}\frac{\partial}{\partial t}\boldsymbol{j}(\boldsymbol{r},t) \tag{2.56}$$

with $\boldsymbol{j}(\boldsymbol{r},t)$ being the current density. A Fourier transform then leads to

$$\nabla\times\nabla\times\boldsymbol{\mathscr{E}}(\boldsymbol{r},\omega)-\frac{\omega^2}{c^2}\boldsymbol{\mathscr{E}}(\boldsymbol{r},\omega) = -\frac{i\omega}{\varepsilon_0 c^2}\boldsymbol{\mathscr{J}}(\boldsymbol{r},\omega)\,. \tag{2.57}$$

Due to the curl on the left side of the equation, a current in a single spatial direction leads to nonzero components of the electric field also in other spatial directions. Therefore, a Green's function relating the current to the electric field needs to be a matrix and is called a dyadic Green's function. Thus, we search for a Green's function $\mathscr{G}_D(\boldsymbol{r}-\boldsymbol{r}',\omega)$ solving the equation [67]

$$\nabla\times\nabla\times\mathscr{G}_D(\boldsymbol{r}-\boldsymbol{r}',\omega)-k^2\mathscr{G}_D(\boldsymbol{r}-\boldsymbol{r}',\omega) = \delta(\boldsymbol{r}-\boldsymbol{r}')\mathbb{1}\,. \tag{2.58}$$

The solution can be given in terms of the earlier derived Green's function of Eq. (2.53), i.e., [67]

$$\mathscr{G}_D(\boldsymbol{r}-\boldsymbol{r}',\omega) = -\left(\mathbb{1}+\frac{1}{k^2}\nabla\otimes\nabla\right)\mathscr{G}(\boldsymbol{r}-\boldsymbol{r}',\omega)\,. \tag{2.59}$$

An explicit calculation of the dyadic Green's function for the outgoing spherical wave gives

$$\mathscr{G}_D(\boldsymbol{r}'',\omega) = \frac{e^{ikr''}}{4\pi r''}\left[\left(1+\frac{i}{kr''}-\frac{1}{k^2r''^2}\right)\mathbb{1}-\left(1+\frac{3i}{kr''}-\frac{3}{k^2r''^2}\right)\frac{\boldsymbol{r}''\otimes\boldsymbol{r}''}{r''^2}\right] \tag{2.60}$$

with $r''=|\boldsymbol{r}''|$. Physically, the dyadic Green's function provides the electric field at a position $\boldsymbol{r}$ radiated by a normalised, oscillating dipole at a position $\boldsymbol{r}'$. By recognising that

$$\Omega_{mn}^{\mu\nu} = \frac{k_0^2}{\hbar\varepsilon_0}\boldsymbol{d}_m\mathrm{Re}\left[\mathscr{G}_D(\boldsymbol{R}_{\mu\nu},\omega_0)\right]\boldsymbol{d}_n^*\,, \tag{2.61}$$

$$\Gamma_{mn}^{\mu\nu} = \frac{k_0^2}{\hbar\varepsilon_0}\boldsymbol{d}_m\mathrm{Im}\left[\mathscr{G}_D(\boldsymbol{R}_{\mu\nu},\omega_0)\right]\boldsymbol{d}_n^*\,, \tag{2.62}$$

we find that the coherent and dissipative couplings between two dipole transitions m and n of atoms μ and ν describe simply the coupling of one dipole to the electric field emitted by the other dipole and vice versa, which gives a clear physical understanding.

2.5 Interaction with coherent fields

For the interactions discussed so far, we assumed $\mathscr{P}\mathscr{L}(t)\mathscr{P} = 0$, which is achieved by $\mathrm{Tr}_R[\hat{H}_I(t)\hat{\tilde{\rho}}_R(0)] = 0$. However, since $\hat{H}_I$ is linear in $\hat{a}_\varepsilon(\boldsymbol{k})$ and $\hat{a}^\dagger_\varepsilon(\boldsymbol{k})$, this does, in general, not hold true for coherent states of the radiation field. In this case, we will keep only the first-order interaction term and neglect all higher-order terms. If we assume that we have a single-mode laser, i.e., a particular mode described by polarisation $\boldsymbol{\varepsilon}_l$ and wave vector $\boldsymbol{k}_l$ is populated by a general coherent state instead of the vacuum, it is convenient to split the Hamiltonian accordingly into

$$\hat{H} = \hat{H}_A + \hat{H}_R + \hat{H}_L + \hat{H}_{I,AR} + \hat{H}_{I,AL}\,. \tag{2.63}$$

Thereby, $\hat{H}_A$ is the atomic Hamiltonian as before,

$$\hat{H}_R = \int d^3k \sum_{\boldsymbol{\varepsilon}} \hbar\omega_k \hat{a}^\dagger_\varepsilon(\boldsymbol{k})\hat{a}_\varepsilon(\boldsymbol{k}) - \hbar\omega_{k_l}\hat{a}^\dagger_{\varepsilon_l}(\boldsymbol{k}_l)\hat{a}_{\varepsilon_l}(\boldsymbol{k}_l) \tag{2.64}$$

is the Hamiltonian of the radiation field without the laser mode,

$$\hat{H}_L = \hbar\omega_{k_l}\hat{a}^\dagger_{\varepsilon_l}(\boldsymbol{k}_l)\hat{a}_{\varepsilon_l}(\boldsymbol{k}_l) \tag{2.65}$$

is the Hamiltonian of the laser mode, and $\hat{H}_{I,AR}$ and $\hat{H}_{I,AL}$ describe the couplings of the atoms with the vacuum modes and the laser mode. In the following, we simplify the notation by replacing $\hat{a}_{\varepsilon_l}(\boldsymbol{k}_l) \to \hat{a}_l$ and $\omega_{k_l} \to \omega_l$, which becomes convenient later on when we treat multiple laser modes. As we see, the Hamiltonian is still the same as before, but we split it conveniently for an initial state of the radiation field given by $|\tilde{\psi}_R(0)\rangle = |\alpha_l\rangle \otimes |0\rangle$, where $|\alpha_l\rangle$ denotes a coherent state of mode $\{\boldsymbol{\varepsilon}_l, \boldsymbol{k}_l\}$ and $|0\rangle$ is the vacuum in all other modes. We note that the derivation of the master equation of the previous section remains valid for the vacuum modes, since we exclude only a single mode, which does not change any of the derived results. However, we need to do the so-called *approximation of independent rates of variation* [65]. We introduced earlier two characteristic time scales for the evolution of the state given by

1. the correlation time τ_c of the reservoir with $\tau_c < \frac{1}{\omega_0}$ for the vacuum,
2. the radiative lifetime $\tau_\gamma \gg \tau_c$ of the atoms.

If we now include the interaction with a laser field, a third time scale appears given by the Rabi frequency Ω_R, which depends on the detuning $\delta_l = \omega_l - \omega_0$. Then, Ω_R^{-1} describes the typical time scale, on which stimulated emission/absorption processes occur, i.e., on which the interaction with the laser photons takes place. If we assume $\tau_c \ll \Omega_R^{-1}$, then the laser photons are only "spectators" during the process of spontaneous emission, but they can couple to the atoms between two spontaneous emission events. Therefore, the two processes do not

interact, but are independent, such that we can simply add the rates of variation of the density operator and calculate both as they were acting alone. Therefore, we first consider again the coupling to the vacuum and treat the coupling to the laser mode afterwards. Performing all the steps of the previous section, we thus arrive at the following master equation

$$\begin{aligned}\frac{\partial}{\partial t}\hat{\rho}_{AL}(t) = &-\frac{i}{\hbar}[\hat{H}_{AL},\hat{\rho}_{AL}(t)] + i\sum_{\substack{\mu,\nu=1\\ \mu\neq\nu}}^{N}\sum_{m,n=1}^{D}\Omega_{mn}^{\mu\nu}\left[\hat{S}_{m+}^{(\mu)}\hat{S}_{n-}^{(\nu)},\hat{\rho}_{AL}(t)\right]\\ &-\sum_{\mu,\nu=1}^{N}\sum_{m,n=1}^{D}\Gamma_{mn}^{\mu\nu}\left(\hat{S}_{m+}^{(\mu)}\hat{S}_{n-}^{(\nu)}\hat{\rho}_{AL}(t)+\hat{\rho}_{AL}(t)\hat{S}_{m+}^{(\mu)}\hat{S}_{n-}^{(\nu)}-2\hat{S}_{n-}^{(\nu)}\hat{\rho}_{AL}(t)\hat{S}_{m+}^{(\mu)}\right),\end{aligned} \tag{2.66}$$

where now $\hat{H}_{AL}=\hat{H}_A+\hat{H}_L+\hat{H}_{I,AL}$ and $\hat{\rho}_{AL}$ denotes the density operator of the composite system of atoms and of the laser field. However, in the end, we want to obtain an equation for the system of atoms alone. Therefore, we transform again into the interaction picture, but now with respect to $\hat{H}_A+\hat{H}_L$ and apply the Nakajima-Zwanzig projection method with $\mathscr{P}$ now defined as

$$\mathscr{P}\hat{\tilde{\rho}}_{AL}(t)=\mathrm{Tr}_L[\hat{\tilde{\rho}}_{AL}(t)]\otimes\hat{\tilde{\rho}}_L(0)=\hat{\tilde{\rho}}_A(t)\otimes\hat{\tilde{\rho}}_L(0)\,. \tag{2.67}$$

The second and third term on the right side of Eq. (2.66) are essentially unaffected, such that we only need to consider the first term and the whole procedure is exactly the same as before. However, as noted earlier, for a coherent state $\hat{\tilde{\rho}}_L(0)=|\alpha_l\rangle\langle\alpha_l|$, $\mathscr{P}\mathscr{L}(t)\mathscr{P}\hat{\tilde{\rho}}_{AL}(t)\neq 0$, such that we keep only the first term of the right side of Eq. (2.18), representing the leading order. Before we proceed, we generalise the situation to W laser modes instead of a single laser mode. Then, the initial state of the laser field becomes $\hat{\tilde{\rho}}_L(0)=|\alpha_{l_1},...,\alpha_{l_W}\rangle\langle\alpha_{l_1},...,\alpha_{l_W}|$ and in the Hamiltonians we additionally get a sum over the laser modes. A straightforward calculation leads to

$$\begin{aligned}&\mathrm{Tr}_L[\mathscr{P}\mathscr{L}(t)\mathscr{P}\hat{\tilde{\rho}}_{AL}(t)]\\ &=\mathrm{Tr}_L\left\{\left[-\frac{1}{\varepsilon_0}\sum_{\mu=1}^{N}\sum_{m=1}^{D}\left\{\hat{S}_{m+}^{(\mu)}(t)\boldsymbol{d}_m\hat{\boldsymbol{D}}_\perp(\boldsymbol{R}_\mu,t)+H.c.\right\},\hat{\tilde{\rho}}_A(t)\otimes\hat{\tilde{\rho}}_L(0)\right]\right\}\\ &=-\frac{1}{\varepsilon_0}\sum_{\mu=1}^{N}\sum_{m=1}^{D}\left\{\left[\hat{S}_{m+}^{(\mu)}(t),\boldsymbol{d}_m\boldsymbol{R}^\mu(t)\hat{\tilde{\rho}}_A(t)\right]+\left[\hat{S}_{m-}^{(\mu)}(t),\boldsymbol{d}_m^*\boldsymbol{R}^\mu(t)\hat{\tilde{\rho}}_A(t)\right]\right\},\end{aligned} \tag{2.68}$$

where we defined

$$\boldsymbol{R}^\mu(t)\coloneqq\frac{1}{\varepsilon_0}\,\mathrm{Tr}_L\left[\hat{\boldsymbol{D}}_\perp(\boldsymbol{R}_\mu,t)\hat{\tilde{\rho}}_L(0)\right]. \tag{2.69}$$

By using $\mathrm{Tr}_L[\hat{a}_{l_h}\hat{\tilde{\rho}}_L(0)] = \alpha_{l_h}e^{-i\omega_{l_h}t}$, $\mathrm{Tr}_L[\hat{a}^\dagger_{l_h}\hat{\tilde{\rho}}_L(0)] = \alpha^*_{l_h}e^{i\omega_{l_h}t}$, and defining

$$\boldsymbol{E}_{l_h 0}(\boldsymbol{R}_\mu) \coloneqq \sqrt{\frac{\hbar\omega_{l_h}}{2\varepsilon_0 V}}\boldsymbol{\varepsilon}_{l_h}\alpha_{l_h}e^{i\boldsymbol{k}_{l_h}\boldsymbol{R}_\mu}\,, \tag{2.70}$$

we obtain

$$\boldsymbol{R}^\mu(t) = i\sum_{h=1}^{W}\left[\boldsymbol{E}_{l_h 0}(\boldsymbol{R}_\mu)e^{-i\omega_{l_h}t} - \boldsymbol{E}^*_{l_h 0}(\boldsymbol{R}_\mu)e^{i\omega_{l_h}t}\right]\,. \tag{2.71}$$

Note that since we only have a sum over discrete laser modes instead of an integral over a continuum of modes, we included the factor $\sqrt{\frac{(2\pi)^3}{V}}$ in $\hat{\boldsymbol{D}}_\perp(\boldsymbol{R}_\mu, t)$, where V is the quantisation volume. Plugging Eq. (2.71) in Eq. (2.68), applying the rotating wave approximation, and defining the Rabi frequency $\Omega_{R,ml_h}(\boldsymbol{R}_\mu) \coloneqq \frac{\boldsymbol{d}_m\boldsymbol{E}_{l_h 0}(\boldsymbol{R}_\mu)}{\hbar}$, we find

$$\mathrm{Tr}_L[\mathscr{P}\mathscr{L}(t)\mathscr{P}\hat{\tilde{\rho}}_{AL}(t)] = -i\hbar\sum_{\mu=1}^{N}\sum_{m=1}^{D}\sum_{h=1}^{W}\left\{\left[\Omega_{R,ml_h}(\boldsymbol{R}_\mu)\hat{S}^{(\mu)}_{m+}e^{i(\omega_m-\omega_{l_h})t} - H.c., \hat{\tilde{\rho}}_A(t)\right]\right\}\,. \tag{2.72}$$

Now, we transform back to the Schrödinger picture and define the Hamiltonian

$$\hat{H}_{LR} \coloneqq -i\hbar\sum_{\mu=1}^{N}\sum_{m=1}^{D}\sum_{h=1}^{W}\left(\Omega_{R,ml_h}(\boldsymbol{R}_\mu)\hat{S}^{(\mu)}_{m+}e^{-i\omega_{l_h}t} - H.c.\right) \tag{2.73}$$

to finally arrive at

$$\frac{\partial}{\partial t}\hat{\rho}_A(t) = -\frac{i}{\hbar}[\hat{H}_A, \hat{\rho}_A(t)] - \frac{i}{\hbar}[\hat{H}_{LR}, \hat{\rho}_A(t)] + \mathscr{L}_\gamma\hat{\rho}_A(t) + \mathscr{L}_{\mathrm{col}}\hat{\rho}_A(t)\,. \tag{2.74}$$

Thereby, the first and second term describe the unitary evolution of the atoms alone and the coupling of the atoms to the coherent laser fields. The third term denotes the spontaneous emission of the individual atoms

$$\mathscr{L}_\gamma\hat{\rho}_A(t) = -\sum_{\mu=1}^{N}\sum_{m,n=1}^{D}\gamma_{mn}\left(\hat{S}^{(\mu)}_{m+}\hat{S}^{(\mu)}_{n-}\hat{\rho}_A(t) + \hat{\rho}_A(t)\hat{S}^{(\mu)}_{m+}\hat{S}^{(\mu)}_{n-} - 2\hat{S}^{(\mu)}_{n-}\hat{\rho}_A(t)\hat{S}^{(\mu)}_{m+}\right) \tag{2.75}$$

with $\gamma_{mn} = \Gamma^{\mu\mu}_{mn}$ and $\gamma_m = \gamma_{mm}$ the so-called half-decay rate of the transition m. Lastly, the fourth term accounts for the collective effects among the different atoms with

$$\mathscr{L}_{\mathrm{col}}\hat{\rho}_A(t) = -\frac{i}{\hbar}[\hat{H}_\Omega, \hat{\rho}_A(t)] + \mathscr{L}_\Gamma\hat{\rho}_A(t)\,, \tag{2.76}$$

where

$$\hat{H}_{\Omega} = -\hbar \sum_{\substack{\mu,\nu=1 \\ \mu \neq \nu}}^{N} \sum_{m,n=1}^{D} \Omega_{mn}^{\mu\nu} \hat{S}_{m+}^{(\mu)} \hat{S}_{n-}^{(\nu)} \tag{2.77}$$

accounts for the coherent coupling between two dipole transitions m and n of two different atoms μ and ν and

$$\mathscr{L}_{\Gamma} \hat{\rho}_A(t) = - \sum_{\substack{\mu,\nu=1 \\ \mu \neq \nu}}^{N} \sum_{m,n=1}^{D} \Gamma_{mn}^{\mu\nu} \left(\hat{S}_{m+}^{(\mu)} \hat{S}_{n-}^{(\nu)} \hat{\rho}_A(t) + \hat{\rho}_A(t) \hat{S}_{m+}^{(\mu)} \hat{S}_{n-}^{(\nu)} - 2 \hat{S}_{n-}^{(\nu)} \hat{\rho}_A(t) \hat{S}_{m+}^{(\mu)} \right) \tag{2.78}$$

describes the modification of the spontaneous emission of one atom due to the presence of all the other atoms.

3 Source field and photon correlation functions

Where quantum phenomena are important the situation is usually quite different. Experiments which detect photons ordinarily do so by absorbing them in one or another way. The use of any absorption process, such as photoionization, means in effect that the field we are measuring is the one associated with photon annihilation, the complex field $\boldsymbol{E}^{(+)}(\boldsymbol{r},t)$.

– Roy J. Glauber

In the following chapter, we define the concept of photon correlation functions, as originally introduced by Glauber in 1963 [6]. Thereby, the detection of a photon leads to the annihilation of this photon and is thus related to the annihilation operator. In terms of electric field operators, the annihilation process is described by the so-called positive electric field operator $\hat{\boldsymbol{E}}^{(+)}(\boldsymbol{r},t)$, which we introduce in a moment. We will first derive this operator for the atomic system discussed in the previous chapter and afterwards proceed with introducing the correlation functions. Before we dive into the derivation, let us first note that outside the system of charges, the polarisation density vanishes, which implies that $\hat{\boldsymbol{D}} = \varepsilon_0 \hat{\boldsymbol{E}}$ with $\hat{\boldsymbol{D}}$ being a transverse field for a globally neutral system. Therefore, the operator describing the electric field outside the system of charges is given by

$$\hat{\boldsymbol{E}}(\boldsymbol{r}) = i \int d^3k \sum_{\boldsymbol{\varepsilon}} \sqrt{\frac{\hbar\omega_k}{2\varepsilon_0(2\pi)^3}} \left[\boldsymbol{\varepsilon}\hat{a}_{\varepsilon}(\boldsymbol{k})e^{i\boldsymbol{kr}} - \boldsymbol{\varepsilon}^* \hat{a}^{\dagger}_{\varepsilon}(\boldsymbol{k})e^{-i\boldsymbol{kr}}\right] . \tag{3.1}$$

Transforming to the Heisenberg picture, the operator becomes time-dependent and we split it into the so-called positive and negative frequency parts $\hat{\boldsymbol{E}}(\boldsymbol{r},t) = \hat{\boldsymbol{E}}^{(+)}(\boldsymbol{r},t) + \hat{\boldsymbol{E}}^{(-)}(\boldsymbol{r},t)$, where

$$\hat{\boldsymbol{E}}^{(+)}(\boldsymbol{r},t) = i \int d^3k \sum_{\boldsymbol{\varepsilon}} \sqrt{\frac{\hbar\omega_k}{2\varepsilon_0(2\pi)^3}} \boldsymbol{\varepsilon}\hat{a}_{\varepsilon}(\boldsymbol{k},t)e^{i\boldsymbol{kr}} . \tag{3.2}$$

Thereby, $\hat{a}_{\varepsilon}(\boldsymbol{k},t)$ denotes the annihilation operator in the Heisenberg picture. To find an expression for the positive electric field operator in terms of atomic operators, we need to

solve the Heisenberg equation of motion

$$\dot{\hat{a}}_\varepsilon(\boldsymbol{k},t) = -\frac{i}{\hbar}[\hat{a}_\varepsilon(\boldsymbol{k},t), \hat{H}(t)]\,, \tag{3.3}$$

where the dot denotes the time derivative and $\hat{H}(t)$ is obtained from Eq. (2.8).

3.1 Source field operator

In the following section, we solve the foregoing equation and derive an expression for the positive electric field operator in the far field by obtaining the so-called source field operator. Defining the mode functions

$$\boldsymbol{u}_{\boldsymbol{k}\boldsymbol{\varepsilon}}(\boldsymbol{r}) \coloneqq \frac{1}{\hbar}\sqrt{\frac{\hbar\omega_k}{2\varepsilon_0(2\pi)^3}}\boldsymbol{\varepsilon}e^{i\boldsymbol{k}\boldsymbol{r}} \tag{3.4}$$

and evaluating the different commutators, leads to

$$\dot{\hat{a}}_\varepsilon(\boldsymbol{k},t) = -i\omega_k\hat{a}_\varepsilon(\boldsymbol{k},t) + \sum_{\mu=1}^{N}\sum_{m=1}^{D}\left\{[\boldsymbol{d}_m\boldsymbol{u}^*_{\boldsymbol{k}\boldsymbol{\varepsilon}}(\boldsymbol{R}_\mu)]\hat{S}^{(\mu)}_{m+}(t) + [\boldsymbol{d}^*_m\boldsymbol{u}^*_{\boldsymbol{k}\boldsymbol{\varepsilon}}(\boldsymbol{R}_\mu)]\hat{S}^{(\mu)}_{m-}(t)\right\}. \tag{3.5}$$

We now follow the route taken by Agarwal in Ref. [61]. Building the second derivative of the previous equation gives

$$\ddot{\hat{a}}_\varepsilon(\boldsymbol{k},t) = -i\omega_k\dot{\hat{a}}_\varepsilon(\boldsymbol{k},t) + \sum_{\mu=1}^{N}\sum_{m=1}^{D}\left\{[\boldsymbol{d}_m\boldsymbol{u}^*_{\boldsymbol{k}\boldsymbol{\varepsilon}}(\boldsymbol{R}_\mu)]\dot{\hat{S}}^{(\mu)}_{m+}(t) + [\boldsymbol{d}^*_m\boldsymbol{u}^*_{\boldsymbol{k}\boldsymbol{\varepsilon}}(\boldsymbol{R}_\mu)]\dot{\hat{S}}^{(\mu)}_{m-}(t)\right\}. \tag{3.6}$$

Therefore, let us consider the time derivative of $\boldsymbol{d}_m\hat{S}^{(\mu)}_{m+}(t) + \boldsymbol{d}^*_m\hat{S}^{(\mu)}_{m-}(t)$, given by the Heisenberg equation of motion

$$\boldsymbol{d}_m\dot{\hat{S}}^{(\mu)}_{m+}(t) + \boldsymbol{d}^*_m\dot{\hat{S}}^{(\mu)}_{m-}(t) = -\frac{i}{\hbar}[\boldsymbol{d}_m\hat{S}^{(\mu)}_{m+}(t) + \boldsymbol{d}^*_m\hat{S}^{(\mu)}_{m-}(t), \hat{H}(t)]\,. \tag{3.7}$$

It is simple to calculate that

$$[\hat{S}^{(\mu)}_{m\pm}(t), \hat{H}_A(t)] = \mp\hbar\omega_m\hat{S}^{(\mu)}_{m\pm}(t)\,, \tag{3.8}$$

$$[\hat{S}^{(\mu)}_{m\pm}(t), \hat{H}_R(t)] = 0\,. \tag{3.9}$$

However, the commutator with the interaction Hamiltonian needs a more detailed discussion. There, we obtain the following commutators $[\boldsymbol{d}_m\hat{S}^{(\mu)}_{m+}(t), \boldsymbol{d}_n\hat{S}^{(\mu)}_{n+}(t)]$, $[\boldsymbol{d}_m\hat{S}^{(\mu)}_{m+}(t), \boldsymbol{d}^*_n\hat{S}^{(\mu)}_{n-}(t)]$, $[\boldsymbol{d}^*_m\hat{S}^{(\mu)}_{m-}(t), \boldsymbol{d}^*_n\hat{S}^{(\mu)}_{n-}(t)]$, and $[\boldsymbol{d}^*_m\hat{S}^{(\mu)}_{m-}(t), \boldsymbol{d}_n\hat{S}^{(\mu)}_{n+}(t)]$. Within our coarse-grained master equation in Markov approximation, the first two commutators can be neglected. Further, for $m \neq n$, the third and fourth term only give a contribution if the two dipole moments are

not orthogonal and either the operator $\hat{S}^{(\mu)}_{m+}\hat{S}^{(\mu)}_{n-}$ or the operator $\hat{S}^{(\mu)}_{m-}\hat{S}^{(\mu)}_{n+}$ must not vanish. We recall that this can not be fulfilled simultaneously for usual angular momentum transitions [63], such that we omitted these terms earlier in the derivation of the master equation. Thus, we are only left with

$$[\boldsymbol{d}_m\hat{S}^{(\mu)}_{m+}(t), \boldsymbol{d}^*_m\hat{S}^{(\mu)}_{m-}(t)] + [\boldsymbol{d}^*_m\hat{S}^{(\mu)}_{m-}(t), \boldsymbol{d}_m\hat{S}^{(\mu)}_{m+}(t)] = 0 \tag{3.10}$$

and therefore we can approximate $[\boldsymbol{d}_m\hat{S}^{(\mu)}_{m+}(t) + \boldsymbol{d}^*_m\hat{S}^{(\mu)}_{m-}(t), \hat{H}_I(t)] \approx 0$. Then, Eq. (3.7) simplifies to

$$\boldsymbol{d}_m\dot{\hat{S}}^{(\mu)}_{m+}(t) + \boldsymbol{d}^*_m\dot{\hat{S}}^{(\mu)}_{m-}(t) = i\omega_m[\boldsymbol{d}_m\hat{S}^{(\mu)}_{m+}(t) - \boldsymbol{d}^*_m\hat{S}^{(\mu)}_{m-}(t)]\,. \tag{3.11}$$

By plugging Eqs. (3.5) and (3.11) in Eq. (3.6), we arrive at

$$\begin{aligned}\ddot{\hat{a}}_\varepsilon(\boldsymbol{k},t) + \omega_k^2\hat{a}_\varepsilon(\boldsymbol{k},t) = i\sum_{\mu,m}\Big\{&[\boldsymbol{d}_m\boldsymbol{u}^*_{\boldsymbol{k}\boldsymbol{\varepsilon}}(\boldsymbol{R}_\mu)](\omega_m-\omega_k)\hat{S}^{(\mu)}_{m+}(t)\\ &-[\boldsymbol{d}^*_m\boldsymbol{u}^*_{\boldsymbol{k}\boldsymbol{\varepsilon}}(\boldsymbol{R}_\mu)](\omega_m+\omega_k)\hat{S}^{(\mu)}_{m-}(t)\Big\}\,.\end{aligned} \tag{3.12}$$

Now, using this equation together with Eq. (3.2), we obtain the wave equation

$$\left(\nabla^2 - \frac{1}{c^2}\frac{\partial^2}{\partial t^2}\right)\hat{\boldsymbol{E}}^{(+)}(\boldsymbol{r},t) = -\frac{1}{\varepsilon_0 c}\hat{\boldsymbol{J}}^{(+)}(\boldsymbol{r},t)\,, \tag{3.13}$$

where we defined the source term as

$$\begin{aligned}\hat{\boldsymbol{J}}^{(+)}(\boldsymbol{r},t) \coloneqq \frac{1}{2(2\pi)^3}\sum_{\mu,m}\int d^3k\sum_{\boldsymbol{\varepsilon}} k e^{i\boldsymbol{k}(\boldsymbol{r}-\boldsymbol{R}_\mu)}\Big[&\boldsymbol{\varepsilon}(\boldsymbol{d}^*_m\boldsymbol{\varepsilon}^*)(\omega_m+\omega_k)\hat{S}^{(\mu)}_{m-}(t)\\ &-\boldsymbol{\varepsilon}(\boldsymbol{d}_m\boldsymbol{\varepsilon}^*)(\omega_m-\omega_k)\hat{S}^{(\mu)}_{m+}(t)\Big]\,.\end{aligned} \tag{3.14}$$

Using the retarded Green's function $G_R(\boldsymbol{r}-\boldsymbol{r}', t-t')$ of Eq. (2.55), a solution of the inhomogeneous wave equation is given by

$$\begin{aligned}\hat{\boldsymbol{E}}^{(+)}_S(\boldsymbol{r},t) &= -\frac{1}{\varepsilon_0 c}\int d^3r'\int dt'\, G_R(\boldsymbol{r}-\boldsymbol{r}', t-t')\hat{\boldsymbol{J}}^{(+)}(\boldsymbol{r}',t')\\ &= \frac{1}{4\pi\varepsilon_0 c}\int d^3r'\,\frac{\hat{\boldsymbol{J}}^{(+)}\left(\boldsymbol{r}', t-\frac{|\boldsymbol{r}-\boldsymbol{r}'|}{c}\right)}{|\boldsymbol{r}-\boldsymbol{r}'|}\,,\end{aligned} \tag{3.15}$$

where the index S indicates that this field stems from a source term and we evaluated the time integral, which leads to the so-called retarded time $t_R = t - \frac{|\boldsymbol{r}-\boldsymbol{r}'|}{c}$. In this context, we already note that due to the oscillating phase $e^{i\boldsymbol{k}(\boldsymbol{r}-\boldsymbol{R}_\mu)}$ in Eq. (3.14), the integral over r' will only pick up contributions from points located around $\boldsymbol{R}_\mu$. Physically, the sources, i.e., the atoms are located at $\boldsymbol{R}_\mu$ and thus the source term $\hat{\boldsymbol{J}}^{(+)}$ should only be nonzero around the

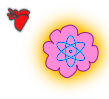

positions of the atoms. In the following, we carry out the integration explicitly. However, since we are only interested in detecting photons in the far field, we first introduce some approximations to simplify the calculations. In general, we can write

$$\hat{S}^{(\mu)}_{m\pm}(t) = \hat{S}^{(\mu),I}_{m\pm}(t) e^{\pm i\omega_m t}\,, \tag{3.16}$$

where $\hat{S}^{(\mu),I}_{m\pm}(t)$ denotes the operator in the interaction picture with respect to the unperturbed Hamiltonian $\hat{H}_0 = \hat{H}_A + \hat{H}_R$. In fact, the operators $\hat{S}^{(\mu)}_{m-}(t)$ and $\hat{S}^{(\mu)}_{m+}(t)$ in Eq. (3.14) need to be evaluated at the retarded time t_R. Therefore, we have

$$\hat{S}^{(\mu)}_{m\pm}\left(t - \frac{|\boldsymbol{r}-\boldsymbol{r}'|}{c}\right) = \hat{S}^{(\mu),I}_{m\pm}\left(t - \frac{|\boldsymbol{r}-\boldsymbol{r}'|}{c}\right) e^{\pm i\omega_m\left(t - \frac{|\boldsymbol{r}-\boldsymbol{r}'|}{c}\right)}\,. \tag{3.17}$$

Now, since $\hat{S}^{(\mu),I}_{m\pm}\left(t - \frac{|\boldsymbol{r}-\boldsymbol{r}'|}{c}\right)$ is a slowly varying operator, it does not change much on a timescale given by $\frac{|\boldsymbol{r}'|}{c} \sim \frac{|\boldsymbol{R}_\mu|}{c}$, such that it is justified to approximate

$$\hat{S}^{(\mu),I}_{m\pm}\left(t - \frac{|\boldsymbol{r}-\boldsymbol{r}'|}{c}\right) \approx \hat{S}^{(\mu),I}_{m\pm}\left(t - \frac{|\boldsymbol{r}|}{c}\right)\,. \tag{3.18}$$

Further, we approximate the exponent by doing the usual far-field Fraunhofer approximation. However, since there is the phase factor $e^{i\boldsymbol{k}(\boldsymbol{r}-\boldsymbol{R}_\mu)}$ in Eq. (3.14), we need to be a bit careful. Therefore, we first consistently insert the positions of the atoms $\boldsymbol{R}_\mu$ and approximate in the exponent

$$|\boldsymbol{r}-\boldsymbol{r}'| = |\boldsymbol{r}-\boldsymbol{R}_\mu - (\boldsymbol{r}'-\boldsymbol{R}_\mu)| \approx |\tilde{\boldsymbol{R}}_\mu| - \frac{\tilde{\boldsymbol{R}}_\mu \tilde{\boldsymbol{R}}'_\mu}{|\tilde{\boldsymbol{R}}_\mu|}\,, \tag{3.19}$$

where $\tilde{\boldsymbol{R}}_\mu = \boldsymbol{r}-\boldsymbol{R}_\mu$, $\tilde{\boldsymbol{R}}'_\mu = \boldsymbol{r}'-\boldsymbol{R}_\mu$, and $|\tilde{\boldsymbol{R}}'_\mu| \ll |\tilde{\boldsymbol{R}}_\mu|$. Now, we can do the usual Fraunhofer approximation for $|\boldsymbol{R}_\mu| \ll |\boldsymbol{r}|$ reading

$$|\tilde{\boldsymbol{R}}_\mu| = |\boldsymbol{r}-\boldsymbol{R}_\mu| \approx |\boldsymbol{r}| - \frac{\boldsymbol{r}\boldsymbol{R}_\mu}{|\boldsymbol{r}|}\,, \tag{3.20}$$

such that in total we have

$$t - \frac{|\boldsymbol{r}-\boldsymbol{r}'|}{c} \approx t - \frac{|\boldsymbol{r}|}{c} + \frac{\boldsymbol{r}\boldsymbol{R}_\mu}{|\boldsymbol{r}|c} + \frac{\tilde{\boldsymbol{R}}_\mu \tilde{\boldsymbol{R}}'_\mu}{|\tilde{\boldsymbol{R}}_\mu|c}\,. \tag{3.21}$$

Applying the discussed steps, we then find

$$\hat{S}^{(\mu)}_{m\pm}\left(t - \frac{|\boldsymbol{r}-\boldsymbol{r}'|}{c}\right) \approx \hat{S}^{(\mu)}_{m\pm}\left(t - \frac{|\boldsymbol{r}|}{c}\right) e^{\pm i k_m\left(\frac{\tilde{\boldsymbol{R}}_\mu \tilde{\boldsymbol{R}}'_\mu}{|\tilde{\boldsymbol{R}}_\mu|} + \frac{\boldsymbol{r}\boldsymbol{R}_\mu}{|\boldsymbol{r}|}\right)} \tag{3.22}$$

with $k_m = \frac{\omega_m}{c}$. In addition, in the denominator of the expression in the integral in Eq. (3.15), we do the usual stronger approximation

$$|\boldsymbol{r} - \boldsymbol{r}'| = |\tilde{\boldsymbol{R}}_\mu - \tilde{\boldsymbol{R}}'_\mu| \approx |\tilde{\boldsymbol{R}}_\mu| = |\boldsymbol{r} - \boldsymbol{R}_\mu| \,. \tag{3.23}$$

Next, we rewrite the sum over the two polarisation directions as

$$\sum_{\boldsymbol{\varepsilon}} \boldsymbol{\varepsilon}(\boldsymbol{d}_m \boldsymbol{\varepsilon}^*) = \boldsymbol{d}_m - \boldsymbol{\kappa}(\boldsymbol{d}_m \boldsymbol{\kappa}) = -\boldsymbol{\kappa} \times (\boldsymbol{\kappa} \times \boldsymbol{d}_m) \tag{3.24}$$

with $\boldsymbol{\kappa} = \frac{\boldsymbol{k}}{k}$. For the source field operator, we then arrive at

$$\begin{aligned}
\hat{\boldsymbol{E}}_S^{(+)}(\boldsymbol{r},t) = &-\frac{1}{8\pi\varepsilon_0 c} \sum_{\mu,m} \int d^3k\, k |\tilde{\boldsymbol{R}}_\mu|^{-1} \times \\
&\Bigg[\underbrace{\frac{1}{(2\pi)^3} \int d^3r'\, e^{i\left(\boldsymbol{k} - k_0 \frac{\tilde{\boldsymbol{R}}_\mu}{|\tilde{\boldsymbol{R}}_\mu|}\right)\boldsymbol{r}'}}_{=\delta\left(\boldsymbol{k} - k_0 \frac{\tilde{\boldsymbol{R}}_\mu}{|\tilde{\boldsymbol{R}}_\mu|}\right)} e^{-i\left(\boldsymbol{k} - k_0 \frac{\tilde{\boldsymbol{R}}_\mu}{|\tilde{\boldsymbol{R}}_\mu|}\right)\boldsymbol{R}_\mu} e^{-ik_0 \frac{\boldsymbol{r}\boldsymbol{R}_\mu}{|\boldsymbol{r}|}} \boldsymbol{\kappa} \times (\boldsymbol{\kappa} \times \boldsymbol{d}_m^*)(\omega_0 + \omega_k) \hat{S}_{m-}^{(\mu)}\left(t - \frac{|\boldsymbol{r}|}{c}\right) \\
&- \underbrace{\frac{1}{(2\pi)^3} \int d^3r'\, e^{i\left(\boldsymbol{k} + k_0 \frac{\tilde{\boldsymbol{R}}_\mu}{|\tilde{\boldsymbol{R}}_\mu|}\right)\boldsymbol{r}'}}_{=\delta\left(\boldsymbol{k} + k_0 \frac{\tilde{\boldsymbol{R}}_\mu}{|\tilde{\boldsymbol{R}}_\mu|}\right)} e^{-i\left(\boldsymbol{k} + k_0 \frac{\tilde{\boldsymbol{R}}_\mu}{|\tilde{\boldsymbol{R}}_\mu|}\right)\boldsymbol{R}_\mu} e^{ik_0 \frac{\boldsymbol{r}\boldsymbol{R}_\mu}{|\boldsymbol{r}|}} \boldsymbol{\kappa} \times (\boldsymbol{\kappa} \times \boldsymbol{d}_m)(\omega_0 - \omega_k) \hat{S}_{m+}^{(\mu)}\left(t - \frac{|\boldsymbol{r}|}{c}\right) \Bigg] ,
\end{aligned} \tag{3.25}$$

where we replaced ω_m by ω_0 and k_m by k_0. The two delta functions give restrictions to the absolute values and the directions of the $\boldsymbol{k}$ vectors. In particular, we only get contributions at magnitudes $\pm k_0$. Since the absolute value integral is only over positive k values, the last line of the previous equation vanishes. Further, the angular integral picks up only the direction of $\tilde{\boldsymbol{R}}_\mu$. Thus, we finally obtain

$$\hat{\boldsymbol{E}}_S^{(+)}(\boldsymbol{r},t) = -\frac{k_0^2}{4\pi\varepsilon_0} \sum_{\mu,m} \underbrace{\frac{\tilde{\boldsymbol{R}}_\mu}{|\tilde{\boldsymbol{R}}_\mu|} \times \left(\frac{\tilde{\boldsymbol{R}}_\mu}{|\tilde{\boldsymbol{R}}_\mu|} \times \boldsymbol{d}_m^*\right) \underbrace{|\tilde{\boldsymbol{R}}_\mu|^{-1} e^{-ik_0 \frac{\boldsymbol{r}\boldsymbol{R}_\mu}{|\boldsymbol{r}|}}}_{\substack{\text{spherical wave in} \\ \text{far-field approximation}}}}_{\text{dipole emission pattern}} \underbrace{\hat{S}_{m-}^{(\mu)}\left(t - \frac{|\boldsymbol{r}|}{c}\right)}_{\substack{\text{photon annihilation} = \\ \text{disexcitation of atoms}}} , \tag{3.26}$$

where we indicated the meaning of the different terms. We note that often we additionally neglect retardation effects and approximate $\hat{S}_{m-}^{(\mu)}\left(t - \frac{|\boldsymbol{r}|}{c}\right) \approx \hat{S}_{m-}^{(\mu)}(t)$. Furthermore, in the far field, the vectors $\tilde{\boldsymbol{R}}_\mu$ are almost parallel and of equal length, such that we usually approximate $\tilde{\boldsymbol{R}}_\mu \approx \boldsymbol{r}$. What we have done so far, is to find a special solution of the inhomogeneous wave equation. The general solution is given by the sum of this particular solution and all solutions

of the homogeneous wave equation. The homogeneous wave equation

$$\left(\nabla^2 - \frac{1}{c^2}\frac{\partial^2}{\partial t^2}\right)\hat{\boldsymbol{E}}^{(+)}(\boldsymbol{r},t) = 0 \tag{3.27}$$

can be derived from the free field equation of the annihilation operator

$$\dot{\hat{a}}_\varepsilon(\boldsymbol{k},t) = -i\omega_k \hat{a}_\varepsilon(\boldsymbol{k},t)\,, \tag{3.28}$$

which is solved by $\hat{a}_\varepsilon(\boldsymbol{k},t) = \hat{a}_\varepsilon(\boldsymbol{k})^{-i\omega_k t}$. Therefore, the general homogeneous solution is given by

$$\hat{\boldsymbol{E}}_0^{(+)}(\boldsymbol{r},t) = i\int d^3k \sum_{\boldsymbol{\varepsilon}} \sqrt{\frac{\hbar\omega_k}{2\varepsilon_0(2\pi)^3}}\boldsymbol{\varepsilon}\hat{a}_\varepsilon(\boldsymbol{k})e^{i(\boldsymbol{k}\boldsymbol{r}-\omega_k t)} \tag{3.29}$$

and the full positive electric field operator reads

$$\hat{\boldsymbol{E}}^{(+)}(\boldsymbol{r},t) = \hat{\boldsymbol{E}}_0^{(+)}(\boldsymbol{r},t) + \hat{\boldsymbol{E}}_S^{(+)}(\boldsymbol{r},t)\,. \tag{3.30}$$

3.2 Photon correlation functions

We continue by defining the photon correlation functions introduced by Glauber [6]. As mentioned in the beginning of this chapter, the detection of a photon annihilates this photon and is thus described by the positive electric field operator. Assuming some initial state $|i\rangle$ and an ideal photon detector, the probability to detect a photon is proportional to [6]

$$\sum_f |\langle f|\hat{\boldsymbol{E}}^{(+)}(\boldsymbol{r},t)|i\rangle|^2 = \langle i|\hat{\boldsymbol{E}}^{(-)}(\boldsymbol{r},t)\hat{\boldsymbol{E}}^{(+)}(\boldsymbol{r},t)|i\rangle\ , \tag{3.31}$$

where the sum runs over all possible final states $|f\rangle$. Generalising to an arbitrary initial state described by a density matrix $\hat{\rho}$, the probability to detect a photon at position $\boldsymbol{r}$ and time t is proportional to the expectation value

$$G^{(1)}(\boldsymbol{r},t) \coloneqq \langle\hat{\boldsymbol{E}}^{(-)}(\boldsymbol{r},t)\hat{\boldsymbol{E}}^{(+)}(\boldsymbol{r},t)\rangle\ , \tag{3.32}$$

which is the so-called first-order photon correlation function. More general, the detection of m photons at positions $\boldsymbol{r}_1$,...,$\boldsymbol{r}_m$ and times t_1,...,t_m is proportional to the expectation value

$$G^{(m)}(\boldsymbol{r}_1,t_1;...;\boldsymbol{r}_m,t_m) \coloneqq \langle\hat{\boldsymbol{E}}^{(-)}(\boldsymbol{r}_1,t_1)...\hat{\boldsymbol{E}}^{(-)}(\boldsymbol{r}_m,t_m)\hat{\boldsymbol{E}}^{(+)}(\boldsymbol{r}_m,t_m)...\hat{\boldsymbol{E}}^{(+)}(\boldsymbol{r}_1,t_1)\rangle\ , \tag{3.33}$$

which is the so-called mth-order photon correlation function. In the following chapters, these correlation functions will play the central role. In particular, on the one hand, we investigate which information about the atomic system can be gained by measuring these higher-order

photon correlation functions, on the other hand, we study how the atomic system can be influenced by those conditional photon measurements. However, before we end this chapter, we want to note that one can also define a normalised version of the mth-order photon correlation function reading

$$g^{(m)}(\boldsymbol{r}_1,t_1;...;\boldsymbol{r}_m,t_m) \coloneqq \frac{\langle \hat{\boldsymbol{E}}^{(-)}(\boldsymbol{r}_1,t_1)...\hat{\boldsymbol{E}}^{(-)}(\boldsymbol{r}_m,t_m)\hat{\boldsymbol{E}}^{(+)}(\boldsymbol{r}_m,t_m)...\hat{\boldsymbol{E}}^{(+)}(\boldsymbol{r}_1,t_1)\rangle}{\langle \hat{\boldsymbol{E}}^{(-)}(\boldsymbol{r}_1,t_1)\hat{\boldsymbol{E}}^{(+)}(\boldsymbol{r}_1,t_1)\rangle ... \langle \hat{\boldsymbol{E}}^{(-)}(\boldsymbol{r}_m,t_m)\hat{\boldsymbol{E}}^{(+)}(\boldsymbol{r}_m,t_m)\rangle}\,, \tag{3.34}$$

which we need in Chapter 6.

Finally, let us make two comments about the evaluation of the correlation functions. First, we usually assume that the state of the environment is the vacuum and therefore the free field operator $\hat{\boldsymbol{E}}_0^{(+)}(\boldsymbol{r},t)$ gives no contribution to the correlation functions. Therefore, we immediately express the correlation functions in terms of the source field operator $\hat{\boldsymbol{E}}_S^{(+)}(\boldsymbol{r},t)$. Second, since the photon correlation functions are multi-time expectation values in the Heisenberg picture using the full unitary dynamics, the question is how these expectation values can be evaluated using the quantum master equation derived in the previous chapter. The answer to this is the so-called quantum regression theorem, which for the interested reader we explain in detail in Appendix C.

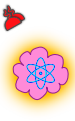

4 Spatio-temporal correlations of a three-atom system

The quantum theory, in other words, has had only a fraction of the influence upon optics that optics has historically had upon quantum theory. The explanation, no doubt, lies in the fact that optical experiments to date have paid very little attention to individual photons. To the extent that observations in optics have been confined to the measurement of ordinary light intensities, it is not surprising that classical theory has offered simple and essentially correct insights. Experiments such as those on quantum correlations suggest, on the other hand, the growing importance of studies of photon statistics. Such studies lie largely outside the grasp of classical theory.

– Roy J. Glauber

In the above quote, Roy J. Glauber indicates the connection between the photon statistics of a given light source, described by higher-order correlation functions, and quantum correlations. In the following sections, we explicitly investigate how quantum correlations can indeed be generated by multi-photon measurements in the case of a system with only a few photons. Concretely, we will consider a system consisting of three atoms and will have a detailed discussion on the measurement of two-photon and three-photon correlations in different atomic configurations. We note that parts of the work presented in the following sections have been previously published in Ref. [68]. We start by discussing first the case of two-level atoms and afterwards extend our work to the case of four-level atoms.

4.1 Spatio-temporal correlations of three two-level atoms

In the first subsection, we introduce the description of the considered two-level atoms and specify the spatial arrangement of the atoms.

4.1.1 Atom description and spatial configuration

We assume three identical two-level atoms with excited state $|e\rangle$, ground state $|g\rangle$, and energy separation $\hbar\omega_0$ as illustrated in Fig. 4.1. Further, the atoms can emit photons with a half-decay rate of γ. In what follows, we consider a particular spatial arrangement of the three

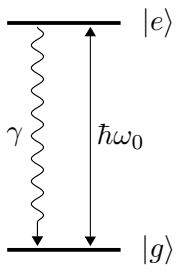

Figure 4.1: Description of a single two-level atom. We denote the lower energy state with $|g\rangle$ for ground state and the higher energy state with $|e\rangle$ for excited state. The energy spacing is given by $\hbar\omega_0$ and the atom can drop from the excited state to the ground state via the spontaneous emission of a photon characterised by the half-decay rate γ.

atoms. Two of the atoms are assumed to have a subwavelength separation, whereas the remaining third atom shall be located far distant, i.e., several wavelengths away from the two-atom subsystem. Therefore, the two close-by atoms interact via the dipole-dipole interaction introduced in Chapter 2, while the third atom evolves independently of the other two atoms. Thus, in the case of the third atom, we neglect the coupling to the other two atoms, which is justified for the aforementioned separation (see Fig. 2.1). Before we describe the three-atom system, it is worth having a look at the coupled two-atom subsystem first. Without any laser interaction, Eq. (2.74) reduces to [63, 69]

$$\begin{aligned}\frac{\partial}{\partial t}\hat{\rho}_A(t) = &-\frac{i}{\hbar}[\hat{H}_A + \hat{H}_\Omega, \hat{\rho}_A(t)] - \sum_{\mu=1}^{2}\gamma\left(\hat{S}_+^{(\mu)}\hat{S}_-^{(\mu)}\hat{\rho}_A(t) + \hat{\rho}_A(t)\hat{S}_+^{(\mu)}\hat{S}_-^{(\mu)} - 2\hat{S}_-^{(\mu)}\hat{\rho}_A(t)\hat{S}_+^{(\mu)}\right)\\ &- \sum_{\substack{\mu,\nu=1\\ \mu\neq\nu}}^{2}\Gamma^{\mu\nu}\left(\hat{S}_+^{(\mu)}\hat{S}_-^{(\nu)}\hat{\rho}_A(t) + \hat{\rho}_A(t)\hat{S}_+^{(\mu)}\hat{S}_-^{(\nu)} - 2\hat{S}_-^{(\nu)}\hat{\rho}_A(t)\hat{S}_+^{(\mu)}\right), \end{aligned} \tag{4.1}$$

where

$$\hat{H}_A + \hat{H}_\Omega = \hbar\omega_0\sum_{\mu=1}^{2}\hat{S}_z^{(\mu)} - \hbar\sum_{\substack{\mu,\nu=1\\ \mu\neq\nu}}^{2}\Omega^{\mu\nu}\hat{S}_+^{(\mu)}\hat{S}_-^{(\nu)} \tag{4.2}$$

and $\hat{S}_z^{(\mu)} = \frac{1}{2}\left(\hat{S}_+^{(\mu)}\hat{S}_-^{(\mu)} - \hat{S}_-^{(\mu)}\hat{S}_+^{(\mu)}\right)$. Since the coupling parameters $\Gamma^{\mu\nu}$ and $\Omega^{\mu\nu}$ are symmetric with respect to the atoms, we define $\Delta\gamma \coloneqq \Gamma^{12} = \Gamma^{21}$ and $\Delta\Omega \coloneqq \Omega^{12} = \Omega^{21}$. For mathematical reasons and also physical insights, it is convenient to diagonalise the Hamiltonian $\hat{H}_A + \hat{H}_\Omega$. This leads to the eigenstates

$$|E\rangle = |e,e\rangle\ , \tag{4.3}$$

$$|S\rangle = \frac{1}{\sqrt{2}}(|e,g\rangle + |g,e\rangle)\,, \tag{4.4}$$

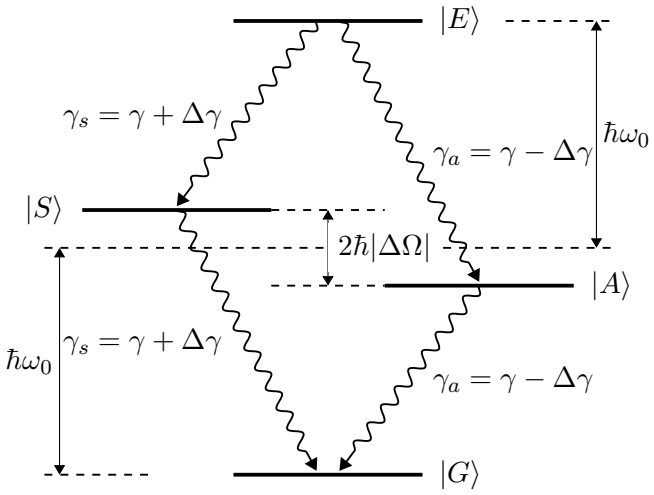

Figure 4.2: Energy level scheme of the coupled two-atom subsystem. The new collective states $|S\rangle$ and $|A\rangle$ are shifted with respect to the bare states $|e,g\rangle$ and $|g,e\rangle$. Note that we assume the dipole moment to be perpendicular to the separation vector of the atoms and a separation smaller than λ, such that $\Delta\Omega < 0$ (see Fig. 2.1). The system features two different decay channels, the so-called symmetric decay channel via the symmetric state $|S\rangle$ and with the symmetric decay rate $\gamma_s = \gamma + \Delta\gamma$ and the so-called antisymmetric decay channel via the antisymmetric state $|A\rangle$ with the antisymmetric decay rate $\gamma_a = \gamma - \Delta\gamma$.

$$|A\rangle = \frac{1}{\sqrt{2}}(|e,g\rangle - |g,e\rangle)\,, \tag{4.5}$$

$$|G\rangle = |g,g\rangle\ , \tag{4.6}$$

with eigenenergies $\hbar\omega_0$, $-\hbar\Delta\Omega$, $\hbar\Delta\Omega$ and $-\hbar\omega_0$, where we refer to the states $|S\rangle$ and $|A\rangle$ as symmetric state and antisymmetric state. Further, we also express the dissipator in this new basis. Therefore, we define the transition operators $\hat{S}_{hl} \coloneqq |h\rangle\langle l|$ with $h,l \in \{E,S,A,G\}$. The master equation in terms of these operators then reads [63, 69]

$$\begin{aligned}
\frac{\partial}{\partial t}\hat{\rho}_A(t) &= -\frac{i}{\hbar}[\hat{H}_A + \hat{H}_\Omega, \hat{\rho}_A(t)] \\
&- \gamma_s \left[(\hat{S}_{EE} + \hat{S}_{SS})\hat{\rho}_A(t) + \hat{\rho}_A(t)(\hat{S}_{EE} + \hat{S}_{SS}) - 2(\hat{S}_{SE} + \hat{S}_{GS})\hat{\rho}_A(t)(\hat{S}_{ES} + \hat{S}_{SG})\right] \\
&- \gamma_a \left[(\hat{S}_{EE} + \hat{S}_{AA})\hat{\rho}_A(t) + \hat{\rho}_A(t)(\hat{S}_{EE} + \hat{S}_{AA}) - 2(\hat{S}_{GA} - \hat{S}_{AE})\hat{\rho}_A(t)(\hat{S}_{AG} - \hat{S}_{EA})\right]\ ,
\end{aligned} \tag{4.7}$$

which allows for a direct physical interpretation. The first term of the dissipator describes the decay cascade $|E\rangle \to |S\rangle \to |G\rangle$ with a rate $\gamma_s = \gamma + \Delta\gamma$, whereas the second term describes the decay cascade $|E\rangle \to |A\rangle \to |G\rangle$ with a rate $\gamma_a = \gamma - \Delta\gamma$. Thus, the coupled two-atom subsystem can be pleasingly illustrated by the energy diagram shown in Fig. 4.2. Now, with the coupled two-atom subsystem discussed, we immediately know the three-atom dynamics, since it is just the sum of the coupled two-atom dynamics and the dynamics of the

independent third atom.

4.1.2 Engineering of spontaneous emission

We investigate the collective spontaneous emission of photons of the three-atom system introduced in the previous subsection. For this purpose, we study Glauber's third-order photon correlation function displaying a so-called *conditional* photon measurement. The third-order photon correlation function $G^{(3)}(\boldsymbol{r}_1, t_1; \boldsymbol{r}_2, t_2; \boldsymbol{r}_3, t_3)$ describes the probability of measuring a photon at a position $\boldsymbol{r}_3$ and time t_3 under the condition that two photons were previously detected at positions $\boldsymbol{r}_1$ and $\boldsymbol{r}_2$ at times t_1 and t_2. Thereby, the first two photon measurements can be viewed as a state preparation process, entangling all three atoms. As we will see, the combination of this conditional measurement with the dipole-dipole interaction of the two close-by atoms, which leads to modified decay rates, gives rise to a pronounced *spatial* modulation of the photon emission rate. This is precisely the particularity of the considered three-atom system. We note that a strong modulation of the decay rates can only be achieved for subwavelength separations of the atoms, for which the emission is, however, almost isotropic. The spatial modulation only comes into play via the third atom located several wavelengths away, but entangled with the other two atoms by conditional photon measurements. Thereby, the interference of the different decay channels, the three-atom system can take, strongly depends on the emission direction. This allows for engineering the collective spontaneous emission behaviour in space and time.
In the following, we assume that the third remote atom can be experimentally controlled. Therefore, we assume that all three atoms are placed along one axis, which we consider to be the x-axis and additionally choose wlog $\boldsymbol{R}_1 = \boldsymbol{0}$ (see Fig. 4.3). Further, the detectors shall be located in the xy-plane, such that we can write the direction of the mth detector as $\hat{\boldsymbol{r}}_m = \frac{\boldsymbol{r}_m}{r_m} = \hat{\boldsymbol{x}}\cos\varphi_m + \hat{\boldsymbol{y}}\sin\varphi_m$, which is characterised by the azimuthal angle φ_m. The source field operator of Eq. (3.26) can then be written as

$$\hat{\boldsymbol{E}}_S^{(+)}(\boldsymbol{r}_m, t_m) = -\frac{k_0^2}{4\pi\varepsilon_0 r_m}\hat{\boldsymbol{r}}_m \times (\hat{\boldsymbol{r}}_m \times \boldsymbol{d}^*)\sum_{\mu=1}^{3} e^{i\delta_{\mu,m}}\hat{S}_-^{(\mu)}(t_m)\,, \tag{4.8}$$

where we defined the phase

$$\delta_{\mu,m} \coloneqq -k_0 \boldsymbol{R}_\mu \hat{\boldsymbol{r}}_m\,, \tag{4.9}$$

which accounts for the geometric phase a photon accumulates by the propagation from the atom at $\boldsymbol{R}_\mu$ to the detector at $\boldsymbol{r}_m$ relative to a photon originating from the coordinate origin (see Fig. 4.3). To calculate the third-order photon correlation function, we assume that the dipole moment $\boldsymbol{d}$ is real and that the atoms are initially prepared in their excited state. Further, the first two photon measurements shall be performed coincidently at the initial time $t_1 = t_2 = 0$ with variable, but fixed positions $\boldsymbol{r}_1$ and $\boldsymbol{r}_2$. The third-order photon correlation

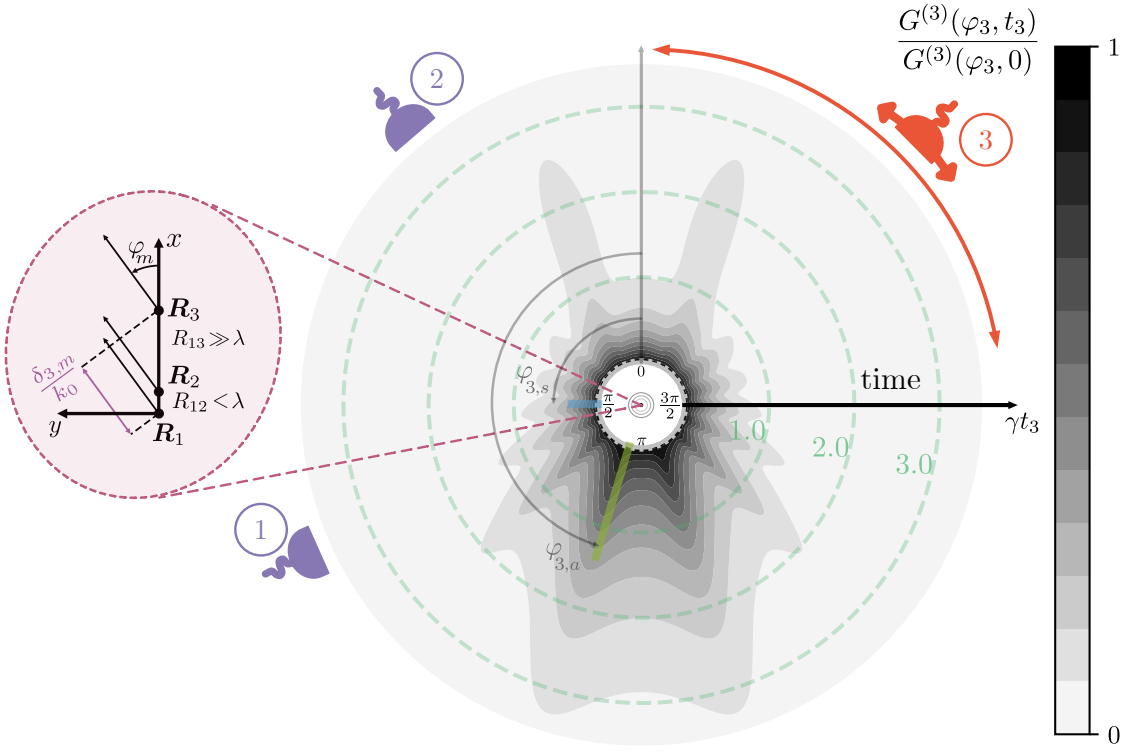

Figure 4.3: Third-order photon correlation function $G^{(3)}(\varphi_3, t_3)$, normalised to its initial value for every angle φ_3, as a function of the third detector position characterised by the azimuthal angle φ_3 and as a function of time γt_3 (radial axis). The first two photon measurements take place at time $t = 0$ and angles $\varphi_1 = \frac{2\pi}{3}$, $\varphi_2 = \frac{\pi}{4.4}$, illustrated by the purple detectors. The atoms are located at positions $\boldsymbol{R}_1 = \boldsymbol{0}$, $\boldsymbol{R}_2 = \frac{\lambda}{3}\hat{\boldsymbol{x}}$, and $\boldsymbol{R}_3 = 4\lambda\hat{\boldsymbol{x}}$ along the x-axis, i.e., the first two atoms have a subwavelength separation $R_{12} < \lambda$, whereas the third atom is placed several wavelengths away, $R_{13} \gg \lambda$. The two angles $\varphi_{3,s}$ and $\varphi_{3,a}$ denote directions, for which an effective decay with the superradiant or subradiant decay rate $\Gamma_s = 2\gamma_s$ or $\Gamma_a = 2\gamma_a$ can be observed.

function is then given by [68, 70]

$$
\begin{aligned}
G^{(3)}(\boldsymbol{r}_3, t_3) \propto \sin^2(\alpha)\times \\
&\Big[|c_{Ge}|^2 e^{-2\gamma t_3} + 2|c_{Sg}|^2 e^{-2(\gamma+\Delta\gamma)t_3}\cos^2\left(\frac{\delta_{2,3}}{2}\right) + 2|c_{Ag}|^2 e^{-2(\gamma-\Delta\gamma)t_3}\sin^2\left(\frac{\delta_{2,3}}{2}\right) \\
&+ 2|c_{Sg}||c_{Ag}|e^{-2\gamma t_3}\sin(\delta_{2,3})\sin\left(\varphi_{Ag} - \varphi_{Sg} - 2\,\Delta\Omega\, t_3\right) \\
&+ 2\sqrt{2}|c_{Sg}||c_{Ge}|e^{-(2\gamma+\Delta\gamma)t_3}\cos\left(\frac{\delta_{2,3}}{2}\right)\cos\left(\varphi_{Sg} + \frac{\delta_{2,3}}{2} - \delta_{3,3} + \Delta\Omega\, t_3\right) \\
&+ 2\sqrt{2}|c_{Ag}||c_{Ge}|e^{-(2\gamma-\Delta\gamma)t_3}\sin\left(\frac{\delta_{2,3}}{2}\right)\sin\left(\varphi_{Ag} + \frac{\delta_{2,3}}{2} - \delta_{3,3} - \Delta\Omega\, t_3\right)\Big] \,,
\end{aligned}
\tag{4.10}
$$

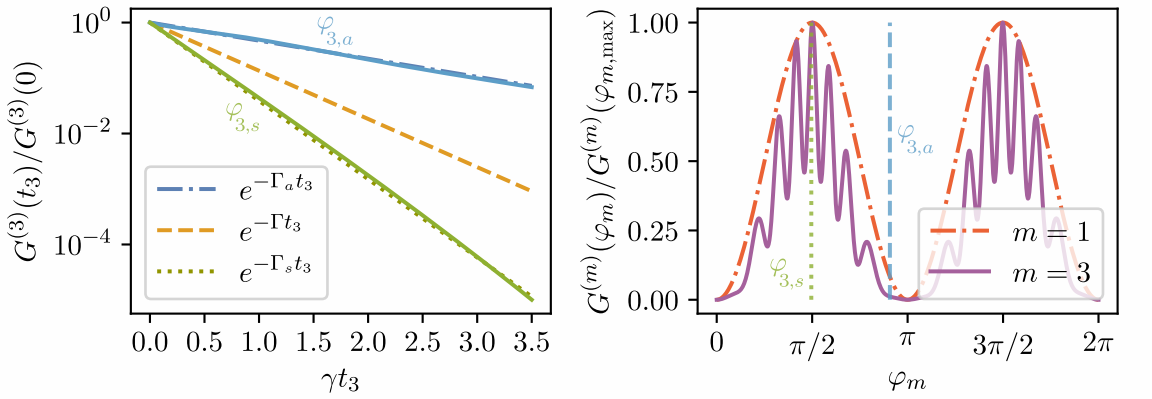

Figure 4.4: On the left, the third-order photon correlation function for the two directions $\varphi_{3,a}$ and $\varphi_{3,s}$ (blue and green solid lines) is shown. By comparing the decay to the three reference decays with the antisymmetric decay rate Γ_a, the unmodified decay rate Γ, and the symmetric decay rate Γ_s, we see that the third-order photon correlation function displays an effective exponential decay with the antisymmetric (subradiant) or the symmetric (superradiant) decay rate in these two directions. On the right, we show the third-order photon correlation function together with the first-order photon correlation function for the initial time $t = 0$ as a function of the detector direction. Whereas the first-order photon correlation function shows only an isotropic emission pattern (up to the dipole radiation pattern), the third-order photon correlation function displays multiple spatial fringes stemming from the entanglement and thus quantum correlations between all three atoms (see Appendix D). Further, we also indicate the directions $\varphi_{3,a}$ and $\varphi_{3,s}$, where an effective subradiant or superradiant decay can be observed.

where we defined the coefficients c_{Ge}, c_{Sg}, and c_{Ag} reading

$$c_{Ge} = \left(e^{i\delta_{2,1}} + e^{i\delta_{2,2}}\right) , \tag{4.11}$$

$$c_{Sg} = \frac{1}{\sqrt{2}}\left(e^{i(\delta_{3,1}+\delta_{2,2})} + e^{i(\delta_{2,1}+\delta_{3,2})} + e^{i\delta_{3,1}} + e^{i\delta_{3,2}}\right) , \tag{4.12}$$

$$c_{Ag} = \frac{1}{\sqrt{2}}\left(e^{i(\delta_{3,1}+\delta_{2,2})} + e^{i(\delta_{2,1}+\delta_{3,2})} - e^{i\delta_{3,1}} - e^{i\delta_{3,2}}\right) . \tag{4.13}$$

Further, the phases $\varphi_{Sg/Ag} = \mathrm{Arg}\left(\frac{c_{Sg/Ag}}{c_{Ge}}\right)$ denote the phases of the complex coefficients c_{Sg} and c_{Ag} with respect to c_{Ge}. In addition, α denotes the angle between the third detector at $\boldsymbol{r}_3$ and the dipole moment $\boldsymbol{d}$. Therefore, the factor $\sin^2(\alpha)$ gives the usual dipole radiation pattern. Finally, we note that in Eq. (4.10), we neglected the prefactor of the source field operator and omitted the fixed positions and times of the first two photon measurements in the argument of the correlation function. In the following, we assume that the dipole moment $\boldsymbol{d} = d\hat{\boldsymbol{x}}$ is parallel to the atomic axis, for which the angle α is equal to the azimuthal angle φ_3 (see Fig. 4.3). In Fig. 4.3, we show the third-order photon correlation function for atom positions $\boldsymbol{R}_1 = \boldsymbol{0}$, $\boldsymbol{R}_2 = \frac{\lambda}{3}\hat{\boldsymbol{x}}$, and $\boldsymbol{R}_3 = 4\lambda\hat{\boldsymbol{x}}$. Thereby, the first two photon detections take

place at detection angles $\varphi_1 = \frac{2\pi}{3}$ and $\varphi_2 = \frac{\pi}{4.4}$, illustrated by the purple detectors in the figure. The third-order photon correlation function is plotted as a function of time (radial direction), normalised to its initial value, for every possible third detector position characterised by the angle φ_3. We find a rich temporal and spatial emission pattern with multiple different emission characteristics, only depending on the direction of the third detector. In particular, in the directions $\varphi_{3,s}$ and $\varphi_{3,a}$, an effective exponential decay with the symmetric or antisymmetric decay rate $\Gamma_s = 2\gamma_s$ or $\Gamma_a = 2\gamma_a$ can be observed simultaneously, i.e., for the same first two detector positions. This is illustrated in Fig. 4.4. Here, on the left, we show the third-order photon correlation functions $G^{(3)}(\varphi_{3,a}, t_3)$ and $G^{(3)}(\varphi_{3,s}, t_3)$ (blue and green solid lines), normalised to their initial value, against time. As a reference, we plot the theoretical decays with the antisymmetric decay rate Γ_a, the unmodified decay rate Γ, and the symmetric decay rate Γ_s. As can be seen, for the two directions $\varphi_{3,a}$ and $\varphi_{3,s}$ an almost perfect effective subradiant or superradiant exponential decay with rate Γ_a or Γ_s can be found. On the right, we show the third-order photon correlation function $G^{(3)}(\varphi_3, t_3 = 0)$ for the time $t_3 = 0$, normalised to its maximum value, against the position of the third detector. We find that not only we get a rich temporal emission pattern, but also spatial interference fringes. Since the third atom becomes entangled with the other two atoms via the first two photon measurements (see Appendix D), the different emission paths of the remote atom and the two-atom subsystem interfere with each other. Due to the large separation of the two systems, many spatial fringes can be found. We note that the two close-by atoms on their own can not produce such a rich spatial pattern.
Furthermore, we also plot the first-order photon correlation function, which shows an isotropic emission characteristics [up to the dipole radiation pattern $\sin^2(\alpha)$]. This demonstrates that the conditional measurement, leading to entanglement between the atoms, is indeed essential to obtain the great spatial variety shown in the Figs. 4.3 and 4.4.
We note that in obtaining the complex emission pattern shown in Fig. 4.3, we adequately balanced the different modes in Eq. (4.10). Thereby, the first two detector positions were chosen such to allow all three modes to substantially contribute to the emission pattern. However, we note that other similar intricate emission patterns can be found for different detector positions, in particular, we could choose positions, where either an isolated superradiant or subradiant decay can be observed. This huge variety allows to engineer the emission dynamics of the presented three-atom system.

To analyse the emission pattern shown in Fig. 4.3 more quantitatively, in Fig. 4.5 the different effective decay rates are illustrated as a function of the detection direction. Thereby, the effective decay rates of the first- and third-order photon correlation functions are obtained by an exponential fit in the time interval $\gamma t \in [0, 0.5]$, i.e., we determine effective decay rates for the early to intermediate time dynamics. Since the emission signal is the superposition of different modes with different decay rates, the time behaviour can not be described by a single exponential. Therefore, the exponential fit is only justifiable for short to intermediate times.

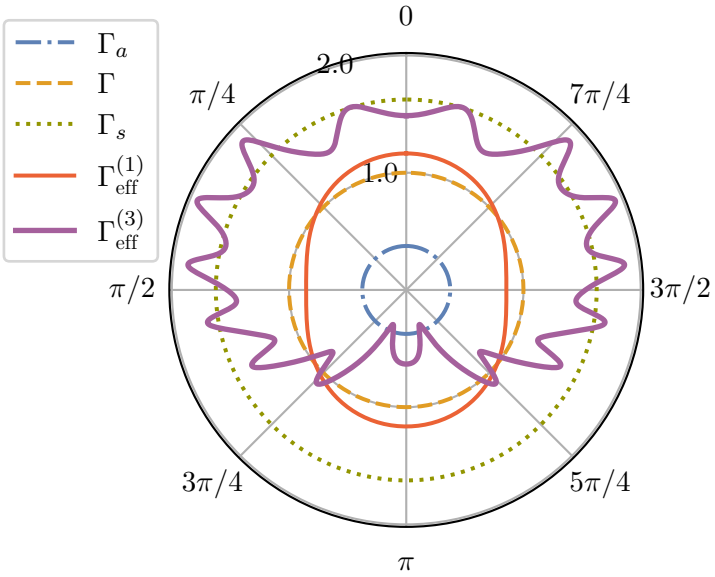

Figure 4.5: Effective decay rates $\Gamma^{(1)}_{\text{eff}}$ and $\Gamma^{(3)}_{\text{eff}}$ of the first- and third-order photon correlation functions. As a reference, we plot again the antisymmetric decay rate Γ_a, the unmodified decay rate Γ, and the symmetric decay rate Γ_s. The decay rates are obtained by an exponential fit in the early to intermediate time dynamics $\gamma t \in [0, 0.5]$ and displayed in units of γ.

Whereas the first-order photon correlation function shows almost no spatial modulation of the decay rates, coming solely from the two close-by atoms alone, the third-order photon correlation function displays a variety of different decay rates. Most remarkably, in the case of $G^{(3)}(\boldsymbol{r}_3, t_3)$, we find multiple directions, for which the effective decay rates are larger or smaller than the symmetric or antisymmetric decay rate. The reason for this is that the different modes do not only have different decay rates, but also different frequency shifts leading to oscillations in the interference terms between the different modes. The decay rates are then effectively increased or decreased depending on the initial phase of these oscillations, leading to decay rates that exceed the symmetric or antisymmetric decay rate.

We end this section with two remarks. First, we note that the antisymmetric coefficient c_{Ag} scales linearly with the separation R_{12} of the two close-by atoms in the limit $R_{12} \to 0$. Therefore, with smaller separation, a substantial superposition of all three modes leading to the obtained intricate emission patterns becomes harder to achieve. Second, since the third-order photon correlation measurement is a conditional measurement, the experimental efficiency is limited by selecting photons in particular directions. The goal of the presented investigations is rather to demonstrate how dipole-dipole interactions and entanglement, i.e., quantum correlations can be combined to engineer particular spontaneous emission features. However, we also note that recent experiments showed a realistic implementation of conditional photon measurements [71–73].

4.1.3 Subwavelength imaging

In this subsection, we consider once more the same three-atom system as before. Two atoms are close to each other and interact via dipole-dipole interactions, whereas the remaining atom is located far distant from the other two atoms. In addition, we investigate again the third-order photon correlation function. However, we slightly change our point of view and ask the question whether the third atom can be used as an auxiliary system to extract information about the two-atom subsystem that is otherwise hard to access. In particular, we investigate how the interference between the third atom and the other two atoms can be utilised to determine the subwavelength separation of the close-by atoms.
We start by assuming that all three atoms are located along the x-axis as before. In what follows, we place the detectors perpendicular to the atomic axis at an angle $\varphi_1 = \varphi_2 = \frac{\pi}{2}$, i.e., we project onto the symmetric state. If we additionally assume that the dipole moment $\boldsymbol{d}$ is perpendicular to the detection plane, the third-order photon correlation function reduces to

$$G^{(3)}(\boldsymbol{r}_3, t_3) \propto \Bigg[|c_{Ge}|^2 e^{-2\gamma t_3} + 2|c_{Sg}|^2 e^{-2(\gamma+\Delta\gamma)t_3} \cos^2\left(\frac{\delta_{2,3}}{2}\right) + 2\sqrt{2}|c_{Sg}||c_{Ge}| e^{-(2\gamma+\Delta\gamma)t_3} \cos\left(\frac{\delta_{2,3}}{2}\right) \cos\left(\varphi_{Sg} + \frac{\delta_{2,3}}{2} - \delta_{3,3} + \Delta\Omega\, t_3\right)\Bigg] . \quad (4.14)$$

As we can see, the third-order photon correlation function depends crucially on the two coupling parameters $\Delta\gamma$ and $\Delta\Omega$. Further, as we already know from Eqs. (2.47) and (2.48) and from Fig. 2.1, the two parameters $\Delta\gamma$ and $\Delta\Omega$ vary quite strongly as a function of the separation between the two atoms. In particular, the coherent coupling parameter $\Delta\Omega$ depends drastically on the separation in the regime $R_{12} \ll \lambda$. Because of this sensitivity, we can deduce the distance of the subwavelength separated atoms if we can accurately determine $\Delta\Omega$. Therefore, let us simplify the expression for the third-order photon correlation function even further by placing also the third detector perpendicular to the atomic chain at an angle $\varphi_3 = \frac{\pi}{2}$. The correlation function now reads

$$G^{(3)}(t_3) \propto 4e^{-2\gamma t_3} + 16e^{-2(\gamma+\Delta\gamma)t_3} + 16e^{-(2\gamma+\Delta\gamma)t_3} \cos\left(\Delta\Omega\, t_3\right) . \quad (4.15)$$

We find that the correlation function decays exponentially with different rates and oscillates in time with the coherent coupling parameter $\Delta\Omega$. Thus, measuring the third-order photon correlation function as a function of time and determining the frequency of the oscillation via a Fourier transform allows us to deduce the coherent coupling parameter and consequently the separation of the close-by atoms. This is illustrated in Fig. 4.6. As can be seen, a peak at the position of the modulus of the coherent coupling parameter can be clearly identified. In addition, from the full width at half maximum (FWHM), we can also define an uncertainty for this determination process. However, note that we plot the analytical Fourier transform

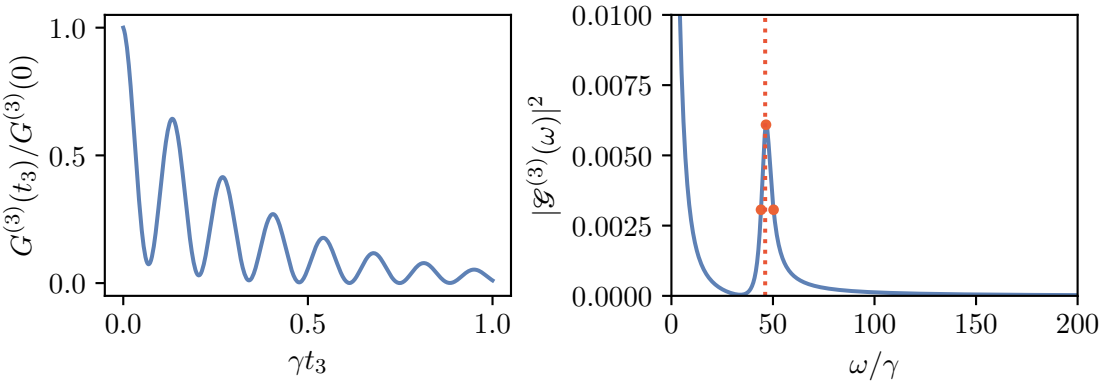

Figure 4.6: The left plot shows $G^{(3)}(t_3)$, normalised to its initial value, as a function of time γt_3 and for a separation of $R_{12}/\lambda = 1/20$. The correlation function decays in an oscillatory manner according to Eq. (4.15). On the right, the modulus square of the Fourier transform $|\mathcal{G}^{(3)}(\omega)|^2$ of the third-order photon correlation function is shown. By determining the slightly shifted position of the peak, the frequency $\Delta\Omega$ of the oscillation can be found. Here, the red dashed line corresponds to the correct value of the modulus of $\Delta\Omega$ and the orange dots mark the position of the peak maximum and the full width at half maximum of the peak.

of the normalised expression of Eq. (4.15), which requires knowledge about the separation of the close-by atoms beforehand. Furthermore, in experiment noise is unavoidable. Therefore, we additionally analyse noisy $G^{(3)}$ signals. In this case, we perform a numerical Fourier transform and determine the frequency via a fit of the analytical expression. This can be seen in Fig. 4.7 for the same separation of the first two atoms as in Fig. 4.6. Thereby, the noise is chosen from a uniform distribution with values of at maximum $\pm 10\%$ of the highest value of $G^{(3)}$. We see that the additional noise does not harm the determination of the coherent coupling parameter.

Now, from Eq. (2.47), we can derive the separation R_{12}/λ and analyse the accuracy of the presented procedure. In Fig. 4.8, we plot the reconstructed separations $R_{12}^{(\mathrm{rec})}/\lambda$ against the correct separations R_{12}/λ. The shaded area gives the uncertainty of the method. We want to emphasise two main points here. First, with the presented method, we obtain values for the reconstructed separations, which are in excellent agreement with the correct separations and second, what is most remarkable, the accuracy of the method increases with decreasing separation of the atoms. That is, it becomes better the smaller the distance of the close-by atoms is. This unintuitive result is based on the functional behaviour of $\Delta\Omega$, which scales as R_{12}^{-3} in the limit $R_{12} \to 0$ and is therefore, in this limit, particularly sensitive to changes in the separation. Finally, by comparing the results obtained from the noisy $G^{(3)}$ function to the noiseless results, we conclude that the method is essentially unaffected by the noise.

Let us now discuss the experimental feasibility and the underlying concept in more detail. As already mentioned in the previous subsection, a $G^{(3)}$ measurement is a conditional mea-

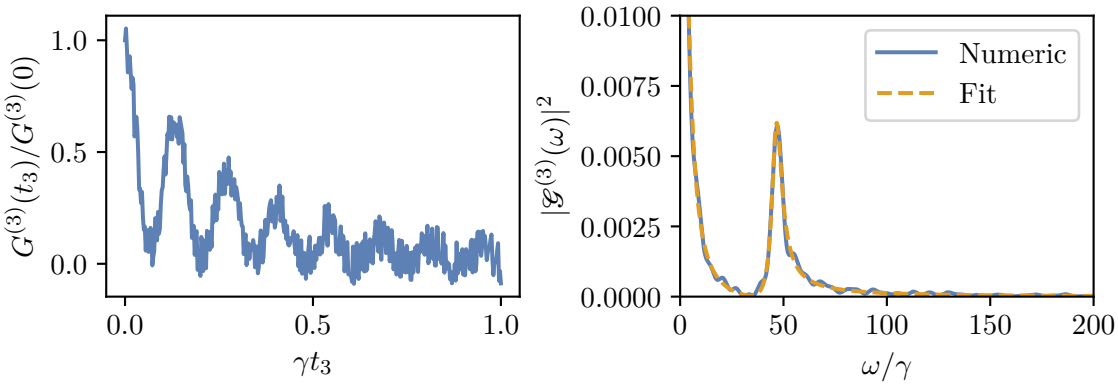

Figure 4.7: The left plot shows the noisy $G^{(3)}(t_3)$ function for a separation of $R_{12}/\lambda = 1/20$ normalised to its initial value. The right plot displays the modulus square of the numerical Fourier transform (blue solid line) as well as a fit of the analytical expression (orange dashed line). We determine the frequency by the peak position and the uncertainty by the FWHM of the peak.

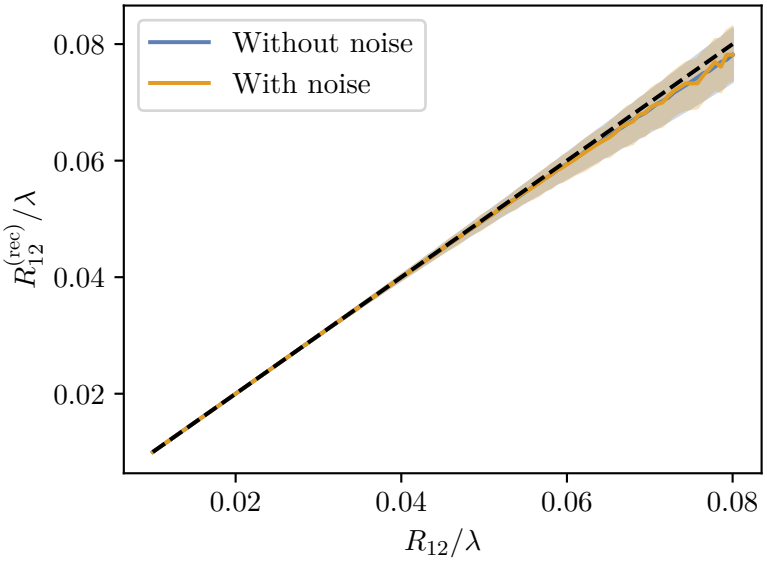

Figure 4.8: Reconstructed separations $R_{12}^{(\mathrm{rec})}/\lambda$ against the correct separations R_{12}/λ. By comparing the reconstructed separations with the black dashed reference curve, representing the identity, we find that the reconstructed separations are in excellent agreement with the correct separations. Furthermore, we highlight that the uncertainty of the obtained values (shaded area) reduces with decreasing distance of the two atoms. Moreover, by comparing the results obtained from the analytical noiseless Fourier transform with the ones obtained from the numerical noisy one, we can conclude that the presented method is essentially unaffected by the noise for realistic experimental noise levels.

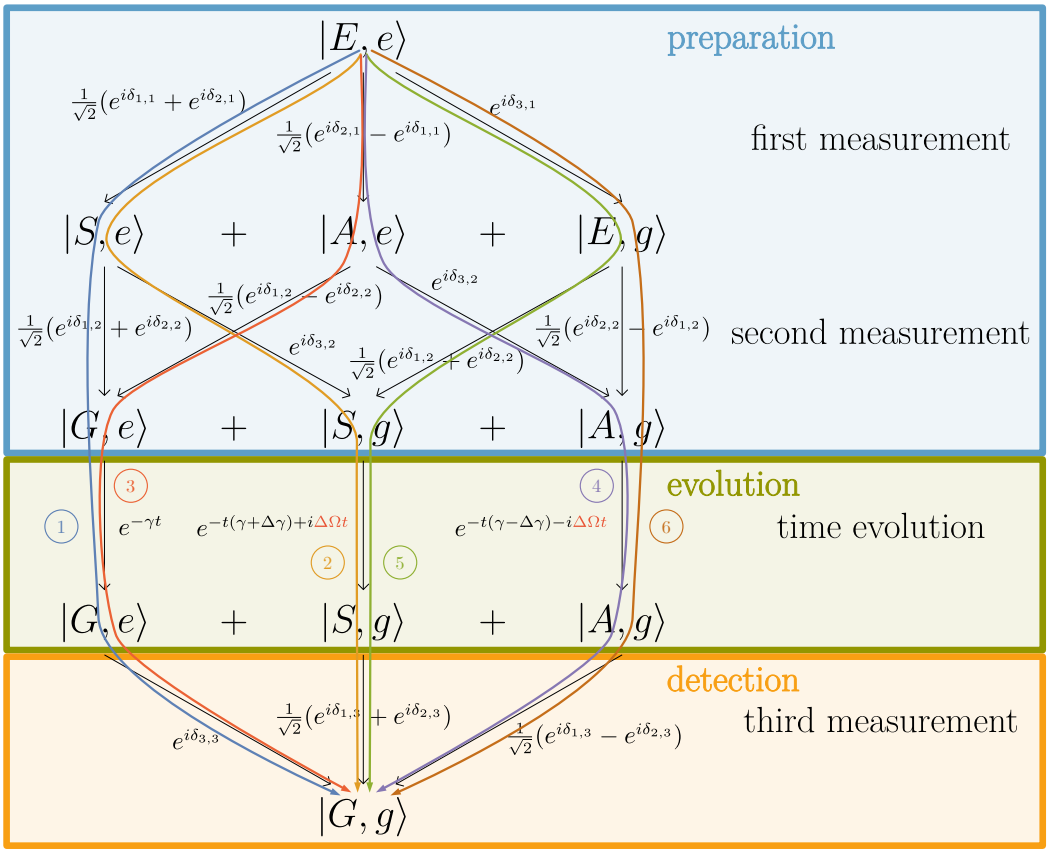

Figure 4.9: Working principle of the conditional $G^{(3)}(\boldsymbol{r}_1, 0; \boldsymbol{r}_2, 0; \boldsymbol{r}_3, t_3)$ measurement. We separate the measurement into three steps. The first two photon measurements at time $t = 0$ are used to prepare an entangled state (blue preparation step, see Appendix D). After the first two photon measurements, the state evolves in time (green evolution step) before the final third photon measurement at a time t_3 is performed (orange detection step). Thereby, the factors along the black arrows give the effect on the corresponding states, the action on the right describes. In total, we get six different quantum paths (coloured paths), where for each path the factors encountered along the path need to be multiplied to find the final prefactor of the state.

surement, which limits the experimental efficiency. This raises the question of whether a $G^{(3)}$ measurement is the only possible measurement or whether a $G^{(2)}$ measurement could also be carried out. Of course, a $G^{(2)}$ measurement is also a conditional measurement and thus comes with a similar drawback of a limited efficiency. However, here, the selection depends on only one photon instead of two photons. If a $G^{(2)}$ measurement is sufficient, a follow up question pops up, namely whether the third atom is actually necessary for the determination process. To answer both questions, we explain the general working principle in more detail based on Fig. 4.9. We separate the $G^{(3)}(\boldsymbol{r}_1, 0; \boldsymbol{r}_2, 0; \boldsymbol{r}_3, t_3)$ measurement into three steps, a preparation step (blue), an evolution step (green), and a detection step (orange). The preparation is done by the first two measurements. Here, an entangled state is created (see Appendix D), which

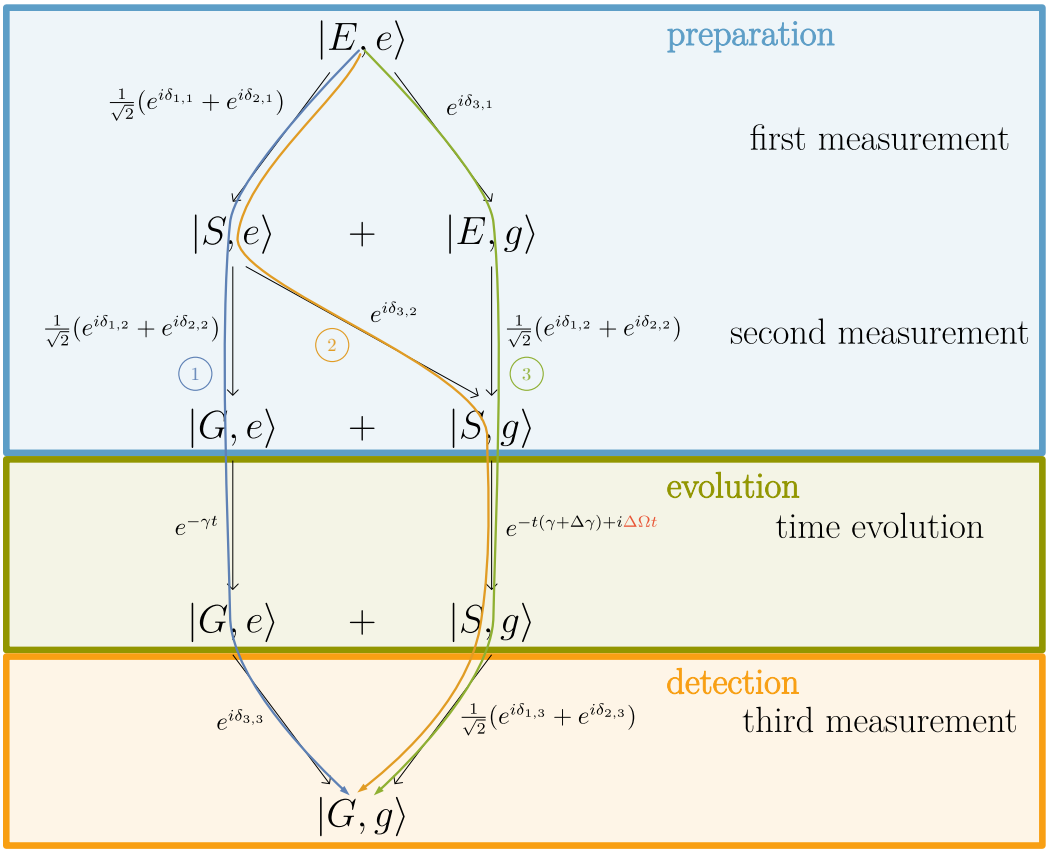

Figure 4.10: Working principle of the conditional $G^{(3)}(\boldsymbol{r}_1,0;\boldsymbol{r}_2,0;\boldsymbol{r}_3,t_3)$ measurement if the antisymmetric state is projected out by the first two photon measurements. The description is analogous to that of Fig. 4.9.

afterwards leads to quantum interferences. During the evolution step, the state evolves in time up to a final time t_3, at which the last photon measurement is performed. In total, we obtain six different quantum paths (coloured paths), which interfere with each other, since all paths lead to the same final state, the complete ground state $|G,g\rangle$. Thereby, the prefactor accumulated along a path is the product of all the factors along the black arrows encountered along the path. In terms of the six paths, the third-order photon correlation function can be calculated symbolically as

$$G^{(3)}(\boldsymbol{r}_1,0;\boldsymbol{r}_2,0;\boldsymbol{r}_3,t_3) = \left|\textcircled{1}+\textcircled{2}+\textcircled{3}+\textcircled{4}+\textcircled{5}+\textcircled{6}\right|^2 \tag{4.16}$$

leading to the general expression of Eq. (4.10). We find three different terms that depend on the coherent coupling parameter $\Delta\Omega$. Thereby, the dependence comes originally from the phase $\Delta\Omega t$ highlighted in Fig. 4.9. The interference term of the paths coming from $|S,g\rangle$ and $|A,g\rangle$ oscillates with $2\Delta\Omega$, whereas the interference terms of the paths coming from $|G,e\rangle$ and $|S,g\rangle$, or from $|G,e\rangle$ and $|A,g\rangle$ oscillate with $\Delta\Omega$ (differences of the different phases).

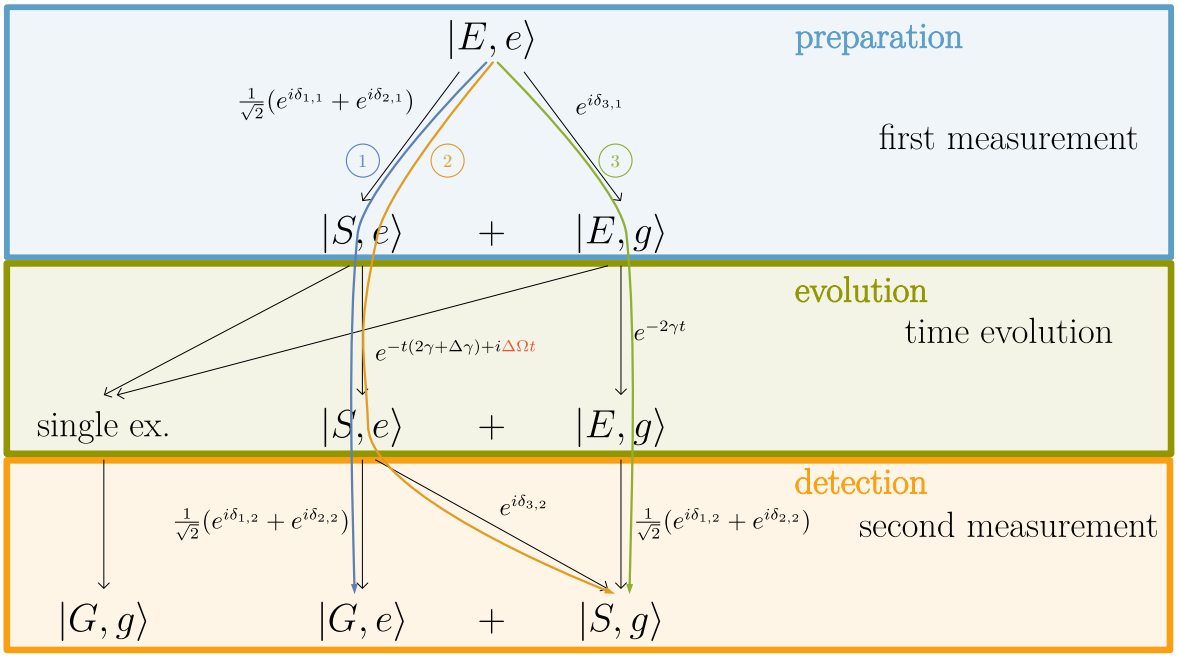

Figure 4.11: Working principle of the conditional $G^{(2)}(\boldsymbol{r}_1,0;\boldsymbol{r}_2,t_2)$ measurement if the antisymmetric state is projected out by the first photon measurement. We split the measurement into the same three steps (preparation, evolution, detection) as before. However, now the preparation only includes the first measurement. Afterwards, we evolve the states in time until the second (final) measurement is performed at a time t_2. We note that the time evolution of the doubly-excited states $|S,e\rangle$ and $|E,g\rangle$ leads additionally to the population of singly-excited states, which also contribute to the $G^{(2)}$ measurement. However, in the figure, we neglect writing all factors explicitly since the contribution from the singly-excited states is irrelevant for the working principle.

If we project out the antisymmetric state, as done in this subsection, the general scheme of Fig. 4.9 reduces to the scheme shown in Fig. 4.10. Three quantum paths remain, which interfere with each other. Thereby, the interference term of the paths coming from the states $|G,e\rangle$ and $|S,g\rangle$ oscillates with $\Delta\Omega$ [last term in Eq. (4.14)]. With this understanding, we are able to decide whether a $G^{(2)}$ measurement is already sufficient or not. The working principle for a $G^{(2)}$ measurement, with the antisymmetric state already projected out, is shown in Fig. 4.11. We see that the two paths (2) and (3) lead to the same final state $|S,g\rangle$ and thus interfere with each other. Since the two states $|S,e\rangle$ and $|E,g\rangle$ evolve with a relative phase of $\Delta\Omega t$ (see Fig. 4.11), the interference term oscillates with a frequency given by $\Delta\Omega$. Mathematically, the contribution coming from the doubly-excited states reads

$$2e^{-2t_2(2\gamma+\Delta\gamma)}\left[2+e^{2t_2\Delta\gamma}+\cos\delta_{2,2}+2e^{t_2\Delta\gamma}\cos\left(\frac{\delta_{2,2}}{2}\right)\cos\left(t_2\Delta\Omega-\frac{\delta_{2,2}}{2}+\delta_{3,2}\right)\right], \quad (4.17)$$

where the interference term of the states $|S,e\rangle$ and $|E,g\rangle$ oscillates with $\Delta\Omega$. As in the case of $G^{(3)}$, this oscillation can be used to determine the distance between the close-by atoms.

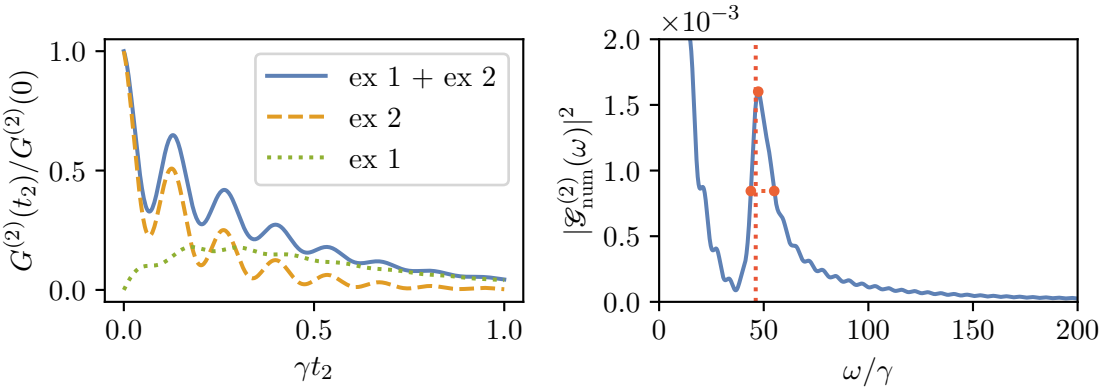

Figure 4.12: Left: $G^{(2)}(t_2)$, normalised to its initial value, for a separation of the close-by atoms of $\lambda/20$ as a function of γt_2. The blue solid curve shows the total second-order photon correlation function, which is the sum of the two contributions coming from the doubly-excited states [see Eq. (4.17)] (dashed orange curve) and singly-excited states (dotted green curve). The oscillation with frequency $\Delta\Omega$ is clearly visible. Right: Absolute value squared of the numeric Fourier transform of the normalised $G^{(2)}(t_2)$. A peak at the coherent coupling parameter can be identified, from which the separation of the two close-by atoms can be inferred.

We note, however, that one gets an additional contribution coming from the singly-excited states. This contribution can be evaluated analytically, but since the expression is quite lengthy, we do not state it explicitly. Rather, we plot both contributions together with the total second-order photon correlation function in Fig. 4.12. In the time domain (left panel), an oscillation of the correlation function with frequency corresponding to the peak at the coherent coupling parameter in the frequency domain (right panel) is clearly visible.

Before we come to the question whether the third atom is necessary for the determination process, we compare the results from the third-order photon correlation function to the ones from the above evaluated second-order photon correlation function. We find that the additional contributions to $G^{(2)}(t_2)$ coming from the singly-excited states are not in phase with the oscillation of the doubly-excited contributions. Furthermore, the interference amplitude in the case of $G^{(2)}(t_2)$ is smaller than the one in the case of $G^{(3)}(t_3)$. This leads to the fact that, in the case of $G^{(2)}(t_2)$, the peak in the Fourier transform is smaller and wider, which would favour to use $G^{(3)}(t_3)$ in this regard (see Fig. 4.13). However, a measurement of $G^{(3)}(t_3)$ comes with a highly reduced signal strength, since three photons have to be measured conditionally. Therefore, for the practical implementation, a measurement of the second-order photon correlation function is still favourable, even though the signal is not as clean as the one of the third-order photon correlation function.

Finally, the remaining question is whether $G^{(2)}(t_2)$ of only two atoms is already sufficient to determine the distance between the two atoms via the coherent coupling parameter. In this case, the first photon measurement only populates the states $|S\rangle$ and $|A\rangle$, which would

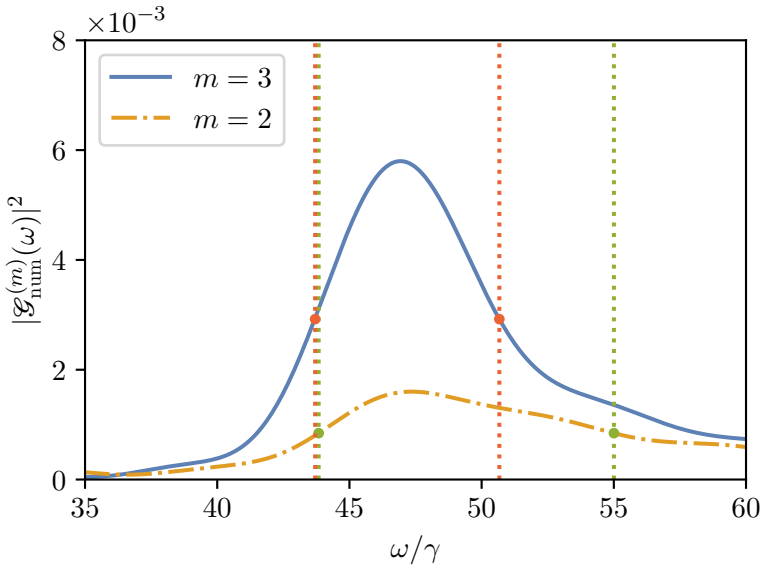

Figure 4.13: Absolute values squared of the numeric FTs of the normalised $G^{(2)}(t_2)$ and $G^{(3)}(t_3)$ functions. We find that, in the case of the third-order photon correlation function, the peak is higher and its FWHM is smaller compared to the one of the second-order photon correlation function. Theoretically, this would favour to use $G^{(3)}(t_3)$ instead of $G^{(2)}(t_2)$.

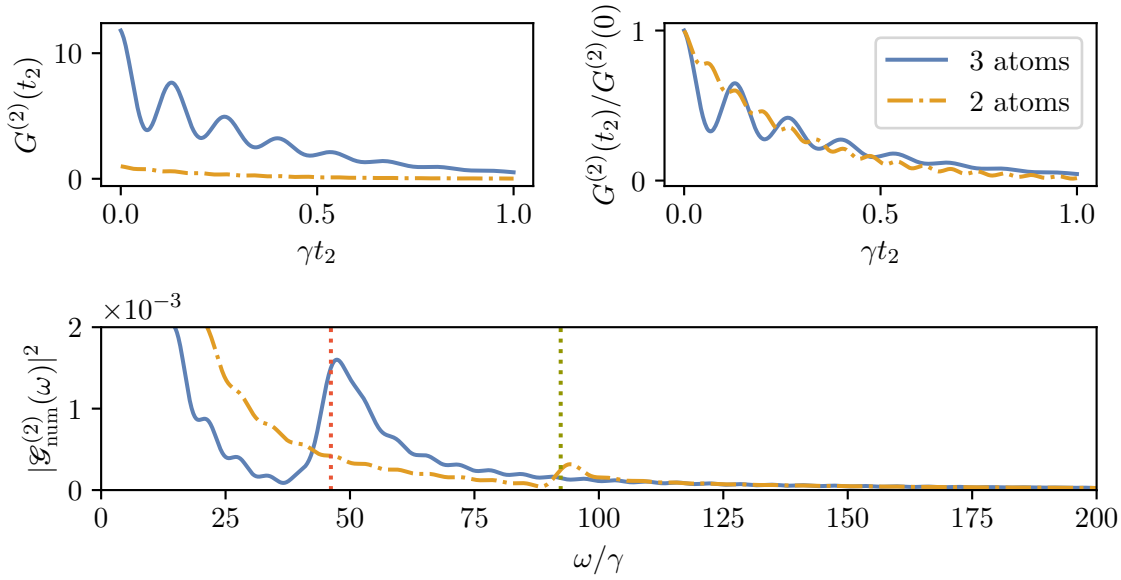

Figure 4.14: Top: $G^{(2)}(t_2)$ for a separation of the close-by atoms of $\lambda/20$ as a function of γt_2. The blue solid line shows the correlation function for the three-atom system, whereas the orange dash-dotted line corresponds to the two-atom case. As can be seen, the correlation function for only two atoms suffers from a total reduced signal strength and a small amplitude of the oscillation (see normalised $G^{(2)}$ plot on the right). Bottom: Absolute values squared of the numeric FTs of the normalised $G^{(2)}$ signals. In theory, for a separation of $\lambda/20$, a slightly shifted peak compared to $2\Delta\Omega$ is still identifiable in the two-atom case.

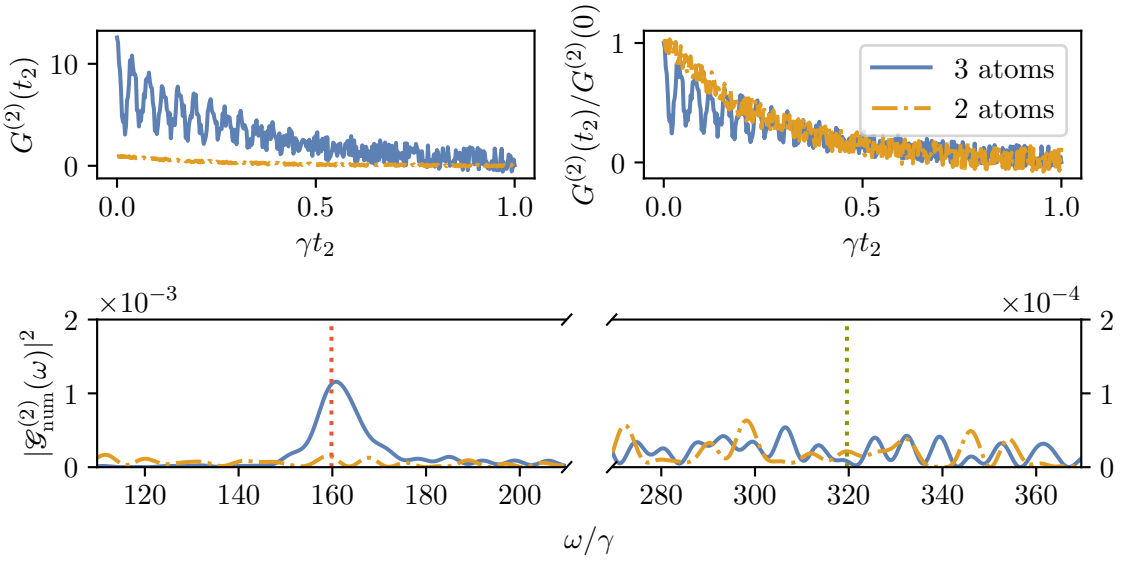

Figure 4.15: Top: Noisy $G^{(2)}(t_2)$ for a separation of the close-by atoms of $\lambda/30$ as a function of γt_2. The blue solid line shows the correlation function for the three-atom system, whereas the orange dash-dotted line corresponds to the two-atom case. Bottom: Absolute values squared of the numeric FTs of the normalised noisy $G^{(2)}$ signals. In the case of our three-atom system, the numeric FT still shows a clear peak around $\Delta\Omega$, whereas in the case of only two atoms, the peak gets lost in the noise.

correspond to the states $|S, g\rangle$ and $|A, g\rangle$ in Fig. 4.9. The subsequent time evolution and final detection is then the same. Therefore, we find an interference term of the two quantum paths, which oscillates with a frequency $2\Delta\Omega$. However, if the separation between the atoms becomes very close, the antisymmetric state is almost unpopulated, which suppresses the interference term in this case. In contrast, in the case of three atoms, the schemes use interferences of combined states of the symmetric state of the first two atoms and the excited or ground state of the third atom, which can be sufficiently populated. Further, the total signal strength of the two-atom setup is reduced compared to the one of the three-atom setup. This is shown in the top plots of Fig. 4.14. In theory, for the shown separation of $R_{12} = \lambda/20$ and a perfect signal, one can, in principle, still determine the coherent coupling parameter, illustrated in the bottom plot of Fig. 4.14. But, we note that the peak is slightly shifted in comparison to the true value of $2\Delta\Omega$ due to interference terms in the square of the absolute value of the numeric FT. Beyond that, if we go to even smaller separations and add noise, which is unavoidable in a real experiment, it is practically impossible to determine the separation of the atoms via the oscillation of the second-order photon correlation function (see Fig. 4.15).

To end this subsection, we want to do a final remark. We note that investigations of using the coherent coupling parameter for the determination of the separation of two close-by atoms have already been carried out [74, 75]. However, while in Refs. [74, 75] the coherent coupling

parameter was extracted by additionally driving the two atoms in a standing wave laser field, here, we extract the coherent coupling parameter by exploiting measurement-induced atomic correlations to an additional third non-interacting remote atom. In this regard, we developed a remote sensing scheme that can be used for more general sensing tasks, as will be shown in the next section.

4.2 Spatio-temporal correlations of three four-level atoms

In this section, we consider the same three-atom system as before, i.e., two atoms are close to each other, whereas the third atom is far away. However, we extend the single-atom level scheme from two levels to *four* levels. First, we give a short description of the concrete three-four-level-atom system. Thereby, we start by introducing a single four-level atom. Afterwards, we investigate the coupled two-atom subsystem and finally we translate the notions to the full three-atom system. After the introduction of the system, we then study once more the third-order photon correlation function and show how it can be used to perform an atomic quantum state reconstruction.

4.2.1 Description of a single four-level atom

The level structure of the atoms shall consist of three excited $J = 1$ states $|m\rangle \coloneqq |1, m\rangle$ with $m \in \{-1, 0, 1\}$ and one ground state $|g\rangle \coloneqq |0, 0\rangle$ ($J = 0$). Here, J denotes the total angular momentum quantum number. Every transition between the ground state and the excited states shall be dipole-allowed with dipole transition matrix element $\boldsymbol{d}_m \coloneqq \langle m|\hat{\boldsymbol{d}}|g\rangle$, where $\hat{\boldsymbol{d}}$ denotes the dipole operator. By use of the Wigner-Eckart theorem (see Appendix E for the application to the dipole operator), one can find that $\boldsymbol{d}_m = \langle m|\hat{d}_m|g\rangle\, \hat{\boldsymbol{\varepsilon}}_m^*$ with the so-called spherical components $\hat{d}_m$ and the polarisation vectors

$$\hat{\boldsymbol{\varepsilon}}_{\pm 1} = \hat{\boldsymbol{\varepsilon}}_{\pm} = \mp\frac{1}{\sqrt{2}}(\hat{\boldsymbol{e}}_x \pm i\hat{\boldsymbol{e}}_y)\,, \qquad \hat{\boldsymbol{\varepsilon}}_0 = \hat{\boldsymbol{e}}_z\,. \tag{4.18}$$

Thus, all three dipole moments are mutually orthogonal, i.e., $\boldsymbol{d}_m^* \boldsymbol{d}_{m'} = \delta_{m,m'}|\boldsymbol{d}_m|^2$.
In the following, we assume that the states $|m\rangle$ are degenerate, i.e., they should have the same energy eigenvalues. Further, we choose the zero energy to be in mid between the excited state energy and the ground state energy, such that the excited state energy reads $\hbar\omega_0/2$ and the ground state energy is $-\hbar\omega_0/2$. The single-atom Hamilton operator is then given by

$$\hat{H}_A = -\frac{\hbar\omega_0}{2}\,|g\rangle\langle g| + \frac{\hbar\omega_0}{2}\,(|-1\rangle\langle -1| + |0\rangle\langle 0| + |1\rangle\langle 1|)\,. \tag{4.19}$$

In addition, the three raising operators connecting the ground state with the excited states can be written as

$$\hat{S}_{-1+} = |-1\rangle\langle g| \,, \qquad \hat{S}_{0+} = |0\rangle\langle g| \,, \qquad \hat{S}_{1+} = |1\rangle\langle g| \,. \tag{4.20}$$

4.2.2 Two four-level atom dynamics

In the following, we investigate the dynamics of two such four-level atoms coupled via the vacuum of the electromagnetic field. Starting from the single-atom operators defined in Eqs. (4.19) and (4.20), the operators for multiple atoms can be obtained by simple tensor product extensions. In terms of the general expressions introduced in Chapter 2, we have the case $N = 2$ and $D = 3$. From Eqs. (2.47) and (2.48), we find that the coupling parameters crucially depend on the orientation of the dipole moments with respect to the separation vector of the atoms. Wlog we assume that the dipole moment $\boldsymbol{d}_0 \in \mathbb{R}^3$ is parallel to the separation vector $\boldsymbol{R}_{12}$. Note that this assumption is simply a definition of the quantisation axis (z-axis). Then, the dipole moments $\boldsymbol{d}_{-1}$ and $\boldsymbol{d}_1$ are perpendicular to $\boldsymbol{R}_{12}$ (see the previous subsection). From Eqs. (2.47) and (2.48), we conclude that

$$\Omega_{mn}^{\mu\nu} = 0 \qquad \text{and} \qquad \Gamma_{mn}^{\mu\nu} = 0 \qquad \forall m \neq n \,. \tag{4.21}$$

Therefore, we only have

$$\Omega_0 \coloneqq \Omega_{00}^{12} = \Omega_{00}^{21} \,, \qquad \Omega_{-1} \coloneqq \Omega_{-1-1}^{12} = \Omega_{-1-1}^{21} \,, \qquad \Omega_1 \coloneqq \Omega_{11}^{12} = \Omega_{11}^{21} \,, \tag{4.22}$$

$$\Gamma_0 \coloneqq \Gamma_{00}^{12} = \Gamma_{00}^{21} \,, \qquad \Gamma_{-1} \coloneqq \Gamma_{-1-1}^{12} = \Gamma_{-1-1}^{21} \,, \qquad \Gamma_1 \coloneqq \Gamma_{11}^{12} = \Gamma_{11}^{21} \,. \tag{4.23}$$

Further, we assume the dipole moments to be of similar strength, i.e., $|\boldsymbol{d}_m| \approx |\boldsymbol{d}_n| \; \forall m \neq n$. We then define

$$\Omega_\perp \coloneqq \Omega_{-1} \approx \Omega_1 \,, \qquad \Omega_\parallel \coloneqq \Omega_0 \,, \tag{4.24}$$

$$\Gamma_\perp \coloneqq \Gamma_{-1} \approx \Gamma_1 \,, \qquad \Gamma_\parallel \coloneqq \Gamma_0 \,. \tag{4.25}$$

In addition, we have $\gamma_{-1} \approx \gamma_0 \approx \gamma_1 =: \gamma$. Considering the general master equation Eq. (2.74), it is useful to study the total Hamilton operator $\hat{H} = \hat{H}_A + \hat{H}_\Omega$. The diagonalisation of this Hamilton operator leads to a convenient basis for the description of the system. The energies and corresponding energy eigenstates are ($\hbar = 1$)

$$-\omega_0 : |G\rangle \coloneqq |g, g\rangle \,, \tag{4.26}$$

$$\omega_0 : |-1,-1\rangle \,, |-1,0\rangle \,, |-1,1\rangle \,, |0,-1\rangle \,, |0,0\rangle \,, |0,1\rangle \,, |1,-1\rangle \,, |1,0\rangle \,, |1,1\rangle \,, \tag{4.27}$$

$$-\Omega_\parallel : |S_0\rangle \coloneqq \frac{1}{\sqrt{2}}(|g,0\rangle + |0,g\rangle) \,, \tag{4.28}$$

$$\Omega_{\parallel} : |A_0\rangle \coloneqq \frac{1}{\sqrt{2}}(|g,0\rangle - |0,g\rangle)\,, \tag{4.29}$$

$$-\Omega_{\perp} : |S_{-1}\rangle \coloneqq \frac{1}{\sqrt{2}}(|g,-1\rangle + |-1,g\rangle), |S_1\rangle \coloneqq \frac{1}{\sqrt{2}}(|g,1\rangle + |1,g\rangle)\,, \tag{4.30}$$

$$\Omega_{\perp} : |A_{-1}\rangle \coloneqq \frac{1}{\sqrt{2}}(|g,-1\rangle - |-1,g\rangle), |A_1\rangle \coloneqq \frac{1}{\sqrt{2}}(|g,1\rangle - |1,g\rangle)\,. \tag{4.31}$$

Now, we investigate the dissipative part of the master equation. The dissipator matrix can be written as

$$\begin{array}{cc} & \begin{array}{cccccc} n=-1 & & n=0 & & n=1 & \\ \nu=1 & \nu=2 & \nu=1 & \nu=2 & \nu=1 & \nu=2 \end{array} \\ \begin{array}{c} m=-1 \\ \\ m=0 \\ \\ m=1 \end{array} & \begin{array}{c} \mu=1 \\ \mu=2 \\ \mu=1 \\ \mu=2 \\ \mu=1 \\ \mu=2 \end{array} \begin{pmatrix} \gamma & \Gamma_{\perp} & 0 & 0 & 0 & 0 \\ \Gamma_{\perp} & \gamma & 0 & 0 & 0 & 0 \\ 0 & 0 & \gamma & \Gamma_{\parallel} & 0 & 0 \\ 0 & 0 & \Gamma_{\parallel} & \gamma & 0 & 0 \\ 0 & 0 & 0 & 0 & \gamma & \Gamma_{\perp} \\ 0 & 0 & 0 & 0 & \Gamma_{\perp} & \gamma \end{pmatrix} \end{array} =: Y\,. \tag{4.32}$$

The diagonalisation of Y reveals the different decay channels. We define the operators $\hat{S}_{h;l} \coloneqq |h\rangle\langle l|$ with h, l being the above written energy eigenstates of $\hat{H}$. The different decay channels can then be characterised by the decay rate and the corresponding Lindblad operator $\hat{L}$ expressed in terms of the operators $\hat{S}_{h;l}$. Explicitly writing down the different decay channels reads

"0" :

$$\begin{aligned} \gamma - \Gamma_{\parallel} : \hat{L}_{\gamma-\Gamma_{\parallel}} = \hat{S}_{G;A_0} - \hat{S}_{A_0;0,0} &+ \frac{1}{2}(\hat{S}_{S_1;1,0} + \hat{S}_{S_{-1};-1,0} - \hat{S}_{S_1;0,1} - \hat{S}_{S_{-1};0,-1} \\ &- \hat{S}_{A_{-1};0,-1} - \hat{S}_{A_{-1};-1,0} - \hat{S}_{A_1;0,1} - \hat{S}_{A_1;1,0}) \end{aligned} \tag{4.33}$$

$$\begin{aligned} \gamma + \Gamma_{\parallel} : \hat{L}_{\gamma+\Gamma_{\parallel}} = \hat{S}_{G;S_0} + \hat{S}_{S_0;0,0} &+ \frac{1}{2}(\hat{S}_{S_1;0,1} + \hat{S}_{S_1;1,0} + \hat{S}_{S_{-1};0,-1} + \hat{S}_{S_{-1};-1,0} \\ &+ \hat{S}_{A_{-1};0,-1} - \hat{S}_{A_{-1};-1,0} + \hat{S}_{A_1;0,1} - \hat{S}_{A_1;1,0}) \end{aligned} \tag{4.34}$$

" -1" :

$$\begin{aligned} \gamma - \Gamma_{\perp} : \hat{L}_{\gamma-\Gamma_{\perp},-1} = \hat{S}_{G;A_{-1}} - \hat{S}_{A_{-1};-1,-1} &+ \frac{1}{2}(\hat{S}_{S_0;0,-1} + \hat{S}_{S_1;1,-1} - \hat{S}_{S_0;-1,0} - \hat{S}_{S_1;-1,1} \\ &- \hat{S}_{A_0;0,-1} - \hat{S}_{A_0;-1,0} - \hat{S}_{A_1;1,-1} - \hat{S}_{A_1;-1,1}) \end{aligned} \tag{4.35}$$

$$\begin{aligned} \gamma + \Gamma_{\perp} : \hat{L}_{\gamma+\Gamma_{\perp},-1} = \hat{S}_{G;S_{-1}} + \hat{S}_{S_{-1};-1,-1} &+ \frac{1}{2}(\hat{S}_{S_1;-1,1} + \hat{S}_{S_1;1,-1} + \hat{S}_{S_0;0,-1} + \hat{S}_{S_0;-1,0} \\ &+ \hat{S}_{A_0;-1,0} - \hat{S}_{A_0;0,-1} + \hat{S}_{A_1;-1,1} - \hat{S}_{A_1;1,-1}) \end{aligned} \tag{4.36}$$

"1" :

$$\begin{aligned} \gamma - \Gamma_{\perp} : \hat{L}_{\gamma-\Gamma_{\perp},1} = \hat{S}_{G;A_1} - \hat{S}_{A_1;1,1} &+ \frac{1}{2}(\hat{S}_{S_0;0,1} + \hat{S}_{S_{-1};-1,1} - \hat{S}_{S_0;1,0} - \hat{S}_{S_{-1};1,-1} \\ &- \hat{S}_{A_0;0,1} - \hat{S}_{A_0;1,0} - \hat{S}_{A_{-1};-1,1} - \hat{S}_{A_{-1};1,-1}) \end{aligned} \tag{4.37}$$

$$\gamma+\Gamma_\perp:\hat{L}_{\gamma+\Gamma_\perp,1}=\hat{S}_{G;S_1}+\hat{S}_{S_1;1,1} \qquad +\frac{1}{2}(\hat{S}_{S_0;0,1}+\hat{S}_{S_0;1,0}+\hat{S}_{S_{-1};-1,1}+\hat{S}_{S_{-1};1,-1} \\ +\hat{S}_{A_0;1,0}-\hat{S}_{A_0;0,1}+\hat{S}_{A_{-1};1,-1}-\hat{S}_{A_{-1};-1,1})\,. \tag{4.38}$$

We note that having the two-level case in mind and considering the possible decay paths, the different contributions of the operators $\hat{S}_{h;l}$ and their corresponding weightings to the Lindblad operators are quite intuitive. With this at hand, we can now discuss the three-atom case.

4.2.3 Three four-level atoms - Excited state determination

In the following, we investigate the situation of three four-level atoms, where the first two atoms are close to each other, such that their dynamics can be described by the formalism of the previous subsection, whereas the third atom shall be far distant. This means that

$$\Gamma_{mn}^{13}=\Gamma_{mn}^{31}=\Gamma_{mn}^{23}=\Gamma_{mn}^{32}=0\,, \qquad \Omega_{mn}^{13}=\Omega_{mn}^{31}=\Omega_{mn}^{23}=\Omega_{mn}^{32}=0 \tag{4.39}$$

with $m,n\in\{-1,0,1\}$, such that the dynamics of the third atom can be treated separately from the two-atom dynamics. Thus, the third atom simply decays independently of the other two atoms with half-decay rate γ. In what follows, we assume that the three atoms are all initially excited. Since the remote atom is meant to be controlled, the state of the third atom shall be known. Our aim is then to determine the state of the close-by atoms by using the interference of the emission paths of the combined three-atom system in terms of a third-order photon correlation measurement. To shorten the notation, we define

$$\boldsymbol{\beta}_{m,n}\coloneqq-\frac{k_0^2}{4\pi\varepsilon_0 r_m}\left[\hat{\boldsymbol{r}}_m\times(\hat{\boldsymbol{r}}_m\times\boldsymbol{d}_n^*)\right]\,. \tag{4.40}$$

Then, the positive electric field operator can be written as

$$\hat{\boldsymbol{E}}_S^{(+)}(\boldsymbol{r}_m,t_m)=\sum_{\mu,n=1}^{3}\boldsymbol{\beta}_{m,n}e^{i\delta_{\mu,m}}\hat{S}_{n-}^{(\mu)}(t_m)\,, \tag{4.41}$$

where $\delta_{\mu,m}$ is defined as before. In a first step, we assume that all three atoms are in a distinct excited state, i.e., the state reads $|h,k,l\rangle$ with $h,k,l\in\{-1,0,1\}$. To calculate the third-order photon correlation function (with $t_1=t_2=0$), we consider the application of $\hat{\boldsymbol{E}}_S^{(+)}(\boldsymbol{r}_2,0)\hat{\boldsymbol{E}}_S^{(+)}(\boldsymbol{r}_1,0)$ onto this state, which gives

$$\begin{aligned}&\hat{\boldsymbol{E}}_S^{(+)}(\boldsymbol{r}_2,0)\hat{\boldsymbol{E}}_S^{(+)}(\boldsymbol{r}_1,0)\,|h,k,l\rangle=c_{Gl}\,|G,l\rangle+c_{gkg}\,|g,k,g\rangle+c_{hgg}\,|h,g,g\rangle\\&=c_{Gl}\,|G,l\rangle+c_{S_kg}\,|S_k,g\rangle+c_{A_kg}\,|A_k,g\rangle+c_{S_hg}\,|S_h,g\rangle+c_{A_hg}\,|A_h,g\rangle\,.\end{aligned} \tag{4.42}$$

Here, the coefficients are defined as follows

$$c_{Gl} \coloneqq \boldsymbol{\beta}_{1,h}\boldsymbol{\beta}_{2,k}e^{i\delta_{1,1}}e^{i\delta_{2,2}} + \boldsymbol{\beta}_{1,k}\boldsymbol{\beta}_{2,h}e^{i\delta_{2,1}}e^{i\delta_{1,2}}\,, \tag{4.43}$$

$$c_{gkg} \coloneqq \boldsymbol{\beta}_{1,h}\boldsymbol{\beta}_{2,l}e^{i\delta_{1,1}}e^{i\delta_{3,2}} + \boldsymbol{\beta}_{1,l}\boldsymbol{\beta}_{2,h}e^{i\delta_{3,1}}e^{i\delta_{1,2}}\,, \tag{4.44}$$

$$c_{hgg} \coloneqq \boldsymbol{\beta}_{1,k}\boldsymbol{\beta}_{2,l}e^{i\delta_{2,1}}e^{i\delta_{3,2}} + \boldsymbol{\beta}_{1,l}\boldsymbol{\beta}_{2,k}e^{i\delta_{3,1}}e^{i\delta_{2,2}}\,, \tag{4.45}$$

$$c_{S_kg} \coloneqq \frac{c_{gkg}}{\sqrt{2}}\,, \quad c_{A_kg} \coloneqq \frac{c_{gkg}}{\sqrt{2}}\,, \tag{4.46}$$

$$c_{S_hg} \coloneqq \frac{c_{hgg}}{\sqrt{2}}\,, \quad c_{A_hg} \coloneqq -\frac{c_{hgg}}{\sqrt{2}}\,. \tag{4.47}$$

Now, let us do the reasonable assumption that the two close-by atoms were equally excited, i.e., they are in the same excited state $|h\rangle = |k\rangle$. The unnormalised post-measurement state of Eq. (4.42) then simplifies to

$$\hat{\boldsymbol{E}}_S^{(+)}(\boldsymbol{r}_2,0)\hat{\boldsymbol{E}}_S^{(+)}(\boldsymbol{r}_1,0)\,|h,h,l\rangle = c_{Gl}\,|G,l\rangle + c_{S_hg}\,|S_h,g\rangle + c_{A_hg}\,|A_h,g\rangle\ , \tag{4.48}$$

where the coefficients are given by

$$c_{Gl} = \boldsymbol{\beta}_{1,h}\boldsymbol{\beta}_{2,h}\left(e^{i(\delta_{1,1}+\delta_{2,2})} + e^{i(\delta_{2,1}+\delta_{1,2})}\right)\,, \tag{4.49}$$

$$c_{S_hg} = \frac{1}{\sqrt{2}}\left[\boldsymbol{\beta}_{1,h}\boldsymbol{\beta}_{2,l}\left(e^{i(\delta_{1,1}+\delta_{3,2})} + e^{i(\delta_{2,1}+\delta_{3,2})}\right) + \boldsymbol{\beta}_{1,l}\boldsymbol{\beta}_{2,h}\left(e^{i(\delta_{3,1}+\delta_{1,2})} + e^{i(\delta_{3,1}+\delta_{2,2})}\right)\right]\,, \tag{4.50}$$

$$c_{A_hg} = \frac{1}{\sqrt{2}}\left[\boldsymbol{\beta}_{1,h}\boldsymbol{\beta}_{2,l}\left(e^{i(\delta_{1,1}+\delta_{3,2})} - e^{i(\delta_{2,1}+\delta_{3,2})}\right) + \boldsymbol{\beta}_{1,l}\boldsymbol{\beta}_{2,h}\left(e^{i(\delta_{3,1}+\delta_{1,2})} - e^{i(\delta_{3,1}+\delta_{2,2})}\right)\right]\,. \tag{4.51}$$

Now, this calculated state above evolves in time. With Section 4.2.2, the evolution of the coefficients can be written as

$$c_{Gl}(t) = c_{Gl}e^{-\gamma t}\,, \tag{4.52}$$

$$c_{S_hg}(t) = c_{S_hg}e^{-(\gamma+\Gamma_h)t+i\Omega_h t}\,, \tag{4.53}$$

$$c_{A_hg}(t) = c_{A_hg}e^{-(\gamma-\Gamma_h)t-i\Omega_h t}\,, \tag{4.54}$$

and the time-evolved unnormalised state reads

$$|\psi(t)\rangle = c_{Gl}(t)\,|G,l\rangle + c_{S_hg}(t)\,|S_h,g\rangle + c_{A_hg}(t)\,|A_h,g\rangle\ . \tag{4.55}$$

We note that in the last equation, we neglected the contribution of the state $|G,g\rangle$, since this state does not contribute to the photon correlation function. Finally, let us calculate the action of the third positive frequency part of the electric field operator at time $t = t_3$, which

gives

$$\begin{aligned}\hat{\boldsymbol{E}}_S^{(+)}(\boldsymbol{r}_3,0)\,|\psi(t_3)\rangle &= \sum_{\mu,n=1}^{3}\boldsymbol{\beta}_{3,n}e^{i\delta_{\mu,3}}\hat{S}_{n-}^{(\mu)}\,|\psi(t_3)\rangle \\ &= \left\{\boldsymbol{\beta}_{3,l}e^{i\delta_{3,3}}c_{Gl}(t_3)+\boldsymbol{\beta}_{3,h}\left[\frac{c_{S_hg}(t_3)}{\sqrt{2}}\left(e^{i\delta_{2,3}}+e^{i\delta_{1,3}}\right)+\frac{c_{A_hg}(t_3)}{\sqrt{2}}\left(e^{i\delta_{2,3}}-e^{i\delta_{1,3}}\right)\right]\right\}|G,g\rangle\,.\end{aligned} \tag{4.56}$$

Thus, the third-order photon correlation function reads

$$\begin{aligned}&G^{(3)}(\boldsymbol{r}_1,0;\boldsymbol{r}_2,0;\boldsymbol{r}_3,t_3)\\ &=\left|\left\{\boldsymbol{\beta}_{3,l}e^{i\delta_{3,3}}c_{Gl}(t_3)+\boldsymbol{\beta}_{3,h}\left[\frac{c_{S_hg}(t_3)}{\sqrt{2}}\left(e^{i\delta_{2,3}}+e^{i\delta_{1,3}}\right)+\frac{c_{A_hg}(t_3)}{\sqrt{2}}\left(e^{i\delta_{2,3}}-e^{i\delta_{1,3}}\right)\right]\right\}\right|^2.\end{aligned} \tag{4.57}$$

Therefore, we have to consider products of the form $\boldsymbol{\beta}_{m,h}^*\boldsymbol{\beta}_{m,l}$. The cross products yield

$$[\boldsymbol{r}_m\times(\boldsymbol{r}_m\times\boldsymbol{d}_h^*)]^*\,[\boldsymbol{r}_m\times(\boldsymbol{r}_m\times\boldsymbol{d}_l^*)]=|\boldsymbol{d}_h|^2r_m^4\delta_{h,l}-r_m^2(\boldsymbol{r}_m\boldsymbol{d}_h)(\boldsymbol{r}_m\boldsymbol{d}_l^*)\,. \tag{4.58}$$

Further, since the polarisation vectors are normalised, $\|\hat{\boldsymbol{\varepsilon}}_q\|=1$, and we assumed $|\boldsymbol{d}_1|\approx|\boldsymbol{d}_0|\approx|\boldsymbol{d}_{-1}|$, we find that

$$\langle 1|\hat{d}_+|g\rangle\approx\langle 0|\hat{d}_0|g\rangle\approx\langle -1|\hat{d}_-|g\rangle=:d\in\mathbb{R}^+\,, \tag{4.59}$$

such that we can write $\boldsymbol{d}_q=d\hat{\boldsymbol{\varepsilon}}_q^*$. Then, we obtain

$$\boldsymbol{\beta}_{m,h}^*\boldsymbol{\beta}_{m,l}=\left(\frac{k_0^2d}{4\pi\varepsilon_0r_m}\right)^2\left[\delta_{h,l}-\frac{(\boldsymbol{r}_m\boldsymbol{d}_h)(\boldsymbol{r}_m\boldsymbol{d}_l^*)}{r_m^2d^2}\right]. \tag{4.60}$$

Thereby, the products $\boldsymbol{r}_m\boldsymbol{d}_q=\boldsymbol{r}_md\hat{\boldsymbol{\varepsilon}}_q^*$ can be calculated by writing $\boldsymbol{r}_m$ in spherical coordinates giving

$$\boldsymbol{r}_m\boldsymbol{d}_0=r_md\cos\theta_m\,, \tag{4.61}$$

$$\boldsymbol{r}_m\boldsymbol{d}_1=\frac{r_md}{\sqrt{2}}\sin\theta_me^{-i(\varphi_m+\pi)}\,, \tag{4.62}$$

$$\boldsymbol{r}_m\boldsymbol{d}_{-1}=\frac{r_md}{\sqrt{2}}\sin\theta_me^{i\varphi_m}\,. \tag{4.63}$$

In addition to the angular distribution of the emission pattern, we also need to calculate the optical phase differences. We assume that all atoms are located along the z-axis, such that the position vector of the μth atom is $\boldsymbol{R}_\mu=Z_\mu\hat{\boldsymbol{z}}$ and the phases read

$$\delta_{\mu,m}=-k_0Z_\mu\cos\theta_m\,. \tag{4.64}$$

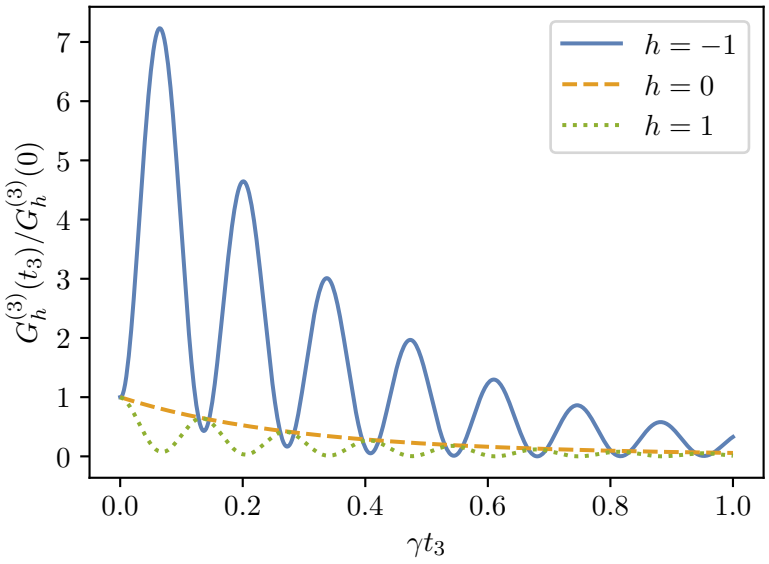

Figure 4.16: Third-order photon correlation functions for different distinct excited states $|h\rangle, h \in \{-1, 0, 1\}$ of the first two atoms. The interference with the third atom leads to clearly distinct time behaviours, which allows to uniquely distinguish the different excited states.

Wlog the first atom shall be located at the origin (as before), i.e., $Z_1 = 0$, such that $\delta_{1,m} = 0, m \in \{1, 2, 3\}$. In addition, we project out the antisymmetric contributions. This can be achieved by performing the first two photon measurements at a detection angle $\theta_1 = \theta_2 = \frac{\pi}{2}$ leading to $\cos\theta_1 = \cos\theta_2 = 0$ and thus $\delta_{\mu,1} = \delta_{\mu,2} = 0, \mu \in \{1, 2, 3\}$. Further, to simplify calculations, the measurements shall be done at an azimuthal angle $\varphi_1 = \varphi_2 = -\frac{\pi}{2}$, such that

$$(\boldsymbol{r}_m \boldsymbol{d}_1)(\boldsymbol{r}_m \boldsymbol{d}_{-1}^*) \propto e^{-i(-\frac{\pi}{2}+\pi)} e^{i\frac{\pi}{2}} \propto 1 \tag{4.65}$$

with $m \in \{1, 2\}$. With this measurement configuration, the coefficients of Eqs. (4.49)-(4.51) simplify to

$$c_{Gl} = 2\boldsymbol{\beta}_{1,h}\boldsymbol{\beta}_{2,h}\,, \tag{4.66}$$

$$c_{S_h g} = \sqrt{2}\left(\boldsymbol{\beta}_{1,h}\boldsymbol{\beta}_{2,l} + \boldsymbol{\beta}_{1,l}\boldsymbol{\beta}_{2,h}\right)\,, \tag{4.67}$$

$$c_{A_h g} = 0\,. \tag{4.68}$$

Since the third atom shall be experimentally controlled, we assume that it can be prepared in the state $|l\rangle = |1\rangle$. Then, if the third measurement is also performed at a polar angle of $\theta_3 = \frac{\pi}{2}$, but with azimuthal angle $\varphi_3 = 0$, the three possible $G^{(3)}$ functions read

$$G_{-1}^{(3)}(t_3) \propto \frac{1}{2}e^{-2\gamma t_3} + 2e^{-2(\gamma+\Gamma_\perp)t_3} - 2e^{-(2\gamma+\Gamma_\perp)t_3}\cos\left(\Omega_\perp t_3\right)\,, \tag{4.69}$$

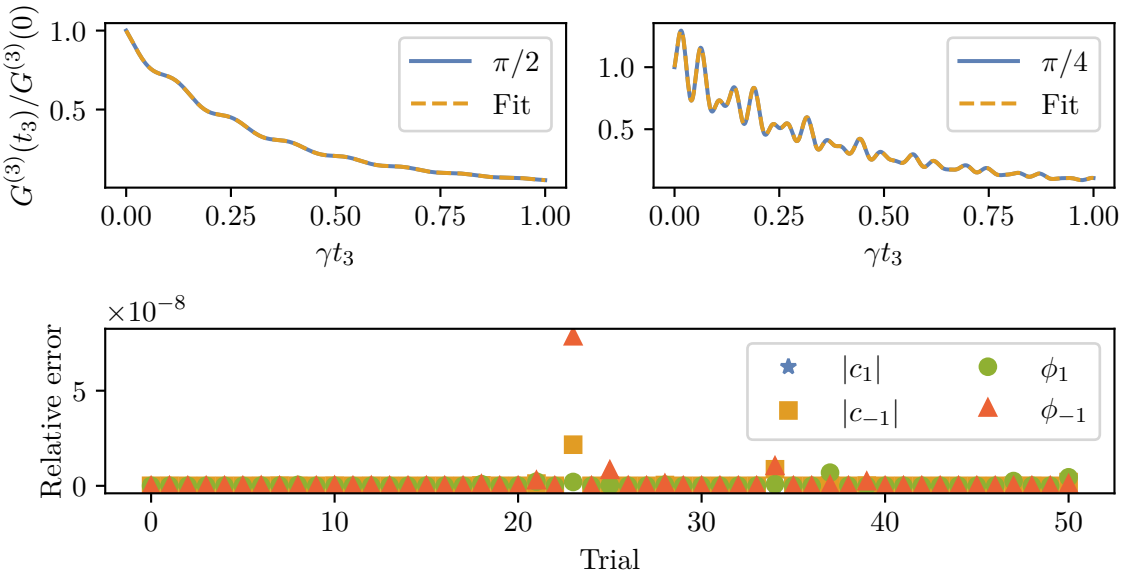

Figure 4.17: Top: Third-order photon correlation functions and fits of the trial 25 for $\theta_3 = \frac{\pi}{2}$ on the left to obtain the absolute values and the phase difference, and for $\theta_3 = \frac{\pi}{4}$ on the right to find the individual phase values. The separation of the atoms is $R_{12} = \lambda/20$. Bottom: Relative errors between the correct values and the reconstructed values from the fit for all four parameters and all 51 trials.

$$G_0^{(3)}(t_3) \propto 2e^{-2\gamma t_3} + 4e^{-2(\gamma+\Gamma_\parallel)t_3}\,, \tag{4.70}$$

$$G_1^{(3)}(t_3) \propto \frac{1}{2}e^{-2\gamma t_3} + 2e^{-2(\gamma+\Gamma_\perp)t_3} + 2e^{-(2\gamma+\Gamma_\perp)t_3}\cos\left(\Omega_\perp t_3\right)\,, \tag{4.71}$$

where the index characterises the state of the first two atoms $|h\rangle$. Note that we neglected the constant prefactor of Eq. (4.60), since we usually normalise the correlation function with respect to its value at the initial time. In Fig. 4.16, we display the three different photon correlation functions, which show clearly distinct time behaviours due to the different interference terms with the third atom. Thus, in this case, the three possible states $|h\rangle\,, h \in \{-1, 0, 1\}$ of the close-by atoms can be uniquely distinguished.

Now, the question is whether this can be generalised to an arbitrary superposition of the possible excited states instead of a single distinct excited state. Therefore, we consider the state $|\psi_s\rangle = \sum_{h=-1}^{1} c_h\,|h\rangle$ and ask the question whether it is possible to determine the coefficients c_h of this superposition. With a proper choice of phase, we can assume wlog that $c_0 \in \mathbb{R}^+$ and thus can be fixed via the normalisation of the state. Consequently, four real parameters, namely the two absolute values $|c_1|$, $|c_{-1}|$ and phases ϕ_1, ϕ_{-1} of the complex coefficients c_1 and c_{-1} need to be determined. As we will see, this can be achieved by measuring the third-order photon correlation function. Thereby, the measurement scheme consists of a first measurement at a polar angle $\theta_3 = \frac{\pi}{2}$ and an azimuthal angle $\varphi_3 = 0$, from which the two absolute values and the phase difference $\phi_1 - \phi_{-1}$ (up to $\pm 2\pi$) can be

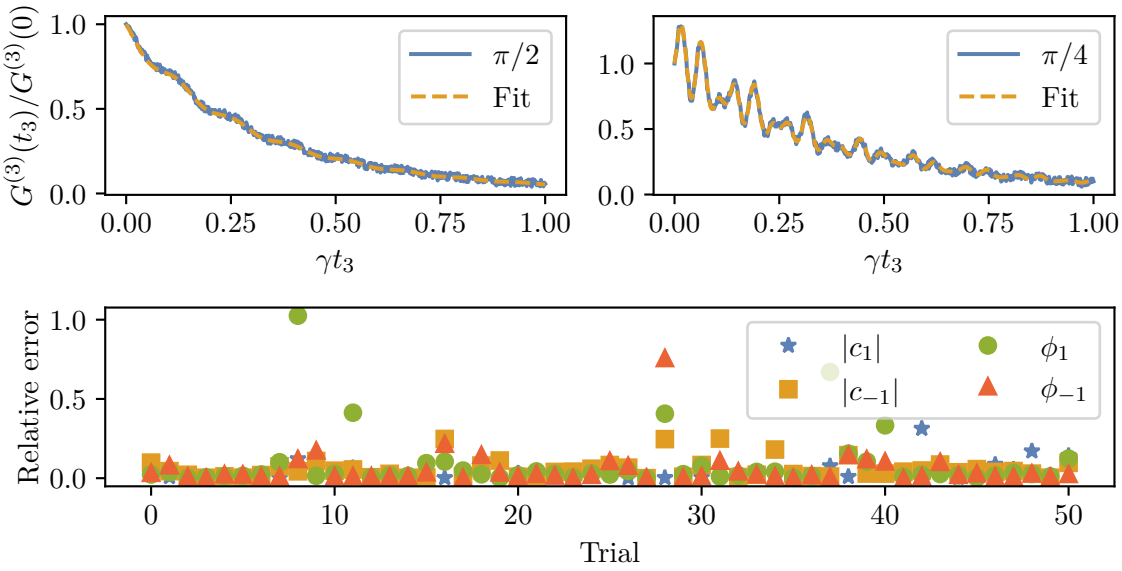

Figure 4.18: Top: Third-order photon correlation function with uniform noise added and fits of the trial 25 for $\theta_3 = \frac{\pi}{2}$ on the left to obtain the absolute values and the phase difference, and for $\theta_3 = \frac{\pi}{4}$ on the right to find the individual phase values. The separation of the atoms is $R_{12} = \lambda/20$. Bottom: Relative errors between the correct values and the reconstructed values from the fit for all four parameters and all 51 trials.

found. Afterwards, a second measurement at a polar angle $\theta_3 = \frac{\pi}{4}$ and an azimuthal angle $\varphi_3 = 0$ is performed. Here, we fix the already found values and determine the two missing phases individually. Since the calculation of the third-order photon correlation function is rather involved, we discard any expressions and rather show the result of the aforementioned procedure in Fig. 4.17. We do 51 random initialisations (trials) of the parameters $|c_1|$, $|c_{-1}|$, ϕ_1, and ϕ_{-1} for a separation of $R_{12} = \lambda/20$ of the close-by atoms and re-obtain the parameters via a fit of the third-order photon correlation function. In the top, we show the third-order photon correlation functions and the fits of the trial 25 (starting from 0). In the bottom, we plot the relative errors between the correct values and the values found from the fit for all four parameters and all 51 trials. As can be seen by analysing the relative errors of the parameters, the coefficients of the excited state superposition can be adequately determined by our method. However, in a real experiment noise is unavoidable. Therefore, we add $\pm 2.5\%$ uniform noise compared to the maximum values of the third-order photon correlation functions for both directions and show the corresponding results for the same 51 initialisations in Fig. 4.18. In this case, we did not fix the absolute values and the phase difference obtained from the first fit. But, in the case of the absolute values, we used them as initial parameters for the second fit. In the case of the phases, we took the correct phases plus a random number from the interval $[-0.5, 0.5]$, since we assume that the phase difference governed from the first fit can be used to preadjust the two phases to reasonable values. As can be seen in Fig. 4.18,

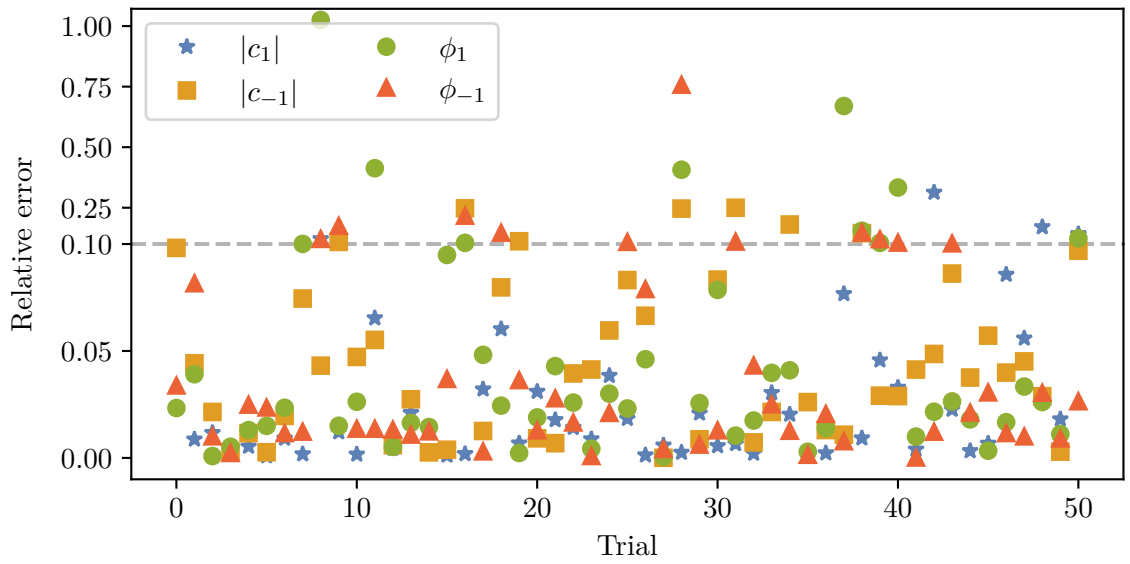

Figure 4.19: Relative errors between the correct parameters and the reconstructed parameters obtained from the fits to the third-order photon correlation functions with uniform noise added. The y-axis is plotted with two different scales, one reaching from 0% to 10% and one starting from 10% on, to show that in a large percentage of trials ($\sim 2/3$) the four relative errors are still below 10%.

the noise affects the performance of the presented method quite heavily. This high sensitivity to noise is based on the high sensitivity of the third-order photon correlation function to small changes in the parameters. In this regard, we want to stress two points. First, in a large percentage of trials of around 2/3, all four relative errors are still below 10%. This can be seen in Fig. 4.19, where we plot the relative errors with two different scales of the y-axis, one reaching from 0% to 10% and one starting from 10% on. In total, we performed 100 runs with 51 trials each. Thereby, the overall percentage of simultaneous relative errors below 10% was 64.0%. The percentage of the run that we show in the Figs. 4.17-4.19 was 62.7%. Second, we also find trials with relative errors of magnitude ~ 1. Even though these errors may be reduced by restricting the absolute values or the phase difference, we want to point out that the obtained fit parameters need to be treated with a certain level of carefulness when the signal is affected by noise.

Let us conclude this section by noting that the key concept is again to exploit the quantum correlations of the system of interest to a remote atom, produced by higher-order conditional photon measurements. We further note, however, that the correlation function is quite sensitive to parameter changes and thus the obtained parameters need to be enjoyed with some caution when the signal is affected by noise. We finally mention that if we have only two atoms, i.e., a state $|\psi\rangle = |\psi_s\rangle \otimes |\psi_s\rangle$, without the remote atom, a measurement of the second-order photon correlation function fails, in general, to provide the correct coefficients. In

particular, in the case of $c_0 = 0$, only the product of $|c_1|$ and $|c_{-1}|$ can be determined, but not the individual values.

After the extensive discussion of the different versions of the three-atom system in the current chapter, in the next chapter, we investigate an atomic ensemble of an arbitrary number of atoms N and analyse how collective effects, such as the superradiant emission of photons, can be engineered by conditional photon measurements.

5 Dicke-like superradiance of distant non-interacting atoms

Coherent radiation is emitted when r is large but $|m|$ small. For example, for even n let

$$r = \frac{1}{2}n\,, \quad m = 0\,; \quad I = \frac{1}{2}n\left(\frac{1}{2}n + 1\right) I_0\,.$$

This is the largest rate at which a gas with an even number of molecules can radiate spontaneously. It should be noted that for large n, it is proportional to the square of the number of molecules. [...] For want of a better term, a gas which is radiating strongly because of coherence will be called "super-radiant".

– Robert H. Dicke

A single two-level atom in its excited state will spontaneously drop down to its ground state and will thereby emit a photon. As can be seen from the quantum master equation, this process happens with exponentially decaying probability leading to an exponential decay of the measured intensity with rate $\Gamma = 2\gamma$ in the ensemble average. If we now, instead of a single atom, consider N independent atoms, i.e., atoms with pairwise separations much larger than the transition wavelength so that they do not interact with each other, the ensemble average of each observable is essentially the same as that of a single atom. Thus, they emit independently of each other and the intensity follows the same exponential decay with rate Γ. If, however, the atoms are closer together than the transition wavelength, their decays are not independent any more, but the atoms emit the photons collectively. In particular, in the limiting case, where all atoms are placed on the same spot, the intensity does not decay exponentially, but shows a burst of photons. Thereby, the maximum intensity scales quadratically in the number of atoms and the duration of the pulse scales inversely with the number of atoms [11]. This phenomenon has been investigated and coined superradiance by Dicke in 1954 (see quote) [7]. Nowadays, a huge conglomeration of theoretical works [7–39] and experimental realisations [40–51] of superradiance exists, whereby the terminology is not unique. Most of the time, however, temporal features are used as a criterion to speak of superradiance. For instance, when a system synchronises or builds up correlations over time leading to a peaked emission, one speaks of a so-called superradiant burst. However, also in the case without a burst of emission, but the emission of photons occurs with a faster decay

rate than the single-atom decay rate, one speaks of a superradiant decay. Another criterion is the magnitude of the emitted intensity, for instance, in a particular direction. If this intensity is higher than the number of excitations, which is the scaling for independent emitters, one also speaks of (spatial) superradiance. Some authors even distinguish between superradiance and measurement-induced cooperativity [35]. In this thesis, we have a broad understanding of superradiance. For us, superradiance has different aspects that sometimes occur in combination, sometimes on their own. In the first section of this chapter, we concretise the foregoing discussion by consolidating it with mathematical expressions.

5.1 Intensity and total emission rate

The intensity measured with a detector at position $\boldsymbol{r}$ in the far field and at a time t is related to the first-order photon correlation function via

$$\begin{aligned} I(\boldsymbol{r},t) &= \varepsilon_0 c G^{(1)}(\boldsymbol{r},t) = \varepsilon_0 c \,\langle \hat{\boldsymbol{E}}^{(-)}(\boldsymbol{r},t)\hat{\boldsymbol{E}}^{(+)}(\boldsymbol{r},t)\rangle \\ &= \frac{\hbar\omega_0}{r^2}\sum_{\mu,\nu}\sum_{m,n}\frac{3}{8\pi}\frac{\gamma_m}{|\boldsymbol{d}_m|^2}[\boldsymbol{d}_m\boldsymbol{d}_n^* - (\boldsymbol{d}_m\hat{\boldsymbol{r}})(\boldsymbol{d}_n^*\hat{\boldsymbol{r}})]e^{ik_0\hat{\boldsymbol{r}}(\boldsymbol{R}_\mu-\boldsymbol{R}_\nu)}\,\langle \hat{S}_{m+}^{(\mu)}(t)\hat{S}_{n-}^{(\nu)}(t)\rangle \ . \end{aligned} \tag{5.1}$$

To obtain the total emitted intensity, we integrate over a sphere at the position of the detector

$$I(t) = \int d\Omega_r\, r^2 I(\boldsymbol{r},t) = \hbar\omega_0 \sum_{\mu,\nu}\sum_{m,n}\Gamma_{mn}^{\mu\nu}\,\langle \hat{S}_{m+}^{(\mu)}(t)\hat{S}_{n-}^{(\nu)}(t)\rangle = \hbar\omega_0 R(t)\,, \tag{5.2}$$

where

$$R(t) = \sum_{\mu,\nu}\sum_{m,n}\Gamma_{mn}^{\mu\nu}\,\langle \hat{S}_{m+}^{(\mu)}(t)\hat{S}_{n-}^{(\nu)}(t)\rangle \tag{5.3}$$

can be interpreted as total emission rate. Next, we rewrite the emission rate in diagonal form and discuss the case investigated by Dicke in more detail. For simplicity, we assume two-level atoms, which means that the sum over the different transitions disappears. The emission rate is then

$$R(t) = \sum_{\mu,\nu}\Gamma^{\mu\nu}\,\langle \hat{S}_{+}^{(\mu)}(t)\hat{S}_{-}^{(\nu)}(t)\rangle \ . \tag{5.4}$$

To obtain the emission rate in diagonal form, we consider the dissipator of the master equation, which is given by

$$\sum_{\mu,\nu}\Gamma^{\mu\nu}\left(\hat{S}_{+}^{(\mu)}\hat{S}_{-}^{(\nu)}\hat{\rho}(t) + \hat{\rho}(t)\hat{S}_{+}^{(\mu)}\hat{S}_{-}^{(\nu)} - 2\hat{S}_{-}^{(\nu)}\hat{\rho}(t)\hat{S}_{+}^{(\mu)}\right) . \tag{5.5}$$

Now, we define the matrix

$$\Gamma = \begin{pmatrix} \Gamma^{11} & \cdots & \Gamma^{1N} \\ \vdots & \ddots & \\ \Gamma^{N1} & \cdots & \Gamma^{NN} \end{pmatrix} \tag{5.6}$$

containing all the decay rates and the vector

$$\hat{\boldsymbol{\Sigma}} = \begin{pmatrix} \hat{S}_-^{(1)} \\ \vdots \\ \hat{S}_-^{(N)} \end{pmatrix} \tag{5.7}$$

containing all the lowering operators. We diagonalise the matrix Γ with the orthogonal matrix V consisting of the eigenvectors of Γ, i.e., $V^{\mathsf{T}}\Gamma V = \Lambda$, where Λ is a diagonal matrix with the eigenvalues of Γ on the diagonal. Now, we define the new jump operator vector $\hat{\boldsymbol{J}} = V^{\mathsf{T}}\hat{\boldsymbol{\Sigma}} \Rightarrow \hat{\boldsymbol{J}}^\dagger = \hat{\boldsymbol{\Sigma}}^\dagger V$ [12]. Then, the dissipator can be written in its diagonal form as

$$\sum_\mu \Lambda^{\mu\mu} \left(\hat{J}_\mu^\dagger \hat{J}_\mu \hat{\rho}(t) + \hat{\rho}(t) \hat{J}_\mu^\dagger \hat{J}_\mu - 2\hat{J}_\mu \hat{\rho}(t) \hat{J}_\mu^\dagger \right) . \tag{5.8}$$

Coming back to the emission rate, we finally obtain

$$R(t) = \sum_{\mu,\nu} \Gamma^{\mu\nu} \langle \hat{S}_+^{(\mu)}(t) \hat{S}_-^{(\nu)}(t) \rangle = \sum_\mu \Lambda^{\mu\mu} \langle \hat{J}_\mu^\dagger(t) \hat{J}_\mu(t) \rangle \ . \tag{5.9}$$

5.2 Dicke superradiance

In the following section, we discuss the phenomenon of Dicke superradiance [7], calculate the corresponding decay rates and the total emission rate, and also have a look at static intensities in the case of so-called (symmetric) Dicke states. Therefore, we first need to introduce the aforementioned Dicke states. We consider N independent two-level atoms described by the Hamilton operator

$$\hat{H}_A = \hbar\omega_0 \sum_{\mu=1}^{N} \hat{S}_z^{(\mu)} = \hbar\omega_0 \hat{S}_z \, , \tag{5.10}$$

where we introduced the z-component of the collective pseudo-spin operator

$$\hat{\boldsymbol{S}} = \sum_{\mu=1}^{N} \hat{\boldsymbol{S}}^{(\mu)} \, . \tag{5.11}$$

One set of eigenstates of $\hat{H}_A$ are, of course, the tensor product states created from the single-atom ground and excited states. Another set of eigenstates, which will be convenient to use later on, are the combined eigenstates of the pseudo-spin operators $\hat{S}^2$ and $\hat{S}_z$. These states can be written as $|J, M, \alpha\rangle$. Here, J accounts for the eigenvalue of $\hat{S}^2$ and M accounts for the eigenvalue of $\hat{S}_z$ according to the following eigenvalue equations

$$\hat{S}^2 |J, M, \alpha\rangle = \hbar^2 J(J+1) |J, M, \alpha\rangle \,, \tag{5.12}$$

$$\hat{S}_z |J, M, \alpha\rangle = \hbar M |J, M, \alpha\rangle \,, \tag{5.13}$$

where

$$J \in \left\{0, 1, ..., \frac{N}{2}\right\} \quad \text{for } N \text{ even}\,, \tag{5.14}$$

$$J \in \left\{\frac{1}{2}, \frac{3}{2}, ..., \frac{N}{2}\right\} \quad \text{for } N \text{ odd}\,, \tag{5.15}$$

$$M \in \{-J, -J+1, ..., J\}\,. \tag{5.16}$$

Further, the parameter $\alpha \in \{1, 2, ..., \beta\}$ with

$$\beta = \frac{N!(2J+1)}{(\frac{N}{2}+J+1)!(\frac{N}{2}-J)!} \tag{5.17}$$

describes the degeneracy of the states for a given value of J. The pseudo-spin eigenstates just introduced are the so-called Dicke states. However, to understand Dicke superradiance, it is enough to consider the symmetric subspace, characterised by $J = N/2$, for which $\beta = 1$, such that we omit the α label of the states in the following. The symmetric Dicke states can be constructed, for instance, by starting with the fully excited state $|J = N/2, M = N/2\rangle = |e, e, ..., e\rangle$ and then applying consecutively the collective lowering operator

$$\hat{S}_- = \sum_{\mu=1}^{N} \hat{S}_-^{(\mu)}\,. \tag{5.18}$$

Alternatively, one can start with the fully ground state and apply the collective raising operator

$$\hat{S}_+ = \sum_{\mu=1}^{N} \hat{S}_+^{(\mu)}\,. \tag{5.19}$$

Now, assume that all atoms are confined to a small volume whose dimensions are smaller than the transition wavelength of the two-level atoms, so that the atoms can be approximately described as being at the same position in space. Then, if the system of atoms is coupled to the vacuum of the electromagnetic field, the foregoing approximation means that the phase

factors of the transverse displacement field in Eq. (2.2) can be omitted in the light-matter interaction Hamiltonian in Eq. (2.11) [7, 61]. As a consequence, the total Hamiltonian of both light and matter commutes with the pseudo-spin operators $\hat{S}_z$ and $\hat{S}^2$, such that subspaces with a fixed value of J are invariant under the time evolution of the system. In particular, if we start with the fully excited state, which is a symmetric Dicke state, only symmetric Dicke states with fewer excitations will be populated in the course of the time evolution. Performing all the steps in Chapter 2 leads to the following quantum master equation in the interaction picture [61]

$$\frac{\partial}{\partial t}\hat{\rho}(t) = -\gamma\left(\hat{S}_+\hat{S}_-\hat{\rho}(t) + \hat{\rho}(t)\hat{S}_+\hat{S}_- - 2\hat{S}_-\hat{\rho}(t)\hat{S}_+\right). \tag{5.20}$$

Thus, in the case of Dicke superradiance, $\Gamma^{\mu\nu} = \gamma$ for all $\mu, \nu \in \{1, ..., N\}$. Then, the Γ matrix has only one nonzero eigenvalue $N\gamma$ and the corresponding jump operator is $\hat{J} = \frac{1}{\sqrt{N}}\hat{S}_-$. This enhanced decay rate $N\gamma$ is one aspect of superradiance. Another aspect is the enhanced (directional) intensity. Therefore, let us first consider the static total emission rate for a single symmetric Dicke state in the case of Dicke superradiance given by

$$R = N\gamma\,\langle J, M|\hat{J}^\dagger\hat{J}|J, M\rangle = \gamma\,\langle J, M|\hat{S}_+\hat{S}_-|J, M\rangle = \gamma(J + M)(J - M + 1)\,. \tag{5.21}$$

For $J = N/2$ and $M = 0$ ($M = n_e - N/2$), this emission rate scales as n_e^2 instead of n_e, where n_e is the mean number of excitations. Usually, this total emission rate is considered in the context of a superradiant burst. However, in the case of Dicke superradiance, one can directly look at the intensity (normalised to be dimensionless)

$$I(\boldsymbol{r}) = \langle J, M|\hat{S}_+\hat{S}_-|J, M\rangle = (J + M)(J - M + 1)\,, \tag{5.22}$$

which is identical to the total emission rate up to a factor of γ, i.e., it shows the same scaling with respect to the number of excitations. In the case of Dicke superradiance, this intensity is isotropic, but for an atomic configuration with far separated atoms, the intensity depends on the detection direction. Therefore, it is useful to define the terminology of *spatial* or *directional* superradiance. Even though the total emission rate $R = \gamma n_e$ does not show a superradiant scaling in the case of far separated atoms, the intensity $I(\boldsymbol{r})$ can show a superradiant scaling in particular directions. We then speak of spatial or directional superradiance if $I(\boldsymbol{r}) > n_e$.

Now, let us investigate the origin of the superradiant behaviour in a single symmetric Dicke state. Therefore, we write the intensity in Eq. (5.22) as [17]

$$I(\boldsymbol{r}) = \langle\hat{S}_+\hat{S}_-\rangle = \sum_{\mu,\nu}\langle\hat{S}_+^{(\mu)}\hat{S}_-^{(\nu)}\rangle$$

$$= \sum_{\mu} \langle \hat{S}_+^{(\mu)} \hat{S}_-^{(\mu)} \rangle + \sum_{\substack{\mu,\nu \\ \mu \neq \nu}} \langle \hat{S}_+^{(\mu)} \rangle \langle \hat{S}_-^{(\nu)} \rangle + \sum_{\substack{\mu,\nu \\ \mu \neq \nu}} \left(\langle \hat{S}_+^{(\mu)} \hat{S}_-^{(\nu)} \rangle - \langle \hat{S}_+^{(\mu)} \rangle \langle \hat{S}_-^{(\nu)} \rangle \right)$$

$$= n_e + \sum_{\substack{\mu,\nu \\ \mu \neq \nu}} \langle \hat{S}_+^{(\mu)} \rangle \langle \hat{S}_-^{(\nu)} \rangle + \sum_{\substack{\mu,\nu \\ \mu \neq \nu}} K(\hat{S}_+^{(\mu)}, \hat{S}_-^{(\nu)}, |J, M\rangle) \,, \tag{5.23}$$

where $K(\hat{S}_+^{(\mu)}, \hat{S}_-^{(\nu)}, |J, M\rangle)$ accounts for dipole-dipole correlations and denotes the correlation function defined in Appendix D. We can simplify this expression by noticing that symmetric Dicke states do not possess any single-atom coherences (and thus no dipole moment), i.e., $\langle \hat{S}_\pm^{(\mu)} \rangle = 0$. Further, they are symmetric with respect to the atoms, such that the correlation function is independent of μ and ν. Thus, the intensity reduces to

$$I(\boldsymbol{r}) = n_e + N(N-1) K(\hat{S}_+^{(1)}, \hat{S}_-^{(2)}, |J, M\rangle) \,. \tag{5.24}$$

Therefore, we find a superradiant behaviour if $K(\hat{S}_+^{(1)}, \hat{S}_-^{(2)}, |J, M\rangle) > 0$. An explicit calculation of the correlation function gives

$$K(\hat{S}_+^{(1)}, \hat{S}_-^{(2)}, |J, M\rangle) = \binom{N-2}{n_e-1} \binom{N}{n_e}^{-1} = \frac{(N-n_e)n_e}{N(N-1)} = \frac{(J-M)(J+M)}{2J(2J-1)} \,, \tag{5.25}$$

which leads to the already calculated intensity

$$I(\boldsymbol{r}) = n_e + (N-n_e)n_e = n_e(N-n_e+1) = (J+M)(J-M+1) \,. \tag{5.26}$$

We find that except for $M = J$ (fully excited state) and $M = -J$ (fully ground state), the correlation function is always positive and thus results in a superradiant behaviour. Further, as we show in Appendix D, in the case of a pure state, a nonzero correlation function implies entanglement, such that we can identify the entanglement of the symmetric Dicke states as the reason for the superradiant behaviour. We can also quantify the entanglement of the symmetric Dicke states by calculating the so-called global entanglement, which gives (see Appendix D)

$$Q_m(|J, M\rangle) = \frac{2^m}{2^m - 1} [1 - \mathrm{Pu}(N, m, n_e)] \,, \tag{5.27}$$

where the purity function $\mathrm{Pu}(N, m, n_e)$ is defined in Section D.4. We find that it is always positive for $n_e \notin \{0, N\}$. Further, $\mathrm{Pu}(N, m, n_e) = \mathrm{Pu}(N, m, N - n_e)$, since interchanging excited states and ground states does not change the amount of entanglement, and the entanglement is highest for $n_e = N/2$ for even N and for $n_e \in \{\lfloor N/2 \rfloor, \lfloor N/2 \rfloor + 1\}$ for odd N (see Fig. 5.1). We note, however, that the last statement needs still to be rigorously proven. Before we discuss the time evolution in more detail, let us give an illustrative explanation for the scaling of the intensity in terms of quantum paths. Consider a pure state with a

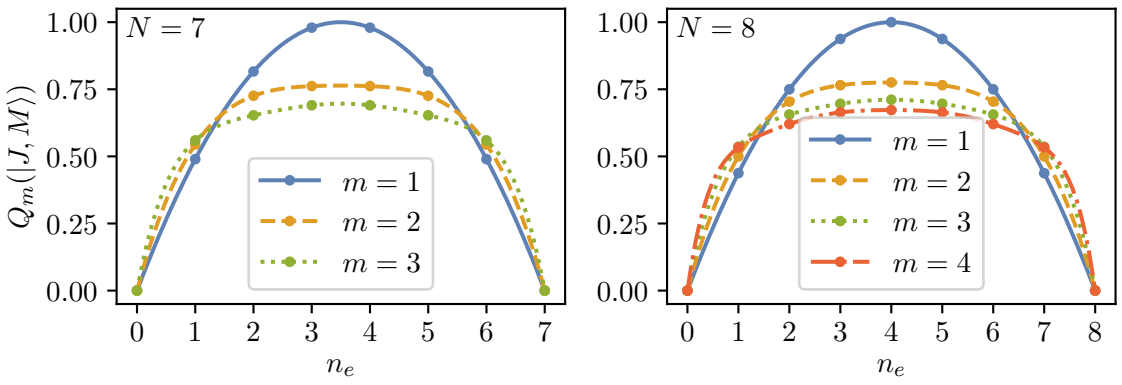

Figure 5.1: Global entanglement $Q_m(|J, M\rangle)$ as a function of the number of excitations n_e and of the possible splittings described by m for odd N ($N = 7$) on the left and for even N ($N = 8$) on the right. The global entanglement is symmetric around $n_e = N/2$, for which it takes its highest value.

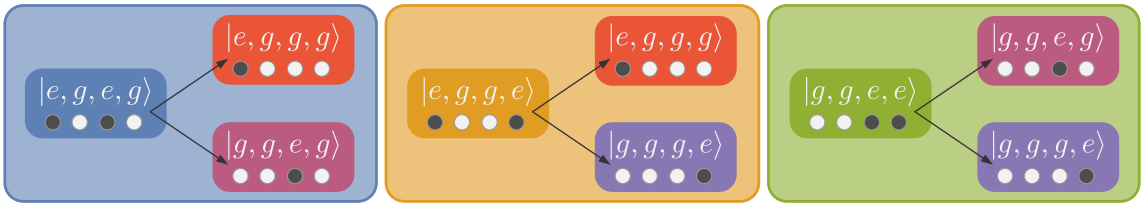

Figure 5.2: Quantum paths of the three states in Eq. (5.29). The state is the superposition of three tensor product states (three coloured boxes). Since in each state two atoms are in the excited state, we have two possibilities or quantum paths for the emission of a photon leading to two different states with one excitation less (splitting in each coloured box). Considering all three states, we find three different final states (red, magenta, and purple coloured smaller boxes). The number of quantum paths per final state is thus $\mathcal{P}_\mathcal{F} = \frac{3\times2}{3} = 2$.

well-defined number of atoms in the ground state $n_g = N - n_e$ that can be written as a tensor product of a symmetric Dicke state and a multi-atom ground state (after reordering of the state). The (maximum) radiated intensity can be calculated by counting interfering (spatial) quantum paths as [17]

$$I = \mathcal{N}^2 \mathcal{P}_\mathcal{F}^2 \mathcal{F} \,. \tag{5.28}$$

Thereby, $\mathcal{N}$ is the normalisation of the state, $\mathcal{P}_\mathcal{F}$ is the number of quantum paths per final state, and $\mathcal{F}$ is the number of different final states. Note that the square of $\mathcal{P}_\mathcal{F}$ comes from the indistinguishability of the quantum paths. Let us consider the state

$$|\psi\rangle = \frac{1}{\sqrt{3}}(|e, g, e, g\rangle + |e, g, g, e\rangle + |g, g, e, e\rangle) \tag{5.29}$$

as a simple example. We see that after reordering the state, we can write $|\psi\rangle = |g\rangle\otimes|3/2, 1/2\rangle$. Since the ground state does not contribute to the intensity, we can calculate the intensity via Eq. (5.26), which gives $I = 4$. To illustrate the applicability of Eq. (5.28), let us count the interfering quantum paths by having a look at the possible detection events drawn in Fig. 5.2. We have a superposition of three different tensor product states with two excitations. Each of these states can emit a photon in two possible ways, i.e., quantum paths. Thereby, we obtain three different final states, which have one excitation less than the original states. The number of quantum paths per final state can thus be calculated to

$$\mathcal{P}_{\mathcal{F}} = \frac{\#\text{product states} \times \#\text{quantum paths per product state}}{\#\text{different final states}} = \frac{3 \times 2}{3} = 2\,. \tag{5.30}$$

Then, using Eq. (5.28), we obtain for the intensity

$$I = \left(\frac{1}{\sqrt{3}}\right)^2 \times 2^2 \times 3 = 4\,, \tag{5.31}$$

i.e., the same value as by a straightforward calculation of the intensity. However, the quantum path picture gives a clear physical interpretation. In particular, we recognise that the enhancement of the intensity ($I > 2 = n_e$) comes from the interference of the quantum paths, which is based on the quantum correlations of the state $|\psi\rangle$.

The same formalism can be applied to an arbitrary symmetric Dicke state. Therefore, we find again that the quantum correlations of the symmetric Dicke states, which lead to the interference of indistinguishable quantum paths, are responsible for the superradiant behaviour. We finally explicitly show that we obtain indeed the same value for the intensity by simply counting the interfering quantum paths. Applying Eq. (5.30) to an arbitrary symmetric Dicke state characterised by the number of atoms in the ground state n_g, we find for the number of quantum paths per final state

$$\mathcal{P}_{\mathcal{F}} = \frac{\binom{N}{n_g} \times (N - n_g)}{\binom{N}{n_g+1}} = n_g + 1\,. \tag{5.32}$$

Now, using Eq. (5.28), the intensity reads

$$I = \binom{N}{n_g}^{-1} \times (n_g + 1)^2 \times \binom{N}{n_g + 1} = (N - n_g)(n_g + 1) = (J + M)(J - M + 1)\,, \tag{5.33}$$

which is the same result as in Eq. (5.26).

As a final step, we analyse the time evolution in the case of Dicke superradiance. Therefore, we unravel the quantum master equation Eq. (5.20) in terms of quantum trajectories (see Appendix F). In the right plot of Fig. 5.3, we show the expectation value $\langle \hat{S}_+ \hat{S}_- \rangle$ (left axis) together with the populated states (right axis) against time for a single trajectory. We find

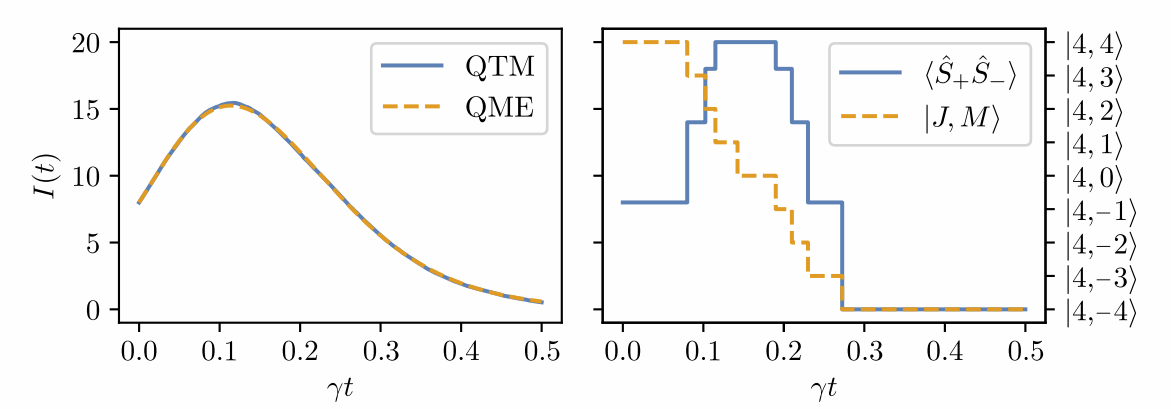

Figure 5.3: In the left plot, we show the radiated intensity as a function of time for $N = 8$ atoms. By passing down the ladder of symmetric Dicke states, the atoms emit the photons in a superradiant burst. The blue solid curve, which is the average over 5000 quantum trajectories (QTM: quantum trajectory method), converges to the expectation value obtained from the master equation, which displays an ensemble average (QME: quantum master equation). In the right plot, a single quantum trajectory is shown. The blue solid curve shows the expectation value $\langle \hat{S}_+ \hat{S}_- \rangle$ (left axis) whose average over many trajectories yields the blue curve in the left plot. The orange dashed curve indicates the symmetric Dicke state, which the system is in for all times (right axis).

that the system descends down the ladder of symmetric Dicke states. Every time a photon is emitted, the state jumps from one symmetric Dicke state to the next symmetric Dicke state with one excitation less. Thereby, the heights of the plateaus of the expectation value $\langle \hat{S}_+ \hat{S}_- \rangle$ can be traced back to the dipole-dipole correlations in the symmetric Dicke states. The question, however, is how this expectation value is connected to superradiance. We found earlier that the emitted intensity is exactly given by the expectation value $\langle \hat{S}_+ \hat{S}_- \rangle$. But, for a single quantum trajectory, the measured intensity consists of single events, namely measured photons at the times the jumps occur. Therefore, the expectation value $\langle \hat{S}_+ \hat{S}_- \rangle$ only describes the intensity if we average over many trajectories. The result of this procedure is shown in the left plot of Fig. 5.3. Here, the blue solid curve shows the average over 5000 trajectories (QTM: quantum trajectory method). This average is equivalent to calculating the intensity via the master equation for the density matrix, which describes an ensemble average (QME: quantum master equation). The resulting curve, displaying the emitted intensity, shows a superradiant burst. Thereby, the height of the maximum scales with the number of atoms squared, while the width scales inversely with the number of atoms, see Fig. 5.4. On the left, we plot the intensity as a function of time for three different numbers of atoms, on the right, the intensity normalised by N is shown to highlight the changes with the number of atoms. By investigating the quantum master equation Eq. (5.20), we find that by starting initially in the fully excited state, the density matrix remains always in the symmetric subspace.

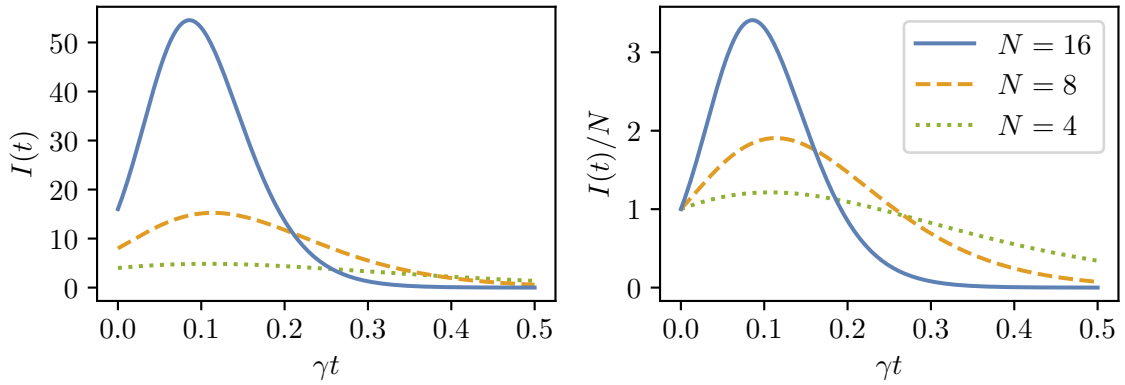

Figure 5.4: Superradiant burst of the intensity calculated via the quantum master equation. On the left, we show the emitted intensity against time for three different numbers of atoms N. The peak of the superradiant burst scales quadratically with the number of atoms, whereas the width scales inversely with the number of atoms. To highlight these scalings, on the right, we plot the intensity normalised by the number of atoms for the same three values of N.

Therefore, the solution of the time evolution can be written as

$$\hat{\rho}(t) = \sum_{M=-J}^{J} \rho_{M,M}(t) \left|J, M\right\rangle\!\left\langle J, M\right| , \tag{5.34}$$

where $\rho_{M,M}(t)$ denotes the population of the respective symmetric Dicke state characterised by M. Using this state for the calculation of the intensity, we immediately find

$$\begin{aligned} I(t) &= n_e(t) + \sum_{\substack{\mu,\nu \\ \mu\neq\nu}} \langle \hat{S}_+^{(\mu)}(t)\rangle \langle \hat{S}_-^{(\nu)}(t)\rangle + \sum_{\substack{\mu,\nu \\ \mu\neq\nu}} K(\hat{S}_+^{(\mu)}, \hat{S}_-^{(\nu)}, \hat{\rho}(t)) \\ &= n_e(t) + \sum_{\substack{\mu,\nu \\ \mu\neq\nu}} K(\hat{S}_+^{(\mu)}, \hat{S}_-^{(\nu)}, \hat{\rho}(t)) , \end{aligned} \tag{5.35}$$

where $n_e(t)$ denotes the average number of excited atoms at time t. We emphasise that the superradiant behaviour is again based on the dipole-dipole correlations of the atoms. However, we also note that in contrast to the case of a single symmetric Dicke state, these correlations may not be based on entanglement, i.e., the incoherent superposition of symmetric Dicke states, as given in Eq. (5.34), may not be an entangled state. We will discuss this mixed state issue in the last section of this chapter. Finally, we note that since the time-evolved density matrix is block-diagonal with respect to the number of atoms in the ground state n_g and the blocks fulfil the condition for the quantum path formalism, we can also interpret the superradiant burst in terms of interfering quantum paths when we apply Eq. (5.28) to each block individually.

In the next section, we investigate the situation of distant non-interacting atoms. Our goal is to mimic a similar (directional) superradiant emission behaviour as in the case of Dicke superradiance by generating dipole-dipole correlations via conditional photon measurements. We note that parts of the following section have been previously published in Ref. [30].

5.3 Dicke-like superradiance of distant non-interacting atoms

In the previous section, we discussed the phenomenon of Dicke superradiance, where the atoms were confined to a small volume. In contrast, in this section, we consider an ensemble of two-level atoms, which are far distant from each other. As such, we can neglect the effects of photon-mediated energy shifts and changes of the decay rates, i.e., dipole-dipole interactions. Therefore, the atoms evolve independently of each other in time, and thus the density matrix does not display any dipole-dipole correlations. However, by intersecting the free time evolution by conditional photon measurements at specific positions in space, we can create dipole-dipole correlations leading to a directional superradiant emission [19, 30, 76]. Depending on the times at which the photon measurements are performed, a similar superradiant burst as in the case of Dicke superradiance can be observed. The resulting time-dependent directional emission behaviour can be transparently interpreted via the quantum path formalism.

5.3.1 Master equation and differential equations for the density matrix elements

If we neglect all dipole-dipole interactions due to the large mutual separations of the atoms, the quantum master equation Eq. (2.46) in the interaction picture simplifies to

$$\frac{\partial}{\partial t}\hat{\rho}(t) = -\gamma \sum_{\mu=1}^{N} \left(\hat{S}_{+}^{(\mu)} \hat{S}_{-}^{(\mu)} \hat{\rho}(t) + \hat{\rho}(t) \hat{S}_{+}^{(\mu)} \hat{S}_{-}^{(\mu)} - 2\hat{S}_{-}^{(\mu)} \hat{\rho}(t) \hat{S}_{+}^{(\mu)} \right) . \tag{5.36}$$

Thus, we immediately find that the atoms simply decay independently of each other. If we project this master equation onto the tensor product basis, where $|\alpha\rangle$, $|\beta\rangle$ denote two basis states, we obtain the following set of first-order differential equations (see Appendix G)

$$\frac{\partial}{\partial t}\rho_{\alpha,\beta}(t) = 2\gamma \sum_{\mu=1}^{N} \rho_{\eta^{(\mu)},\delta^{(\mu)}}(t) - \gamma \sum_{\mu=1}^{N} \rho_{S_{+}^{(\mu)}\chi,\beta}(t) - \gamma \sum_{\mu=1}^{N} \rho_{\alpha,S_{+}^{(\mu)}\zeta}(t) . \tag{5.37}$$

Thereby, the indices on the right side of Eq. (5.37) specify the following three conditions

$$\text{1. sum:} \quad \hat{S}_{-}^{(\mu)} |\eta\rangle = |\alpha\rangle \ , \ \hat{S}_{-}^{(\mu)} |\delta\rangle = |\beta\rangle \ , \tag{5.38}$$

$$\text{2. sum:} \quad \hat{S}_{+}^{(\mu)} |\chi\rangle = |\alpha\rangle \ , \tag{5.39}$$

$$\text{3. sum:} \quad \hat{S}_{+}^{(\mu)} |\zeta\rangle = |\beta\rangle \tag{5.40}$$

that need to be fulfilled to get a contribution from the respective term in the sums.
It is convenient to characterise the tensor product states by the number of ground state atoms. Therefore, we define the fully excited state as $|g^{(0)}\rangle \coloneqq |e, e, ..., e\rangle$. A state, in which atom ν is in the ground state, but all other atoms are in the excited state, we define as $|g_\nu^{(1)}\rangle \coloneqq \hat{S}_-^{(\nu)} |g^{(0)}\rangle$. Analogously, we define and denote all states with a higher number of atoms in the ground state. In this notation, "g" reminds us that we characterise the states with respect to the atoms being in the ground state. In addition, the superscript indicates how many atoms are in the ground state, and the index specifies which atoms are in the ground state.
Now, let us show a simple example of how Eqs. (5.37)-(5.40) need to be applied. Consider the population $\rho_{g^{(0)},g^{(0)}}(t)$ of the fully excited state $|g^{(0)}\rangle$. We see that $|\alpha\rangle = |\beta\rangle = |g^{(0)}\rangle$ and therefore the first condition means that we need to find states $|\eta\rangle$ and $|\delta\rangle$ that fulfil $\hat{S}_-^{(\mu)} |\eta\rangle = \hat{S}_-^{(\mu)} |\delta\rangle = |g^{(0)}\rangle$. Obviously, there are no states that fulfil this equation since $|g^{(0)}\rangle$ is the fully excited state. Next, we consider the second and third sum. Here, we need to find states $|\chi\rangle$ and $|\zeta\rangle$ that fulfil $\hat{S}_+^{(\mu)} |\chi\rangle = \hat{S}_+^{(\mu)} |\zeta\rangle = |g^{(0)}\rangle$. There is only one state, which fulfils this equation, namely the state $|g_\mu^{(1)}\rangle$, where atom μ is in the ground state and all other atoms are in the excited state. From each sum, we additionally obtain a factor of N, such that the differential equation for the population of the fully excited state is given by

$$\frac{\partial}{\partial t}\rho_{g^{(0)},g^{(0)}}(t) = -2\gamma N \rho_{g^{(0)},g^{(0)}}(t)\,. \tag{5.41}$$

This yields the usual exponential decay with rate $2\gamma N$. We note that instead of applying the condition $\hat{S}_+^{(\mu)} |\chi\rangle = \hat{S}_+^{(\mu)} |\zeta\rangle = |g^{(0)}\rangle$ for a specific μ and afterwards considering the sum over all atoms, one can directly view this condition for $\mu \in \{1, 2, ..., N\}$, which immediately gives the factor of N.
The same procedure can be applied to every other density matrix element characterised by two tensor product states. This yields in general a set of $2^{2N} - 1$ real first-order differential equations. However, if we assume two reasonable restrictions, which we specify in Appendix G, we can reduce the number of real differential equations to N^2. This allows us to analytically solve the full time evolution intersected by conditional photon measurements performed in a particular direction.

5.3.2 Photon correlation functions

In general, we need to solve the set of differential equations derived in the previous subsection to find the higher-order photon correlation functions defined in Eq. (3.33). However, since we consider independent atoms, the time evolution is rather simple, such that the correlation functions can be straightforwardly obtained using the quantum regression theorem (see Appendix C). To connect the results to superradiance, we need to consider intensities.

Therefore, by rewriting Eq. (3.33) as

$$G^{(m)}_{\hat{\rho}}(\boldsymbol{r}_1,t_1;...;\boldsymbol{r}_m,t_m) = G^{(1)}_{\hat{\rho}_{m-1}}(\boldsymbol{r}_1,t_1;...;\boldsymbol{r}_m,t_m)G^{(m-1)}_{\hat{\rho}}(\boldsymbol{r}_1,t_1;...;\boldsymbol{r}_{m-1},t_{m-1})\,, \tag{5.42}$$

where [7, 19, 77, 78]

$$\hat{\rho}_{m-1} = \frac{\hat{E}^{(+)}(\boldsymbol{r}_{m-1},t_{m-1})...\hat{E}^{(+)}(\boldsymbol{r}_1,t_1)\hat{\rho}\hat{E}^{(-)}(\boldsymbol{r}_1,t_1)...\hat{E}^{(-)}(\boldsymbol{r}_{m-1},t_{m-1})}{\mathrm{Tr}[\hat{E}^{(+)}(\boldsymbol{r}_{m-1},t_{m-1})...\hat{E}^{(+)}(\boldsymbol{r}_1,t_1)\hat{\rho}\hat{E}^{(-)}(\boldsymbol{r}_1,t_1)...\hat{E}^{(-)}(\boldsymbol{r}_{m-1},t_{m-1})]} \tag{5.43}$$

is the density operator after the measurement of $m-1$ photons at positions $\boldsymbol{r}_1$ to $\boldsymbol{r}_{m-1}$ and times t_1 to t_{m-1} with $\hat{\rho}_0 = \hat{\rho}$, we define the *conditional* intensities

$$G^{(1)}_{\hat{\rho}_{m-1}}(\boldsymbol{r}_1,t_1;...;\boldsymbol{r}_m,t_m) = \frac{G^{(m)}_{\hat{\rho}}(\boldsymbol{r}_1,t_1;...;\boldsymbol{r}_m,t_m)}{G^{(m-1)}_{\hat{\rho}}(\boldsymbol{r}_1,t_1;...;\boldsymbol{r}_{m-1},t_{m-1})}\,. \tag{5.44}$$

Note that we write the correlation functions with the density operator as an index to explicitly specify the state which the expectation values are calculated with. Further, we note that $G^{(1)}_{\hat{\rho}_{m-1}}(\boldsymbol{r}_1,t_1;...;\boldsymbol{r}_m,t_m)$ depends, in general, on all positions $\boldsymbol{r}_1$ to $\boldsymbol{r}_m$ and times t_1 to t_m via the conditional state $\hat{\rho}_{m-1}$.

In the following, we assume an atomic chain with regular spacing much larger than the transition wavelength. All conditional photon measurements are performed perpendicular to this chain, such that in the far field approximation, all photons accumulate the same phase by the propagation from the respective atom to the detector. Further, for comparison, we consider again dimensionless intensities as in Section 5.2. For the described setup, the dimensionless higher-order photon correlation functions are then given by multi-time pseudo-spin expectation values, i.e.,

$$G^{(m)}_{\hat{\rho}}(t_1,...,t_m) = \langle \hat{S}_+(t_1)...\hat{S}_+(t_m)\hat{S}_-(t_m)...\hat{S}_-(t_1)\rangle\ . \tag{5.45}$$

Using Eq. (G.14) of Appendix G, computed via the quantum regression theorem, the conditional intensities therefore read

$$G^{(1)}_{\rho_{m-1}}(t_1,...,t_m) = \frac{\left(\prod_{s=1}^{m} e^{-2\gamma t_s}\right)\langle \overbrace{\hat{S}_+(0)...\hat{S}_+(0)}^{m\text{ times}}\overbrace{\hat{S}_-(0)...\hat{S}_+(0)}^{m\text{ times}}\rangle}{\left(\prod_{s=1}^{m-1} e^{-2\gamma t_s}\right)\langle \underbrace{\hat{S}_+(0)...\hat{S}_+(0)}_{m-1\text{ times}}\underbrace{\hat{S}_-(0)...\hat{S}_+(0)}_{m-1\text{ times}}\rangle} = e^{-2\gamma t_m}G^{(1)}_{\hat{\rho}_{m-1}}(0,...,0)\,. \tag{5.46}$$

We find that in the case of independently decaying atoms and photon measurements perpendicular to the atomic chain, the conditional intensities only depend on the latest time t_m. Furthermore, the amplitude is given by the conditional intensity at $t_1 = ... = t_m = 0$, i.e., $G^{(1)}_{\hat{\rho}_{m-1}}(0,...,0)$.

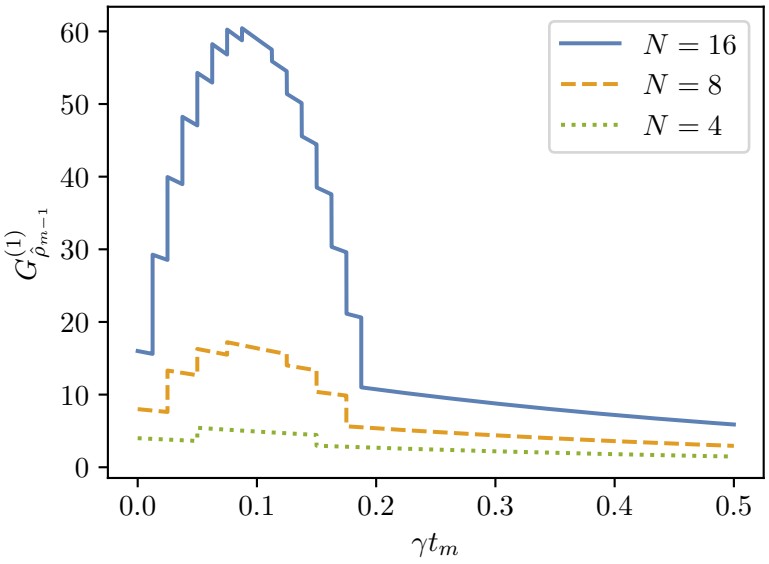

Figure 5.5: Conditional intensities against time for an equal time-spacing of the conditional photon measurements. The jumps of the conditional intensities occur at times at which conditional photon measurements are performed. As can be seen, a similar Dicke-like superradiant burst for the conditional intensities can be obtained.

If we start, as in the case of Dicke superradiance, with the fully excited state $\hat{\rho}_0 = |g^{(0)}\rangle\langle g^{(0)}|$, the state after $m-1$ photon measurements at time $t = 0$ and perpendicular to the atomic chain is simply given by $\hat{\rho}_{m-1} = |J, M\rangle\langle J, M|$, where $J = N/2$ and $M = N/2 - m + 1$. Therefore, we find for the conditional intensities

$$\begin{aligned} G^{(1)}_{\rho_{m-1}}(t_1, ..., t_m) &= \langle J, M|\hat{S}_+\hat{S}_-|J, M\rangle\, e^{-2\gamma t_m} \\ &= (J + M)(J - M + 1)e^{-2\gamma t_m} = m(N - m + 1)e^{-2\gamma t_m}\,. \end{aligned} \tag{5.47}$$

In the case that conditional photon measurements are performed at equidistant times, we plot the conditional intensities against time in Fig. 5.5. The free evolutions are intersected by conditional photon measurements. The explanation of the different sections is as follows. In the first section from time $t = 0$ to a time t_1, the usual intensity emitted by an ensemble of independent atoms is shown. The second section corresponds to the intensity that one would measure after the time t_1 to a time t_2 if at the time t_1 a photon was detected. Analogously, the curve in the mth section corresponds to the intensity that one would measure after a time t_{m-1} if at times t_1 to t_{m-1} photons were detected. Thereby, the heights of the conditional intensities are based on dipole-dipole correlations generated by the photon measurements. We will give more details on that in the next subsections when we explicitly investigate the state of the atoms for all times, interpret the emitted intensity via interfering quantum paths, and analyse the role of the measurement process quantitatively. Before that, we

finally highlight that even in the case of distant non-interacting atoms, a similar Dicke-like (directional) superradiant burst of the conditional intensities can be obtained, as can be seen in Fig. 5.5.

5.3.3 Quantum path interference interpretation

Instead of solving directly for the photon correlation functions, i.e., the conditional intensities, we can also solve the set of differential equations derived in Subsection 5.3.1 and Appendix G to obtain the time-dependent density operator, with which we can then calculate the conditional intensities afterwards. The time-dependent density operator allows, in particular, to explain the occurring directional superradiant behaviour via interfering quantum paths, which provides an illustrative physical picture.
We start with the fully excited state $\hat{\rho}_0(t_1 = 0) = |g^{(0)}\rangle\langle g^{(0)}|$, where the argument of the density operator refers to times between two intersections, i.e., we consider the free time evolution of the states after conditional photon measurements. For the initial state, we can easily find that $\mathcal{N} = 1$, $\mathcal{P}_\mathcal{F} = 1$, and $\mathcal{F} = N$, such that the initial emitted intensity equals N, the number of atoms. Now, let us investigate the first free time evolution. The time-evolved density operator can be written as

$$\hat{\rho}_0(t_1) = p_{0,0}(t_1)\,|g^{(0)}\rangle\langle g^{(0)}| + p_{0,1}(t_1)\sum_\mu |g^{(1)}_\mu\rangle\langle g^{(1)}_\mu| + p_{0,2}(t_1)\sum_{\mu<\nu} |g^{(2)}_{\mu\nu}\rangle\langle g^{(2)}_{\mu\nu}| + \dots\,, \quad (5.48)$$

where the probabilities read

$$p_{0,s}(t_1) = e^{-2N\gamma t_1}(e^{2\gamma t_1} - 1)^s\,, \quad (5.49)$$

which we obtain by solving the set of differential equations derived in Appendix G. Note that we can write the probabilities in front of the different blocks of the density operator since every state with the same number of ground state atoms evolves equally in time if we consider initially the symmetric fully excited state. We note, further, that every state in the incoherent sum in Eq. (5.48) can be written as a tensor product of the fully excited state of a reduced number of atoms and the fully ground state of a reduced number of atoms. Thus, every state fulfils the condition for the applicability of Eq. (5.28), such that we are able to compute the maximum intensity, which can be measured perpendicular to the atomic axis due to constructive interference, by counting the interfering quantum paths. For each state in each block, the normalisation is $\mathcal{N} = 1$. Further, every state is a tensor product state with a certain number of ground state atoms n_g and excited atoms $N - n_g$. Therefore, the number of single quantum paths per product state is $N - n_g$ and the number of different final states is $\mathcal{F} = \binom{N-n_g}{1} = N - n_g$. Consequently, the number of quantum paths per final state reads

$\mathcal{P}_{\mathcal{F}} = 1$. The intensity can then be calculated as

$$\begin{aligned} G^{(1)}_{\hat{\rho}_0}(t_1) &= \sum_{s=0}^{N-1} p_{0,s}(t_1) \binom{N}{s} \mathcal{N}^2 \mathcal{P}_{\mathcal{F}}^2 \mathcal{F} \\ &= \sum_{s=0}^{N-1} e^{-2N\gamma t_1} (e^{2\gamma t_1} - 1)^s \binom{N}{s} \times 1 \times 1^2 \times \binom{N-s}{1} \\ &= 1 \times (N - 1 + 1) e^{-2\gamma t_1} = N e^{-2\gamma t_1} \,, \end{aligned} \tag{5.50}$$

where $\binom{N}{s}$ accounts for the number of product states in each block of the density matrix with well-defined number of ground state atoms. Note that in the first expression of the last line of Eq. (5.50), we wrote the intensity as in Eq. (5.47) to show the equality for $m = 1$.
Next, we come to the state after the first conditional photon measurement, which can be obtained by applying the collective pseudo-spin lowering operator from the left and the collective pseudo-spin raising operator from the right to the state of Eq. (5.48). The application to the individual states of each block reads as follows:

$$|g^{(0)}\rangle \to |g^{(0)}_{S_-}\rangle \coloneqq S_- |g^{(0)}\rangle = \sum_{\mu=1}^{N} S_-^{(\mu)} |g^{(0)}\rangle = \sum_{\mu=1}^{N} |g^{(1)}_{\mu}\rangle \tag{5.51}$$

$$|g^{(1)}_{\mu}\rangle \to |g^{(1)}_{\mu,S_-}\rangle \coloneqq S_- |g^{(1)}_{\mu}\rangle = \sum_{\nu=1}^{N} S_-^{(\nu)} |g^{(1)}_{\mu}\rangle = \sum_{\substack{\nu=1 \\ \nu\neq\mu}}^{N} |g^{(2)}_{\mu\nu}\rangle \tag{5.52}$$

$$|g^{(2)}_{\mu\nu}\rangle \to |g^{(2)}_{\mu\nu,S_-}\rangle \coloneqq S_- |g^{(2)}_{\mu\nu}\rangle = \sum_{\xi=1}^{N} S_-^{(\xi)} |g^{(2)}_{\mu\nu}\rangle = \sum_{\substack{\xi=1 \\ \xi\neq\mu,\xi\neq\nu}}^{N} |g^{(3)}_{\mu\nu\xi}\rangle \tag{5.53}$$

$$\vdots$$

Then, if we evolve the state after the first conditional photon measurement in time, we find

$$\begin{aligned} \hat{\rho}_1(t_2) = \frac{1}{N} \Bigg\{ & p_{1,0}(t_2) |g^{(0)}_{S_-}\rangle\langle g^{(0)}_{S_-}| + p_{1,1}(t_2) \sum_{\mu} |g^{(1)}_{\mu,S_-}\rangle\langle g^{(1)}_{\mu,S_-}| \\ & + p_{1,2}(t_2) \sum_{\mu,\nu} |g^{(2)}_{\mu\nu,S_-}\rangle\langle g^{(2)}_{\mu\nu,S_-}| + \dots \Bigg\} \,, \end{aligned} \tag{5.54}$$

where the probabilities are given by

$$p_{1,s}(t_2) = e^{-2(N-1)\gamma t_2} (e^{2\gamma t_2} - 1)^s \,. \tag{5.55}$$

Since we only applied the collective lowering operator, the symmetry of the states remains unchanged, so we can again apply Eq. (5.28) to find the radiated conditional intensity. The normalisation can be read off as $\mathcal{N} = 1/\sqrt{N}$. Now, a single state in Eq. (5.54) with n_g many

atoms in the ground state came from a state with $N - n_g + 1$ many excited states before the application of the collective lowering operator. Therefore, the number of product states in each superposition state after the first conditional photon measurement is $N - n_g + 1$. Together with the number of single quantum paths per product state given by $N - n_g$ and the number of different final states, which can be obtained by distributing two ground states over $N - n_g + 1$ previously excited states, i.e., $\mathcal{F} = \binom{N-n_g+1}{2}$, the number of quantum paths per final state can be calculated to

$$\mathcal{P}_{\mathcal{F}} = \frac{(N - n_g + 1) \times (N - n_g)}{\binom{N-n_g+1}{2}} = 2\,. \tag{5.56}$$

Then, the conditional intensity after the first photon measurement reads

$$\begin{aligned} G^{(1)}_{\hat{\rho}_1}(t_2) &= \sum_{s=1}^{N-1} p_{1,s-1}(t_2) \binom{N}{s-1} \mathcal{N}^2 \mathcal{P}_{\mathcal{F}}^2 \mathcal{F} \\ &= \sum_{s=1}^{N-1} e^{-2(N-1)\gamma t_2} (e^{2\gamma t_2} - 1)^{s-1} \binom{N}{s-1} \times \frac{1}{N} \times 2^2 \times \binom{N-s+1}{2} \\ &= \sum_{s=0}^{N-2} e^{-2(N-1)\gamma t_2} (e^{2\gamma t_2} - 1)^{s} \binom{N}{s} \times \frac{1}{N} \times 2^2 \times \binom{N-s}{2} \\ &= 2(N - 2 + 1)e^{-2\gamma t_2} = 2(N-1)e^{-2\gamma t_2}\,. \end{aligned} \tag{5.57}$$

Note that we wrote the first expression in the last line of Eq. (5.57) to show the equality to Eq. (5.47) for $m = 2$.

This explicitly demonstrated calculation of the conditional intensity after the first photon measurement by simply counting interfering quantum paths can be analogously applied to the state after $m - 1$ photon measurements. In this case, the probabilities are given by

$$p_{m-1,s}(t_m) = e^{-2(N-m+1)\gamma t_m} (e^{2\gamma t_m} - 1)^s\,, \tag{5.58}$$

where s characterises, as before, the number of ground state atoms before the first photon measurement [see Eqs. (5.48) and (5.54)]. Further, the normalisation is

$$\mathcal{N} = \binom{N}{m-1}^{-1/2}. \tag{5.59}$$

Now, let us count the interfering quantum paths. For each state with n_g many atoms in the ground state, the number of different final states can be obtained by distributing m ground states over $N - n_g + (m-1)$ previously excited states, i.e., $\mathcal{F} = \binom{N-n_g+(m-1)}{m}$. Moreover, the number of product states in a superposition state with n_g many atoms in the ground state can be counted to $\binom{N-n_g+(m-1)}{m-1}$ and the number of single quantum paths per product state

is $N - n_g$. Therefore, the number of quantum paths per final state reads

$$\mathcal{P}_{\mathcal{F}} = \frac{\binom{N-n_g+(m-1)}{m-1} \times (N-n_g)}{\binom{N-n_g+(m-1)}{m}} = m\,. \tag{5.60}$$

The conditional intensity after $m-1$ photon measurements is thus given by

$$\begin{aligned} G^{(1)}_{\hat{\rho}_{m-1}}(t_m) &= \sum_{s=0}^{N-m} p_{m-1,s}(t_m)\binom{N}{s}\mathcal{N}^2\mathcal{P}_{\mathcal{F}}^2\mathcal{F} \\ &= \sum_{s=0}^{N-m} e^{-2(N-m+1)\gamma t_m}(e^{2\gamma t_m}-1)^s\binom{N}{s} \times \binom{N}{m-1}^{-1} \times m^2 \times \binom{N-s}{m} \\ &= m(N-m+1)e^{-2\gamma t_m}\,. \end{aligned} \tag{5.61}$$

As can be seen, we obtain the same result for the conditional intensities as calculated via the quantum regression theorem in the previous subsection. However, by tracing the directional Dicke-like superradiant behaviour back to interfering quantum paths based on the generated dipole-dipole correlations, we have a clear physical interpretation. What remains is to show that the photon measurement indeed creates dipole-dipole correlations. Therefore, we analyse the role of the measurement process quantitatively in the next subsection. In this context, we also investigate the distance of the time-evolved state after m photon measurements to the symmetric subspace.

5.3.4 Role of the measurement process

As mentioned above, in this subsection, we have a closer look at the consequences of the conditional photon measurements.

Creation of dipole-dipole correlations

To verify that the conditional photon measurements create dipole-dipole correlations, we make use of the splitting of the intensity introduced in the second line of Eq. (5.23). Since the density operator is always block-diagonal with respect to the number of atoms in the ground state, there are no single-atom coherences, i.e., $\langle \hat{S}^{(\mu)}_{\pm}\rangle = 0$ for all $\mu \in \{1,...,N\}$. Therefore, the conditional intensities can be written as

$$G^{(1)}_{\hat{\rho}_{m-1}}(t_m) = n_{e,m-1}(t_m) + \sum_{\substack{\mu,\nu \\ \mu\neq\nu}} K(\hat{S}^{(\mu)}_{+}, \hat{S}^{(\nu)}_{-}, \hat{\rho}_{m-1}(t_m))\,. \tag{5.62}$$

With the number of product states $\binom{N-n_g+(m-1)}{m-1}$ and the number of excitations $N-n_g$ for a superposition state with n_g many ground state atoms after $m-1$ photon measurements,

the average number of excitations is given by

$$\begin{aligned} n_{e,m-1}(t_m) &= \sum_{s=0}^{N-m} p_{m-1,s}(t_m) \binom{N}{s} \binom{N}{m-1}^{-1} \binom{N-s}{m-1} [N-s-(m-1)] \\ &= (N-m+1)e^{-2\gamma t_m} \,. \end{aligned} \tag{5.63}$$

Now, by rewriting Eq. (5.62), the dipole-dipole correlations can be calculated as

$$\begin{aligned} \sum_{\substack{\mu,\nu \\ \mu\neq\nu}} K(\hat{S}_+^{(\mu)}, \hat{S}_-^{(\nu)}, \hat{\rho}_{m-1}(t_m)) &= G^{(1)}_{\hat{\rho}_{m-1}}(t_m) - n_{e,m-1}(t_m) = (m-1)(N-m+1)e^{-2\gamma t_m} \\ &= n_{e,m-1}(0)[N - n_{e,m-1}(0)]e^{-2\gamma t_m} \,. \end{aligned} \tag{5.64}$$

Thereby, the prefactor of the exponential function is equal to the dipole-dipole correlations of the symmetric Dicke state $|J, M\rangle$ with $n_{e,m-1}(0)$ many excitations [see Eq. (5.26)], which is not surprising since we already saw that $\hat{\rho}_{m-1}(0) = |J, M\rangle\langle J, M|$. We thus explicitly showed that the photon measurements create dipole-dipole correlations.

Distance to symmetric subspace

Besides creating dipole-dipole correlations, the photon measurement also projects the density operator closer to the symmetric subspace spanned by the symmetric Dicke states and thus enhances the emission of photons perpendicular to the atomic axis (directional superradiance of symmetric Dicke states [17]). To prove this quantitatively, we calculate the trace distance

$$T(\hat{\rho}_m, \hat{\rho}_{m,\mathrm{proj}}) = \frac{1}{2} \mathrm{Tr}\left[\sqrt{(\hat{\rho}_m - \hat{\rho}_{m,\mathrm{proj}})^\dagger (\hat{\rho}_m - \hat{\rho}_{m,\mathrm{proj}})}\right] \tag{5.65}$$

between the time-evolved state $\hat{\rho}_m$ after m conditional photon measurements and its projection onto the symmetric subspace

$$\hat{\rho}_{m,\mathrm{proj}} = \sum_{M,M'} |J, M\rangle\langle J, M|\hat{\rho}_m|J, M'\rangle\langle J, M'| \,. \tag{5.66}$$

For the detailed calculation, we refer the reader to Appendix G. Here, we state the final result reading

$$T(\hat{\rho}_m, \hat{\rho}_{m,\mathrm{proj}}) = \frac{1}{2} \binom{N}{m}^{-1} \sum_{n_g=0}^{N} \binom{N}{n_g} \mathcal{T}(m, n_g)[\mathcal{D}(m, n_g) - \mathcal{D}_{\mathrm{proj}}(m, n_g)] \,, \tag{5.67}$$

where the functions $\mathcal{T}(m, n_g)$, $\mathcal{D}(m, n_g)$, and $\mathcal{D}_{\mathrm{proj}}(m, n_g)$ are defined in Appendix G. We show the result of the measurement process in Fig. 5.6. Here, we plot the trace distance together with the conditional intensities against time for $N = 8$ atoms. We see that every time

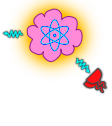

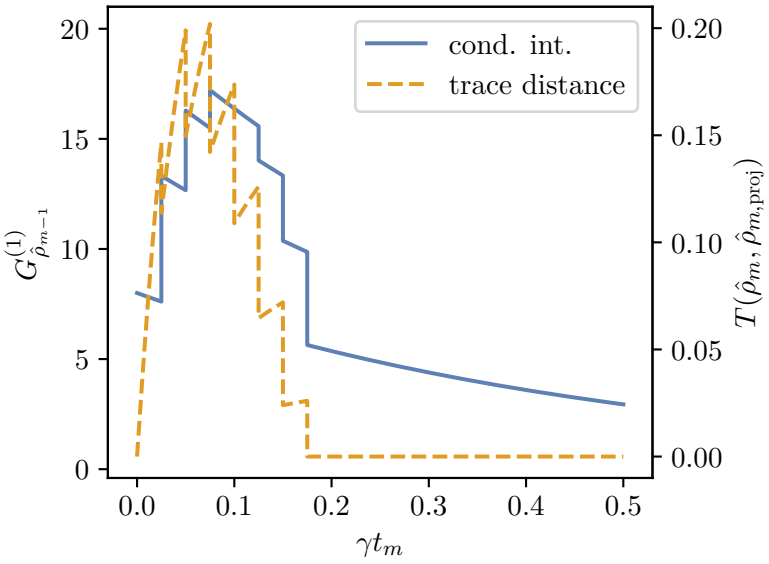

Figure 5.6: Conditional intensities (left axis) and trace distance (right axis) against time for $N = 8$ atoms. It can be clearly seen that the conditional photon measurements project the state closer to the symmetric subspace and thus enhance the directional emission leading to a Dicke-like superradiant radiation behaviour.

a photon is detected, the measurement projects the state closer to the symmetric subspace leading to an enhancement of the directional emission perpendicular to the atomic chain. Viewed in time, this leads to a Dicke-like superradiant radiation profile.

Let us conclude this subsection by noting again that the measurement process leads to the creation of dipole-dipole correlations, which enhance the (directional) emission of photons. Similar, in the small sample limit of Dicke superradiance, the superradiant burst is also based on the dipole-dipole correlations of the atoms. The question that arises is whether these correlations are classical correlations or quantum correlations, or even hint at entanglement. This will be the topic of the next section.

5.4 Dipole-dipole correlations - quantum or classical?

Before we come to the cases of Dicke superradiance and Dicke-like superradiance, we start by discussing an introductory example to explain the main issues.

5.4.1 Introductory example

Let us define the states

$$|P_\pm\rangle \coloneqq \alpha\,|g\rangle \pm \beta\,|e\rangle \tag{5.68}$$

with $\alpha, \beta \in \mathbb{R}$ and $\alpha^2 + \beta^2 = 1$. Now, consider the tensor product state $|P_{++}\rangle = |P_+\rangle \otimes |P_+\rangle$. In Ref. [76], we investigated the emitted (dimensionless) intensity of this state reading

$$I(\boldsymbol{r}) = 2\beta^2[1 + \alpha^2 \cos(\delta)] \tag{5.69}$$

with $\delta = -k_0 \hat{\boldsymbol{r}} \boldsymbol{R}_{12}$ as usual. Since the average number of excitations is given by $n_e = 2\beta^2$, we find a directional superradiant behaviour if both α and β are nonzero. Furthermore, since the state is a tensor product state, there are no dipole-dipole correlations. This implies that the origin of the superradiant emission can be addressed to the single-atom coherences of the atoms [see Eq. (5.23)]. In addition, the state is neither entangled nor possesses any classical or quantum correlations. Analogously, the superradiant behaviour of the tensor product state $|P_{--}\rangle = |P_-\rangle \otimes |P_-\rangle$ can be explained. But, what can be said about the mixed state

$$\hat{\rho}_{+-} = \frac{1}{2} |P_{++}\rangle\langle P_{++}| + \frac{1}{2} |P_{--}\rangle\langle P_{--}| \,, \tag{5.70}$$

i.e., the incoherent superposition of the introduced product states with equal weightings? The radiated intensity of this state reads

$$I(\boldsymbol{r}) = 2\beta^2[1 + \alpha^2 \cos(\delta)] \,, \tag{5.71}$$

i.e., it shows the same directional superradiance. Further, it is easy to verify that this state is not entangled. However, for this state the single-atom coherences are zero implying that the superradiant behaviour stems from dipole-dipole correlations. Thus, by incoherently superposing two classical states with no correlations but only single-atom coherences, we obtain a state without single-atom coherences, but with dipole-dipole correlations. By applying the formalism developed in Ref. [79], we can also identify whether these correlations are classical or quantum. We analytically calculate the mutual information $\mathcal{I}_{\hat{\rho}_{+-}}$ describing the total amount of correlations, the classical correlations $\mathcal{J}_{\hat{\rho}_{+-}}$, and the quantum discord $\mathcal{D}_{\hat{\rho}_{+-}}$ describing the amount of quantum correlations. Since the expressions are rather lengthy, we omit writing down the explicit results, but rather plot all three quantities against β in Fig. 5.7. We see that unless $\beta = 0$ or $\beta = 1$, the state always possesses correlations quantified by the mutual information $\mathcal{I}_{\hat{\rho}_{+-}}$. Furthermore, for almost the whole range, the classical correlations ($\mathcal{J}_{\hat{\rho}_{+-}}$) dominate over the quantum correlations ($\mathcal{D}_{\hat{\rho}_{+-}}$), only at the edges the quantum correlations do surpass the classical ones. A particular point is at $\beta = 1/\sqrt{2}$, where we have an equal superposition of the ground and excited state. Here, the correlations reach a maximum, however, these correlations are purely classical, i.e., $\mathcal{D}_{\hat{\rho}_{+-}} = 0$ at this point.
Let us now extent the foregoing discussion by considering an at first glance completely different state. For this, let us define the two states

$$|S\rangle := \frac{1}{\sqrt{2}}(|e, g\rangle + |g, e\rangle) \,, \tag{5.72}$$

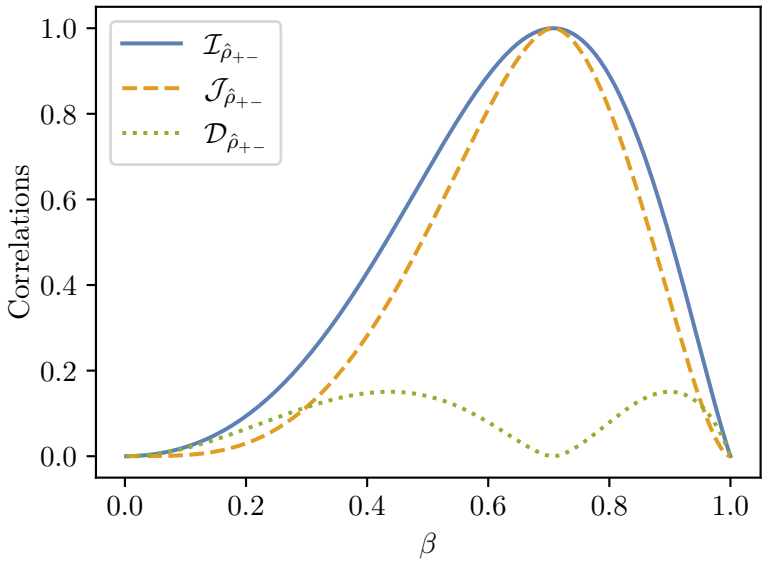

Figure 5.7: Total amount of correlations $\mathcal{I}_{\hat{\rho}_{+-}}$ together with the splitting in classical correlations $\mathcal{J}_{\hat{\rho}_{+-}}$ and quantum correlations $\mathcal{D}_{\hat{\rho}_{+-}}$ for the state $\hat{\rho}_{+-}$ against β. Only at the edges, the quantum correlations are higher than the classical correlations. A particular point is at $\beta = 1/\sqrt{2}$, where the correlations reach a maximum, but are solely classical, i.e., $\mathcal{D}_{\hat{\rho}_{+-}} = 0$ at this point.

$$|\Phi^+\rangle := \frac{1}{\sqrt{2}}(|g,g\rangle + |e,e\rangle)\,. \tag{5.73}$$

As can be easily verified, both states are maximally entangled states. Now, if we consider the incoherent superposition

$$\hat{\rho}_I = \frac{1}{2}\,|S\rangle\langle S| + \frac{1}{2}\,|\Phi^+\rangle\langle\Phi^+|\,, \tag{5.74}$$

we would intuitively expect that this state is also an entangled state. However, by writing the density matrix $\hat{\rho}_{+-}$ of Eq. (5.70) in its spectral decomposition given by

$$\hat{\rho}_{+-} = w_1\,|v_1\rangle\langle v_1| + w_2\,|v_2\rangle\langle v_2|\,, \tag{5.75}$$

where the eigenvalues are

$$w_1 = \alpha^4 + \beta^4\,, \tag{5.76}$$

$$w_2 = 2\alpha^2\beta^2\,, \tag{5.77}$$

and the corresponding orthonormal eigenvectors read

$$|v_1\rangle = \frac{1}{\sqrt{\alpha^4+\beta^4}}(\alpha^2\,|g,g\rangle + \beta^2\,|e,e\rangle)\,, \tag{5.78}$$

$$|v_2\rangle = \frac{1}{\sqrt{2}}(|e,g\rangle + |g,e\rangle)\,, \tag{5.79}$$

we find that $\hat{\rho}_I = \hat{\rho}_{+-}$ for $\alpha = \beta = 1/\sqrt{2}$. Therefore, the state $\hat{\rho}_I$ is actually an unentangled state. Even more, it possesses no quantum correlations at all, but only classical correlations. This example clearly demonstrates the issue of mixed states. The incoherent superposition of entangled states does not have to be an entangled state since entanglement is sublinear.

5.4.2 Dicke superradiance vs. Dicke-like superradiance

After having discussed the simple example of the previous subsection, let us now come back to Dicke superradiance on the one hand and to the engineered Dicke-like superradiance based on conditional photon measurements on the other hand. We start with the simplest case of only two atoms and afterwards conclude the entire chapter by analysing the general N atom case.

Two atoms

In the following, we investigate the situation of *two* atoms in more detail both in the case of Dicke superradiance and in the case of distant non-interacting atoms. For two atoms, the amount of entanglement can be quantified by the so-called concurrence. As the calculation shows, in the case of Dicke superradiance, the density matrix $\hat{\rho}(t)$ is actually unentangled for all times t ($C_{\hat{\rho}} = 0$, see left plot of Fig. 5.8). However, by determining the mutual information $\mathcal{I}_{\hat{\rho}}$, the classical correlations $\mathcal{J}_{\hat{\rho}}$, and the quantum discord $\mathcal{D}_{\hat{\rho}}$, we find that the state develops quantum correlations, which are always higher than the classical correlations (see left plot of Fig. 5.8). Before we come to the case of distant atoms, let us note that, as can be seen, the quantum and classical correlations show a small kink at around $\gamma t \approx 0.46$. However, this kink is an artefact of the calculation, which is based on Ref. [79]. As was later shown, the general formula of the quantum discord presented in Ref. [79] is not entirely correct, i.e., it does not capture all of the extrema [80]. But, the obtained results are approximately correct with a very small worst case error [81, 82]. Further, by referring to Ref. [83], we can state that our calculations of the correlations are completely correct up to $\gamma t \approx 0.45$, i.e., up to around the kink.

Now, in the case of distant atoms, it can be easily shown that the state before the measurement is a separable state that possesses no correlations at all. Therefore, we consider immediately the state after the first photon measurement $\hat{\rho}_1(t_2)$. As can be seen in the right plot of Fig. 5.8, this conditional state possesses quantum correlations $\mathcal{D}_{\hat{\rho}_1}$ at any point in time,

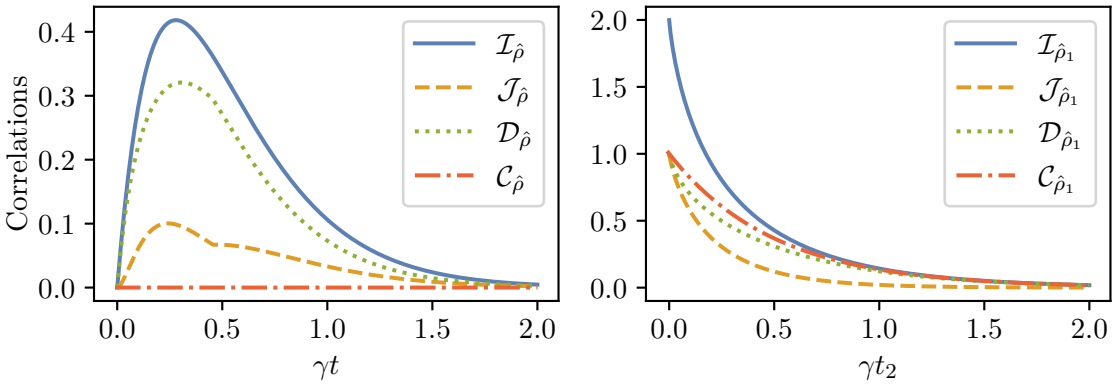

Figure 5.8: In the left plot, we show the mutual information $\mathcal{I}_{\hat{\rho}}$, the classical correlations $\mathcal{J}_{\hat{\rho}}$, the quantum correlations $\mathcal{D}_{\hat{\rho}}$, and the entanglement $C_{\hat{\rho}}$ as a function of time for the two-atom density matrix in the case of Dicke superradiance. As can be seen, the state is unentangled for all times, but develops quantum correlations, which are always higher than the classical ones. In the right plot, we show the mutual information $\mathcal{I}_{\hat{\rho}_1}$, the classical correlations $\mathcal{J}_{\hat{\rho}_1}$, the quantum correlations $\mathcal{D}_{\hat{\rho}_1}$, and the entanglement $C_{\hat{\rho}_1}$ as a function of time for the two-atom density matrix after the first conditional photon measurement in the case of distant non-interacting atoms. We find that the state possesses always quantum correlations surpassing the classical correlations. Even more, the conditional state is always entangled.

which are always higher than the classical correlations $\mathcal{J}_{\hat{\rho}_1}$, except for the time $t_2 = 0$, where both coincide. But even more, as we show by calculating the concurrence $C_{\hat{\rho}_1}$, which is maximal for $t_2 = 0$ and then decays exponentially with the single-atom decay rate, in the case of conditional photon measurements, we create an entangled state.

N atoms

After the detailed discussion of the two-atom case, let us now come to the general case of N atoms. We note that for a general mixed state of N qubits, it seems rather hopeless to determine its (multipartite) entanglement or correlation splitting since both are still not well understood. However, regarding entanglement, one can construct so-called entanglement witnesses (see Appendix D), which are more easily accessible. Here, a negative value of the expectation value of the entanglement witness indicates entanglement, whereas for positive values no conclusion can be drawn. Even more, in the case of Dicke superradiance, one can actually make statements about the separability of the density operator due to its special form as an incoherent superposition of symmetric Dicke states [18].
But let us first come back to the entanglement witnesses. In Appendix D, we introduce an entanglement witness, which is based on the so-called structure factor, and calculate it for the case of Dicke superradiance. Thereby, we choose the parameters such to detect symmetric Dicke states. The obtained result is shown in the bottom plot of Fig. 5.9. As a reference,

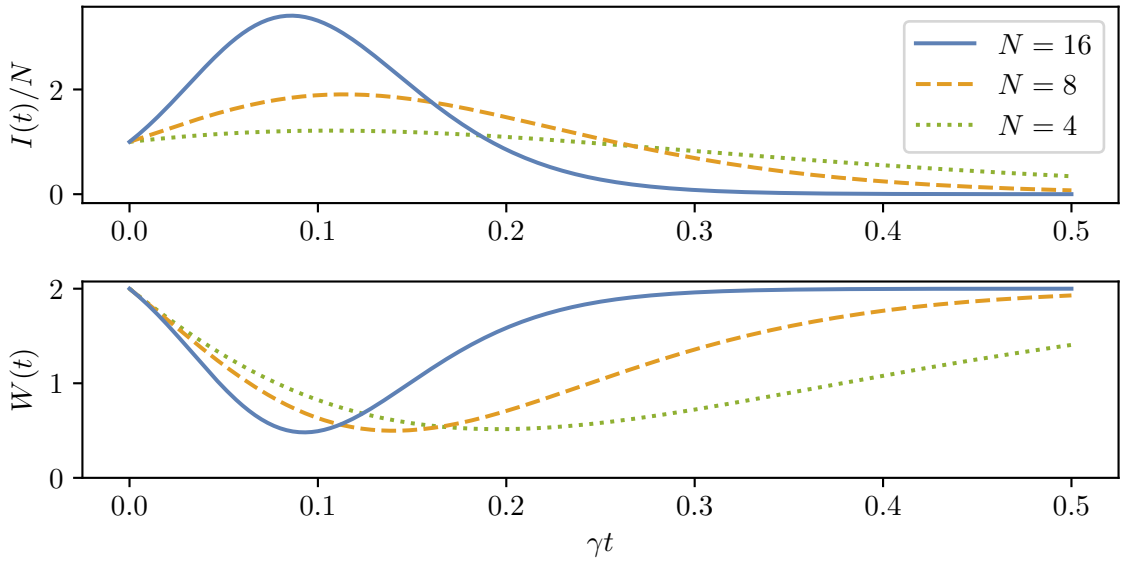

Figure 5.9: Top: Normalised intensity in the case of Dicke superradiance as a reference. Bottom: Expectation value of the entanglement witness calculated in Appendix D. As can be inferred from the figure, even around the maximal value of the superradiant burst, where the entanglement witness works best, no entanglement of the state is indicated.

we also plot the normalised intensity in the top plot. As we can see, even around the maximum of the superradiant burst, where the population of Dicke states with $M \approx 0$ is highest and the entanglement witness works best, the entanglement witness does not indicate any entanglement. Even more, as already teasered, we can make use of the separability equations developed in Ref. [18] and explained in more detail in Appendix D.6 to numerically show that the state is separable in the case of Dicke superradiance. In this context, we extend the work of Ref. [18] up to an atom number of $N = 16$. In Fig. 5.10, we show the mapping of the state obtained from the time evolution in the small sample limit to a separable state. Since all parameters x_j, y_j lay between 0 and 1 for all times γt, the state mapping is valid and demonstrates that the state is separable for all times γt in the case of Dicke superradiance (see details in Appendix D).

Now, let us consider the case of distant non-interacting atoms, but influenced by conditional photon measurements, and let us calculate the expectation value of the same entanglement witness for this system. The details of the calculation are shown in Appendix D. Here, we rather show the result for the case of $N = 8$ atoms in Fig. 5.11. In the left plot, we show the conditional intensity (blue solid line and left axis) together with the expectation value of the entanglement witness (dashed orange line and right axis). As can be seen, for intermediate times γt_m, the entanglement witness is negative and thus indicates entanglement, even though the value is rather small. However, by considering the right plot, where we illustrate the expectation value of the entanglement witness for all states $\hat{\rho}_{m-1}$ over the whole range of times,

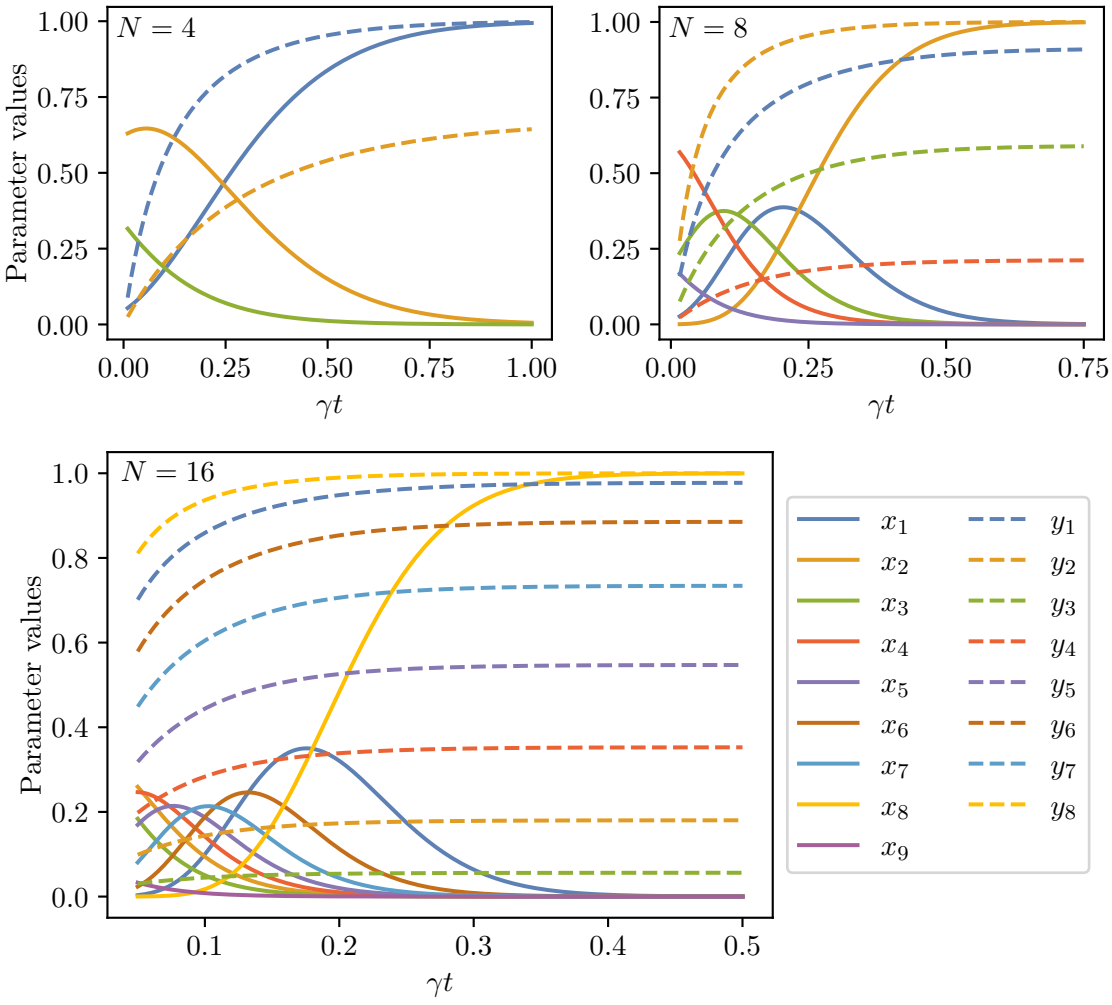

Figure 5.10: Mapping of the state obtained in the case of Dicke superradiance to a separable state for $N \in \{4, 8, 16\}$ atoms. As can be seen, all parameters x_j, y_j lay between 0 and 1 for all times implying that the mapping to the separable state is valid. Thus, in the case of Dicke superradiance, the time-evolved state, which is an incoherent superposition of symmetric Dicke states, is separable, i.e., not entangled.

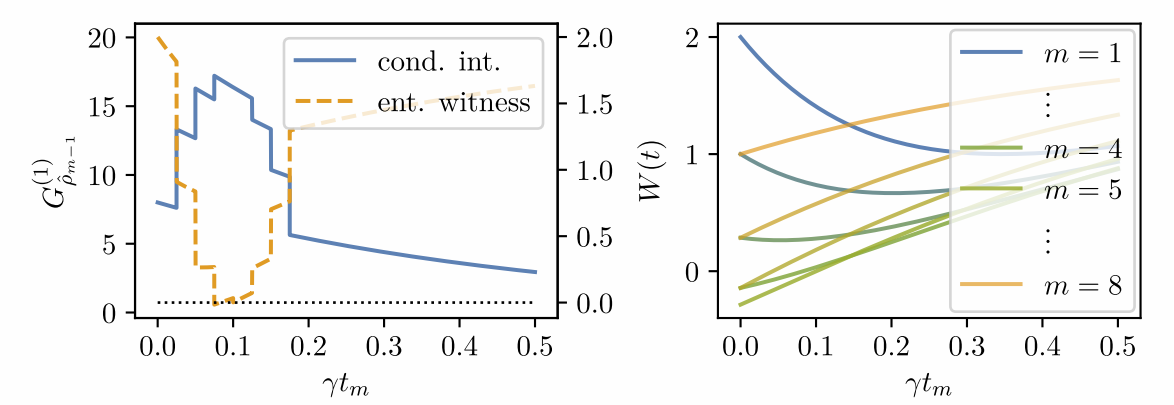

Figure 5.11: On the left, we plot the conditional intensity (blue solid line and left axis) together with the expectation value of the entanglement witness (orange dashed line and right axis). As can be inferred from the figure, for intermediate values of γt_m, the conditional state is entangled, characterised by a negative expectation value of the entanglement witness. On the right, we plot the expectation value of the entanglement witness for all conditional states $\hat{\rho}_{m-1}$, but starting from the time $\gamma t_m = 0$. As can be seen, for some of the conditional states (around $M \approx 0$), the entanglement witness clearly indicates entanglement. This allows to enhance the amount of entanglement and still to obtain a Dicke-like superradiant burst by properly engineering the times of the photon measurements.

i.e., starting from $\gamma t_m = 0$, we recognise two points. First, for some of the post-measurement states (around $M \approx 0$), the entanglement witness clearly indicates entanglement. Thus, by engineering the times of the photon measurements properly, one can enhance the amount of entanglement and still obtain a Dicke-like superradiant burst. Second, even though all states except $m = 1$ are entangled at the time $\gamma t_m = 0$, since we simply have pure symmetric Dicke states at that time, the entanglement witness does not rigorously indicate entanglement. Thus, the conditional states may be entangled, even though the entanglement witness does not detect the entanglement.

Let us conclude this section by summarising the main points of the entanglement and correlation investigations. In the case of two atoms, the superradiant behaviour in the Dicke superradiance setup is based on dipole-dipole correlations, which we were able to trace back to quantum correlations that the state develops over time. Strictly speaking, the state possesses quantum and classical correlations, which together are the origin of the enhanced radiation. We note that also in the case of a single symmetric Dicke state, which is an entangled state, the superradiant emission, strictly speaking, stems from quantum and classical correlations equally contributing, since for pure states the amount of entanglement, quantum correlations, and classical correlations is completely equal. Similar, in the case of two distant atoms with conditional photon measurements, the directional superradiant emission of photons can also be explained by both quantum and classical correlations, whereby the quantum correlations

dominate. However, here, we can trace the radiation behaviour even back to entanglement of the two atoms. Afterwards, we analysed the situation of N atoms, where similar conclusions can be drawn. In the case of distant non-interacting atoms, we demonstrated that the state becomes entangled via the conditional photon measurements. Thus, it possesses quantum correlations, which the superradiant emission is based on. In the case of Dicke superradiance, however, one can show that the state is separable at any time. Nevertheless, it may develop quantum correlations in the course of photon emission. Therefore, we finally note that in both cases a thorough analysis of the amount of correlations needs still to be done.

After discussing in this chapter how an ensemble of distant non-interacting atoms can be influenced by photon measurements, in the next chapter, we analyse the statistics of such independent emitters in more detail and in particular investigate under which conditions such an ensemble of atoms emits light with a statistics similar to the one of a thermal source.

6 Classical and non-classical features of the light emitted by an independent atomic ensemble

To speak of nonclassical states of light might seem an oxymoron. After all, aren't all states of light quantum mechanical? Well, yes, all states of light are quantum mechanical, but, waxing Orwellian, it turns out that some states are more quantum mechanical than others.

– Christopher C. Gerry and Peter L. Knight

Inspired by the famous line "all animals are equal, but some animals are more equal than others" in the beast fable *Animal Farm* by George Orwell, Christopher C. Gerry and Peter L. Knight speak of states of light that are more quantum mechanical than others (see quote). This is based on the fact that there exist states, for which the so-called Glauber-Sudarshan P function does not describe a proper probability distribution, but is negative in some regions of phase space or is more singular than a delta function. These states are particularly desirable in several fields, e.g., in quantum information processing, in the context of quantum parameter estimation theory, and in quantum simulation and quantum computing [84–86]. In contrast, in the case of 'classical' states, the Glauber-Sudarshan P function is a true (classical) probability distribution. In the first section of this chapter, we recapitulate the Glauber-Sudarshan P-representation, define the notion of classical and non-classical or quantum light, establish the relation to the normalised second-order photon correlation function, and discuss a particular class of classical states, namely thermal states.

6.1 Classical light and quantum light

In this section, we define some general notions needed for the next sections. We start by introducing the so-called Glauber-Sudarshan P-representation. To simplify the notation, we consider a single mode in the following. However, all derivations can easily be extended to the multi-mode case.

6.1.1 Glauber-Sudarshan *P*-representation

In many cases, we can write the density operator $\hat{\rho}$ as a function of products of the annihilation and creation operators $\hat{a}$ and $\hat{a}^\dagger$. By rearranging the operators, we can bring the density operator in anti-normal order, i.e., all annihilation operators to the left of all creation operators. The density operator then reads [87]

$$\hat{\rho} = \sum_{m,n} c_{mn} \hat{a}^m [\hat{a}^\dagger]^n \,. \tag{6.1}$$

Inserting an identity $\mathbb{1} = \frac{1}{\pi} \int d^2\alpha \, |\alpha\rangle\langle\alpha|$, we obtain

$$\hat{\rho} = \int d^2\alpha \, \frac{1}{\pi} \sum_{m,n} c_{mn} \alpha^m [\alpha^*]^n \, |\alpha\rangle\langle\alpha| = \int d^2\alpha \, P(\alpha) \, |\alpha\rangle\langle\alpha| \,, \tag{6.2}$$

where

$$P(\alpha) = \frac{1}{\pi} \sum_{m,n} c_{mn} \alpha^m [\alpha^*]^n \tag{6.3}$$

is the so-called Glauber-Sudarshan P function. Since $\hat{\rho}$ is Hermitian and $\mathrm{Tr}[\hat{\rho}] = 1$, the P function is real and normalised to one, i.e., $\int d^2\alpha \, P(\alpha) = 1$.

6.1.2 Optical equivalence theorem

Consider an operator in normal order, i.e., all annihilation operators to the right of all creation operators, written as

$$\hat{g}^{(N)}(\hat{a}, \hat{a}^\dagger) = \sum_{m,n} \tilde{g}_{mn} [\hat{a}^\dagger]^m \hat{a}^n \,. \tag{6.4}$$

By using the Glauber-Sudarshan P-representation, the expectation value of this operator can be calculated as [87]

$$\langle \hat{g}^{(N)}(\hat{a}, \hat{a}^\dagger) \rangle = \mathrm{Tr}\left[\hat{\rho} \hat{g}^{(N)}(\hat{a}, \hat{a}^\dagger) \right] = \int d^2\alpha \, P(\alpha) g^{(N)}(\alpha, \alpha^*) = \langle g^{(N)}(\alpha, \alpha^*) \rangle \,. \tag{6.5}$$

That is, we can write the expectation value as an expectation value of the corresponding phase space function $g^{(N)}(\alpha, \alpha^*)$ with $P(\alpha)$ as weighting function. This is the so-called optical equivalence theorem and suggests to interpret $P(\alpha)$ as a probability density. However, there exist states, for which the P function is negative in some regions of phase space or is more singular than a delta function. Therefore, on the one hand, the P function is usually called a quasi-probability density, and on the other hand, the states for which the P function is not a true probability density are called non-classical.

6.1.3 Relation between non-classical light and the normalised second-order photon correlation function

If only the free field is present without any atoms as sources, using Eq. (3.29), the normalised second-order photon correlation function for a single mode and time difference $\tau = t_2 - t_1 = 0$ can be written as [88]

$$g^{(2)}(\tau = 0) = \frac{\langle \hat{a}^\dagger \hat{a}^\dagger \hat{a}\hat{a} \rangle}{\langle \hat{a}^\dagger \hat{a} \rangle^2} = 1 + \frac{\langle \hat{a}^\dagger \hat{a}^\dagger \hat{a}\hat{a} \rangle - \langle \hat{a}^\dagger \hat{a} \rangle^2}{\langle \hat{a}^\dagger \hat{a} \rangle^2} = 1 + \frac{\int d^2\alpha \, P(\alpha) \left[|\alpha|^2 - \langle \hat{a}^\dagger \hat{a} \rangle \right]^2}{\langle \hat{a}^\dagger \hat{a} \rangle^2} . \tag{6.6}$$

So, for a classical state for which $P(\alpha) \geq 0$ applies everywhere, we immediately find $g^{(2)}(0) \geq 1$. However, for a non-classical state for which $P(\alpha) < 0$ holds in some regions, it is possible to have $g^{(2)}(0) < 1$. Therefore, a value of the normalised second-order photon correlation function less than 1 implies that we have quantum light.

6.1.4 Thermal states and Gaussian Moment Theorem

In this last subsection, we discuss a particular class of classical states of light, so-called thermal states. In the case of the free electromagnetic field and a single mode, the Hamiltonian reads $\hat{H} = \hbar\omega \hat{a}^\dagger \hat{a}$. Therefore, the thermal states can be written as

$$\hat{\rho} = \frac{e^{-\beta \hat{H}}}{\mathrm{Tr}[e^{-\beta \hat{H}}]} = \int d^2\alpha \, \underbrace{\frac{1}{\pi \langle \hat{a}^\dagger \hat{a} \rangle} e^{-\frac{|\alpha|^2}{\langle \hat{a}^\dagger \hat{a} \rangle}}}_{= P(\alpha)} |\alpha\rangle\langle\alpha| \, , \tag{6.7}$$

where $\beta = \frac{1}{k_B T}$ with k_B the Boltzmann constant and T the temperature. Now, let us consider M independent modes, such that the total density operator is simply the tensor product of the individual density operators. Then, the P function becomes the product of the individual P functions, i.e.,

$$P(\alpha_1, ..., \alpha_M) = \prod_{m=1}^{M} \frac{1}{\pi \langle \hat{a}_m^\dagger \hat{a}_m \rangle} e^{-\frac{|\alpha_m|^2}{\langle \hat{a}_m^\dagger \hat{a}_m \rangle}} . \tag{6.8}$$

Thus, we see that the P function for thermal states is a multivariate Gaussian function, for which the so-called Gaussian Moment Theorem applies. It states that all higher-order correlations of the complex variates $\alpha_1, ..., \alpha_M$ can be written as a sum of products of second-order correlations (second order in the variates). Concretely, let $i_1, ..., i_n$ be a set of n indices and $j_1, ..., j_m$ be a set of m indices, the Gaussian Moment Theorem for zero-mean Gaussian

complex variates reads [87]

$$\langle \alpha_{i_1}^* ... \alpha_{i_n}^* \alpha_{j_m} ... \alpha_{j_1} \rangle = \begin{cases} 0\,, & n \neq m\,, \\ \sum\limits_{\substack{\text{all } n! \\ \text{pairings}}} \langle \alpha_{i_1}^* \alpha_{j_1} \rangle ... \langle \alpha_{i_n}^* \alpha_{j_n} \rangle\,, & n = m\,. \end{cases} \tag{6.9}$$

In terms of (normalised) higher-order photon correlation functions, this theorem implies that in the case of thermal light sources, all higher orders can be expressed in terms of the so-called (normalised) first-order field correlation function [6]

$$G^{(1)}(\boldsymbol{r}_1, t_1; \boldsymbol{r}_2, t_2) \coloneqq \langle \hat{E}^{(-)}(\boldsymbol{r}_1, t_1) \hat{E}^{(+)}(\boldsymbol{r}_2, t_2) \rangle\,, \tag{6.10}$$

$$g^{(1)}(\boldsymbol{r}_1, t_1; \boldsymbol{r}_2, t_2) \coloneqq \frac{\langle \hat{E}^{(-)}(\boldsymbol{r}_1, t_1) \hat{E}^{(+)}(\boldsymbol{r}_2, t_2) \rangle}{\sqrt{\langle \hat{E}^{(-)}(\boldsymbol{r}_1, t_1) \hat{E}^{(+)}(\boldsymbol{r}_1, t_1) \rangle \langle \hat{E}^{(-)}(\boldsymbol{r}_2, t_2) \hat{E}^{(+)}(\boldsymbol{r}_2, t_2) \rangle}}\,. \tag{6.11}$$

Explicitly, the Gaussian Moment Theorem for photon correlation functions reads

$$G^{(m)}(\boldsymbol{r}_1, t_1; ...; \boldsymbol{r}_m, t_m) = \sum_{\sigma \in S_m} \prod_{p=1}^{m} G^{(1)}(\boldsymbol{r}_p, t_p; \boldsymbol{r}_{\sigma(p)}, t_{\sigma(p)})\,, \tag{6.12}$$

$$g^{(m)}(\boldsymbol{r}_1, t_1; ...; \boldsymbol{r}_m, t_m) = \sum_{\sigma \in S_m} \prod_{p=1}^{m} g^{(1)}(\boldsymbol{r}_p, t_p; \boldsymbol{r}_{\sigma(p)}, t_{\sigma(p)})\,, \tag{6.13}$$

where S_m denotes the set of all permutations of m elements. We note that the correlation functions on the left are photon correlation functions, while the correlation functions on the right are field correlation functions. In the next section, we investigate under which conditions the light emitted by an ensemble of independent atoms shows thermal light statistics in terms of higher-order photon correlation functions. Therefore, we identify a parameter regime wherein the Gaussian Moment Theorem approximately holds.

6.2 Classical feature - Gaussian Moment Theorem

Let us consider N two-level atoms with excited state $|e\rangle$ and ground state $|g\rangle$. Since we investigate the behaviour of the *normalised* mth-order photon correlation function, we neglect the dipole radiation pattern and a general constant prefactor, which would provide a meaningful physical unit. But, as usual, we account for the different accumulated travelling phases in the positive electric source field operator. Furthermore, we analyse the stationary case, i.e., all photon measurements are performed at the same time $t = 0$. We therefore use the scalar positive electric source field operator

$$\hat{E}_S^{(+)}(\boldsymbol{r}) = \sum_{\mu=1}^{N} e^{-ik_0 \hat{\boldsymbol{r}} \boldsymbol{R}_\mu} \hat{S}_-^{(\mu)}\,, \tag{6.14}$$

where we most of the time assume that the positions of the atoms $\boldsymbol{R}_\mu$, $\mu \in \{1, ..., N\}$, are randomly distributed, but fixed. For convenience, we define $\boldsymbol{k} \coloneqq k_0 \hat{\boldsymbol{r}}$ and write the positive electric source field operator as a function of $\boldsymbol{k}$ instead of $\boldsymbol{r}$ as

$$\hat{E}_S^{(+)}(\boldsymbol{k}) = \sum_{\mu=1}^{N} e^{-i\boldsymbol{k}\boldsymbol{R}_\mu} \hat{S}_-^{(\mu)} \,. \tag{6.15}$$

We note that if the atoms are driven by a plane wave laser field with wave vector $\boldsymbol{k}_L$, we can do a basis transformation to include the additional phase coming from the laser in the electric field operators instead of the atomic states. In this case, the positive electric source field operator would read (see Appendix J)

$$\hat{E}_S^{(+)}(\boldsymbol{r}) = \sum_{\mu=1}^{N} e^{-i(k_0\hat{\boldsymbol{r}}-\boldsymbol{k}_L)\boldsymbol{R}_\mu} \hat{S}_-^{(\mu)} \,. \tag{6.16}$$

Therefore, we would define the momentum transfer vector $\boldsymbol{k} \coloneqq k_0\hat{\boldsymbol{r}} - \boldsymbol{k}_L$ to obtain again the same form as in Eq. (6.15). This means that the case of an atomic ensemble driven by a plane wave laser field can be easily included by a redefinition of $\boldsymbol{k}$.

As already mentioned, in what follows, we only consider equal-time photon correlation functions. Moreover, we consider only atomic tensor product states, i.e., $\hat{\rho} = \otimes_{\mu=1}^{N} \hat{\rho}_\mu$, where $\hat{\rho}_\mu$ denotes the state of atom μ. In addition, we assume that the differences of the atomic expectation values are 'small' compared to the mean values over all atoms. We define the mean values as

$$\bar{S}_\pm \coloneqq \frac{1}{N} \sum_{\mu=1}^{N} \langle \hat{S}_\pm^{(\mu)} \rangle \,, \tag{6.17}$$

$$\overline{S_+ S_-} \coloneqq \frac{1}{N} \sum_{\mu=1}^{N} \langle \hat{S}_+^{(\mu)} \hat{S}_-^{(\mu)} \rangle \,, \tag{6.18}$$

with which we can concretise the meaning of 'small' by the conditions

$$\frac{\left| \langle \hat{S}_\pm^{(\mu)} \rangle - \langle \hat{S}_\pm^{(\nu)} \rangle \right|}{\left| \bar{S}_\pm \right|} \ll 1 \,, \forall \mu \neq \nu \in \{1, ..., N\} \,, \tag{6.19}$$

$$\frac{\left| \langle \hat{S}_+^{(\mu)} \hat{S}_-^{(\mu)} \rangle - \langle \hat{S}_+^{(\nu)} \hat{S}_-^{(\nu)} \rangle \right|}{\overline{S_+ S_-}} \ll 1 \,, \forall \mu \neq \nu \in \{1, ..., N\} \,. \tag{6.20}$$

With these foregoing definitions, we now investigate the conditions that must be satisfied to obtain thermal statistics, i.e., the Gaussian Moment Theorem, in this atomic ensemble.

6.2.1 Conditions for obtaining thermal light statistics

Let us consider the unnormalised mth-order photon correlation function. Since $[\hat{S}_{\pm}^{(\mu)}]^n = 0$ for $n \geq 2$, we can write

$$\begin{aligned} G^{(m)}(\boldsymbol{k}_1, ..., \boldsymbol{k}_m) = & \sum_{\substack{\mu_1,...,\mu_m=1,\\ \text{mutually different}}}^{N} \sum_{\substack{\nu_1,...,\nu_m=1,\\ \text{mutually different}}}^{N} e^{i\boldsymbol{k}_1\boldsymbol{R}_{\mu_1}} ... e^{i\boldsymbol{k}_m\boldsymbol{R}_{\mu_m}} e^{-i\boldsymbol{k}_m\boldsymbol{R}_{\nu_m}} ... e^{-i\boldsymbol{k}_1\boldsymbol{R}_{\nu_1}} \times \\ & \langle \hat{S}_{+}^{(\mu_1)} ... \hat{S}_{+}^{(\mu_m)} \hat{S}_{-}^{(\nu_m)} ... \hat{S}_{-}^{(\nu_1)} \rangle \\ = & \sum_{\substack{\mu_1,...,\mu_m=1,\\ \text{mutually different}}}^{N} \sum_{\nu_1<...<\nu_m=1}^{N} \sum_{\sigma\in S_m} \prod_{p=1}^{m} e^{i\boldsymbol{k}_p\boldsymbol{R}_{\mu_p}} e^{-i\boldsymbol{k}_{\sigma(p)}\boldsymbol{R}_{\nu_p}} \langle \hat{S}_{+}^{(\mu_p)} \hat{S}_{-}^{(\nu_p)} \rangle \ . \end{aligned} \tag{6.21}$$

On the other hand, the first-order field correlation function reads

$$G^{(1)}(\boldsymbol{k}_1, \boldsymbol{k}_2) = \sum_{\mu,\nu=1}^{N} e^{i\boldsymbol{k}_1\boldsymbol{R}_{\mu}} e^{-i\boldsymbol{k}_2\boldsymbol{R}_{\nu}} \langle \hat{S}_{+}^{(\mu)} \hat{S}_{-}^{(\nu)} \rangle \ , \tag{6.22}$$

such that

$$\begin{aligned} \sum_{\sigma\in S_m} \prod_{p=1}^{m} G^{(1)}(\boldsymbol{k}_p, \boldsymbol{k}_{\sigma(p)}) = & \sum_{\sigma\in S_m} \prod_{p=1}^{m} \sum_{\mu,\nu=1}^{N} e^{i\boldsymbol{k}_p\boldsymbol{R}_{\mu}} e^{-i\boldsymbol{k}_{\sigma(p)}\boldsymbol{R}_{\nu}} \langle \hat{S}_{+}^{(\mu)} \hat{S}_{-}^{(\nu)} \rangle \\ = & \sum_{\mu_1,...,\mu_m=1}^{N} \sum_{\nu_1,...,\nu_m=1}^{N} \sum_{\sigma\in S_m} \prod_{p=1}^{m} e^{i\boldsymbol{k}_p\boldsymbol{R}_{\mu_p}} e^{-i\boldsymbol{k}_{\sigma(p)}\boldsymbol{R}_{\nu_p}} \langle \hat{S}_{+}^{(\mu_p)} \hat{S}_{-}^{(\nu_p)} \rangle \ . \end{aligned} \tag{6.23}$$

Comparing Eq. (6.21) to Eq. (6.23), we find two differences, namely the different sums

$$\sum_{\substack{\mu_1,...,\mu_m=1,\\ \text{mutually different}}}^{N} \leftrightarrow \sum_{\mu_1,...,\mu_m=1}^{N} \ , \tag{6.24}$$

$$\sum_{\nu_1<...<\nu_m=1}^{N} \leftrightarrow \sum_{\nu_1,...,\nu_m=1}^{N} \ . \tag{6.25}$$

Now, with the definitions

$$S_1(N, m) \coloneqq \sum_{\mu_1,...,\mu_m=1}^{N} 1 = N^m \, , \tag{6.26}$$

$$S_2(N, m) \coloneqq \sum_{\substack{\mu_1,...,\mu_m=1,\\ \text{mutually different}}}^{N} 1 = m! \binom{N}{m} \, , \tag{6.27}$$

$$S_3(N,m) \coloneqq \sum_{\mu_1<\ldots<\mu_m=1}^{N} 1 = \binom{N}{m}\,, \tag{6.28}$$

we find that

$$\lim_{N\to\infty}\left(\frac{S_1(N,m)-S_2(N,m)}{S_1(N,m)}\right) = 0\,, \tag{6.29}$$

$$\lim_{N\to\infty}\left(\frac{S_1(N,m)-S_3(N,m)}{S_1(N,m)}\right) = 1-\frac{1}{m!}\,. \tag{6.30}$$

This means, the relative error between the first two sums vanishes for $N\to\infty$, whereas the relative error between the first and the third sum is finite for $m>2$. This implies that we can not properly approximate the first sum by the third sum in the thermodynamic limit for $m>2$. However, the difference in the correlation functions is only present if there are nonzero single-atom coherences $\langle\hat{S}_{\pm}^{(\mu)}\rangle \neq 0$. If it would hold that $\langle\hat{S}_{+}^{(\mu_p)}\hat{S}_{-}^{(\nu_p)}\rangle = \langle\hat{S}_{+}^{(\mu_p)}\hat{S}_{-}^{(\mu_p)}\rangle\,\delta_{\mu_p,\nu_p}$, the sums over the νs disappear and we can potentially obtain the Gaussian Moment Theorem. Therefore, we now investigate the ratio of the coherences and the populations of the atoms. If the atoms have randomly distributed positions $\boldsymbol{R}_\mu$, the sums over the phases $e^{i\boldsymbol{k}\boldsymbol{R}_\mu}$ statistically scale as $\sqrt{N}$. However, in the direction $\boldsymbol{k}=\boldsymbol{0}$, the sums over these phases scale as N, such that this direction gives a particular strong constraint. We note, however, that there might be some outlying directions, which are even more disadvantageous. Nevertheless, to obtain a condition, which is a strict condition almost everywhere (and can even be loosened in most directions), we consider the direction $\boldsymbol{k}=\boldsymbol{0}$. Here, we have

$$\begin{aligned} G^{(m)}(\boldsymbol{0},\ldots,\boldsymbol{0}) &= \sum_{\mu_1,\ldots,\mu_m,\nu_1,\ldots,\nu_m=1}^{N} \langle\hat{S}_{+}^{(\mu_1)}\ldots\hat{S}_{+}^{(\mu_m)}\hat{S}_{-}^{(\nu_m)}\ldots\hat{S}_{-}^{(\nu_1)}\rangle \\ &\approx \sum_{j=0}^{m}\binom{m}{j}^2 j!(2m-j)!\binom{N}{2m-j}(\overline{S_+S_-})^j\left(\bar{S}_+\bar{S}_-\right)^{m-j}\,, \end{aligned} \tag{6.31}$$

where we write an approximation sign since we use the mean values in the second line. We note that if all N atoms are in the same state, both sides are exactly equal. To determine under which condition the contributions from the coherences can be neglected compared to those from the populations, we calculate the ratio between the terms corresponding to $j-1$ and j, which is given by

$$\frac{\bar{S}_+\bar{S}_-}{\overline{S_+S_-}}\frac{j(j+N-2m)}{(m-j+1)^2}\,. \tag{6.32}$$

To be able to keep only the term with $j = m$, this ratio has to be much smaller than 1 for all j. The maximal constraint is obtained for $j = m$. Therefore, we require

$$\frac{\langle \hat{S}_+^{(\mu)} \rangle \langle \hat{S}_-^{(\mu)} \rangle}{\langle \hat{S}_+^{(\mu)} \hat{S}_-^{(\mu)} \rangle} m(N-m) \ll 1 \Leftrightarrow \frac{\langle \hat{S}_+^{(\mu)} \rangle \langle \hat{S}_-^{(\mu)} \rangle}{\langle \hat{S}_+^{(\mu)} \hat{S}_-^{(\mu)} \rangle} \ll \frac{1}{m(N-m)} \,, \forall \mu \in \{1, ..., N\} \,. \tag{6.33}$$

However, we note that if one is only interested in the *normalised* mth-order photon correlation function, a weaker condition based on the second-order correction instead of the first-order correction is actually sufficient (see Appendix H). Nevertheless, if condition (6.33) is fulfilled, we can approximate Eq. (6.21) almost everywhere in leading order by

$$G^{(m)}(\boldsymbol{k}_1, ..., \boldsymbol{k}_m) \approx \sum_{\substack{\mu_1,...,\mu_m=1, \\ \text{mutually different}}}^{N} \sum_{\sigma \in S_m} \prod_{p=1}^{m} e^{i(\boldsymbol{k}_p - \boldsymbol{k}_{\sigma(p)})\boldsymbol{R}_{\mu_p}} \langle \hat{S}_+^{(\mu_p)} \hat{S}_+^{(\mu_p)} \rangle \tag{6.34}$$

and Eq. (6.23) by

$$\sum_{\sigma \in S_m} \prod_{p=1}^{m} G^{(1)}(\boldsymbol{k}_p, \boldsymbol{k}_{\sigma(p)}) \approx \sum_{\mu_1,...,\mu_m=1}^{N} \sum_{\sigma \in S_m} \prod_{p=1}^{m} e^{i(\boldsymbol{k}_p - \boldsymbol{k}_{\sigma(p)})\boldsymbol{R}_{\mu_p}} \langle \hat{S}_+^{(\mu_p)} \hat{S}_-^{(\mu_p)} \rangle \,. \tag{6.35}$$

Further, the first-order photon correlation function can be approximated by

$$G^{(1)}(\boldsymbol{k}) \approx \sum_{\mu=1}^{N} \langle \hat{S}_+^{(\mu)} \hat{S}_-^{(\mu)} \rangle = n_e \,, \tag{6.36}$$

where n_e is the average number of excitations. In the following, we investigate under which additional condition Eqs. (6.34) and (6.35) are approximately equal. The indices of summation $\mu_1, ..., \mu_m$ in Eq. (6.34) need to be mutually different. This can be accounted for by including an additional product reading

$$\begin{aligned} &\prod_{\nu_1 \in \{\mu_2,...,\mu_m\}} (1 - \delta_{\mu_1,\nu_1}) \times \prod_{\nu_2 \in \{\mu_3,...,\mu_m\}} (1 - \delta_{\mu_2,\nu_2}) \times ... \times (1 - \delta_{\mu_{m-1},\mu_m}) \\ &= 1 + f(\delta_{\mu_1,\mu_2}, ..., \delta_{\mu_1,\mu_m}, \delta_{\mu_2,\mu_3}, ..., \delta_{\mu_2,\mu_m}, ..., \delta_{\mu_{m-1},\mu_m}) \,, \end{aligned} \tag{6.37}$$

where $f(\delta_{\mu_1,\mu_2}, ..., \delta_{\mu_1,\mu_m}, \delta_{\mu_2,\mu_3}, ..., \delta_{\mu_2,\mu_m}, ..., \delta_{\mu_{m-1},\mu_m})$ is a multivariate polynomial of degree $m - 1$. We note that the lowest monomial of f has a degree of 1.
Let us now consider again the direction $\boldsymbol{k} = \boldsymbol{0}$, for which we find

$$\sum_{\mu=1}^{N} e^{i\boldsymbol{k}\boldsymbol{R}_\mu} \langle \hat{S}_+^{(\mu)} \hat{S}_-^{(\mu)} \rangle \Big|_{\boldsymbol{k}=\boldsymbol{0}} = \sum_{\mu=1}^{N} \langle \hat{S}_+^{(\mu)} \hat{S}_-^{(\mu)} \rangle = n_e \approx G^{(1)}(\boldsymbol{k}) \tag{6.38}$$

and

$$\sum_{\mu_1,...,\mu_m=1}^{N}\prod_{p=1}^{m} e^{i\boldsymbol{k}_p\boldsymbol{R}_{\mu_p}}\langle\hat{S}_+^{(\mu_p)}\hat{S}_-^{(\mu_p)}\rangle\Big|_{\boldsymbol{k}_p=\boldsymbol{0}} = n_e^m \approx [G^{(1)}(\boldsymbol{k})]^m\,. \tag{6.39}$$

Further, in the case of a Kronecker delta of indices μ_p and μ_s we have

$$\sum_{\mu_p,\mu_s=1}^{N}\delta_{\mu_p,\mu_s}\prod_{q\in\{p,s\}}\langle\hat{S}_+^{(\mu_q)}\hat{S}_-^{(\mu_q)}\rangle = \sum_{\mu_p=1}^{N}\langle\hat{S}_+^{(\mu_p)}\hat{S}_-^{(\mu_p)}\rangle^2 \approx \overline{S_+S_-}\sum_{\mu_p=1}^{N}\langle\hat{S}_+^{(\mu_p)}\hat{S}_-^{(\mu_p)}\rangle = \overline{S_+S_-}n_e\,, \tag{6.40}$$

so we find that

$$\sum_{\mu_1,...,\mu_p,...,\mu_s,...,\mu_m=1}^{N}\delta_{\mu_p,\mu_s}\prod_{q=1}^{m} e^{i\boldsymbol{k}_q\boldsymbol{R}_{\mu_q}}\langle\hat{S}_+^{(\mu_q)}\hat{S}_-^{(\mu_q)}\rangle\Big|_{\boldsymbol{k}_q=\boldsymbol{0}} \approx \overline{S_+S_-}n_e^{m-1} \approx \overline{S_+S_-}[G^{(1)}(\boldsymbol{k})]^{m-1}\,. \tag{6.41}$$

Therefore, the terms coming from the function f are at most of order $[G^{(1)}(\boldsymbol{k})]^{m-1}$. Now, we also need to take into account the number of summands of a specific order of $G^{(1)}(\boldsymbol{k})$. Therefore, let us calculate

$$\sum_{\substack{\mu_1,...,\mu_m=1,\\ \text{mutually different}}}^{N} 1 = \sum_{\mu_1,...,\mu_m=1}^{N}(1+f) = m!\binom{N}{m} = N(N-1)...(N-m+1)\,, \tag{6.42}$$

which gives a falling factorial, a polynomial in N. The coefficients of this polynomial are the so-called Stirling numbers of the first kind. Now, the number of summands of order $[G^{(1)}(\boldsymbol{k})]^n$ is exactly given by the coefficient, i.e., the corresponding Stirling number of the N^n term for $n\in\{1,...,m-1\}$ in the falling factorial. Let $\mathcal{L}=\{-1,...,-m+1\}$, then the Stirling number of the first kind for a given m and n is [89]

$$s(m,n) = \sum_{\substack{T\subset\mathcal{L},\\ |T|=m-n}}\prod_{p=1}^{m-n}T_p = (-1)^{m-n}\sum_{i_1<i_2<...<i_{m-n}}^{m-1}\prod_{p=1}^{m-n}i_p\,. \tag{6.43}$$

We can estimate the product from above by

$$\prod_{p=1}^{m-n} i_p \leq (m-1)(m-2)...n < m^{m-n}\,. \tag{6.44}$$

In addition, we count

$$\sum_{i_1<i_2<...<i_{m-n}}^{m-1} 1 = \binom{m-1}{m-n} < m^{m-n}\,, \tag{6.45}$$

such that $|s(m,n)| < m^{2(m-n)}$. Finally, taking the normalisation factor $[G^{(1)}(\boldsymbol{k})]^{-m}$ in the normalised $g^{(m)}(\boldsymbol{k}_1,...,\boldsymbol{k}_m)$ function into account, we obtain

$$\begin{aligned}\frac{1}{m!}g^{(m)}(\mathbf{0},...,\mathbf{0}) &= \frac{1}{[G^{(1)}(\boldsymbol{k})]^m}\sum_{\mu_1,...,\mu_m=1}^{N}(1+f)\prod_{p=1}^{m}\langle\hat{S}_+^{(\mu_p)}\hat{S}_-^{(\mu_p)}\rangle \\ &< \frac{1}{[G^{(1)}(\boldsymbol{k})]^m}\left\{[G^{(1)}(\boldsymbol{k})]^m + m^2\overline{S_+S_-}[G^{(1)}(\boldsymbol{k})]^{m-1} + ... + (m^2)^{m-1}(\overline{S_+S_-})^{m-1}G^{(1)}(\boldsymbol{k})\right\}.\end{aligned} \tag{6.46}$$

Taking also the sum over the permutations into consideration, it is justified to keep only the zeroth order of the mth-order photon correlation function if $\frac{m!\,m^2\overline{S_+S_-}}{G^{(1)}(\boldsymbol{k})} \ll 1$. However, we note that it is usually enough to have $\frac{m^2\overline{S_+S_-}}{G^{(1)}(\boldsymbol{k})} \ll 1$ since also the terms contributing to the Gaussian Moment Theorem are $m!$ many (see e.g. the case of $\boldsymbol{k}=\mathbf{0}$). Using Eq. (6.34), approximating the normalised mth-order photon correlation function in zeroth order gives

$$\begin{aligned}g^{(m)}(\boldsymbol{k}_1,...,\boldsymbol{k}_m) &\approx \frac{1}{[G^{(1)}(\boldsymbol{k})]^m}\sum_{\mu_1,...,\mu_m=1}^{N}\sum_{\sigma\in S_m}\prod_{p=1}^{m}e^{i(\boldsymbol{k}_p-\boldsymbol{k}_{\sigma(p)})\boldsymbol{R}_{\mu_p}}\langle\hat{S}_+^{(\mu_p)}\hat{S}_-^{(\mu_p)}\rangle \\ &= \sum_{\sigma\in S_m}\prod_{p=1}^{m}\frac{1}{G^{(1)}(\boldsymbol{k})}\sum_{\mu_p=1}^{N}e^{i(\boldsymbol{k}_p-\boldsymbol{k}_{\sigma(p)})\boldsymbol{R}_{\mu_p}}\langle\hat{S}_+^{(\mu_p)}\hat{S}_-^{(\mu_p)}\rangle \\ &= \sum_{\sigma\in S_m}\prod_{p=1}^{m}g^{(1)}(\boldsymbol{k}_p,\boldsymbol{k}_{\sigma(p)})\,,\end{aligned} \tag{6.47}$$

which is the Gaussian Moment Theorem. If we further approximate $G^{(1)}(\boldsymbol{k}) \approx n_e \approx \overline{S_+S_-}N$, we thus find the following two conditions for the applicability of the Gaussian Moment Theorem, namely

$$\frac{\langle\hat{S}_+^{(\mu)}\rangle\langle\hat{S}_-^{(\mu)}\rangle}{\langle\hat{S}_+^{(\mu)}\hat{S}_-^{(\mu)}\rangle} \ll \frac{1}{m(N-m)} \approx \frac{1}{mN}\,,\forall\mu\in\{1,...,N\} \qquad \text{and} \qquad \frac{(m!)\,m^2}{N} \ll 1\,. \tag{6.48}$$

If these two conditions are satisfied, the light emitted by the atomic ensemble shows thermal statistics in terms of higher-order photon correlation functions. As a remark, we note that if instead of all N atoms only $\tilde{N} = N - N_g$ many atoms are partially excited and N_g many atoms are in the ground state, all derived results remain true if we replace N by $\tilde{N}$.
In the next section, we demonstrate the found results on some examples. However, before we end this section, we note that for the interested reader we analyse a similar question as in

the current section in Appendix I. Since thermal light sources are incoherent in first order, in Appendix I we split the radiation emitted by the atomic ensemble in a first-order coherent and a first-order incoherent part and investigate when the incoherent higher-order photon correlation functions show thermal statistics.

6.2.2 Validity of the conditions - Examples

In this subsection, we investigate the applicability of the Gaussian Moment Theorem using several examples.

Fully excited state

In the case of the fully excited state, the state of a single atom is given by $\hat{\rho}_\mu = |e\rangle\langle e|$ for all $\mu \in \{1, ..., N\}$. Thus, $\langle \hat{S}_+^{(\mu)} \hat{S}_-^{(\mu)} \rangle = 1$ and $\langle \hat{S}_+^{(\mu)} \rangle = \langle \hat{S}_-^{(\mu)} \rangle = 0$ for all $\mu \in \{1, ..., N\}$. Further, in the limit $G^{(1)}(\boldsymbol{k}) = n_e = N \gg m!\, m^2$, we expect the Gaussian Moment Theorem to hold. We can explicitly calculate

$$G^{(1)}(\boldsymbol{k}) = n_e = N\,, \tag{6.49}$$

$$g^{(1)}(\boldsymbol{k}_1, \boldsymbol{k}_2) = \frac{1}{N} \sum_{\mu=1}^{N} e^{i(\boldsymbol{k}_1 - \boldsymbol{k}_2)\boldsymbol{R}_\mu}\,, \tag{6.50}$$

and

$$\begin{aligned} g^{(m)}(\boldsymbol{k}_1, ..., \boldsymbol{k}_m) &= \frac{1}{N^m} \sum_{\substack{\mu_1,...,\mu_m=1,\\ \text{mutually different}}}^{N} \sum_{\sigma \in S_m} \prod_{p=1}^{m} e^{i(\boldsymbol{k}_p - \boldsymbol{k}_{\sigma(p)})\boldsymbol{R}_{\mu_p}} \\ &= \sum_{\sigma \in S_m} \prod_{p=1}^{m} g^{(1)}(\boldsymbol{k}_p, \boldsymbol{k}_{\sigma(p)}) + \mathcal{O}\left(\frac{m!\, m^2}{N}\right) \end{aligned} \tag{6.51}$$

using the approximation from the previous subsection. We note that the factor of $m!$ comes from the sum over all permutations. As concrete examples, let us consider the second- and third-order photon correlation functions $g^{(2)}(\boldsymbol{k}_1, \boldsymbol{k}_2)$ and $g^{(3)}(\boldsymbol{k}_1, \boldsymbol{k}_2, \boldsymbol{k}_3)$ explicitly. A straightforward calculation leads to

$$g^{(2)}(\boldsymbol{k}_1, \boldsymbol{k}_2) = 1 + |g^{(1)}(\boldsymbol{k}_1, \boldsymbol{k}_2)|^2 - \frac{2}{N} \tag{6.52}$$

$$\begin{aligned} g^{(3)}(\boldsymbol{k}_1, \boldsymbol{k}_2, \boldsymbol{k}_3) &= 1 + |g^{(1)}(\boldsymbol{k}_1, \boldsymbol{k}_2)|^2 + |g^{(1)}(\boldsymbol{k}_2, \boldsymbol{k}_3)|^2 + |g^{(1)}(\boldsymbol{k}_1, \boldsymbol{k}_3)|^2 \\ &\quad + 2\mathrm{Re}\{g^{(1)}(\boldsymbol{k}_1, \boldsymbol{k}_2) g^{(1)}(\boldsymbol{k}_2, \boldsymbol{k}_3) g^{(1)}(\boldsymbol{k}_3, \boldsymbol{k}_1)\} \\ &\quad - \frac{6}{N} + \frac{12}{N^2} - \frac{4}{N}[|g^{(1)}(\boldsymbol{k}_1, \boldsymbol{k}_2)|^2 + |g^{(1)}(\boldsymbol{k}_2, \boldsymbol{k}_3)|^2 + |g^{(1)}(\boldsymbol{k}_1, \boldsymbol{k}_3)|^2]\,, \end{aligned} \tag{6.53}$$

where we already ordered the terms to see the deviations from the Gaussian Moment Theorem. In the case of $g^{(2)}$, the deviation is $-\frac{2}{N}$, which we can directly find from our calculations in

the previous subsection. The factor of 2 comes from the number of permutations, which is in general $m!$. This factor needs to be multiplied with the coefficient given in Eq. (6.43). For $n = m - 1$, we generally find $s(m, m-1) = (-1)^{\frac{m(m-1)}{2}}$, which for $m = 2$ gives $s(2,1) = -1$. From this we can also see that the leading deviation is of order $\frac{m^2}{N}$ (excluding the permutations), which we identified earlier. Now, let us move on to $g^{(3)}$, here the highest deviation is obtained for $\boldsymbol{k}_1 = \boldsymbol{k}_2 = \boldsymbol{k}_3$. In this case, the leading deviation is $-\frac{18}{N}$, whereas the deviation of the next order is $\frac{12}{N^2}$. The leading deviation can again be found by the multiplication of the number of permutations 3! with the coefficient $s(3,2) = -3$ giving -18. For the deviation of the next order, we need the coefficient $s(m, m-2)$, which is, in general, given by

$$s(m, m-2) = \frac{1}{24} m(m-1)(m-2)(3m-1)\,. \tag{6.54}$$

For $m = 3$, we obtain $s(3,1) = 2$, which together with 3! gives the factor of 12. Again, we can also identify the general scaling, which is of order $\frac{m^4}{N^2}$.

Doubly excited state

As a second example, we consider an ensemble of N two-level atoms, where atoms $\tilde{\mu}$ and $\tilde{\nu}$ are excited, but all other atoms are in the ground state. Here, $N_g = N - 2$ and $\tilde{N} = 2$. Moreover, $\langle \hat{S}_+^{(\mu)} \hat{S}_-^{(\mu)} \rangle = \delta_{\mu,\tilde{\mu}} + \delta_{\mu,\tilde{\nu}}$ and $\langle \hat{S}_+^{(\mu)} \rangle = \langle \hat{S}_-^{(\mu)} \rangle = 0$. Therefore, all higher-order photon correlation functions with $m \geq 3$ are zero and can thus not be approximated by the Gaussian Moment Theorem. However, also in the case of $m = 2$, we have $\tilde{N} = 2 = m$, such that we expect that the Gaussian Moment Theorem can not be applied either. We check this explicitly by calculating the correlation functions. The first-order correlation functions read

$$G^{(1)}(\boldsymbol{k}) = \tilde{N} = 2\,, \tag{6.55}$$

$$g^{(1)}(\boldsymbol{k}_1, \boldsymbol{k}_2) = \frac{1}{2}(e^{i(\boldsymbol{k}_1 - \boldsymbol{k}_2)\boldsymbol{R}_{\tilde{\mu}}} + e^{i(\boldsymbol{k}_1 - \boldsymbol{k}_2)\boldsymbol{R}_{\tilde{\nu}}})\,. \tag{6.56}$$

Now, with

$$\langle \hat{S}_+^{(\mu_1)} \hat{S}_+^{(\mu_2)} \hat{S}_-^{(\mu_3)} \hat{S}_-^{(\mu_4)} \rangle = (\delta_{\mu_1,\mu_3}\delta_{\mu_2,\mu_4} + \delta_{\mu_1,\mu_4}\delta_{\mu_2,\mu_3})(\delta_{\mu_1,\tilde{\mu}}\delta_{\mu_2,\tilde{\nu}} + \delta_{\mu_1,\tilde{\nu}}\delta_{\mu_2,\tilde{\mu}}) \tag{6.57}$$

we obtain for the second-order photon correlation function

$$\begin{aligned} g^{(2)}(\boldsymbol{k}_1, \boldsymbol{k}_2) &= \frac{1}{2^2} \left(\sum_{\sigma \in S_2} e^{i(\boldsymbol{k}_1 - \boldsymbol{k}_{\sigma(1)})\boldsymbol{R}_{\tilde{\mu}}} e^{i(\boldsymbol{k}_2 - \boldsymbol{k}_{\sigma(2)})\boldsymbol{R}_{\tilde{\nu}}} + e^{i(\boldsymbol{k}_1 - \boldsymbol{k}_{\sigma(1)})\boldsymbol{R}_{\tilde{\nu}}} e^{i(\boldsymbol{k}_2 - \boldsymbol{k}_{\sigma(2)})\boldsymbol{R}_{\tilde{\mu}}} \right) \\ &= \sum_{\sigma \in S_2} \prod_{p=1}^{2} g^{(1)}(\boldsymbol{k}_p, \boldsymbol{k}_{\sigma(p)}) - \frac{1}{2^2} \sum_{\sigma \in S_2} 2 = \sum_{\sigma \in S_2} \prod_{p=1}^{2} g^{(1)}(\boldsymbol{k}_p, \boldsymbol{k}_{\sigma(p)}) - 1\,, \end{aligned} \tag{6.58}$$

which is not approximative the Gaussian Moment Theorem due to the additional -1. The reason is that m is of the same order as $\tilde{N}$. Moreover, using the calculations of the previous subsection, we can immediately identify the deviation as $-m!\frac{m(m-1)}{2\tilde{N}}$, which gives -1 for $m = \tilde{N} = 2$.

Symmetric Dicke state

As a third example, we consider a symmetric Dicke state, which can not be written as a tensor product of the individual atomic states. This means, we can not apply our conditions to find approximately the Gaussian Moment Theorem. However, we choose this example on purpose to show that in the case of a correlated state, the condition $\frac{m!\,m^2}{\tilde{N}} \ll 1$ does indeed not imply thermal statistics. Therefore, let us consider the symmetric Dicke state with $\tilde{N} = N - 1$ excitations reading

$$|D^N_{N-1}\rangle = \frac{1}{\sqrt{N}}\sum_{\mu=1}^{N}\hat{S}_-^{(\mu)}\,|e,...,e\rangle = \frac{1}{\sqrt{N}}\hat{S}_-\,|e,...,e\rangle = \frac{1}{\sqrt{N}}\hat{E}_S^{(+)}(\mathbf{0})\,|e,...,e\rangle\ . \tag{6.59}$$

This means, we can relate the second-order photon correlation function of the symmetric Dicke state to the third-order photon correlation function of the fully excited state as

$$G^{(2)}_{|D^N_{N-1}\rangle}(\boldsymbol{k}_1,\boldsymbol{k}_2) = \frac{1}{N}G^{(3)}_{|e,...,e\rangle}(\mathbf{0},\boldsymbol{k}_1,\boldsymbol{k}_2) = N^2 g^{(3)}_{|e,...,e\rangle}(\mathbf{0},\boldsymbol{k}_1,\boldsymbol{k}_2)\,. \tag{6.60}$$

For simplicity, let us consider the case of $\boldsymbol{k}_1 = \boldsymbol{k}_2 = \mathbf{0}$. In this case, the correlation functions are given by

$$G^{(1)}_{|D^N_{N-1}\rangle}(\mathbf{0}) = 2(N-1)\,, \tag{6.61}$$

$$g^{(1)}_{|D^N_{N-1}\rangle}(\mathbf{0},\mathbf{0}) = 1\,, \tag{6.62}$$

$$g^{(2)}_{|D^N_{N-1}\rangle}(\mathbf{0},\mathbf{0}) = \frac{3(N-2)}{2(N-1)}\,. \tag{6.63}$$

Thus, for $\frac{m!\,m^2}{\tilde{N}} \ll 1$, e.g., by considering the limit of N going to infinity, we have

$$\lim_{N\to\infty} g^{(2)}_{|D^N_{N-1}\rangle}(\mathbf{0},\mathbf{0}) = \frac{3}{2} \neq 2 = \sum_{\sigma\in S_2}\prod_{p=1}^{2} g^{(1)}_{|D^N_{N-1}\rangle}(\mathbf{0},\mathbf{0})\,. \tag{6.64}$$

Therefore, we conclude that correlated states do, in general, not show thermal light statistics even in the thermodynamic limit.

Atoms in steady state driven by a plane wave laser field

As a last example, we consider an ensemble of identical two-level atoms driven by a plane wave laser field. For simplicity, we assume that the laser frequency is in resonance with the transition frequency of the atoms. The single-atom steady state is then given by (see Appendix J)

$$\hat{\rho}_\mu = \begin{pmatrix} \frac{s}{2(1+s)} & -\frac{\sqrt{s}}{\sqrt{2}(1+s)} \\ -\frac{\sqrt{s}}{\sqrt{2}(1+s)} & \frac{2+s}{2(1+s)} \end{pmatrix} \tag{6.65}$$

for all $\mu \in \{1, ..., N\}$, where s denotes the saturation parameter. The atomic expectation values can be calculated to

$$\langle \hat{S}_+^{(\mu)} \hat{S}_-^{(\mu)} \rangle = \frac{s}{2(1+s)} , \tag{6.66}$$

$$\langle \hat{S}_+^{(\mu)} \rangle = -\frac{\sqrt{s}}{\sqrt{2}(1+s)} , \tag{6.67}$$

$$\langle \hat{S}_-^{(\mu)} \rangle = -\frac{\sqrt{s}}{\sqrt{2}(1+s)} , \tag{6.68}$$

$$\langle \hat{S}_+^{(\mu)} \rangle \langle \hat{S}_-^{(\mu)} \rangle = \frac{s}{2(1+s)^2} . \tag{6.69}$$

Thus, the fraction of the coherences and the populations of the atoms given by

$$\frac{\langle \hat{S}_+^{(\mu)} \rangle \langle \hat{S}_-^{(\mu)} \rangle}{\langle \hat{S}_+^{(\mu)} \hat{S}_-^{(\mu)} \rangle} = \frac{1}{1+s} \tag{6.70}$$

crucially depends on the saturation parameter s. In what follows, we calculate the second-order photon correlation function and show that under the conditions of Eq. (6.48), it is approximatively given by the Gaussian Moment Theorem. Let us first calculate the unnormalised first-order field correlation function. A straightforward calculation gives

$$G^{(1)}(\boldsymbol{k}_1, \boldsymbol{k}_2) = \frac{s}{2(1+s)^2} \left[s\Phi(\boldsymbol{k}_1 - \boldsymbol{k}_2) + \Phi(\boldsymbol{k}_1)\Phi(-\boldsymbol{k}_2) \right] , \tag{6.71}$$

where we defined the so-called structure factor

$$\Phi(\boldsymbol{k}) \coloneqq \sum_{\mu=1}^{N} e^{i\boldsymbol{k}\boldsymbol{R}_\mu} . \tag{6.72}$$

Then, with

$$G^{(1)}(\boldsymbol{k}, \boldsymbol{k}) = \frac{s}{2(1+s)^2} \left[sN + \Phi(\boldsymbol{k})\Phi(-\boldsymbol{k}) \right] \tag{6.73}$$

the normalised first-order field correlation function reads

$$g^{(1)}(\boldsymbol{k}_1,\boldsymbol{k}_2)=\frac{s\Phi(\boldsymbol{k}_1-\boldsymbol{k}_2)+\Phi(\boldsymbol{k}_1)\Phi(-\boldsymbol{k}_2)}{\sqrt{sN+\Phi(\boldsymbol{k}_1)\Phi(-\boldsymbol{k}_1)}\sqrt{sN+\Phi(\boldsymbol{k}_2)\Phi(-\boldsymbol{k}_2)}}\,, \tag{6.74}$$

from which we obtain

$$\sum_{\sigma\in S_2}\prod_{p=1}^{2}g^{(1)}(\boldsymbol{k}_p,\boldsymbol{k}_{\sigma(p)})=1+\frac{\left[s\Phi(\boldsymbol{k}_1-\boldsymbol{k}_2)+\Phi(\boldsymbol{k}_1)\Phi(-\boldsymbol{k}_2)\right]\left[s\Phi(\boldsymbol{k}_2-\boldsymbol{k}_1)+\Phi(-\boldsymbol{k}_1)\Phi(\boldsymbol{k}_2)\right]}{\left[sN+\Phi(\boldsymbol{k}_1)\Phi(-\boldsymbol{k}_1)\right]\left[sN+\Phi(\boldsymbol{k}_2)\Phi(-\boldsymbol{k}_2)\right]}\,. \tag{6.75}$$

Similarly, we can calculate the second-order photon correlation function, which is given by

$$\begin{aligned}g^{(2)}(\boldsymbol{k}_1,\boldsymbol{k}_2)=&\frac{1}{\left[sN+\Phi(\boldsymbol{k}_1)\Phi(-\boldsymbol{k}_1)\right]\left[sN+\Phi(\boldsymbol{k}_2)\Phi(-\boldsymbol{k}_2)\right]}\times\big[s^2N^2-2s^2N+4sN\\&+s^2\Phi(\boldsymbol{k}_1-\boldsymbol{k}_2)\Phi(\boldsymbol{k}_2-\boldsymbol{k}_1)+s\Phi(-\boldsymbol{k}_1)\Phi(\boldsymbol{k}_2)\Phi(\boldsymbol{k}_1-\boldsymbol{k}_2)+s\Phi(\boldsymbol{k}_1)\Phi(-\boldsymbol{k}_2)\Phi(\boldsymbol{k}_2-\boldsymbol{k}_1)\\&-\Phi(\boldsymbol{k}_1)\Phi(\boldsymbol{k}_2)\Phi(-\boldsymbol{k}_1-\boldsymbol{k}_2)+\Phi(-\boldsymbol{k}_1)\Phi(\boldsymbol{k}_1)\Phi(-\boldsymbol{k}_2)\Phi(\boldsymbol{k}_2)+\Phi(-\boldsymbol{k}_1-\boldsymbol{k}_2)\Phi(\boldsymbol{k}_1+\boldsymbol{k}_2)\\&-\Phi(-\boldsymbol{k}_1)\Phi(-\boldsymbol{k}_2)\Phi(\boldsymbol{k}_1+\boldsymbol{k}_2)+sN\Phi(-\boldsymbol{k}_1)\Phi(\boldsymbol{k}_1)-4s\Phi(-\boldsymbol{k}_1)\Phi(\boldsymbol{k}_1)+sN\Phi(-\boldsymbol{k}_2)\Phi(\boldsymbol{k}_2)\\&-4s\Phi(-\boldsymbol{k}_2)\Phi(\boldsymbol{k}_2)\big]\,.\end{aligned} \tag{6.76}$$

Now, let us consider the first condition of Eq. (6.48). Together with Eq. (6.70) we can write this condition as ($m=2$)

$$\frac{1}{1+s}\ll\frac{1}{2N}\Leftrightarrow\frac{2N-1}{s}\approx\frac{2N}{s}\ll 1\,. \tag{6.77}$$

This suggests to define the expansion parameter $r:=\frac{2N}{s}$ and to do a Taylor expansion of both Eqs. (6.75) and (6.76) up to the leading order in r. We obtain

$$\sum_{\sigma\in S_2}\prod_{p=1}^{2}g^{(1)}(\boldsymbol{k}_p,\boldsymbol{k}_{\sigma(p)})=1+\frac{1}{N^2}\Phi(\boldsymbol{k}_1-\boldsymbol{k}_2)\Phi(\boldsymbol{k}_2-\boldsymbol{k}_1)+\mathcal{O}(r)\,, \tag{6.78}$$

$$g^{(2)}(\boldsymbol{k}_1,\boldsymbol{k}_2)=1+\frac{1}{N^2}\Phi(\boldsymbol{k}_1-\boldsymbol{k}_2)\Phi(\boldsymbol{k}_2-\boldsymbol{k}_1)-\frac{2}{N}+\mathcal{O}(r)\,, \tag{6.79}$$

which are equal except for the term $-\frac{2}{N}$. This is the same deviation that we found earlier, given by $-m!\frac{m(m-1)}{2N}$ for $m=2$, and can thus be neglected if the second condition of Eq. (6.48) holds. We illustrate this transition to the Gaussian Moment Theorem by considering a dilute cloud of atoms uniformly distributed in a sphere (see Fig. 6.1). Since only the product $\boldsymbol{kR}_{\mu\nu}$ is important, we can effectively control the diluteness of the cloud by adjusting the absolute value k of the wave vector. Therefore, we are allowed to place the atoms within a sphere of radius 1 in units of the wavelength. The state of such a driven dilute cloud of atoms, where dipole-dipole interactions can be neglected, is given by the Nth tensor product of the state written in Eq. (6.65). Further, let us assume that the wave vector of the laser is parallel to

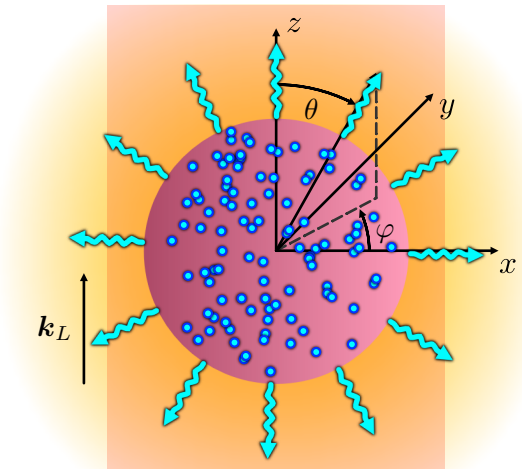

Figure 6.1: Cloud of 100 atoms uniformly distributed in a sphere of radius 1 in units of the transition wavelength. The laser with wave vector $\boldsymbol{k}_L \parallel \hat{\boldsymbol{z}}$ drives the atoms to steady state, of which the emission properties are analysed. The angle φ denotes the azimuthal angle in the xy-plane, while the angle θ is the usual polar angle.

the z-axis.

In the following, we consider the autocorrelation function $g^{(2)}(\boldsymbol{k})$ ($\boldsymbol{k}_1 = \boldsymbol{k}_2 = \boldsymbol{k}$) given by

$$g^{(2)}(\boldsymbol{k}) = \frac{1}{(sN + |\Phi(\boldsymbol{k})|^2)^2}\{2sN[2 + s(N-1)] + 4s(N-2)|\Phi(\boldsymbol{k})|^2 + |[\Phi(\boldsymbol{k})]^2 - \Phi(2\boldsymbol{k})|^2\} \tag{6.80}$$

in two different setups. In the first setup, we scan around the sphere in the xz-plane, i.e., including the direction of the laser, so the effective wave vector can be written as $\boldsymbol{k} = \boldsymbol{k}_{xz} = 2\pi\tilde{k}(\sin\theta, 0, \cos\theta - 1)^\mathsf{T}$, where $\tilde{k}$ determines the diluteness. In the second setup, we scan around the sphere in the xy-plane, i.e., perpendicular to the direction of the laser, such that the effective wave vector is given by $\boldsymbol{k} = \boldsymbol{k}_{xy} = 2\pi\tilde{k}(\cos\varphi, \sin\varphi, -1)^\mathsf{T}$. We note that in the next section, we also consider a $2D$ scan of the correlation function. Nevertheless, let us first investigate the aforementioned two particular setups. In Fig. 6.2, we show the autocorrelation function for both setups for $N = 100$ atoms and different values of the saturation parameter s when we average over $M = 100$ realisations of the atomic positions. In the left plot, we show the autocorrelation function for the first setup. By increasing the saturation parameter s for a fixed number of atoms N, we can clearly see the transition to the Gaussian Moment Theorem. However, by considering both plots (in the right plot we show the autocorrelation function for the second setup), we see that the condition $\frac{2N}{s} \ll 1$ is only needed in the direction of the laser. In other directions, a weaker condition is already sufficient. In what follows, we explain these both behaviours quantitatively. First, we note that the derivation of the conditions was based on the direction $\boldsymbol{k} = \boldsymbol{0}$, which characterises the direction of the laser. Therefore, in the direction of the laser we indeed need $\frac{2N}{s} \ll 1$. This can also be seen

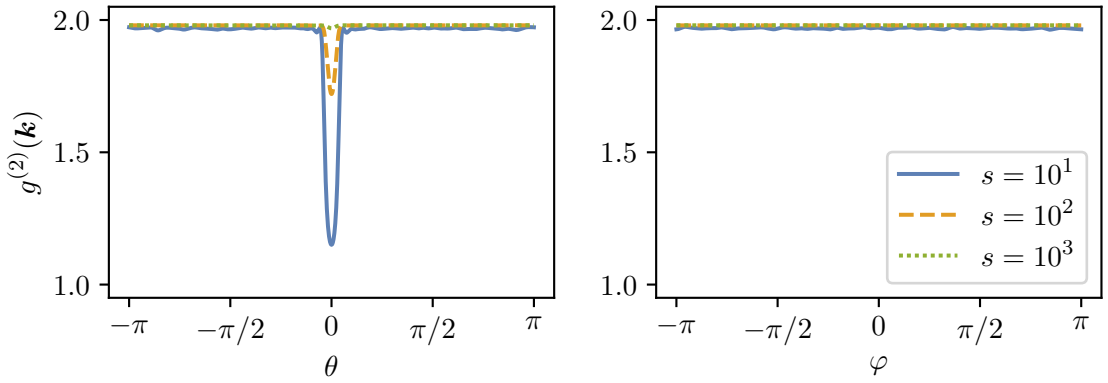

Figure 6.2: Left: Autocorrelation function for the first setup, i.e., $\boldsymbol{k} = \boldsymbol{k}_{xz}$ and $\tilde{k} = 4$. Right: Autocorrelation function for the second setup, i.e., $\boldsymbol{k} = \boldsymbol{k}_{xy}$ and $\tilde{k} = 4$. We want to highlight that we can clearly see the transition towards the Gaussian Moment Theorem by increasing the saturation parameter s for fixed N, such that $\frac{2N}{s}$ becomes small compared to 1. Concretely, the dip in the left plot becomes smaller and smaller and we approximately find the value obtained from the Gaussian Moment Theorem. However, we also want to mention that except for a vicinity around the direction of the laser (left plot, $\theta = 0$), the Gaussian Moment Theorem can already be found for saturation parameters s, for which $\frac{2N}{s}$ is not yet negligibly small.

by doing a Taylor expansion of the autocorrelation function up to the second order in the parameter r that we defined earlier. Using $\Phi(\boldsymbol{k} = \boldsymbol{0}) = N$, we find

$$g^{(2)}(\boldsymbol{k}) = 2 - \frac{2}{N} + \frac{4[N - |\Phi(\boldsymbol{k})|^2]}{N^2 s} + \frac{1}{N^3 s^2}[N|\Phi(2\boldsymbol{k})|^2 - N\Phi(2\boldsymbol{k})[\Phi(-\boldsymbol{k})]^2 - N\Phi(-2\boldsymbol{k})[\Phi(\boldsymbol{k})]^2 - N|\Phi(\boldsymbol{k})|^4 + 10|\Phi(\boldsymbol{k})|^4 - 8N|\Phi(\boldsymbol{k})|^2] + \mathcal{O}(r^3)\,. \tag{6.81}$$

Now, the direction of the laser is characterised by $\boldsymbol{k} = \boldsymbol{0}$, so we have

$$g^{(2)}(\boldsymbol{0}) = 2 - \frac{2}{N} + \frac{4(1-N)}{Ns} - \frac{(N-7)(N-1)}{s^2} + \mathcal{O}(r^3)\,. \tag{6.82}$$

Therefore, the leading correction is of second order and scales as $\frac{N^2}{s^2}$ (see Appendix H), which needs to be much smaller than 1 if we want to approximately obtain the Gaussian Moment Theorem. However, if we consider a direction far away from the direction of the laser, for example perpendicular to the laser, then the function $\Phi(\boldsymbol{k})$ describes for sufficiently large wave numbers for which the phase is randomly distributed in the interval $[0, 2\pi)$, a random walk. This is illustrated in Fig. 6.3. Here, we plot on the left the root mean square distance $\sqrt{\langle|\Phi|^2\rangle}$ for $N = 20$ atoms against the wave number k for $\boldsymbol{k} = \frac{k}{\sqrt{2}}(1, 0, -1)^\mathsf{T}$, i.e., for a detection in the x-direction. On the right, the products $\boldsymbol{k}\boldsymbol{R}_\mu$, which enter the phases of the exponentials of $\Phi(\boldsymbol{k})$, are shown, sorted from small to big. As can be seen, if we consider only a single realisation of the atomic positions, the phases are not uniformly distributed and

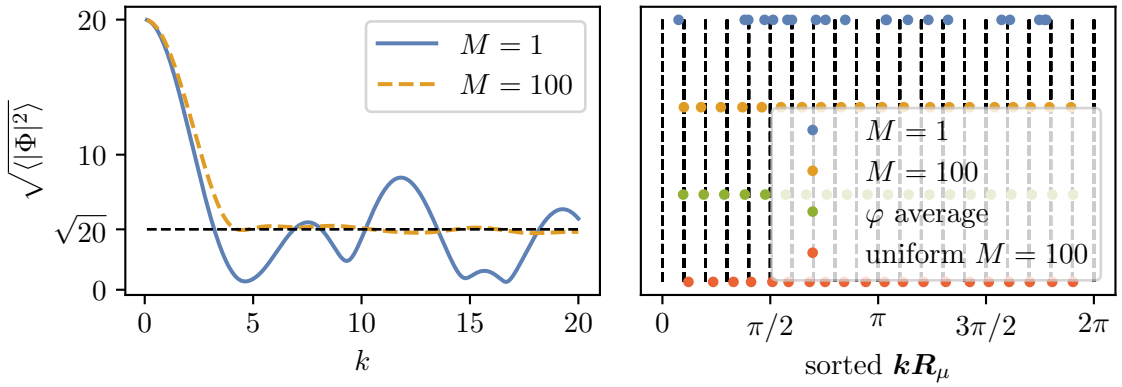

Figure 6.3: Left: Root mean square distance $\sqrt{\langle|\Phi|^2\rangle}$ for $N = 20$ atoms against the wave number k for $\boldsymbol{k} = \frac{k}{\sqrt{2}}(1, 0, -1)^\mathsf{T}$, i.e., for a detection in the x-direction. For a single realisation, the $\sqrt{N}$ scaling of a random walk can not be observed. However, the average over $M = 100$ realisations follows the $\sqrt{N}$ behaviour in the case of a sufficiently large wave number k. Right: Products $\boldsymbol{kR}_\mu$, which enter the phases of the exponentials of $\Phi(\boldsymbol{k})$, sorted from small to big. In concordance with the results for the root mean square distance, when comparing the results with those from a pseudo-uniform distribution (red), we see that the phases exhibit fluctuations in the case of a single realisation (blue), but are almost perfectly uniformly distributed in the case of an ensemble average over many realisations (orange). As additional information, we plot the average over all angles φ for a single realisation, which also shows a uniform distribution of the phases (green).

no $\sqrt{N}$ scaling for the root mean square distance can be observed. However, if we average over many realisations ($M = 100$ in the plots), the phases become uniformly distributed for sufficiently large wave numbers and the statistics of a random walk can be found. As a side remark, if we average a single realisation over all angles φ, the phases are also uniformly distributed. Now, using the scalings

$$\langle|\Phi(\boldsymbol{k})|^2\rangle, \langle|\Phi(2\boldsymbol{k})|^2\rangle \sim N\,, \tag{6.83}$$

$$\langle|\Phi(\boldsymbol{k})|^4\rangle \sim N^2\,, \tag{6.84}$$

$$|\langle\Phi(2\boldsymbol{k})[\Phi(-\boldsymbol{k})]^2\rangle|, |\langle\Phi(-2\boldsymbol{k})[\Phi(\boldsymbol{k})]^2\rangle| \sim N\,, \tag{6.85}$$

which apply in the case of a random walk, the averaged $g^{(2)}(\boldsymbol{k})$ function reads

$$g^{(2)}(\boldsymbol{k}) \sim 2 - \frac{2}{N} + \frac{N^2 - N^3}{N^3 s^2} + \mathcal{O}(r^3)\,. \tag{6.86}$$

We notice that the second-order correction is essentially independent of the number of atoms for N large enough, but is determined by the saturation parameter s. That is, also for $N \geq s$, we obtain approximately the Gaussian Moment Theorem if s is sufficiently large. This is illustrated in Fig. 6.4, where we plot the averaged $g^{(2)}$ function for $s = 100$ and three

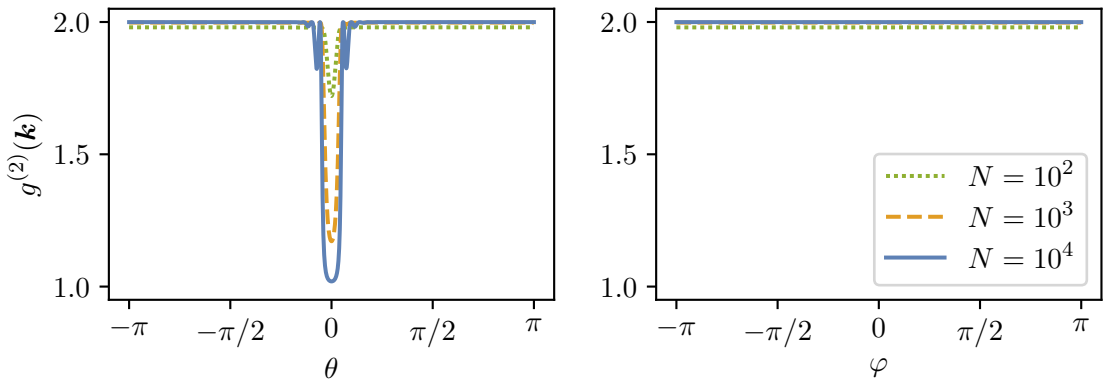

Figure 6.4: Autocorrelation function for $s = 100$ and three different numbers of atoms $N \geq s$ in the case of a detection in the xz-plane (left plot) and in the case of a detection in the xy-plane (right plot). Apart from the direction of the laser, the autocorrelation function is a flat curve whose value is approximately given by the Gaussian Moment Theorem.

different numbers of atoms $N \geq s$. We find that except for the direction of the laser, a flat curve is obtained, the value of which is approximately given by the Gaussian Moment Theorem. We end this subsection by noting that to find the Gaussian Moment Theorem in all directions, we need a particularly large saturation parameter $s \gg 2N$. In the next section, we consider exactly the opposite regime of small saturation parameters s. Then, the atomic ensemble emits mainly coherently and the dynamics can be approximatively described via a classical dipole model [20, 34, 46, 52, 90–99]. However, as we will see, the light emitted by this coherently driven atomic ensemble exhibits unintuitive non-classical features.

6.3 Non-classical features of a weakly laser driven atomic cloud

In this section, we consider the limit of small saturation parameters s, i.e., $s \ll 1$ (or even the stronger condition $sN \ll 1$). In this case, the atoms are driven coherently and the dynamics can be essentially described by a classical dipole model, whereby the individual dipole moments are given by the off-diagonal elements of the single-atom density matrices [20, 34, 46, 52, 90–99]. Based on this picture of classical dipoles, one would assume that the light emitted by the atomic ensemble will be classical coherent light. In fact, this is not the case, but rather the atoms emit quantum light in certain directions, which is characterised by a value of the second-order autocorrelation function less than 1. In Fig. 6.5, we plot a characteristic course of the second-order autocorrelation function for a single realisation of $N = 100$ atoms and saturation parameters $s \in \{10^{-6}, 10^{-5}, 10^{-4}\}$. Here, we want to highlight three features. First, for some observation directions, we obtain so-called superbunching, i.e., $g^{(2)}(\boldsymbol{k}) \gg 2$. Second, for other observation directions, we find quantum light, i.e., $g^{(2)}(\boldsymbol{k}) < 1$, and third, the curves are basically independent of the saturation parameter s. The latter

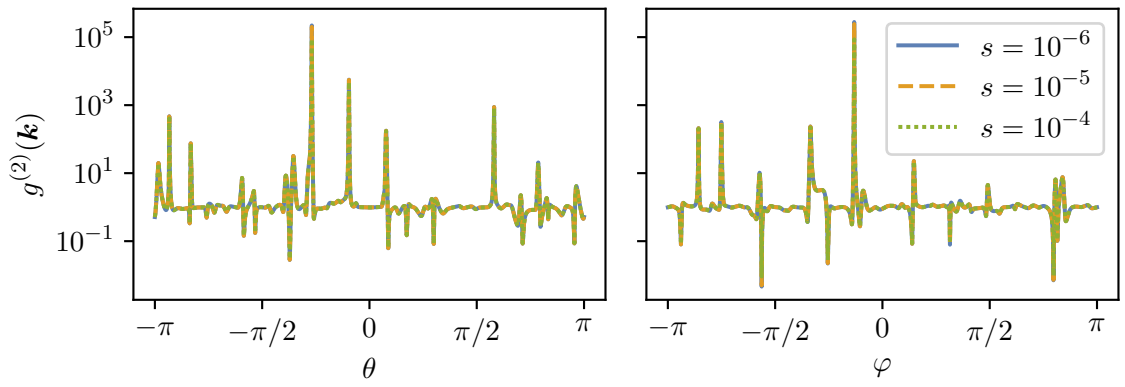

Figure 6.5: Autocorrelation function for a single realisation of the atomic positions with $N = 100$ and $s \in \{10^{-6}, 10^{-5}, 10^{-4}\}$ in the case of $\boldsymbol{k} = \boldsymbol{k}_{xz}$ (left) and in the case of $\boldsymbol{k} = \boldsymbol{k}_{xy}$ (right). The curves are essentially independent of the saturation parameter s. Further, we find a plethora of different emission behaviours reaching from superbunching ($g^{(2)}(\boldsymbol{k}) \gg 2$) to antibunching ($g^{(2)}(\boldsymbol{k}) < 1$).

is easy to understand, since in the so-called linear regime, i.e., for a very small drive of the atoms, the emitted intensity is proportional to the strength of the driving laser, i.e., proportional to s, while the second-order photon correlation function is proportional to s^2. Thus, in the normalised second-order photon correlation function, the saturation parameters in the numerator and denominator cancel each other out, so that the function is independent of s in the zeroth-order approximation. We can also verify this quantitatively by calculating the Taylor expansion of the second-order autocorrelation function around $r := sN = 0$, which reads

$$g^{(2)}(\boldsymbol{k}) = \frac{|[\Phi(\boldsymbol{k})]^2 - \Phi(2\boldsymbol{k})|^2}{|\Phi(\boldsymbol{k})|^4} + \mathcal{O}(r) \tag{6.87}$$

and is thus independent of s. In Fig. 6.6, we illustrate this result by plotting $g^{(2)}(\boldsymbol{k})$ and $\frac{|[\Phi(\boldsymbol{k})]^2 - \Phi(2\boldsymbol{k})|^2}{|\Phi(\boldsymbol{k})|^4}$ for $s = 10^{-6}$, i.e., $sN = 10^{-4}$ and $\boldsymbol{k} = \boldsymbol{k}_{xy}$. As can be clearly seen, both curves are basically identical. Therefore, all superbunching peaks and antibunching dips are determined by the expression $\frac{|[\Phi(\boldsymbol{k})]^2 - \Phi(2\boldsymbol{k})|^2}{|\Phi(\boldsymbol{k})|^4}$.
However, to gain more physical insight, let us first show the normalised second-order autocorrelation function $g^{(2)}(\boldsymbol{k})$ together with the unnormalised second-order autocorrelation function $G^{(2)}(\boldsymbol{k})$ and the first-order correlation function squared $[G^{(1)}(\boldsymbol{k})]^2$ in Fig. 6.7. As can be inferred from the plots, the superbunching peaks can be explained by a strong destructive first-order interference of the emitted photons. On the other hand, the antibunching dips are not based on a strong constructive first-order interference, but we rather find that the destructive second-order interference is stronger than the destructive first-order interference. To analyse this behaviour in more detail, we plot the different terms entering the expression

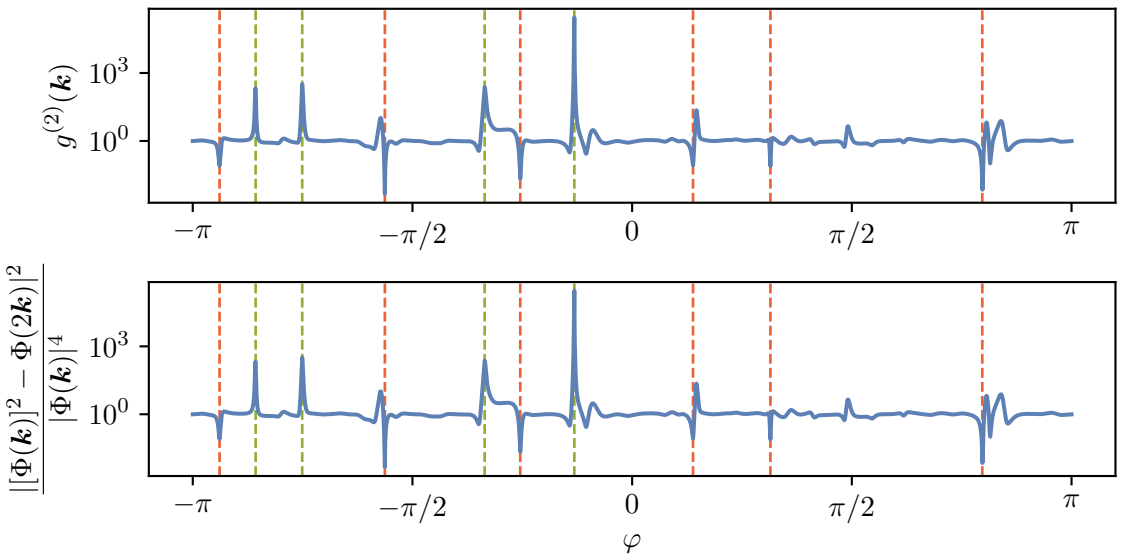

Figure 6.6: Autocorrelation function (top) and $\frac{|[\Phi(\boldsymbol{k})]^2-\Phi(2\boldsymbol{k})|^2}{|\Phi(\boldsymbol{k})|^4}$ (bottom) for $sN = 10^{-4}$ and $\boldsymbol{k} = \boldsymbol{k}_{xy}$. As can be seen, in the limit of $sN \ll 1$ both curves are basically identical. Thus, the directions and values of the superbunching peaks and antibunching dips are determined by the expression $\frac{|[\Phi(\boldsymbol{k})]^2-\Phi(2\boldsymbol{k})|^2}{|\Phi(\boldsymbol{k})|^4}$. In the figure, we mark all superbunching peaks with a value greater than 100 (green dashed lines) and all antibunching dips with a value less than 0.1 (red dashed lines).

$\frac{|[\Phi(\boldsymbol{k})]^2-\Phi(2\boldsymbol{k})|^2}{|\Phi(\boldsymbol{k})|^4}$ together with the normalised autocorrelation function in Fig. 6.8. First, let us note that we see again that the superbunching stems from the strong destructive first-order interference, expressed by $|\Phi(\boldsymbol{k})|^2 \ll 1$ [see Eq. (6.73)]. Second, by writing the expression $[\Phi(\boldsymbol{k})]^2 - \Phi(2\boldsymbol{k})$ in the numerator as

$$[\Phi(\boldsymbol{k})]^2 - \Phi(2\boldsymbol{k}) = \sum_{\mu,\nu=1}^{N} e^{i\boldsymbol{k}(\boldsymbol{R}_\mu+\boldsymbol{R}_\nu)} - \sum_{\mu=1}^{N} e^{i2\boldsymbol{k}\boldsymbol{R}_\mu} = \sum_{\mu\neq\nu=1}^{N} e^{i\boldsymbol{k}(\boldsymbol{R}_\mu+\boldsymbol{R}_\nu)}, \tag{6.88}$$

we see that the term $\Phi(2\boldsymbol{k})$ assures that every atom emits only one photon. This term is the essential difference of a two-level atom compared to a classical oscillating dipole and leads to the emission of quantum light in certain directions. Without this term, the numerator and the denominator in the expression $\frac{|[\Phi(\boldsymbol{k})]^2-\Phi(2\boldsymbol{k})|^2}{|\Phi(\boldsymbol{k})|^4}$ would be identical, but including this term, the numerator may actually be smaller than the denominator for certain wave vectors $\boldsymbol{k}$. In accordance with this, we find in Fig. 6.8 that the numerator exhibits dips in the particular directions of antibunched light.

So far, we have only considered two particular sets of observation directions. In contrast, in Fig. 6.9, we plot the inverse exponential of the second-order autocorrelation function against both angles φ and θ scanning the entire sphere of possible observation directions. The inverse

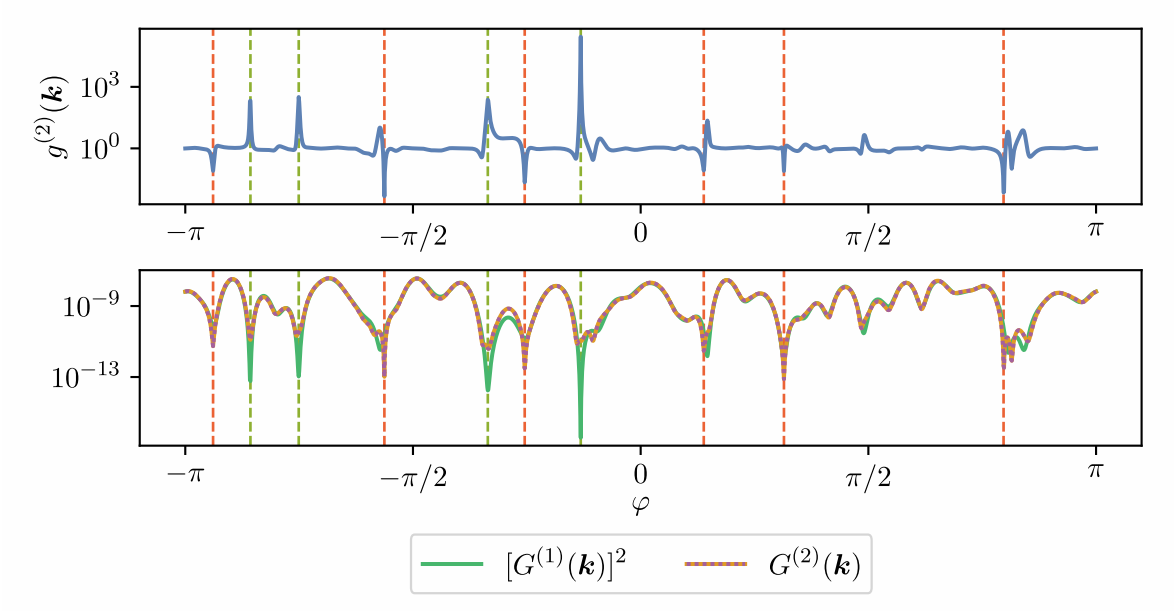

Figure 6.7: Normalised second-order autocorrelation function $g^{(2)}(\boldsymbol{k})$ (top) together with the unnormalised second-order autocorrelation function $G^{(2)}(\boldsymbol{k})$ (bottom) and the first-order correlation function squared $[G^{(1)}(\boldsymbol{k})]^2$ (bottom). As can be seen, the superbunching peaks can be explained by a strong destructive first-order interference, whereas the antibunching dips result from a strong destructive second-order interference, stronger than the first-order one.

exponential is taken to be able to show the richness of the autocorrelation function, which would otherwise be dominated by the large superbunching peaks. We can clearly identify multiple regions of superbunching [$\exp\left(-g^{(2)}(\boldsymbol{k})\right) \approx 0$] and antibunching [$\exp\left(-g^{(2)}(\boldsymbol{k})\right) \approx 1$]. In what follows, let us analyse particular directions of superbunching and antibunching. Since $\Phi(\boldsymbol{k})$ and $[\Phi(\boldsymbol{k})]^2 - \Phi(2\boldsymbol{k})$ are randomly fluctuating functions, we expect that both functions are approximately zero in some directions. But what is the particularity of these two conditions? We first consider $\Phi(\boldsymbol{k}) \approx 0$, which characterises a strong destructive first-order interference and we thus expect superbunching. In contrast, as we will show later on, the condition $[\Phi(\boldsymbol{k})]^2 - \Phi(2\boldsymbol{k}) \approx 0$ can lead to strong antibunching depending on the value of $\Phi(\boldsymbol{k})$. Before we analyse these two regimes mathematically, let us plot the correlation function and the inverse correlation function in Fig. 6.10. At first glance, the two plots seem rather featureless. However, this results from the several superbunching peaks and antibunching dips that can be observed. In particular, we mark the directions of the highest value of $g^{(2)}(\boldsymbol{k})$ (left plot) and the lowest value of $g^{(2)}(\boldsymbol{k})$ (right plot). The two cuts drawn in Fig. 6.10, which contain the highest and lowest values of $g^{(2)}(\boldsymbol{k})$ are shown in Figs. 6.11 and 6.12. As can be seen, the strong superbunching peak results from a structure factor $\Phi(\boldsymbol{k}) \approx 0$ indicating strong destructive first-order interference. On the other hand, the remaining structure factor expressions $\Phi(2\boldsymbol{k})$ and $[\Phi(\boldsymbol{k})]^2 - \Phi(2\boldsymbol{k})$ have finite absolute values. Considering now the anti-

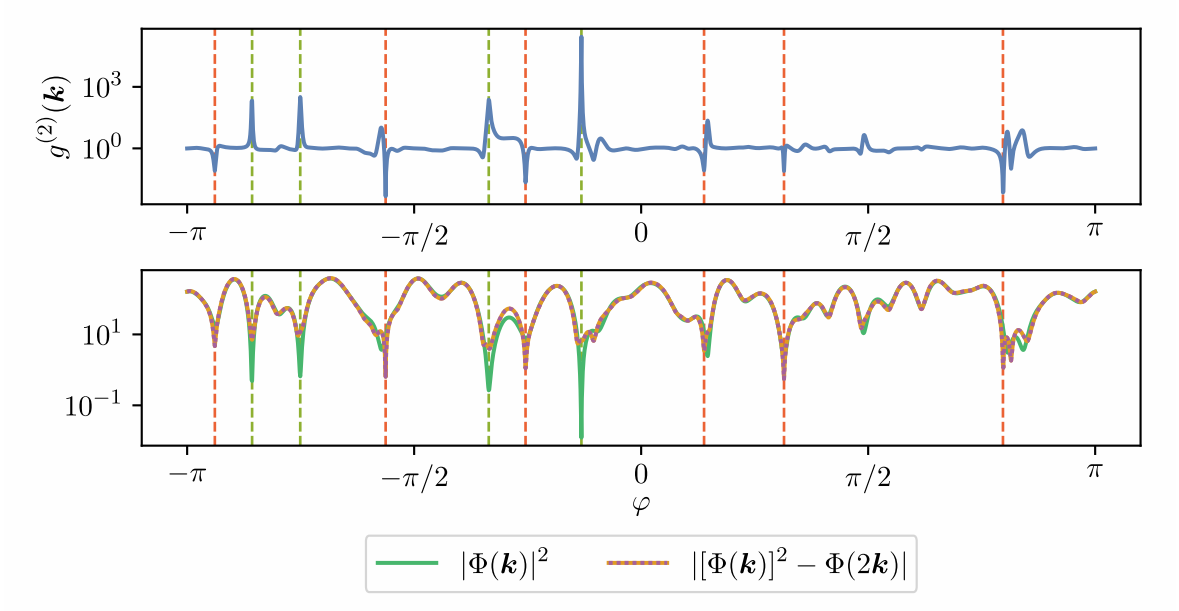

Figure 6.8: Autocorrelation function (top) together with the different terms entering the expression $\frac{|[\Phi(\boldsymbol{k})]^2-\Phi(2\boldsymbol{k})|^2}{|\Phi(\boldsymbol{k})|^4}$ (bottom). We find again that the superbunching peaks stem from a strong destructive first-order interference, expressed by $|\Phi(\boldsymbol{k})|^2 \ll 1$. Further, the term $\Phi(2\boldsymbol{k})$ represents exactly the difference between two-level atoms, which can emit only one photon at a time, and a coherent light source. Subtracting this term from the coherent term $[\Phi(\boldsymbol{k})]^2$ opens the possibility of finding particular observation directions for which $g^{(2)}(\boldsymbol{k})$ can be smaller than 1.

bunching dip in Fig. 6.12, we find that here $[\Phi(\boldsymbol{k})]^2 - \Phi(2\boldsymbol{k}) \approx 0$ indicating strong destructive second-order interference. In contrast, the remaining structure factor expressions have again finite absolute values. The most remarkable feature we want to highlight is that the height of the superbunching peak as well as the depth of the antibunching dip can be controlled by the saturation parameter s. In what follows, we analyse these dependencies quantitatively by doing appropriate Taylor expansions of the second-order autocorrelation function to derive the scaling with the saturation parameter. Afterwards, we check our findings using the explicit values of the example realisation.

Let us start with the case of $\Phi(\boldsymbol{k}) \approx 0$. A Taylor expansion of the normalised second-order autocorrelation function leads to

$$g^{(2)}(\boldsymbol{k}) = \frac{|\Phi(2\boldsymbol{k})|^2 + 2sN[2 + s(N-1)]}{s^2N^2} + \mathcal{O}(|\Phi(\boldsymbol{k})|^2)\,. \tag{6.89}$$

We note that the absolute value squared of the structure factor $\Phi(2\boldsymbol{k})$ usually fluctuates around N, whereas the other terms in the numerator scale at least linearly with s. Since the saturation parameter is much smaller than 1 ($s \ll 1$), the autocorrelation function can be

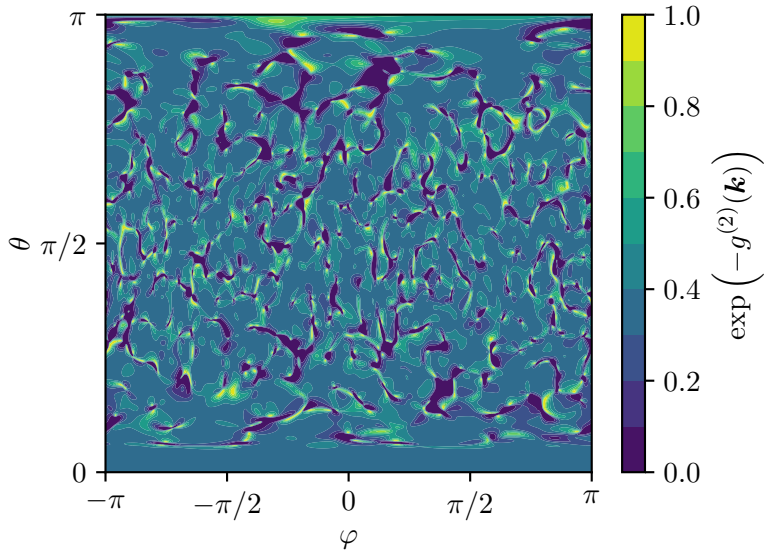

Figure 6.9: Inverse exponential of the second-order autocorrelation function against both angles φ and θ. Several superbunching and antibunching regions characterised by $\exp\left(-g^{(2)}(\boldsymbol{k})\right) \approx 0$ and $\exp\left(-g^{(2)}(\boldsymbol{k})\right) \approx 1$ can be observed.

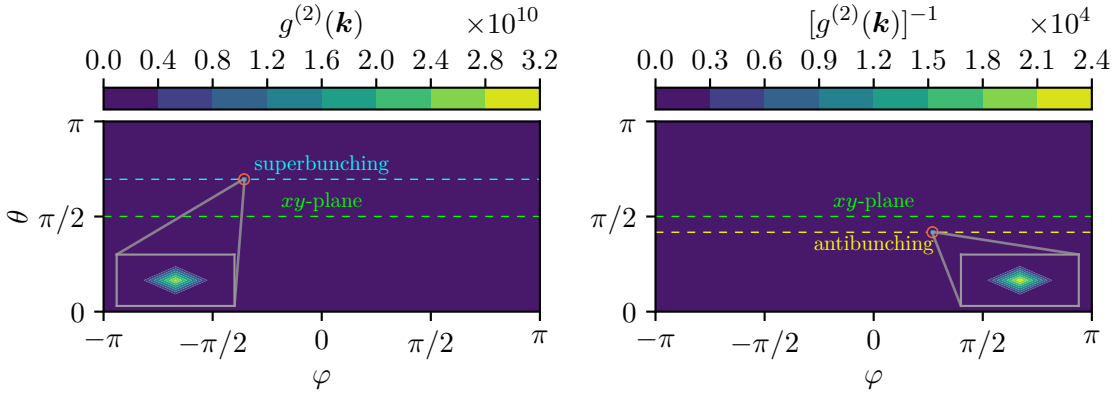

Figure 6.10: Left plot: Normalised second-order autocorrelation function for all observation directions, characterised by the angles φ and θ. Right plot: Inverse normalised second-order autocorrelation function for all observation directions. The plots seem rather featureless. However, this is based on the strong superbunching peaks as well as antibunching dips (the maximum and minimum of $g^{(2)}$ are indicated by the insets) that can be observed in several directions.

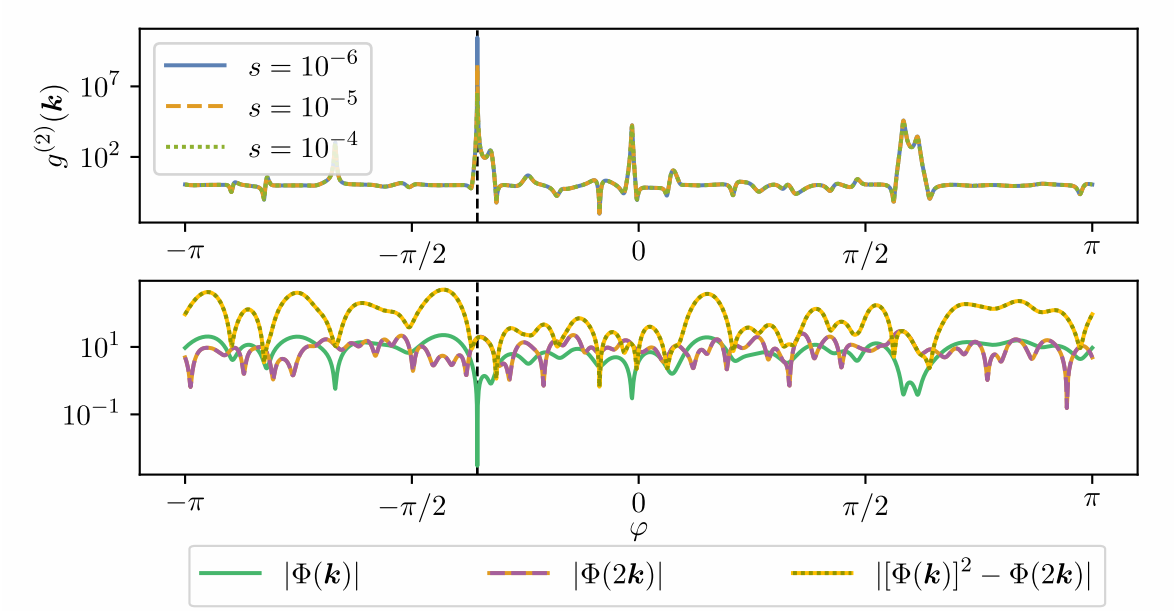

Figure 6.11: Normalised second-order autocorrelation function (top) for the superbunching cut drawn in the left plot of Fig. 6.10 together with the absolute values of the structure factor expressions $\Phi(\boldsymbol{k})$, $\Phi(2\boldsymbol{k})$, and $[\Phi(\boldsymbol{k})]^2 - \Phi(2\boldsymbol{k})$ (bottom). At the superbunching peak, the structure factor $\Phi(\boldsymbol{k})$ is approximately zero, indicating strong destructive first-order interference, whereas the absolute values of the two remaining structure factor expressions are finite. As can be seen in the top plot, the height of the superbunching peak can be controlled by the saturation parameter.

approximated by

$$g^{(2)}(\boldsymbol{k}) \approx \frac{|\Phi(2\boldsymbol{k})|^2}{s^2 N^2}\,. \tag{6.90}$$

Thus, we find that the correlation function scales inversely with the square of the saturation parameter. This means, by lowering the saturation parameter by a factor of 10, we expect an increase of the superbunching peak by a factor of 100. Indeed, in the example realisation considered, the increase of the superbunching peak is by a factor of 98.4 when going from $s = 10^{-4}$ to $s = 10^{-5}$, and by a factor of 85.7 when going from $s = 10^{-5}$ to $s = 10^{-6}$. To explain the deviation in the latter case, we note that, in general, the denominator of the autocorrelation function reads $\left(sN + |\Phi(\boldsymbol{k})|^2\right)^2$. When going from $s = 10^{-5}$ to $s = 10^{-6}$, the correction in the denominator given by $|\Phi(\boldsymbol{k})|^2 \approx 9 \times 10^{-6}$ becomes already important in comparison to the leading term $sN = 10^{-4}$. Indeed, if we calculate

$$\frac{\left(sN + |\Phi(\boldsymbol{k})|^2\right)^2|_{s=10^{-5}}}{\left(sN + |\Phi(\boldsymbol{k})|^2\right)^2|_{s=10^{-6}}} \approx 85.7\,, \tag{6.91}$$

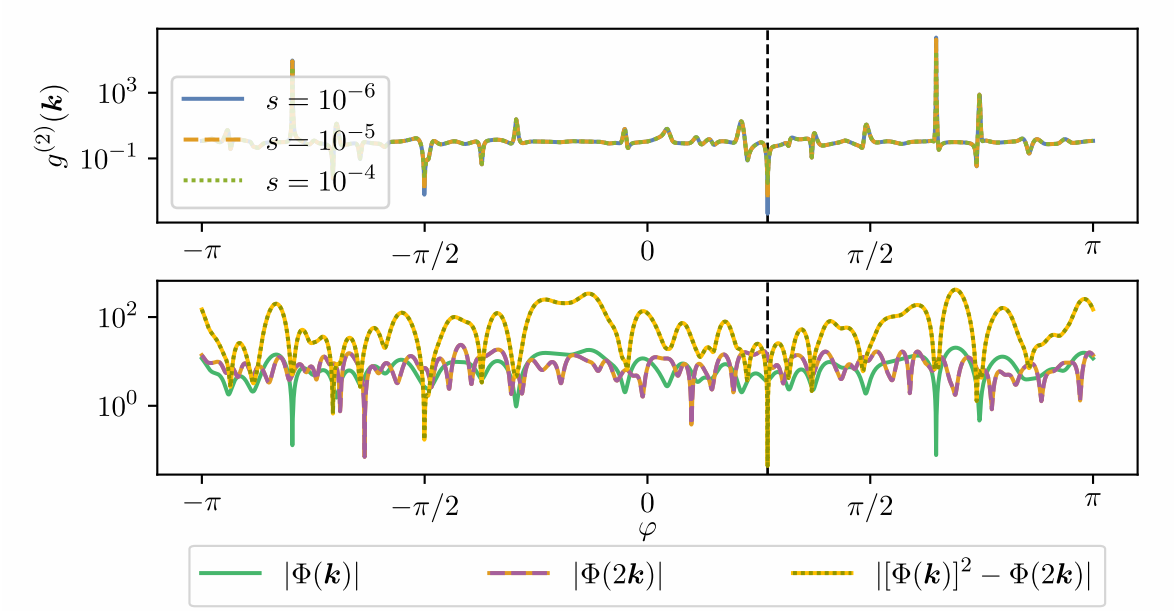

Figure 6.12: Normalised second-order autocorrelation function (top) for the antibunching cut drawn in the right plot of Fig. 6.10 together with the absolute values of the structure factor expressions $\Phi(\boldsymbol{k})$, $\Phi(2\boldsymbol{k})$, and $[\Phi(\boldsymbol{k})]^2 - \Phi(2\boldsymbol{k})$ (bottom). At the antibunching dip, the structure factor expression $[\Phi(\boldsymbol{k})]^2 - \Phi(2\boldsymbol{k})$ is approximately zero, indicating strong destructive second-order interference, whereas the absolute values of the two remaining structure factor expressions are finite. As can be seen in the top plot, the depth of the antibunching dip can be controlled by the saturation parameter.

we find exactly the factor by which the value of the peak increases. Now, let us come to the case of $[\Phi(\boldsymbol{k})]^2 - \Phi(2\boldsymbol{k}) \approx 0$. We perform again a Taylor expansion leading to

$$g^{(2)}(\boldsymbol{k}) = \frac{2sN[2 + s(N-1)] + 4s(N-2)|\Phi(\boldsymbol{k})|^2}{(sN + |\Phi(\boldsymbol{k})|^2)^2} + \mathcal{O}(|[\Phi(\boldsymbol{k})]^2 - \Phi(2\boldsymbol{k})|^2)\,. \tag{6.92}$$

Since we consider saturation parameters for which $sN \ll 1$, we do a second Taylor expansion, which gives

$$g^{(2)}(\boldsymbol{k}) = \left(\frac{4s[N + (N-2)|\Phi(\boldsymbol{k})|^2]}{|\Phi(\boldsymbol{k})|^4} + \mathcal{O}(s^2N^2)\right) + \mathcal{O}(|[\Phi(\boldsymbol{k})]^2 - \Phi(2\boldsymbol{k})|^2)\,. \tag{6.93}$$

Therefore, we expect that the autocorrelation function is linear in the saturation parameter. Indeed, in the example realisation considered, the decrease of the antibunching dip is by a factor of 9.7 when going from $s = 10^{-4}$ to $s = 10^{-5}$, and by a factor of 7.7 when going from $s = 10^{-5}$ to $s = 10^{-6}$. In the latter case, the first-order correction given by

$$\frac{|[\Phi(\boldsymbol{k})]^2 - \Phi(2\boldsymbol{k})|^2}{|\Phi(\boldsymbol{k})|^4} \tag{6.94}$$

becomes already important. Indeed, the calculation

$$\frac{\left(\frac{4s[N+(N-2)|\Phi(\boldsymbol{k})|^2]}{|\Phi(\boldsymbol{k})|^4}+\frac{|[\Phi(\boldsymbol{k})]^2-\Phi(2\boldsymbol{k})|^2}{|\Phi(\boldsymbol{k})|^4}\right)\Big|_{s=10^{-5}}}{\left(\frac{4s[N+(N-2)|\Phi(\boldsymbol{k})|^2]}{|\Phi(\boldsymbol{k})|^4}+\frac{|[\Phi(\boldsymbol{k})]^2-\Phi(2\boldsymbol{k})|^2}{|\Phi(\boldsymbol{k})|^4}\right)\Big|_{s=10^{-6}}}=7.7 \tag{6.95}$$

leads exactly to the factor by which the value of the antibunching dip decreases.

Let us conclude this section by noting that we have demonstrated that coherently driven two-level atoms, even in the linear driving regime, show a unique, unintuitive emission characteristics that is in strong contrast to the emission of classical oscillating dipoles. However, we also note that all the previous plots and discussions were based on a *single* realisation of the atomic positions. If we were to average over multiple realisations, the signal would wash out and, in particular, lose its quantumness, i.e., we would no longer find directions for which $g^{(2)}(\boldsymbol{k}) < 1$.

7 Summary and Outlook

> *What really matters for me is [...] the more active role of the observer in quantum physics [...]. According to quantum physics the observer has indeed a new relation to the physical events around him in comparison with the classical observer, who is merely a spectator.*
>
> – Wolfgang E. Pauli

After the introduction of a general open system approach to describe light matter interactions and of the concept of higher-order correlation functions, in Chapter 4, we have shown that the combination of dipole-dipole interactions and measurement-induced entanglement allows for engineering the spontaneous emission properties of a three-atom system, in which two atoms are close to each other, while the third atom is far distant from the two-atom subsystem. In this context, we found that by properly balancing the different interference channels, one can observe a strong superradiant and subradiant decay simultaneously, only depending on the observation angle. Afterwards, in the same chapter, we have demonstrated how the interference of the different emission paths of the remote atom and the two-atom subsystem can be used to gain information about properties of the two close-by atoms, which would be inaccessible without the remote atom. With our developed measurement protocol, using either the second-order or third-order photon correlation function, the distance of the subwavelength separated atoms can be determined with sub-Abbe resolution. Then, we extended the system by adding additional energy levels and excited states and presented a method how the interference can be utilised to reconstruct the initially excited superposition state of the two-atom subsystem. In the future, we plan to investigate further quantum sensing tasks that can potentially be performed utilising the entanglement of a system of interest with a remote quantum system created via conditional photon measurements.
In the subsequent Chapter 5, we extended the number of atoms from three to an arbitrary number N. In a first step, we recapitulated the prominent phenomenon of Dicke superradiance and traced the emission behaviour back to dipole-dipole correlations that emerge during the course of the time evolution. We used this understanding to mimic a temporal Dicke-like superradiant burst in a particular observation direction even in the case of far distant non-interacting atoms, with the necessary dipole-dipole correlations created via consecutive conditional photon measurements. To give a transparent physical explanation of the result-

ing light emission, we applied a quantum path interference formalism, which allowed us to calculate the full time course of the emission using combinatorics, i.e., by simply counting interfering quantum paths. In the end, we gave a short outlook on the quantumness of the correlations by explicitly calculating measures of entanglement and quantum correlations in the case of two atoms, and by computing an entanglement witness and solving separability equations in the general case of N atoms. In the latter case, in future investigations, a comparison with other entanglement witnesses and an analysis of proper measures of entanglement and quantum correlations need to be done to unravel confusions and to be able to clearly identify the origin of superradiance.

In the last chapter, Chapter 6, we considered once more an arbitrary number of atoms N, all independent of each other, so that the total state is a simple tensor product of the individual atomic states, and analysed the statistical moments of the emitted light. In particular, we derived two conditions, one relating the number of atoms to the correlation order and one relating the strength of the coherences to the populations of the atoms, which need to be fulfilled to observe thermal light statistics in terms of photon correlation functions. In the future, we plan to extend these investigations by additionally deriving conditions for the field correlation functions. After establishing the two conditions, we demonstrated the validity of the two conditions by considering several examples, one of them being a dilute cloud of atoms driven by a plane wave laser field. In the last section of this chapter, we analysed the aforementioned system in more detail in the small driving regime. Even though the dynamics can be adequately described by a classical dipole model, the emission statistics differs drastically from that of classical oscillating dipoles, showing the difference of the latter in comparison to two-level atoms. In particular, we explicitly calculated the second-order autocorrelation function and identified conditions for strong superbunching and antibunching. Thereby, the heights of the superbunching peaks and the depths of the antibunching dips can be controlled by the saturation parameter. These astonishing results motivate us to analyse the correlation functions of even higher orders in the future and also to investigate a system of weakly laser driven *interacting* atoms, i.e., a densely packed cloud of atoms.

A Power-Zienau-Woolley transformation

In this appendix, we derive the Hamiltonian describing the interaction between charges and the quantised electromagnetic field in the long-wavelength approximation by introducing the so-called Power-Zienau-Woolley transformation. The following derivation is based on Chapter IV.C in Ref. [100].

A.1 Polarisation and magnetisation density

Assume a charge q_α at position $\boldsymbol{r}_\alpha$ with respect to the origin. This charge can be represented by a charge q_α at the origin plus a dipole chain where the $-q_\alpha$ and q_α charges cancel each other, such that only the charge q_α at $\boldsymbol{r}_\alpha$ remains (see Fig. A.1). For n such dipoles their separation reads $\frac{\boldsymbol{r}_\alpha}{n}$. By letting n go to infinity, one arrives at a continuous distribution with polarisation density

$$\boldsymbol{P}(\boldsymbol{r}) = \lim_{n\to\infty} \sum_{p=0}^{n-1} q_\alpha \frac{\boldsymbol{r}_\alpha}{n} \delta\left(\boldsymbol{r} - \frac{p+\frac{1}{2}}{n}\boldsymbol{r}_\alpha\right) = \int_0^1 du\, q_\alpha \boldsymbol{r}_\alpha \delta(\boldsymbol{r} - u\boldsymbol{r}_\alpha)\,. \tag{A.1}$$

This polarisation density together with the charge q_α at the origin is an alternative description of the charge q_α at $\boldsymbol{r}_\alpha$. Here, the dipoles are distributed along the line $\mathcal{O}\boldsymbol{r}_\alpha$, but any curve is possible (with dipoles tangentially aligned), i.e., we have a certain freedom in choosing the polarisation density. The made choice of a straight line gives the minimum polarisation field. If we consider now a system of charges, we can describe them by the sum of all charges at

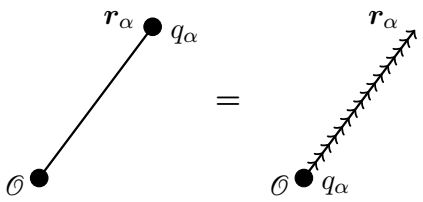

Figure A.1: A charge q_α at point $\boldsymbol{r}_\alpha$ is equivalent to a charge q_α at the origin $\mathcal{O}$ plus a dipole chain consisting of n dipoles $\frac{q_\alpha \boldsymbol{r}_\alpha}{n}$.

the origin (which is zero for a globally neutral system) and a polarisation density

$$\boldsymbol{P}(\boldsymbol{r}) = \sum_\alpha \int_0^1 du\, q_\alpha \boldsymbol{r}_\alpha \delta(\boldsymbol{r} - u\boldsymbol{r}_\alpha)\,. \tag{A.2}$$

For the following calculations, it is convenient to introduce the Fourier transform of $\boldsymbol{P}(\boldsymbol{r})$ reading

$$\boldsymbol{\mathscr{P}}(\boldsymbol{k}) = \sum_\alpha \int_0^1 du\, \frac{q_\alpha \boldsymbol{r}_\alpha}{(2\pi)^{\frac{3}{2}}} e^{-i\boldsymbol{k}\boldsymbol{r}_\alpha u}\,. \tag{A.3}$$

From the divergence of $\boldsymbol{P}$ in Fourier space

$$i\boldsymbol{k}\boldsymbol{\mathscr{P}}(\boldsymbol{k}) = -\sum_\alpha q_\alpha \frac{e^{-i\boldsymbol{k}\boldsymbol{r}_\alpha}}{(2\pi)^{\frac{3}{2}}} + \sum_\alpha q_\alpha \frac{1}{(2\pi)^{\frac{3}{2}}} \tag{A.4}$$

follows that $\nabla\boldsymbol{P}(\boldsymbol{r}) = -\rho(\boldsymbol{r}) + \rho_0(\boldsymbol{r})$ with $\rho(\boldsymbol{r})$ the charge density and $\rho_0(\boldsymbol{r}) = (\sum_\alpha q_\alpha)\,\delta(\boldsymbol{r})$ the reference charge density. Further, from Maxwell's equations, we have $\nabla\boldsymbol{E} = \frac{\rho}{\varepsilon_0}$. This leads to the definition of the so-called displacement field $\boldsymbol{D} = \varepsilon_0\boldsymbol{E} + \boldsymbol{P}$, for which $\nabla\boldsymbol{D} = \rho_0$. Writing the Fourier transform of $\boldsymbol{D}$ in terms of its so-called longitudinal and transverse components as $\boldsymbol{\mathscr{D}} = \boldsymbol{\mathscr{D}}_\parallel + \boldsymbol{\mathscr{D}}_\perp$, where $\boldsymbol{\mathscr{D}}_\parallel$ is parallel and $\boldsymbol{\mathscr{D}}_\perp$ perpendicular to $\boldsymbol{k}$, we find $\boldsymbol{D}_\parallel = \varepsilon_0\boldsymbol{E}_0$ with $\boldsymbol{E}_0$ being the static electric field produced by the charge density ρ_0. If we assume a globally neutral system, i.e., $\sum_\alpha q_\alpha = 0$, $\rho_0 = 0$ and thus $\boldsymbol{D}$ is a transverse field, i.e., $\boldsymbol{D}_\parallel = 0$ and $\boldsymbol{D} = \boldsymbol{D}_\perp$, with which we obtain $\varepsilon_0\boldsymbol{E}_\parallel = -\boldsymbol{P}_\parallel$. This allows us to write the Coulomb energy as

$$\begin{aligned} V_{\text{coul}} &= \frac{1}{8\pi\varepsilon_0} \iint d^3r d^3r'\, \frac{\rho(\boldsymbol{r})\rho(\boldsymbol{r}')}{|\boldsymbol{r} - \boldsymbol{r}'|} = \frac{1}{2\varepsilon_0} \int d^3k\, \frac{\rho^*(\boldsymbol{k})\rho(\boldsymbol{k})}{k^2} \\ &= \frac{\varepsilon_0}{2} \int d^3k\, |\boldsymbol{\mathscr{E}}_\parallel(\boldsymbol{k})|^2 = \frac{\varepsilon_0}{2} \int d^3r\, |\boldsymbol{E}_\parallel(\boldsymbol{r})|^2 = \frac{1}{2\varepsilon_0} \int d^3r\, |\boldsymbol{P}_\parallel(\boldsymbol{r})|^2\,, \end{aligned} \tag{A.5}$$

where we applied the Parseval-Plancherel identity and the convolution theorem. Further, we used $\boldsymbol{\mathscr{E}}_\parallel = -\frac{i}{\varepsilon_0}\rho\frac{\boldsymbol{k}}{k^2}$ resulting from the Maxwell equation $i\boldsymbol{k}\boldsymbol{\mathscr{E}} = \frac{\rho}{\varepsilon_0}$ in Fourier space.
Connected to the motion of the charges, there is a current $\boldsymbol{j}$, which is related to a change of the polarisation density $\dot{\boldsymbol{P}}$. With $\dot\rho + \nabla\dot{\boldsymbol{P}} = 0$ and the conservation of charge $\dot\rho + \nabla\boldsymbol{j} = 0$, we find $\nabla(\boldsymbol{j} - \dot{\boldsymbol{P}}) = 0$, i.e., $\boldsymbol{j} - \dot{\boldsymbol{P}}$ is divergence free. Thus, we can write

$$\boldsymbol{j}(\boldsymbol{r}) = \boldsymbol{j}_p(\boldsymbol{r}) + \boldsymbol{j}_m(\boldsymbol{r}) \tag{A.6}$$

with $\boldsymbol{j}_p(\boldsymbol{r}) = \dot{\boldsymbol{P}}(\boldsymbol{r})$ the polarisation current and $\boldsymbol{j}_m(\boldsymbol{r})$ the divergence free magnetisation current. Calculating the Fourier transform of Eq. (A.6) and transforming back to real space,

leads to

$$\boldsymbol{j}_m(\boldsymbol{r}) = \nabla \times \boldsymbol{M}(\boldsymbol{r}) \quad \text{with} \quad \boldsymbol{M}(\boldsymbol{r}) = \sum_\alpha \int_0^1 du\, u q_\alpha \boldsymbol{r}_\alpha \times \dot{\boldsymbol{r}}_\alpha \delta(\boldsymbol{r} - u\boldsymbol{r}_\alpha) \tag{A.7}$$

interpreted as magnetisation density.

A.2 Power-Zienau-Woolley transformation

We now introduce the Power-Zienau-Woolley transformation by considering the standard Lagrangian of electrodynamics in Coulomb gauge given by

$$L = \sum_\alpha \frac{1}{2} m_\alpha \dot{\boldsymbol{r}}_\alpha^2 - V_{\text{coul}} + \int d^3r\, \frac{\varepsilon_0}{2} [\dot{\boldsymbol{A}}^2 - c^2 (\nabla \times \boldsymbol{A})^2] + \boldsymbol{j}\boldsymbol{A}\,, \tag{A.8}$$

where $\boldsymbol{A}$ is the vector potential. If we add the total time derivative of a function F to this standard Lagrangian, we obtain an equivalent Lagrangian L' with respect to the principle of least action. Power, Zienau, and Woolley introduced the function

$$F = -\int d^3r\, \boldsymbol{P}(\boldsymbol{r}) \boldsymbol{A}(\boldsymbol{r}) \tag{A.9}$$

to obtain a new equivalent formulation. Grouping the resulting additional term together with the interaction between charges and field leads to

$$L'_I = \int d^3r\, \boldsymbol{j}\boldsymbol{A} - \int d^3r\, (\dot{\boldsymbol{P}}\boldsymbol{A} + \boldsymbol{P}\dot{\boldsymbol{A}}) = \int d^3r\, \boldsymbol{M}\boldsymbol{B} + \int d^3r\, \boldsymbol{P}\boldsymbol{E}_\perp\,, \tag{A.10}$$

where we used $\boldsymbol{B} = \nabla \times \boldsymbol{A}$ and $\dot{\boldsymbol{A}} = -\boldsymbol{E}_\perp$. Therefore, we find that the interaction is given by the coupling of the magnetisation density to the magnetic field and the polarisation density to the transverse electric field. The new conjugate particle and field momenta are [$\boldsymbol{\mathscr{A}}(\boldsymbol{k})$ is the Fourier transform of $\boldsymbol{A}(\boldsymbol{r})$]

$$\boldsymbol{p}_{\alpha L'} = m_\alpha \dot{\boldsymbol{r}}_\alpha + \int_0^1 du\, u q_\alpha \boldsymbol{B}(\boldsymbol{r}_\alpha u) \times \boldsymbol{r}_\alpha\,, \tag{A.11}$$

$$\boldsymbol{\Pi}_{L'}(\boldsymbol{k}) = \varepsilon_0 \dot{\boldsymbol{\mathscr{A}}}(\boldsymbol{k}) - \boldsymbol{\mathscr{P}}_\perp(\boldsymbol{k})\,, \tag{A.12}$$

with which the new Hamiltonian can be found via the Legendre transform giving

$$H_{L'} = \sum_\alpha \dot{\boldsymbol{r}}_\alpha \boldsymbol{p}_{\alpha L'} + \fint d^3k\, (\dot{\boldsymbol{\mathscr{A}}} \boldsymbol{\Pi}^*_{L'} + \dot{\boldsymbol{\mathscr{A}}}^* \boldsymbol{\Pi}_{L'}) - L'\,. \tag{A.13}$$

Here, $\fint$ denotes the integral over one reciprocal half space. This procedure would give us a new equivalent description of quantum electrodynamics, which is particularly suited for a multipole expansion. However, for simplicity, we do immediately the so-called long-wavelength

approximation, which will give us a pure electric dipole coupling. Let the system of charges have an extent of a around the origin. Then, if the charges and the field couple mainly via modes whose wavelengths λ are much larger than the extent a, such that $\frac{a}{\lambda} \ll 1$ holds, we can approximate $\boldsymbol{A}(\boldsymbol{r}) \approx \boldsymbol{A}(\boldsymbol{0})$ in the coupling terms. The function F reduces to

$$F = -\boldsymbol{A}(\boldsymbol{0}) \int d^3r\, \boldsymbol{P}(\boldsymbol{r}) = -\boldsymbol{d}\boldsymbol{A}(\boldsymbol{0}) \tag{A.14}$$

with $\boldsymbol{d} = \sum_\alpha q_\alpha \boldsymbol{r}_\alpha$ being the total dipole moment. Further, the interaction term in the Lagrangian simplifies to

$$L_I' = \int d^3r\, \boldsymbol{j}\boldsymbol{A} - \int d^3r\, (\dot{\boldsymbol{P}}\boldsymbol{A} + \boldsymbol{P}\dot{\boldsymbol{A}}) = \int d^3r\, \boldsymbol{P}\boldsymbol{E}_\perp\,, \tag{A.15}$$

since $\nabla \times \boldsymbol{A}(\boldsymbol{0}) = 0$ and the new conjugate momenta are

$$\boldsymbol{p}_{\alpha L'} = m_\alpha \dot{\boldsymbol{r}}_\alpha\,, \tag{A.16}$$

$$\boldsymbol{\Pi}_{L'}(\boldsymbol{k}) = \varepsilon_0 \dot{\boldsymbol{\mathscr{A}}}(\boldsymbol{k}) - \boldsymbol{\mathscr{P}}_\perp(\boldsymbol{k})\,. \tag{A.17}$$

We now present the new Hamiltonian, obtained via the Legendre transform of Eq. (A.13). It can be split into a part describing the particles $H_{PL'}$, a part describing the radiation field $H_{RL'}$, and a part accounting for the interaction $H_{IL'}$. The particle Hamiltonian reads

$$H_{PL'} = \sum_\alpha \frac{\boldsymbol{p}_{\alpha L'}^2}{2m_\alpha} + V_{\text{coul}} + \frac{1}{\varepsilon_0} \fint d^3k\, |\boldsymbol{\mathscr{P}}_\perp(\boldsymbol{k})|^2 = \sum_\alpha \frac{\boldsymbol{p}_{\alpha L'}^2}{2m_\alpha} + \frac{1}{2\varepsilon_0} \int d^3r\, |\boldsymbol{P}(\boldsymbol{r})|^2\,, \tag{A.18}$$

where we extended the integral over one half reciprocal plane to the full plane, used the Parseval-Plancherel theorem, and applied Eq. (A.5). The radiation field Hamiltonian is given by

$$H_{RL'} = \frac{\varepsilon_0}{2} \int d^3r\, \left\{ \frac{\boldsymbol{\Pi}_{L'}^2(\boldsymbol{r})}{\varepsilon_0^2} + c^2 [\nabla \times \boldsymbol{A}(\boldsymbol{r})]^2 \right\}\,, \tag{A.19}$$

where $\boldsymbol{\Pi}_{L'}(\boldsymbol{r})$ is the Fourier transform of $\boldsymbol{\Pi}_{L'}(\boldsymbol{k})$, and for the interaction Hamiltonian we find

$$H_{IL'} = \int d^3r\, \frac{\boldsymbol{P}(\boldsymbol{r})\boldsymbol{\Pi}_{L'}(\boldsymbol{r})}{\varepsilon_0} \approx \frac{\boldsymbol{d}\boldsymbol{\Pi}_{L'}(\boldsymbol{0})}{\varepsilon_0}\,. \tag{A.20}$$

A.3 Quantisation and physical variables

Now, we come to the usual quantisation procedure. Therefore, in the following, we denote with a superscript (2) the operators in the new representation, whereas operators in the old representation are labelled by a superscript (1). The position variables $\boldsymbol{r}_\alpha$ and conjugate

momenta $\boldsymbol{p}_{\alpha L'}$ now become operators that have to satisfy the fundamental canonical commutation relations. This can be achieved by choosing the operators $\hat{\boldsymbol{r}}_\alpha^{(2)} = \hat{\boldsymbol{r}}_\alpha = \boldsymbol{r}_\alpha$ (i.e., multiplication with $\boldsymbol{r}_\alpha$) and $\hat{\boldsymbol{p}}_\alpha^{(2)} = \hat{\boldsymbol{p}}_\alpha = -i\hbar\nabla_{\boldsymbol{r}_\alpha}$. The new field variables are represented by operators $\hat{\boldsymbol{\mathscr{A}}}^{(2)}(\boldsymbol{k}) = \hat{\boldsymbol{\mathscr{A}}}(\boldsymbol{k}) = \boldsymbol{\varepsilon}\hat{\mathscr{A}}_\varepsilon(\boldsymbol{k}) + \boldsymbol{\varepsilon}'\hat{\mathscr{A}}_{\varepsilon'}(\boldsymbol{k})$ and $\hat{\boldsymbol{\Pi}}_{L'}^{(2)}(\boldsymbol{k}) = \hat{\boldsymbol{\Pi}}(\boldsymbol{k}) = \boldsymbol{\varepsilon}\hat{\Pi}_\varepsilon(\boldsymbol{k}) + \boldsymbol{\varepsilon}'\hat{\Pi}_{\varepsilon'}(\boldsymbol{k})$, which have to fulfil the commutation relations

$$[\hat{\mathscr{A}}_\varepsilon(\boldsymbol{k}), \hat{\Pi}_{\varepsilon'}(\boldsymbol{k}')] = 0\,, \tag{A.21}$$

$$[\hat{\mathscr{A}}_\varepsilon(\boldsymbol{k}), \hat{\Pi}_{\varepsilon'}^\dagger(\boldsymbol{k}')] = i\hbar\delta_{\varepsilon,\varepsilon'}\delta(\boldsymbol{k}-\boldsymbol{k}')\,. \tag{A.22}$$

Thereby, $\boldsymbol{\varepsilon}$ and $\boldsymbol{\varepsilon}'$ denote two polarisation directions orthogonal to each other and to the wave vector $\boldsymbol{k}$. With these operators, one can define a new operator

$$\hat{a}_\varepsilon(\boldsymbol{k}) \coloneqq \sqrt{\frac{\varepsilon_0}{2\hbar\omega_k}}\left[\omega_k\hat{\mathscr{A}}_\varepsilon(\boldsymbol{k}) + \frac{i}{\varepsilon_0}\hat{\Pi}_\varepsilon(\boldsymbol{k})\right] \tag{A.23}$$

whose Hermitian conjugate is

$$\hat{a}_\varepsilon^\dagger(\boldsymbol{k}) = \sqrt{\frac{\varepsilon_0}{2\hbar\omega_k}}\left[\omega_k\hat{\mathscr{A}}_\varepsilon^\dagger(\boldsymbol{k}) - \frac{i}{\varepsilon_0}\hat{\Pi}_\varepsilon^\dagger(\boldsymbol{k})\right]. \tag{A.24}$$

The commutation relations for the field operators then imply for the commutation relations of these two new operators

$$[\hat{a}_\varepsilon(\boldsymbol{k}), \hat{a}_{\varepsilon'}(\boldsymbol{k}')] = 0\,, \tag{A.25}$$

$$[\hat{a}_\varepsilon^\dagger(\boldsymbol{k}), \hat{a}_{\varepsilon'}^\dagger(\boldsymbol{k}')] = 0\,, \tag{A.26}$$

$$[\hat{a}_\varepsilon(\boldsymbol{k}), \hat{a}_{\varepsilon'}^\dagger(\boldsymbol{k}')] = \delta_{\varepsilon,\varepsilon'}\delta(\boldsymbol{k}-\boldsymbol{k}')\,, \tag{A.27}$$

which shows that $\hat{a}_\varepsilon(\boldsymbol{k})$ and $\hat{a}_\varepsilon^\dagger(\boldsymbol{k})$ are the annihilation and creation operators of the mode characterised by $\boldsymbol{k}$ and $\boldsymbol{\varepsilon}$. Inverting Eqs. (A.23) and (A.24), and performing a Fourier transform gives the field operators in real space

$$\hat{\boldsymbol{A}}(\boldsymbol{r}) = \int d^3k \sum_{\boldsymbol{\varepsilon}} \sqrt{\frac{\hbar}{2\varepsilon_0\omega_k(2\pi)^3}}\left[\boldsymbol{\varepsilon}\hat{a}_\varepsilon(\boldsymbol{k})e^{i\boldsymbol{kr}} + \boldsymbol{\varepsilon}^*\hat{a}_\varepsilon^\dagger(\boldsymbol{k})e^{-i\boldsymbol{kr}}\right], \tag{A.28}$$

$$\hat{\boldsymbol{\Pi}}(\boldsymbol{r}) = -i\varepsilon_0 \int d^3k \sum_{\boldsymbol{\varepsilon}} \sqrt{\frac{\hbar\omega_k}{2\varepsilon_0(2\pi)^3}}\left[\boldsymbol{\varepsilon}\hat{a}_\varepsilon(\boldsymbol{k})e^{i\boldsymbol{kr}} - \boldsymbol{\varepsilon}^*\hat{a}_\varepsilon^\dagger(\boldsymbol{k})e^{-i\boldsymbol{kr}}\right]. \tag{A.29}$$

Before we state the Hamilton operator in the new representation, we want to note that depending on which representation one uses, the same physical quantity G is, in general, described by different operators $\hat{G}^{(2)}$ and $\hat{G}^{(1)}$, where the operators are related to each other

by the unitary transformation

$$\hat{T} = \exp\left(\frac{i}{\hbar}\hat{F}\right) = \exp\left(-\frac{i}{\hbar}\hat{\boldsymbol{d}}\hat{\boldsymbol{A}}(\boldsymbol{0})\right) , \tag{A.30}$$

i.e., $\hat{G}^{(2)} = \hat{T}\hat{G}^{(1)}\hat{T}^{\dagger}$. Vice versa, the same operator in the two representations corresponds, in general, to different physical variables.
Coming back to the Hamiltonian obtained via the Legendre transform of Eq. (A.13), we can now give the operators of the different parts. The particle Hamiltonian is given by

$$\hat{H}'_P = \hat{H}^{(2)}_{PL'} = \sum_{\alpha} \frac{\hat{\boldsymbol{p}}^2_{\alpha}}{2m_{\alpha}} + \frac{1}{2\varepsilon_0}\int d^3r\, |\hat{\boldsymbol{P}}(\boldsymbol{r})|^2 \,. \tag{A.31}$$

Further, the radiation field Hamiltonian can be written as

$$\begin{aligned}\hat{H}'_R = \hat{H}^{(1)}_{RL} = \hat{H}^{(2)}_{RL'} &= \frac{\varepsilon_0}{2}\int d^3r \left\{ \frac{\hat{\boldsymbol{\Pi}}^2(\boldsymbol{r})}{\varepsilon_0^2} + c^2[\nabla \times \hat{\boldsymbol{A}}(\boldsymbol{r})]^2 \right\} \\ &= \int d^3k \sum_{\boldsymbol{\varepsilon}} \hbar\omega_k \left[\hat{a}^{\dagger}_{\varepsilon}(\boldsymbol{k})\hat{a}_{\varepsilon}(\boldsymbol{k}) + \frac{1}{2}\right]\end{aligned} \tag{A.32}$$

and for the interaction Hamiltonian we find

$$\hat{H}'_I = \hat{H}^{(2)}_{IL'} = \frac{1}{\varepsilon_0}\hat{\boldsymbol{d}}\hat{\boldsymbol{\Pi}}(\boldsymbol{0}) \,. \tag{A.33}$$

Since the displacement field is $\hat{\boldsymbol{D}}^{(2)}(\boldsymbol{r}) = \varepsilon_0\hat{\boldsymbol{E}}^{(2)}(\boldsymbol{r}) + \hat{\boldsymbol{P}}^{(2)}(\boldsymbol{r})$, we find $\hat{\boldsymbol{\Pi}}(\boldsymbol{r}) = -\hat{\boldsymbol{D}}^{(2)}_{\perp}(\boldsymbol{r}) = -\varepsilon_0\hat{\boldsymbol{E}}^{(1)}_{\perp}(\boldsymbol{r})$, such that the interaction can be written as $\hat{H}'_I = -\hat{\boldsymbol{d}}\hat{\boldsymbol{E}}^{(1)}_{\perp}(\boldsymbol{0})$, i.e., as an electric dipole coupling to the transverse electric field in representation (1). However, we should note that the transverse electric field in representation (2) is not described by the operator $\hat{\boldsymbol{E}}^{(1)}$. Therefore, we should rather write the coupling as $\hat{H}'_I = -\frac{\hat{\boldsymbol{d}}\hat{\boldsymbol{D}}^{(2)}_{\perp}(\boldsymbol{0})}{\varepsilon_0}$, i.e., as a coupling of the dipole moment to the transverse displacement field at the origin given by

$$\hat{\boldsymbol{D}}^{(2)}_{\perp}(\boldsymbol{0}) = i\varepsilon_0 \int d^3k \sum_{\boldsymbol{\varepsilon}} \sqrt{\frac{\hbar\omega_k}{2\varepsilon_0(2\pi)^3}} \left[\boldsymbol{\varepsilon}\hat{a}_{\varepsilon}(\boldsymbol{k}) - \boldsymbol{\varepsilon}^*\hat{a}^{\dagger}_{\varepsilon}(\boldsymbol{k})\right] . \tag{A.34}$$

Thus, the total Hamiltonian reads

$$\hat{H}' = \sum_{\alpha} \frac{\hat{\boldsymbol{p}}^2_{\alpha}}{2m_{\alpha}} + \int d^3k \sum_{\boldsymbol{\varepsilon}} \hbar\omega_k \left[\hat{a}^{\dagger}_{\varepsilon}(\boldsymbol{k})\hat{a}_{\varepsilon}(\boldsymbol{k}) + \frac{1}{2}\right] + \frac{1}{2\varepsilon_0}\int d^3r\, |\hat{\boldsymbol{P}}(\boldsymbol{r})|^2 - \frac{\hat{\boldsymbol{d}}\hat{\boldsymbol{D}}^{(2)}_{\perp}(\boldsymbol{0})}{\varepsilon_0} \,. \tag{A.35}$$

A.4 Extension to two globally neutral systems

In this section, we extend the previous description to the case of two separated globally neutral systems. Let us denote the two subsystems with letters A and B, and indices α and β. The charges of subsystem A shall be placed around a point $\boldsymbol{R}_A$, and that of subsystem B around a point $\boldsymbol{R}_B$. The polarisation densities now read

$$\boldsymbol{P}_{A/B}(\boldsymbol{r}) = \sum_{\alpha/\beta} \int_0^1 du\, q_{\alpha/\beta} \boldsymbol{s}_{\alpha/\beta} \delta(\boldsymbol{r} - \boldsymbol{R}_{A/B} - u\boldsymbol{s}_{\alpha/\beta})\,, \tag{A.36}$$

where $\boldsymbol{s}_{\alpha/\beta} = \boldsymbol{r}_{\alpha/\beta} - \boldsymbol{R}_{A/B}$ are the relative position vectors. Again, since $\sum_{\alpha/\beta} q_{\alpha/\beta} = 0$, we have $\boldsymbol{E}_{\parallel A/B}(\boldsymbol{r}) = -\frac{1}{\varepsilon_0}\boldsymbol{P}_{\parallel A/B}(\boldsymbol{r})$, which we can use to express the individual Coulomb energies. To obtain the new description from the standard Lagrangian in Coulomb gauge, again the total time derivative of the function

$$F = -\int d^3r\, \boldsymbol{P}(\boldsymbol{r})\boldsymbol{A}(\boldsymbol{r}) \tag{A.37}$$

is added to the Lagrangian. However, here $\boldsymbol{P}(\boldsymbol{r}) = \boldsymbol{P}_A(\boldsymbol{r}) + \boldsymbol{P}_B(\boldsymbol{r})$ denotes the total polarisation density given by the sum of the individual polarisation densities. Applying the long-wavelength approximation and performing the transformation, leads to the Hamiltonian (for details see Ref. [100])

$$H_{L'} = H^A_{PL'} + H^B_{PL'} + H_{RL'} + H^A_{IL'} + H^B_{IL'} + V^{AB}\,, \tag{A.38}$$

where the particle Hamiltonians $H^{A/B}_{PL'}$, the radiation field Hamiltonian $H_{RL'}$, and the interaction Hamiltonians $H^{A/B}_{IL'}$ are given as before. However, in addition, a term

$$V^{AB} = \underbrace{\frac{1}{2\varepsilon_0}\int d^3k\, (\boldsymbol{\mathscr{P}}_{\perp A}\boldsymbol{\mathscr{P}}^*_{\perp B} + \boldsymbol{\mathscr{P}}^*_{\perp A}\boldsymbol{\mathscr{P}}_{\perp B})}_{\text{=self-energy for transverse polarisation}} + \underbrace{\sum_{\alpha,\beta}\frac{q_\alpha q_\beta}{4\pi\varepsilon_0|\boldsymbol{r}_\alpha - \boldsymbol{r}_\beta|}}_{=V^{AB}_{\text{coul}}\text{ Coulomb energy between systems A and B}} \tag{A.39}$$

arises describing the interaction of the two subsystems. The Coulomb energy between the two subsystems can be written as

$$\begin{aligned} V^{AB}_{\text{coul}} &= V^{\text{tot}}_{\text{coul}} - V^{AA}_{\text{coul}} - V^{BB}_{\text{coul}} \\ &= \frac{1}{2\varepsilon_0}\int d^3r \left\{\left[\boldsymbol{P}_{\parallel A}(\boldsymbol{r}) + \boldsymbol{P}_{\parallel B}(\boldsymbol{r})\right]^2 - \boldsymbol{P}^2_{\parallel A}(\boldsymbol{r}) - \boldsymbol{P}^2_{\parallel B}(\boldsymbol{r})\right\} = \frac{1}{\varepsilon_0}\int d^3r\, \boldsymbol{P}_{\parallel A}(\boldsymbol{r})\boldsymbol{P}_{\parallel B}(\boldsymbol{r})\,. \end{aligned} \tag{A.40}$$

By combining this expression with the self-energy, we finally find

$$V^{AB} = \frac{1}{\varepsilon_0} \int d^3r \, \left[\boldsymbol{P}_{\perp A}(\boldsymbol{r}) \boldsymbol{P}_{\perp B}(\boldsymbol{r}) + \boldsymbol{P}_{\parallel A}(\boldsymbol{r}) \boldsymbol{P}_{\parallel B}(\boldsymbol{r}) \right] = \frac{1}{\varepsilon_0} \int d^3r \, \boldsymbol{P}_A(\boldsymbol{r}) \boldsymbol{P}_B(\boldsymbol{r}) \,. \tag{A.41}$$

Since $\boldsymbol{P}_A(\boldsymbol{r})$ is strictly zero outside of system A and $\boldsymbol{P}_B(\boldsymbol{r})$ outside of system B, V^{AB} vanishes if the distance $|\boldsymbol{R}_A - \boldsymbol{R}_B|$ between the two subsystems is larger than the extents of the two subsystems. With that, we obtain a natural extension of the case of one system of charges.

B Explicit calculation of the coupling parameters

In this appendix, we carry out the explicit calculation of the coupling parameters appearing in the quantum master equation. Therefore, we start with the function $F_{pq}(k, \boldsymbol{R})$, which was defined in the main text as

$$F_{pq}(k, \boldsymbol{R}) \coloneqq \int d\Omega_k \sum_{\boldsymbol{\varepsilon}} e^{i\boldsymbol{k}\boldsymbol{R}} [\boldsymbol{e}_p \boldsymbol{\varepsilon}][\boldsymbol{e}_q \boldsymbol{\varepsilon}^*] \,. \tag{B.1}$$

In spherical coordinates, the wave vector is $\boldsymbol{k} = k\boldsymbol{e}_r$. The two polarisation vectors are orthogonal to the wave vector, such that we can wlog choose $\boldsymbol{\varepsilon} = \boldsymbol{e}_\theta$ and $\boldsymbol{\varepsilon}' = \boldsymbol{e}_\phi$. Thereby,

$$\boldsymbol{e}_r = \begin{pmatrix} \cos\phi \sin\theta \\ \sin\phi \sin\theta \\ \cos\theta \end{pmatrix} , \quad \boldsymbol{e}_\theta = \begin{pmatrix} \cos\phi \cos\theta \\ \sin\phi \cos\theta \\ -\sin\theta \end{pmatrix} , \quad \boldsymbol{e}_\phi = \begin{pmatrix} -\sin\phi \\ \cos\phi \\ 0 \end{pmatrix} \tag{B.2}$$

are the spherical coordinate unit vectors. We see that, within this choice, the polarisation vectors $\boldsymbol{\varepsilon}$ and $\boldsymbol{\varepsilon}'$ are real vectors. However, we note that one could, e.g., also use complex spherical unit vectors $\boldsymbol{\varepsilon}_\pm = \frac{1}{\sqrt{2}}(\boldsymbol{\varepsilon} \pm i\boldsymbol{\varepsilon}')$. Since we integrate over the whole solid angle, we can choose wlog $\boldsymbol{R} = R\boldsymbol{e}_z$ with $R = |\boldsymbol{R}|$ and $\boldsymbol{e}_z$ being the Cartesian unit vector in the z direction. With this choice, a straightforward calculation gives

$$\int_0^{2\pi} d\phi \sum_{\boldsymbol{\varepsilon}} [\boldsymbol{e}_p \boldsymbol{\varepsilon}][\boldsymbol{e}_q \boldsymbol{\varepsilon}^*] = \pi(1 + \cos^2\theta)\delta_{p,q} + \pi(2\sin^2\theta - 1 - \cos^2\theta)\frac{[\boldsymbol{e}_p \boldsymbol{R}][\boldsymbol{e}_q \boldsymbol{R}]}{R^2} \,. \tag{B.3}$$

Now, only the θ integration remains. With $e^{i\boldsymbol{k}\boldsymbol{R}} = e^{ikR\cos\theta} = e^{i\eta\cos\theta}$, where $\eta = kR$, we obtain the following three integrals

$$\int_0^\pi d\theta \, \sin\theta e^{i\eta\cos\theta} = \frac{2\sin\eta}{\eta} \,, \tag{B.4}$$

$$\int_0^\pi d\theta \, \sin\theta\cos^2\theta e^{i\eta\cos\theta} = \frac{4\cos\eta}{\eta^2} + \left(\frac{2}{\eta} - \frac{4}{\eta^3}\right)\sin\eta \,, \tag{B.5}$$

$$\int_0^\pi d\theta \, \sin\theta\sin^2\theta e^{i\eta\cos\theta} = \frac{4\sin\eta}{\eta^3} - \frac{4\cos\eta}{\eta^2} \,. \tag{B.6}$$

Putting everything together and simplifying, we finally arrive at

$$F_{pq}(k,\boldsymbol{R}) = 4\pi\left\{\delta_{p,q}\left[\left(\frac{1}{\eta}-\frac{1}{\eta^3}\right)\sin\eta+\frac{1}{\eta^2}\cos\eta\right]\right.$$
$$\left.-\frac{[\boldsymbol{e}_p\boldsymbol{R}][\boldsymbol{e}_q\boldsymbol{R}]}{R^2}\left[\left(\frac{1}{\eta}-\frac{3}{\eta^3}\right)\sin\eta+\frac{3}{\eta^2}\cos\eta\right]\right\}. \tag{B.7}$$

With this at hand, we can now explicitly calculate the coupling parameters of the final master equation Eq. (2.46). We use Eqs. (2.38) and (2.42) to find

$$\Gamma^{\mu\nu}_{mn} = \frac{\omega_0^3}{4\pi\varepsilon_0\hbar c^3}\left\{\boldsymbol{d}_m\boldsymbol{d}_n^*\left[\left(\frac{1}{\eta_{0\mu\nu}}-\frac{1}{\eta_{0\mu\nu}^3}\right)\sin\eta_{0\mu\nu}+\frac{1}{\eta_{0\mu\nu}^2}\cos\eta_{0\mu\nu}\right]\right.$$
$$\left.-\frac{[\boldsymbol{d}_m\boldsymbol{R}_{\mu\nu}][\boldsymbol{d}_n^*\boldsymbol{R}_{\mu\nu}]}{R_{\mu\nu}^2}\left[\left(\frac{1}{\eta_{0\mu\nu}}-\frac{3}{\eta_{0\mu\nu}^3}\right)\sin\eta_{0\mu\nu}+\frac{3}{\eta_{0\mu\nu}^2}\cos\eta_{0\mu\nu}\right]\right\}, \tag{B.8}$$

where $\eta_{0\mu\nu} = k_0 R_{\mu\nu}$ and $k_0 = \frac{\omega_0}{c}$. The coherent coupling parameter $\Omega^{\mu\nu}_{mn}$ needs a more detailed treatment. Using Eqs. (2.39), (2.43), (2.44), and $\Omega^{\mu\nu}_{mn} \coloneqq -\left(\Delta^{\mu\nu}_{mn+}+\Delta^{\mu\nu}_{mn-}\right)$, we find

$$\Omega^{\mu\nu}_{mn} = \frac{1}{\varepsilon_0\hbar(2\pi c)^3}\,\mathrm{p.v.}\left(\int_0^{\omega_c} d\omega_k\,[\boldsymbol{d}_m F(k,\boldsymbol{R}_{\mu\nu})\boldsymbol{d}_n^*]\,\frac{\omega_k^4}{\omega_k^2-\omega_0^2}\right). \tag{B.9}$$

In the following, we omit the index $\mu\nu$ and adopt the notation to $z = \eta_{\mu\nu}$, $z_0 = \eta_{0\mu\nu}$, and $z_c = k_c R_{\mu\nu}$, where $k_c = \frac{\omega_c}{c}$. In addition, we write

$$F_{pq}(z,\boldsymbol{R}_{\mu\nu}) = 4\pi\left[\delta_{p,q}F_1(z)-\frac{[\boldsymbol{e}_p\boldsymbol{R}_{\mu\nu}][\boldsymbol{e}_q\boldsymbol{R}_{\mu\nu}]}{R_{\mu\nu}^2}F_2(z)\right], \tag{B.10}$$

where we defined

$$F_1(z) \coloneqq \left(\frac{1}{z}-\frac{1}{z^3}\right)\sin z+\frac{1}{z^2}\cos z\,, \tag{B.11}$$
$$F_2(z) \coloneqq \left(\frac{1}{z}-\frac{3}{z^3}\right)\sin z+\frac{3}{z^2}\cos z\,. \tag{B.12}$$

To solve the integral in Eq. (B.9), we regularise it by replacing the sharp frequency cutoff by the smooth step function [63]

$$\xi(\omega_k,\omega_c) = \frac{\omega_c^2}{\omega_k^2+\omega_c^2} \tag{B.13}$$

and expand the integral to infinity. Note that the step function is ≈ 1 for $\omega_k \ll \omega_c$ and ≈ 0 for $\omega_k \gg \omega_c$. We also note that the choice of the step function is not unique and the integral depends on the specific choice. However, as we will see in the end, effects coming from the

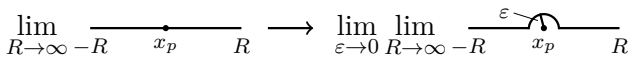

Figure B.1: Extension of the integral to the complex plane and avoiding the pole at x_p by going around it with a semi-circle.

step function can be neglected. We now have

$$\Omega_{mn}^{\mu\nu} = \frac{1}{4\varepsilon_0\hbar\pi^2}\frac{1}{R_{\mu\nu}^3}\text{p.v.}\left(\int_{-\infty}^{\infty} dz\left[\boldsymbol{d}_m\boldsymbol{d}_n^* F_1(z) - \frac{[\boldsymbol{d}_m\boldsymbol{R}_{\mu\nu}][\boldsymbol{d}_n^*\boldsymbol{R}_{\mu\nu}]}{R_{\mu\nu}^2}F_2(z)\right]\frac{z^4}{z^2-z_0^2}\frac{z_c^2}{z_c^2+z^2}\right), \tag{B.14}$$

where we used that the integrand is an even function of z to extend the integral to $-\infty$. Before we proceed, let us do a small excursion in calculating Cauchy principal values. The Cauchy principal value for any function $f(x)$, which has a singularity at some point x_p is defined by

$$\text{p.v.}\left(\int_{-\infty}^{\infty} dx\, f(x)\right) = \lim_{\varepsilon\to 0}\left[\int_{-\infty}^{x_p-\varepsilon} dx\, f(x) + \int_{x_p+\varepsilon}^{\infty} dx\, f(x)\right]. \tag{B.15}$$

Let us assume that the function $f(x)$ is real and has a single pole of order 1 at x_p on the real axis. We can write $f(x) = \frac{g(x)}{x-x_p}$ with some function $g(x)$ and extend the integration to the complex plane assuming $g(z)$, $z \in \mathbb{C}$, to be holomorphic in the following. We can avoid the pole at x_p by going around it with a semi-circle (see Fig. B.1). We then consider the integral

$$I_\cap = \int_{-\infty}^{x_p-\varepsilon} dx\, f(x) + \int_{x_p+\varepsilon}^{\infty} dx\, f(x) + \int_\cap dz\,\frac{g(z)}{z-x_p}, \tag{B.16}$$

from which we find

$$\lim_{\varepsilon\to 0} I_\cap = \text{p.v.}\left(\int_{-\infty}^{\infty} dx\, f(x)\right) + \lim_{\varepsilon\to 0}\int_\cap dz\,\frac{g(z)}{z-x_p}. \tag{B.17}$$

Now, we consider the second term of the right side of the previous equation. Since the function $g(z)$ is holomorphic, we can expand it in a Taylor series around x_p, i.e.,

$$g(z) = \sum_{m=0}^{\infty}\frac{g^{(m)}(x_p)}{m!}(z-x_p)^m, \tag{B.18}$$

where $g^{(m)}(x_p)$ denotes the mth derivative at position x_p. With $z-x_p = \varepsilon e^{i\theta}$ and $dz = i\varepsilon e^{i\theta} d\theta$, we obtain for the integral

$$\lim_{\varepsilon\to 0}\int_{\frown} dz\,\frac{g(z)}{z-x_p} = -\int_0^{\pi} d\theta\, i g(x_p) - \underbrace{\lim_{\varepsilon\to 0}\sum_{m=1}^{\infty}\frac{g^{(m)}(x_p)}{m!} i\varepsilon^m \int_0^{\pi} d\theta\, e^{im\theta}}_{=0} = -i\pi g(x_p)\,. \quad \text{(B.19)}$$

We note that since $g(z)$ is holomorphic, we can expand $f(z)$ in a Laurent series around x_p, from which we can read off $g(x_p) = \mathrm{Res}_{x_p} f(z)$, where $\mathrm{Res}_{x_p} f(z)$ denotes the residue of $f(z)$ at x_p. Now, to calculate the integral $I_{\frown}$, we can close the contour sketched in Fig. B.1 in the upper half plane. Then, assuming $zf(z) \to 0$ uniformly for $|z| \to \infty$, we have

$$I_{\frown} = 2\pi i \sum_{z_p \in P_{\mathbb{C}}, \mathrm{Im}(z_p)>0} \mathrm{Res}_{z_p} f(z) \Rightarrow \lim_{\varepsilon\to 0} I_{\frown} = I_{\frown}, \quad \text{(B.20)}$$

where $P_{\mathbb{C}}$ denotes the set of all poles of $f(z)$ and the Cauchy principal value reads

$$\text{p.v.}\left(\int_{-\infty}^{\infty} dx\, f(x)\right) = 2\pi i \sum_{z_p \in P_{\mathbb{C}}, \mathrm{Im}(z_p)>0} \mathrm{Res}_{z_p} f(z) + i\pi \mathrm{Res}_{x_p} f(z)\,. \quad \text{(B.21)}$$

If there are multiple poles of order 1 on the real axis, we simply need to replace $i\pi \mathrm{Res}_{x_p} f(z)$ by $i\pi \sum_{x_p \in P_{\mathbb{R}}} \mathrm{Res}_{x_p} f(z)$, where $P_{\mathbb{R}}$ is the set of all poles on the real axis. Now, let us come back to the expression of $\Omega^{\mu\nu}_{mn}$ in Eq. (B.14). We replace the sines and cosines in the functions $F_1(z)$ and $F_2(z)$ by e^{iz} and take later on the real and imaginary parts. Then, we need to evaluate the following three integrals

$$I_m = \text{p.v.}\left(\int_{-\infty}^{\infty} dz\, \underbrace{\frac{z^m}{z^2-z_0^2}\frac{z_c^2}{z_c^2+z^2} e^{iz}}_{=:f_m(z)}\right) \quad \text{(B.22)}$$

with $m \in \{1,2,3\}$. We find poles at $\pm z_0$ on the real axis and at $\pm i z_c$ on the imaginary axis. Since e^{iz} drops to zero for $|z| \to \infty$ in the upper half plane, we close the contour in the upper half plane. Thus, we get a contribution from the pole at iz_c, but not from the pole at $-iz_c$. We write

$$f_m(z) = \frac{z^m}{(z-z_0)(z+z_0)}\frac{z_c^2}{(z+iz_c)(z-iz_c)} e^{iz} = \frac{g_{m1}(z)}{z-z_0} = \frac{g_{m2}(z)}{z+z_0} = \frac{g_{m3}(z)}{z-iz_c}\,, \quad \text{(B.23)}$$

where we implicitly defined the functions $g_{m1}(z)$, $g_{m2}(z)$, and $g_{m3}(z)$. Thereby, $g_{m1}(z)$ is holomorphic in a neighbourhood of z_0, $g_{m2}(z)$ in a neighbourhood of $-z_0$, and $g_{m3}(z)$ in a neighbourhood of iz_c. Thus, we obtain

$$I_m = 2\pi i \mathrm{Res}_{iz_c} f(z) + i\pi \mathrm{Res}_{z_0} f(z) + i\pi \mathrm{Res}_{-z_0} f(z)$$

$$= 2\pi i g_{m3}(iz_c) + i\pi g_{m1}(z_0) + i\pi g_{m2}(-z_0)\,. \tag{B.24}$$

Explicitly plugging in the expressions, leads to

$$I_1 = i\pi\left(\frac{z_c^2 z_0^2\cos z_0}{z_0^2+z_c^2} + \frac{z_c^4 e^{-z_c}}{z_0^2+z_c^2}\right) = i\pi[z_0^2\cos z_0 + G_1(z_0,z_c)]\,, \tag{B.25}$$

$$I_2 = \pi\left(-\frac{z_0 z_c^2\sin z_0}{z_0^2+z_c^2} + \frac{z_c^3 e^{-z_c}}{z_0^2+z_c^2}\right) = \pi[-z_0\sin z_0 + G_2(z_0,z_c)]\,, \tag{B.26}$$

$$I_3 = i\pi\left(\frac{z_c^2\cos z_0}{z_0^2+z_c^2} - \frac{z_c^2 e^{-z_c}}{z_0^2+z_c^2}\right) = i\pi[\cos z_0 + G_3(z_0,z_c)]\,, \tag{B.27}$$

where we defined the functions

$$G_1(z_0,z_c) = \frac{1}{z_0^2+z_c^2}(z_c^4 e^{-z_c} - z_0^4\cos z_0)\,, \tag{B.28}$$

$$G_2(z_0,z_c) = \frac{1}{z_0^2+z_c^2}(z_c^3 e^{-z_c} + z_0^3\sin z_0)\,, \tag{B.29}$$

$$G_3(z_0,z_c) = \frac{1}{z_0^2+z_c^2}(-z_c^2 e^{-z_c} - z_0^2\cos z_0)\,. \tag{B.30}$$

Changing back to the "η"-notation, we finally find ($\eta_{c\mu\nu} = k_c R_{\mu\nu}$)

$$\begin{aligned}\Omega_{mn}^{\mu\nu} &= \frac{1}{4\varepsilon_0\hbar\pi^2}\frac{1}{R_{\mu\nu}^3}\Bigg\{\boldsymbol{d}_m\boldsymbol{d}_n^*[\mathrm{Im}(I_1) - \mathrm{Im}(I_3) + \mathrm{Re}(I_2)] \\ &\quad - \frac{[\boldsymbol{d}_m\boldsymbol{R}_{\mu\nu}][\boldsymbol{d}_n^*\boldsymbol{R}_{\mu\nu}]}{R_{\mu\nu}^2}[\mathrm{Im}(I_1) - 3\mathrm{Im}(I_3) + 3\mathrm{Re}(I_2)]\Bigg\} \\ &= \frac{\omega_0^3}{4\pi\varepsilon_0\hbar c^3}\Bigg\{\boldsymbol{d}_m\boldsymbol{d}_n^*\left[\left(\frac{1}{\eta_{0\mu\nu}} - \frac{1}{\eta_{0\mu\nu}^3}\right)\cos\eta_{0\mu\nu} - \frac{1}{\eta_{0\mu\nu}^2}\sin\eta_{0\mu\nu} + C_1(\eta_{0\mu\nu},\eta_{c\mu\nu})\right] \\ &\quad - \frac{[\boldsymbol{d}_m\boldsymbol{R}_{\mu\nu}]\,[\boldsymbol{d}_n^*\boldsymbol{R}_{\mu\nu}]}{R_{\mu\nu}^2}\left[\left(\frac{1}{\eta_{0\mu\nu}} - \frac{3}{\eta_{0\mu\nu}^3}\right)\cos\eta_{0\mu\nu} - \frac{3}{\eta_{0\mu\nu}^2}\sin\eta_{0\mu\nu} + C_2(\eta_{0\mu\nu},\eta_{c\mu\nu})\right]\Bigg\}\,,\end{aligned} \tag{B.31}$$

where

$$C_1(\eta_{0\mu\nu},\eta_{c\mu\nu}) \coloneqq \frac{1}{\eta_{0\mu\nu}^3}[G_1(\eta_{0\mu\nu},\eta_{c\mu\nu}) - G_3(\eta_{0\mu\nu},\eta_{c\mu\nu}) + G_2(\eta_{0\mu\nu},\eta_{c\mu\nu})]\,, \tag{B.32}$$

$$C_2(\eta_{0\mu\nu},\eta_{c\mu\nu}) \coloneqq \frac{1}{\eta_{0\mu\nu}^3}[G_1(\eta_{0\mu\nu},\eta_{c\mu\nu}) - 3G_3(\eta_{0\mu\nu},\eta_{c\mu\nu}) + 3G_2(\eta_{0\mu\nu},\eta_{c\mu\nu})]\,. \tag{B.33}$$

The functions C_1 and C_2 depend on the chosen regularisation function via $\eta_{c\mu\nu}$. However, on the one hand, $\lim_{\eta_{c\mu\nu}\to\infty} C_1 = 0 = \lim_{\eta_{c\mu\nu}\to\infty} C_2$, on the other hand, for finite $\eta_{c\mu\nu}$ the contributions from C_1 and C_2 are negligible if $\frac{1}{\eta_{c\mu\nu}} \ll 1$ and $e^{-\eta_{c\mu\nu}}\eta_{c\mu\nu}^2 \ll 1$, which is well satisfied if $\eta_{c\mu\nu} = k_c R_{\mu\nu} \gg 1$ or equivalently $R_{\mu\nu} \gg k_c^{-1}$. Since $k_c^{-1} \approx a_0$, where a_0 is the Bohr radius,

this is well satisfied if the separation of the atoms is much larger than their extent, which we already assumed earlier to neglect the coupling of the polarisation densities. Therefore, it is justified to omit the two functions C_1 and C_2 in Eq. (B.31) and we arrive at the expression given in the main text [see Eq. (2.47)].

C Quantum regression theorem

In this appendix, we derive the so-called quantum regression theorem, which links multi-time expectation values of some product of operators to single-time expectation values of the same product of operators when the unitary time evolution of the full system is replaced by the time evolution of a reduced system. In the following, we show two different formulations, a rather abstract one via the Laplace transform and a more practical one using the projection onto an operator basis. We start with the Laplace transform formulation.

C.1 Laplace transform formulation

The following derivation of the quantum regression theorem is based on Ref. [101]. The basic idea of the so-called quantum regression theorem is to connect two-time correlation functions $\langle \hat{O}_1(t')\hat{O}_2(t)\rangle$ to single-time expectation values. Therefore, we write

$$\begin{aligned}\langle \hat{O}_1(t')\hat{O}_2(t)\rangle &= \mathrm{Tr}[\hat{\rho}(0)\hat{O}_1(t')\hat{O}_2(t)] = \mathrm{Tr}[\hat{\rho}(0)\hat{U}^\dagger(t',0)\hat{O}_1\hat{U}(t',0)\hat{U}^\dagger(t,0)\hat{O}_2\hat{U}(t,0)] \\ &= \mathrm{Tr}[\hat{U}(t,t')\underbrace{\hat{U}(t',0)\hat{\rho}(0)\hat{U}^\dagger(t',0)}_{=\hat{\rho}(t')}\hat{O}_1\hat{U}(t',0)\hat{U}^\dagger(t,0)\hat{O}_2] \\ &= \mathrm{Tr}[\hat{O}_2\underbrace{\hat{U}(t,t')\hat{\rho}(t')\hat{O}_1\hat{U}^\dagger(t,t')}_{=:\hat{\Omega}(t,t')}] = \mathrm{Tr}[\hat{O}_2\hat{\Omega}(t,t')]\,, \end{aligned} \tag{C.1}$$

which has the form of an expectation value, where $\hat{\rho}(t)$ is replaced by $\hat{\Omega}(t,t')$. Since $\hat{\rho}(t) = \hat{U}(t,0)\hat{\rho}(0)\hat{U}^\dagger(t,0)$, it is obvious from the definition of $\hat{\Omega}(t,t')$ that $\hat{\rho}(t)$ and $\hat{\Omega}(t,t')$ fulfil the same equation of motion with respect to t. Thus, if one is able to solve the equation of motion for the density matrix $\hat{\rho}(t)$, one immediately has the solution for $\hat{\Omega}(t,t')$ and the two-time correlation function. However, note that $\hat{\rho}(t)$ is the total density operator, which describes usually a composed system, i.e., the total Hamiltonian often reads

$$\hat{H} = \hat{H}_S + \hat{H}_R + \hat{H}_{SR} = \hat{H}_0 + \hat{H}_1\,, \tag{C.2}$$

where $\hat{H}_S, \hat{H}_R$ are the system and reservoir Hamilton operators, and $\hat{H}_{SR}$ accounts for interactions between the two subsystems. Note that we assumed that the Hamilton operator is time-independent. We are not interested in the dynamics of both the system and the reser-

voir, but only of the system alone. Therefore, we use projection operators $\mathscr{P}$ and $\mathscr{Q} = \mathbb{1} - \mathscr{P}$, as given in Eq. (2.13), and define the operators

$$\hat{\rho}_1(t) \coloneqq \mathscr{P}\hat{\rho}(t)\,, \tag{C.3}$$

$$\hat{\rho}_2(t) \coloneqq \mathscr{Q}\hat{\rho}(t)\,. \tag{C.4}$$

Now, we Laplace transform the Liouville-von Neumann equation

$$\frac{\partial}{\partial t}\hat{\rho}(t) = -i[\hat{H}, \hat{\rho}(t)] = -i\mathscr{L}\hat{\rho}(t) \tag{C.5}$$

with Liouvillian $\mathscr{L}\ldots = [\hat{H}, \ldots]$ leading to

$$z\hat{\tilde{\rho}}(z) - \hat{\rho}(0) = -i\mathscr{L}\hat{\tilde{\rho}}(z)\,. \tag{C.6}$$

Here,

$$\hat{\tilde{\rho}}(z) \coloneqq \int_0^\infty dt\, \hat{\rho}(t) e^{-zt} \tag{C.7}$$

is the Laplace transform of $\hat{\rho}(t)$. Note that we set $\hbar = 1$ for simplicity. Projecting onto the relevant and irrelevant parts then gives

$$z\hat{\tilde{\rho}}_1(z) - \hat{\rho}_1(0) = -i\mathscr{P}\mathscr{L}\hat{\tilde{\rho}}_1(z) - i\mathscr{P}\mathscr{L}\hat{\tilde{\rho}}_2(z)\,, \tag{C.8}$$

$$z\hat{\tilde{\rho}}_2(z) - \hat{\rho}_2(0) = -i\mathscr{Q}\mathscr{L}\hat{\tilde{\rho}}_1(z) - i\mathscr{Q}\mathscr{L}\hat{\tilde{\rho}}_2(z)\,. \tag{C.9}$$

By rearranging and solving Eq. (C.9) for $\hat{\tilde{\rho}}_2(z)$ and plugging the solution in Eq. (C.8), we obtain

$$\left(z + i\mathscr{P}\mathscr{L} + \mathscr{P}\mathscr{L}\frac{1}{z + i\mathscr{Q}\mathscr{L}}\mathscr{Q}\mathscr{L}\right)\hat{\tilde{\rho}}_1(z) = \hat{\rho}_1(0) - i\mathscr{P}\mathscr{L}\frac{1}{z + i\mathscr{Q}\mathscr{L}}\hat{\rho}_2(0)\,. \tag{C.10}$$

A usual assumption is that the initial state does not have any correlations, i.e., $\hat{\rho}(0) = \hat{\rho}_S(0) \otimes \hat{\rho}_R(0)$, such that $\hat{\rho}_2(0) = 0$. This simplifies Eq. (C.10) to

$$\left(z + i\mathscr{P}\mathscr{L} + \mathscr{P}\mathscr{L}\frac{1}{z + i\mathscr{Q}\mathscr{L}}\mathscr{Q}\mathscr{L}\right)\hat{\tilde{\rho}}_1(z) = \hat{\rho}_1(0)\,. \tag{C.11}$$

Analogously to $\hat{\rho}_1(t)$, we can define $\hat{\Omega}_1(t, t') \coloneqq \mathscr{P}\hat{\Omega}(t, t')$. Then, assuming $\hat{O}_1$ and $\hat{O}_2$ to be system variables, we can rewrite the expectation values as

$$\langle \hat{O}_2(t)\rangle = \mathrm{Tr}_S[\hat{O}_2\, \mathrm{Tr}_R[\hat{\rho}_1(t)]]\,, \tag{C.12}$$

$$\langle \hat{O}_1(t')\hat{O}_2(t)\rangle = \mathrm{Tr}_S[\hat{O}_2\, \mathrm{Tr}_R[\hat{\Omega}_1(t, t')]]\,, \tag{C.13}$$

where we used $\mathrm{Tr}_R[\hat{\rho}(t)] = \mathrm{Tr}_R[\mathscr{P}\hat{\rho}(t)] = \mathrm{Tr}_R[\hat{\rho}_1(t)]$ and analogously for $\hat{\Omega}(t,t')$. We now assume $t \geq t'$, such that we can choose $\hat{\Omega}(t,t') = 0$ for $t < t'$. Defining the Laplace transform $\hat{\tilde{\Omega}}(z,t')$ of $\hat{\Omega}(t,t')$ analogously to the one of the density operator, we immediately find the same equation of motion for $\hat{\tilde{\Omega}}_1(z,t')$ as for $\hat{\tilde{\rho}}_1(z)$, i.e.,

$$\left(z + i\mathscr{P}\mathscr{L} + \mathscr{P}\mathscr{L}\frac{1}{z + i\mathscr{Q}\mathscr{L}}\mathscr{Q}\mathscr{L}\right)\hat{\tilde{\Omega}}_1(z,t') = \hat{\Omega}_1(t',t') + \hat{\tilde{\Phi}}(z,t')\,, \tag{C.14}$$

where

$$\hat{\tilde{\Phi}}(z,t') = -i\mathscr{P}\mathscr{L}\frac{1}{z + i\mathscr{Q}\mathscr{L}}\hat{\Omega}_2(t',t') = -i\mathscr{P}\mathscr{L}\frac{1}{z + i\mathscr{Q}\mathscr{L}}[\hat{\rho}(t') - \hat{\rho}_S(t') \otimes \hat{\rho}_R(0)]\hat{O}_1\,. \tag{C.15}$$

Thus, we find that if no correlations build up within the time interval $[0,t']$ and the reservoir state remains unchanged, the inhomogeneous part $\hat{\tilde{\Phi}}(z,t') = 0$ and we obtain the same type of equation of motion as in Eq. (C.11). Then, $\hat{\Omega}_1(t,t')$ obeys the same equation of motion as $\hat{\rho}_1(t)$, such that the time evolution in the interval $[t',t]$ is given by the solution of the master equation for $\hat{\rho}_1(t)$. This is the quantum regression theorem. Usually, if the coupling between the two subsystems is weak, one assumes $\hat{\rho}(t') \approx \hat{\rho}_S(t') \otimes \hat{\rho}_R(0)$ for all times t', such that the use of the quantum regression theorem for the calculation of multi-time correlation functions is justified.

C.2 Operator basis projected formulation

In the following section, we derive the quantum regression theorem again, but in a more practical formulation. Therefore, we write it in an operator basis projected form given in Ref. [77]. We assume, as before, that the Hamilton operator is time-independent, such that also the Liouvillian superoperator is time-independent. The generalisation to the time-dependent case is then found by small replacements, which we will address at the end of the section. We assume that the time evolution of the reduced system is governed by a master equation of the form

$$\dot{\hat{\rho}}_S(t) = \mathscr{L}\hat{\rho}_S(t)\,, \tag{C.16}$$

where $\mathscr{L}$ is the corresponding Liouvillian superoperator for the time evolution of the reduced system. We are interested in two-time correlation functions $\langle \hat{O}_1(t')\hat{O}_2(t)\rangle = \mathrm{Tr}[\hat{\rho}(0)\hat{O}_1(t')\hat{O}_2(t)]$, where $\hat{O}_1$ and $\hat{O}_2$ are two system operators as before. Further, we write the two-time correlation function in the same way as in the previous section as

$$\langle \hat{O}_1(t')\hat{O}_2(t)\rangle = \mathrm{Tr}[\hat{U}(t,t')\hat{\rho}(t)\hat{O}_1\hat{U}^\dagger(t,t')\hat{O}_2] = \mathrm{Tr}[\hat{O}_2\hat{\rho}_{\hat{O}_1}(\tau)]\,, \tag{C.17}$$

where we assumed $t \geq t'$ and defined $\hat{\rho}_{O_1}(\tau) = \hat{U}(\tau,0)\hat{\rho}(t')\hat{O}_1\hat{U}^\dagger(\tau,0)$ with $\tau = t - t'$. Note that we used that the time evolution depends only on the time difference, i.e., $\hat{U}(t,t') = \hat{U}(\tau,0)$, since we assumed a time-independent Hamilton operator. Further, note that the operator $\hat{\rho}_{O_1}(\tau)$ is the same as $\hat{\Omega}(t,t')$ of the previous section. Thus, it obeys the Liouville-von Neumann equation with respect to τ, i.e.,

$$\frac{\partial}{\partial\tau}\hat{\rho}_{O_1}(\tau) = -\frac{i}{\hbar}[\hat{H}, \hat{\rho}_{O_1}(\tau)] \tag{C.18}$$

with initial condition $\hat{\rho}_{O_1}(0) = \hat{\rho}(t')\hat{O}_1$. The corresponding system operators are found by tracing over the reservoir degrees of freedom reading

$$\hat{\rho}_{S,O_1}(\tau) = \mathrm{Tr}_R[\hat{\rho}_{O_1}(\tau)]\,, \tag{C.19}$$

$$\hat{\rho}_{S,O_1}(0) = \mathrm{Tr}_R[\hat{\rho}_{O_1}(0)] = \mathrm{Tr}_R[\hat{\rho}(t')\hat{O}_1] = \hat{\rho}_S(t')\hat{O}_1\,. \tag{C.20}$$

If we now do the crucial assumption that the density operator $\hat{\rho}(t')$ factorises for all times t' with some fixed initial reservoir state, i.e., $\hat{\rho}(t') = \hat{\rho}_S(t') \otimes \hat{\rho}_R(0)$, we find that

$$\hat{\rho}_{O_1}(0) = \hat{\rho}(t')\hat{O}_1 = \hat{\rho}_S(t')\hat{O}_1 \otimes \hat{\rho}_R(0) = \hat{\rho}_{S,O_1}(0) \otimes \hat{\rho}_R(0)\,. \tag{C.21}$$

Note that in the previous section, we found that this assumption is the condition for the correctness of the quantum regression theorem as it implies that $\hat{\rho}_{O_1}(\tau)$ factorises at $\tau = 0$. Therefore, we can derive the same master equation for $\hat{\rho}_{S,O_1}(\tau)$ with respect to τ as for $\hat{\rho}_S(t)$ with respect to t, i.e.,

$$\dot{\hat{\rho}}_{S,O_1}(\tau) = \mathscr{L}\hat{\rho}_{S,O_1}(\tau)\,, \tag{C.22}$$

for which the solution is given by $\hat{\rho}_{S,O_1}(\tau) = e^{\mathscr{L}\tau}\hat{\rho}_{S,O_1}(0)$. Then, we find for the two-time correlation function

$$\begin{aligned}\langle\hat{O}_1(t')\hat{O}_2(t)\rangle &= \langle\hat{O}_1(t')\hat{O}_2(t'+\tau)\rangle = \mathrm{Tr}[\hat{O}_2\hat{\rho}_{O_1}(\tau)] = \mathrm{Tr}_S[\hat{O}_2\,\mathrm{Tr}_R[\hat{\rho}_{O_1}(\tau)]] \\ &= \mathrm{Tr}_S[\hat{O}_2\hat{\rho}_{S,O_1}(\tau)] = \mathrm{Tr}_S[\hat{O}_2 e^{\mathscr{L}\tau}\hat{\rho}_{S,O_1}(0)] = \mathrm{Tr}_S[\hat{O}_2 e^{\mathscr{L}\tau}(\hat{\rho}_S(t')\hat{O}_1)]\,,\end{aligned} \tag{C.23}$$

which means that we can evolve the unnormalised state of the system after the application of the operator $\hat{O}_1$ at time t', $\hat{\rho}_S(t')\hat{O}_1$, with the same master equation as for the initial state at time $t' = 0$. The last equation is thus just another formulation of the quantum regression theorem.

We now project the last expression onto an operator basis to get a direct connection between the equations of motion of single-time expectation values and multi-time correlation functions.

If we can find a complete set of system operators $\hat{A}_\mu$ with $\mu \in \{1, 2, ...\}$, which fulfil

$$\mathrm{Tr}_S[\hat{A}_\mu(\mathscr{L}\hat{O})] = \sum_\lambda M_{\mu\lambda}\,\mathrm{Tr}_S[\hat{A}_\lambda \hat{O}] \tag{C.24}$$

for all system operators $\hat{O}$ and $M_{\mu\lambda}$ being constants, we can relate the differential equations of two-time correlation functions to the one of one-time expectation values. Note that this equation holds true, for example, for the operators $\hat{A}_{nm} = |n\rangle\langle m|$, where $|n\rangle$ is any orthonormal basis. We now find for the time derivative of the one-time expectation values of the operators $\hat{A}_\mu$ that

$$\langle \dot{\hat{A}}_\mu(t)\rangle = \mathrm{Tr}_S[\hat{A}_\mu \dot{\hat{\rho}}_S(t)] = \mathrm{Tr}_S[\hat{A}_\mu \mathscr{L}\hat{\rho}_S(t)] = \sum_\lambda M_{\mu\lambda}\,\langle \hat{A}_\lambda(t)\rangle\ . \tag{C.25}$$

Equivalently, we can write

$$\langle \dot{\hat{\boldsymbol{A}}}(t)\rangle = M\,\langle \hat{\boldsymbol{A}}(t)\rangle \tag{C.26}$$

if we define the vector $\hat{\boldsymbol{A}} \coloneqq (\hat{A}_1, \hat{A}_2, ...)^\mathsf{T}$ and the matrix

$$M \coloneqq \begin{pmatrix} M_{11} & M_{12} & \cdots \\ M_{22} & M_{22} & \cdots \\ \vdots & \vdots & \ddots \end{pmatrix}\ . \tag{C.27}$$

Then, we obtain for the time derivative of the two-time correlation functions

$$\begin{aligned} \frac{d}{d\tau}\,\langle \hat{O}_1(t)\hat{A}_\mu(t+\tau)\rangle &= \frac{d}{d\tau}\,\mathrm{Tr}_S[\hat{A}_\mu e^{\mathscr{L}\tau}(\hat{\rho}_S(t)\hat{O}_1)] = \mathrm{Tr}_S[\hat{A}_\mu \mathscr{L} e^{\mathscr{L}\tau}(\hat{\rho}_S(t)\hat{O}_1)] \\ &= \sum_\lambda M_{\mu\lambda}\,\mathrm{Tr}_S[\hat{A}_\lambda e^{\mathscr{L}\tau}(\hat{\rho}_S(t)\hat{O}_1)] = \sum_\lambda M_{\mu\lambda}\,\langle \hat{O}_1(t)\hat{A}_\lambda(t+\tau)\rangle\ , \end{aligned} \tag{C.28}$$

i.e., the two-time correlation functions fulfil the same equations of motion as the single-time expectation values. Again equivalently, in vectorial form we have

$$\frac{d}{d\tau}\,\langle \hat{O}_1(t)\hat{\boldsymbol{A}}(t+\tau)\rangle = M\,\langle \hat{O}_1(t)\hat{\boldsymbol{A}}(t+\tau)\rangle\ . \tag{C.29}$$

This is the quantum regression theorem projected onto an operator basis.
Now, finally, we have a look at the generalisation to time-dependent systems. If the Hamilton operator is time-dependent, the time evolution operator $\hat{U}(t, t')$ does not only depend on the time difference, but we need to keep both times t and t'. For the following discussion, it is then convenient to define the one-parameter family $\{\hat{V}(t)|t \geq 0\}$ of dynamical maps, where the dynamical map $\hat{V}(t)$ is defined via the commutative diagram shown in Fig. C.1 [62]. In addition, we assume that the Markov approximation can be applied. Then, in the time-

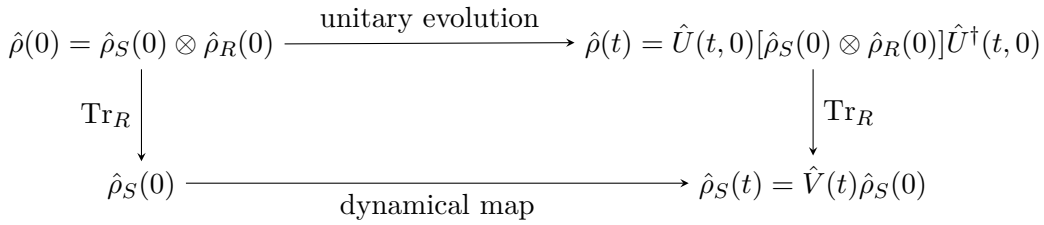

Figure C.1: Commutative diagram to define the dynamical map $\hat{V}(t)$ for the reduced system.

independent case, the dynamical map $\hat{V}(t)$ fulfils the semigroup property

$$\hat{V}(t_1)\hat{V}(t_2) = \hat{V}(t_1 + t_2) \tag{C.30}$$

with $t_1, t_2 \geq 0$. Under certain mathematical conditions (see Ref. [62]), one then finds a linear map $\mathscr{L}$, the generator of the semigroup, such that one can represent the semigroup in its exponential form as

$$\hat{V}(t) = e^{\mathscr{L}t}\,. \tag{C.31}$$

Thereby, $\mathscr{L}$ will be the Liouvillian of the time evolution of the reduced density matrix, i.e.,

$$\frac{\partial}{\partial t}\hat{\rho}_S(t) = \mathscr{L}\hat{\rho}_S(t)\,. \tag{C.32}$$

Now, if the Hamilton operator is explicitly time-dependent, $\mathscr{L}$ in Eq. (C.32) changes to $\mathscr{L}(t)$ and Eq. (C.31) changes to a time-ordered exponential. In addition, instead of the semigroup property, the dynamical map $\hat{V}(t, t_0)$ can be split as

$$\hat{V}(t, t_1)\hat{V}(t_1, t_0) = \hat{V}(t, t_0) \tag{C.33}$$

in analogy to the unitary time evolution operator.

D Quantum coherence, quantum correlations, and entanglement

Since we use the notions of *quantum coherence*, *quantum correlations*, and *entanglement* throughout this thesis and also quantify them in several places, we briefly discuss calculated quantities in this appendix.

D.1 Measures

To quantify quantum coherence [102], quantum correlations [103, 104], and entanglement [105], several measures can be used, which may be related to each other (see references for respective reviews). In the following, we focus primarily on quantum correlations and entanglement.

D.1.1 Quantum discord

A measure of quantum correlations is the so-called *quantum discord*, which captures quantum correlations even beyond entanglement [103] and quantifies basis-free quantum coherence [106]. Consider a composite system AB with subsystems A and B. The quantum discord with respect to subsystem A is defined as [103, 104]

$$\mathcal{D}_A(\hat{\rho}_{AB}) \coloneqq \mathcal{I}(\hat{\rho}_{AB}) - \mathcal{J}_A(\hat{\rho}_{AB})\,. \tag{D.1}$$

Thereby,

$$\mathcal{I}(\hat{\rho}_{AB}) \coloneqq \mathcal{S}(\hat{\rho}_A) + \mathcal{S}(\hat{\rho}_B) - \mathcal{S}(\hat{\rho}_{AB}) \tag{D.2}$$

is the mutual information accounting for the total amount of correlations between the subsystems A and B. Here, $\mathcal{S}(\hat{\rho}_A)$, $\mathcal{S}(\hat{\rho}_B)$ denote the von Neumann entropies of the reduced systems and $\mathcal{S}(\hat{\rho}_{AB})$ is the von Neumann entropy of the total system AB. Further,

$$\mathcal{J}_A(\hat{\rho}_{AB}) \coloneqq \sup_{\Pi_A} \left[\mathcal{S}(\hat{\rho}_B) - \mathcal{S}^{\Pi_A}_{B|A}(\hat{\rho}_{AB})\right] \tag{D.3}$$

quantifies the one-sided classical correlations with respect to subsystem A. Thereby,

$$\mathcal{S}_{B|A}^{\Pi_A}(\hat{\rho}_{AB}) \coloneqq \sum_a p_a \mathcal{S}(\hat{\rho}_{B|a}) \tag{D.4}$$

is the conditional von Neumann entropy, where

$$\hat{\rho}_{B|a} = \frac{\mathrm{Tr}_A[\hat{\Pi}_{A,a}\hat{\rho}_{AB}]}{p_a} \tag{D.5}$$

is the conditional post-selected state of outcome a of a measurement on subsystem A described by the positive operator-valued measure $\hat{\Pi}_A$. Moreover, $p_a = \mathrm{Tr}[\hat{\Pi}_{A,a}\hat{\rho}_{AB}]$ denotes the probability of outcome a. Analogously, the quantum discord with respect to subsystem B can be defined. We also note that a two-sided quantum discord $\mathcal{D}_{AB}(\hat{\rho}_{AB})$ can be defined by considering local measurements on both subsystems $\{\hat{\Pi}_{AB,ab} = \hat{\Pi}_{A,a} \otimes \hat{\Pi}_{B,b}\}$ and by replacing the one-sided classical correlations with the two-sided 'classical mutual information' defined as [104]

$$\mathcal{J}_{AB}(\hat{\rho}_{AB}) \coloneqq \sup_{\Pi_{AB}} \mathcal{I}_{AB}^{\Pi_{AB}}(\hat{\rho}_{AB})\,. \tag{D.6}$$

We end this subsection with two remarks regarding the application to pure states. First, for pure states, the two one-sided quantum discords and the two-sided quantum discord coincide, i.e., $\mathcal{D}_A(\hat{\rho}_{AB}) = \mathcal{D}_B(\hat{\rho}_{AB}) = \mathcal{D}_{AB}(\hat{\rho}_{AB})$ [104]. Second, for pure states, all quantum correlations are directly related to entanglement and no quantum correlations beyond entanglement exist.

D.1.2 Concurrence

The *concurrence* is a measure of entanglement. To arrive at the concurrence, we first introduce the so-called entanglement of formation, which for a pure state $|\psi\rangle$ of the total system AB with subsystems A and B is defined as [105]

$$\mathcal{E}(|\psi\rangle) \coloneqq \mathcal{S}(\hat{\rho}_A) = \mathcal{S}(\hat{\rho}_B)\,. \tag{D.7}$$

The entanglement of formation for a mixed state $\hat{\rho}$ can then be defined by the so-called convex-roof construction as the minimum over all decompositions of $\hat{\rho}$ reading [105]

$$\mathcal{E}(\hat{\rho}) \coloneqq \min \sum_i p_i \mathcal{E}(|\psi_i\rangle)\,. \tag{D.8}$$

In the case of a mixed state $\hat{\rho}$ of two qubits, it was shown that this entanglement of formation can be written as [107]

$$\mathcal{E}(\hat{\rho}) = H\left(\frac{1+\sqrt{1-C(\hat{\rho})^2}}{2}\right), \tag{D.9}$$

where $C(\hat{\rho})$ denotes the so-called concurrence and H is the binary entropy function reading

$$H(x) = -x\log_2 x - (1-x)\log_2(1-x). \tag{D.10}$$

The concurrence is given by

$$C(\hat{\rho}) = \max\{0, \sqrt{\lambda_1} - \sqrt{\lambda_2} - \sqrt{\lambda_3} - \sqrt{\lambda_4}\}, \tag{D.11}$$

where the λ_is ($i \in \{1,2,3,4\}$) are the eigenvalues of the operator $\hat{\rho}\hat{\tilde{\rho}}$, in decreasing order. Thereby, the operator $\hat{\tilde{\rho}}$ is defined as

$$\hat{\tilde{\rho}} \coloneqq \hat{\sigma}_y \otimes \hat{\sigma}_y \hat{\rho}^* \hat{\sigma}_y \otimes \hat{\sigma}_y, \tag{D.12}$$

where $\hat{\sigma}_y$ denotes the y-Pauli matrix and $\hat{\rho}^*$ is the complex conjugate of $\hat{\rho}$. Since the concurrence is a positive and monotonous function, the concurrence can directly be considered as a measure of entanglement instead of the entanglement of formation. Thereby, $C(\hat{\rho}) = 0$ indicates no entanglement, while a value of $C(\hat{\rho}) > 0$ quantifies the amount of entanglement, with maximal entanglement for $C(\hat{\rho}) = 1$. In the case of pure states, the concurrence can be written as [105]

$$C(|\psi\rangle) = \sqrt{2(1-\mathrm{Tr}[\hat{\rho}^2])} = \sqrt{2\mathcal{S}_L(\hat{\rho})}, \tag{D.13}$$

where $\hat{\rho}$ is one of the reduced density matrices and $\mathcal{S}_L(\hat{\rho})$ is the linear entropy function. We note that first, from this expression, it is clear that the concurrence measures the entanglement of the state in terms of the purity of the marginal density matrices. And second, the relation of the concurrence to the linear entropy function allows for the construction of entanglement measures based on the linear entropy function.

D.1.3 Global entanglement

The *global entanglement* is a multipartite entanglement measure defined as the average over bipartite entanglement measures. Thereby, the amount of bipartite entanglement is quantified by the linear entropy function defined in the previous subsection. The global entanglement

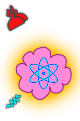

for pure states of N qubits reads [108–111]

$$Q(|\psi\rangle) \coloneqq \frac{1}{N}\sum_{k=1}^{N} 2\mathcal{S}_L(\hat{\rho}_k) = \frac{1}{N}\sum_{k=1}^{N} 2(1-\mathrm{Tr}[\hat{\rho}_k^2])\,, \tag{D.14}$$

where $\hat{\rho}_k$ is the reduced density matrix of the kth qubit. Here, the linear entropy function measures the entanglement between the kth qubit and all other qubits. This definition allows for a straightforward generalisation to bipartite divisions consisting of subsets of qubits, which can be written as [110, 111]

$$Q_m(|\psi\rangle) \coloneqq \binom{N}{m}^{-1} \sum_{|S|=m} \frac{2^m}{2^m-1}(1-\mathrm{Tr}[\hat{\rho}_S^2])\,. \tag{D.15}$$

Thereby, S denotes a subset of m qubits and $\hat{\rho}_S = \mathrm{Tr}_{S'}[\hat{\rho}]$ is the corresponding reduced density matrix of this m-qubit subsystem (S' consists of the remaining $N-m$ qubits). This defines a class of $\lfloor N/2 \rfloor$ measures, all with values $0 \leq Q_m \leq 1$. A measure for mixed states can be obtained again by the convex-roof construction.

D.2 Correlation function

Let us consider two operators $\hat{O}_A$ and $\hat{O}_B$ on the subsystems A and B. We define the correlation function

$$K(\hat{O}_A, \hat{O}_B, \hat{\rho}) \coloneqq \langle \hat{O}_A \hat{O}_B \rangle - \langle \hat{O}_A \rangle \langle \hat{O}_B \rangle\,. \tag{D.16}$$

In the case of pure states, this correlation function can be used as an entanglement measure if we take the supremum over all operators $\hat{O}_A$, $\hat{O}_B$. In particular, a nonzero value of K corresponds to quantum correlations due to entanglement. The reason is quite simple. For a pure separable state, it is easy to show that $K = 0$. Therefore, a value of $K \neq 0$ implies that the state can not be separable, i.e., the state must be entangled. We use this property mainly throughout our explanations in Chapter 5.

D.3 Explicit calculations for the three-two-level-atom system

In Chapter 4, we consider a second- and third-order photon correlation measurement. Thereby, the measurements at $t = 0$ are seen as a preparation of the quantum state. At several locations, we note that these measurements can be used to create entangled states, which then lead to the interference phenomena that we discuss in detail in Chapter 4. In this section, we explicitly prove that the encountered states are indeed entangled by calculating the global entanglement and also the concurrences for the reduced two-atom states.

D.3.1 State after the first photon measurement

The normalised state after the first photon measurement is given by

$$|\psi_1\rangle = \frac{1}{\sqrt{3}}(e^{i\delta_{1,1}}\,|g,e,e\rangle + e^{i\delta_{2,1}}\,|e,g,e\rangle + e^{i\delta_{3,1}}\,|e,e,g\rangle)\,. \tag{D.17}$$

Since the amount of entanglement does not depend on the relative phases of the state, the global entanglement as well as the concurrences between the different atoms are independent of the δ-phases and read

$$Q(|\psi_1\rangle) = \frac{8}{9}\,, \tag{D.18}$$

$$C(\hat{\rho}_{12}) = C(\hat{\rho}_{13}) = C(\hat{\rho}_{23}) = \frac{2}{3}\,. \tag{D.19}$$

Here, $\hat{\rho}_{12}$ denotes the marginal state when we trace out the third atom and analogously $\hat{\rho}_{13}$, $\hat{\rho}_{23}$ are the marginal states when we trace out the second and first atom, respectively. As can be inferred from the values, a highly entangled state is produced via the first photon detection.

D.3.2 State after the second photon measurement

The normalised state after the second photon measurement is a bit more complicated reading

$$\begin{aligned}|\psi_2\rangle = \mathcal{N}^{-1/2}\Big[&\left(e^{i(\delta_{2,2}+\delta_{3,1})} + e^{i(\delta_{2,1}+\delta_{3,2})}\right)|e,g,g\rangle + \left(e^{i(\delta_{1,2}+\delta_{3,1})} + e^{i(\delta_{1,1}+\delta_{3,2})}\right)|g,e,g\rangle \\ &+ \left(e^{i(\delta_{1,2}+\delta_{2,1})} + e^{i(\delta_{1,1}+\delta_{2,2})}\right)|g,g,e\rangle\Big]\end{aligned} \tag{D.20}$$

with normalisation

$$\begin{aligned}\mathcal{N} = 2[3 &+ \cos(\delta_{1,1} - \delta_{1,2} - \delta_{2,1} + \delta_{2,2}) + \cos(\delta_{1,1} - \delta_{1,2} - \delta_{3,1} + \delta_{3,2}) \\ &+ \cos(\delta_{2,1} - \delta_{2,2} - \delta_{3,1} + \delta_{3,2})]\,.\end{aligned} \tag{D.21}$$

Using this state the global entanglement can be calculated as a function of the δ-phases. Since the general expression is quite involved, we omit writing down the explicit form and rather evaluate it below for the two special cases discussed in this work.

Engineering of spontaneous emission

In the case of our engineering of spontaneous emission setup (see Section 4.1.2), the positions of the atoms are $\boldsymbol{R}_1 = \boldsymbol{0}$, $\boldsymbol{R}_2 = \frac{\lambda}{3}\hat{\boldsymbol{x}}$, and $\boldsymbol{R}_3 = 4\lambda\hat{\boldsymbol{x}}$. Further, the detectors are located at azimuthal angles $\varphi_1 = \frac{2\pi}{3}$ and $\varphi_2 = \frac{\pi}{4.4}$. For this configuration, the global entanglement is

given by

$$Q(|\psi_2\rangle) \approx 0.34 \tag{D.22}$$

and the concurrences between the atoms are

$$C(\hat{\rho}_{12}) \approx 0.43\,, \tag{D.23}$$
$$C(\hat{\rho}_{13}) \approx 0.14\,, \tag{D.24}$$
$$C(\hat{\rho}_{23}) \approx 0.55\,. \tag{D.25}$$

This shows that all three atoms are entangled with each other, with biqubit entanglement particularly between atoms 1 and 2 and between 2 and 3.

Subwavelength imaging

In the case of our subwavelength imaging setup, we project out the antisymmetric state by measuring perpendicular to the atomic chain. Thus, we have $\delta_{1,1} = \delta_{2,1} = \delta_{3,1} = \delta_{1,2} = \delta_{2,2} = \delta_{3,2} = 0$, so that the state is given by the symmetric Dicke state

$$|\psi_2\rangle = \frac{1}{\sqrt{3}}(|e,g,g\rangle + |g,e,g\rangle + |g,g,e\rangle)\,, \tag{D.26}$$

for which the global entanglement and the concurrences are easy to calculate reading

$$Q(|\psi_2\rangle) = \frac{8}{9}\,, \tag{D.27}$$
$$C(\hat{\rho}_{12}) = C(\hat{\rho}_{13}) = C(\hat{\rho}_{23}) = \frac{2}{3}\,. \tag{D.28}$$

Note that the values are exactly the same as for the state $|\psi_1\rangle$, which obviously needs to be the case since we simply swap the ground and excited states. This does not change the amount of entanglement.

D.4 Global entanglement of symmetric Dicke states

In this section, we calculate the global entanglement of symmetric Dicke states. Let us consider a symmetric Dicke state written as (the state $|J,M\rangle$ is defined in Chapter 5)

$$|D^N_{n_e}\rangle \coloneqq |J = N/2, M = n_e - N/2\rangle = \binom{N}{n_e}^{-1/2} \sum_{|S|=n_e} |N;S\rangle\ , \tag{D.29}$$

where S denotes a subset of the N atoms and $|N;S\rangle$ is a tensor product state of N atoms with n_e many atoms in the excited state. Thereby, the subset S specifies which atoms are in

the excited state. We need to calculate the reduced density matrices $\hat{\rho}_{N-m}$, where we trace out m qubits. Since the state is symmetric with respect to the atoms, the density matrices do not depend on the specific atoms, such that we choose to trace out the first m atoms in the following. Further, we choose the symmetric Dicke states

$$|D^m_{n'_e}\rangle = \binom{m}{n'_e}^{-1/2} \sum_{|S'|=n'_e} |m; S'\rangle \tag{D.30}$$

to be part of the basis used for the partial traces and we calculate

$$(\langle D^m_{n'_e}| \otimes \mathbb{1}_{N-m})\, |D^N_{n_e}\rangle = \binom{m}{n'_e}^{1/2} \binom{N}{n_e}^{-1/2} \binom{N-m}{n_e-n'_e}^{1/2} |D^{N-m}_{n_e-n'_e}\rangle \ . \tag{D.31}$$

Therefore, the reduced density matrices read

$$\hat{\rho}_{N-m} = \bigoplus_{n'_e=0}^{m} \binom{m}{n'_e} \binom{N-m}{n_e-n'_e} \binom{N}{n_e}^{-1} |D^{N-m}_{n_e-n'_e}\rangle\langle D^{N-m}_{n_e-n'_e}| \ , \tag{D.32}$$

where $\binom{n}{k} = 0$ if $k < 0$. Then, we find for the trace of the squared reduced density matrices

$$\begin{aligned} \mathrm{Tr}[\hat{\rho}^2_{N-m}] &= \sum_{n'_e=0}^{m} \binom{m}{n'_e}^2 \binom{N-m}{n_e-n'_e}^2 \binom{N}{n_e}^{-2} \\ &= \binom{N-m}{n_e}^2 \binom{N}{n_e}^{-2} {}_4F_3(a_1, a_2, a_3, a_4; b_1, b_2, b_3; 1) =: \mathrm{Pu}(N, m, n_e)\,, \end{aligned} \tag{D.33}$$

where we defined the purity function $\mathrm{Pu}(N, m, n_e)$, and $a_1 = a_2 = -m$, $a_3 = a_4 = -n_e$, $b_1 = 1$, and $b_2 = b_3 = N + 1 - m - n_e$. Here, ${}_pF_q(a_1, ..., a_p; b_1, ..., b_q; z)$ is the so-called generalised hypergeometric function. Now, we finally obtain for the global entanglement of a symmetric Dicke state

$$Q_m(|D^N_{n_e}\rangle) = \binom{N}{m}^{-1} \sum_{|S|=m} \frac{2^m}{2^m-1}[1 - \mathrm{Pu}(N, m, n_e)] = \frac{2^m}{2^m-1}[1 - \mathrm{Pu}(N, m, n_e)]\,. \tag{D.34}$$

D.5 Entanglement witness based on the structure factor

An entanglement witness is not a strict entanglement measure, but explicitly designed to detect a certain class of entangled states. It is a Hermitian operator whose expectation value is greater than or equal to 0 for all separable states, such that any value less than 0 implies entanglement. In this section, we present the entanglement witness introduced in Ref. [112], which is based on the structure factor of coherent diffractive imaging. It is defined as

$$\hat{W}(k) := \mathbb{1} - \hat{\Sigma}(k)\,, \tag{D.35}$$

where

$$\hat{\Sigma}(k) = \frac{1}{2}\left[\hat{\tilde{\Sigma}}(k) + \hat{\tilde{\Sigma}}(-k)\right] \tag{D.36}$$

and

$$\hat{\tilde{\Sigma}}(k) = \binom{N}{2}^{-1}\left[c_x\hat{S}_{xx}(k) + c_y\hat{S}_{yy}(k) + c_z\hat{S}_{zz}(k)\right] . \tag{D.37}$$

Here, the operators

$$\hat{S}_{\alpha\alpha}(k) = 4\sum_{\mu<\nu}^{N} e^{ik(R_\nu - R_\mu)}\hat{S}_\alpha^{(\mu)}\hat{S}_\alpha^{(\nu)} , \; \alpha \in \{x, y, z\} \tag{D.38}$$

are based on the structure factor and account for pair correlations of the atoms. Further, R_μ is the position of the μth atom (one dimensional). If the goal is to detect symmetric (Dicke) states, it is best to use $k = 0$ and $c_x = c_y = 1$, $c_z = -1$. In this case, the expressions reduce to

$$\hat{W} = \mathbb{1} - \binom{N}{2}^{-1}\left[\hat{S}_{xx} + \hat{S}_{yy} - \hat{S}_{zz}\right] \tag{D.39}$$

and

$$\hat{S}_{\alpha\alpha} = 4\sum_{\mu<\nu}^{N} \hat{S}_\alpha^{(\mu)}\hat{S}_\alpha^{(\nu)} , \; \alpha \in \{x, y, z\} . \tag{D.40}$$

Thereby, the constructed entanglement witness reliably detects entanglement of symmetric Dicke states with approximately $N/2$ many excitations [112], i.e., $\langle\hat{W}\rangle < 0$, but fails to detect entanglement for small (≈ 1) or large ($\approx N$) number of excitations, i.e., $\langle\hat{W}\rangle \geq 0$ in these cases.

D.5.1 Entanglement witness for Dicke superradiance

In the case of Dicke superradiance, the density operator at any time t can be written as an incoherent sum of symmetric Dicke states as in Eq. (5.34). Thus, the expectation value of the entanglement witness is simply given by [112]

$$W(t) = \mathrm{Tr}[\hat{W}\hat{\rho}(t)] = 1 - \sum_{n_e=0}^{N} \rho_{n_e,n_e}(t)\frac{4n_e(N-n_e) - (N-2n_e)^2 + N}{N(N-1)} , \tag{D.41}$$

where we characterised the density matrix elements by the number of excited atoms n_e ($n_e = M + N/2$).

D.5.2 Entanglement witness for Dicke-like superradiance of distant non-interacting atoms

In the case of Dicke-like superradiance via consecutive photon measurements, we need to calculate the expectation value of the entanglement witness with respect to the conditional states $\hat{\rho}_{m-1}(t_m)$. First of all, we recognise that

$$\langle \hat{S}_{\alpha\alpha} \rangle = 2 \langle \hat{S}_\alpha \hat{S}_\alpha \rangle - \frac{N}{2} \,. \tag{D.42}$$

Since $\langle \hat{S}_+^2 \rangle = \langle \hat{S}_-^2 \rangle = 0$ for the states $\hat{\rho}_{m-1}(t_m)$, we have

$$\langle \hat{S}_x \hat{S}_x \rangle = \langle \hat{S}_y \hat{S}_y \rangle = \frac{1}{4} \Big(\langle \hat{S}_+ \hat{S}_- \rangle + \langle \hat{S}_- \hat{S}_+ \rangle \Big) \,. \tag{D.43}$$

We already know that

$$\langle \hat{S}_+ \hat{S}_- \rangle = \mathrm{Tr}[\hat{S}_+ \hat{S}_- \hat{\rho}_{m-1}(t_m)] = G^{(1)}_{\rho_{m-1}}(t_1, ..., t_m) = m(N-m+1)e^{-2\gamma t_m} \,. \tag{D.44}$$

Further, by using ($\hat{n}_e$ is the excited state number operator)

$$\langle \hat{S}_z \rangle = \langle \hat{n}_e \rangle - \frac{N}{2} \tag{D.45}$$

and Eq. (5.63), we find

$$\langle \hat{S}_- \hat{S}_+ \rangle = -2 \langle \hat{S}_z \rangle + \langle \hat{S}_+ \hat{S}_- \rangle = (m-2)(N-m+1)e^{-2\gamma t_m} + N \,. \tag{D.46}$$

Therefore, the two expectation values for the x and y components are

$$\langle \hat{S}_{xx} \rangle = \langle \hat{S}_{yy} \rangle = (m-1)(N-m+1)e^{-2\gamma t_m} \,. \tag{D.47}$$

Now, we calculate the remaining z component. By writing

$$\langle \hat{S}_z \hat{S}_z \rangle = \langle \hat{n}_e^2 \rangle - N \langle \hat{n}_e \rangle + \frac{N^2}{4} \,, \tag{D.48}$$

we recognise that the only expectation value that is left to calculate is $\langle \hat{n}_e^2 \rangle$, which can be evaluated as

$$\begin{aligned} \langle \hat{n}_e^2 \rangle &= \sum_{s=0}^{N-m} p_{m-1,s}(t_m) \binom{N}{s} \binom{N}{m-1}^{-1} \binom{N-s}{m-1} [N-s-(m-1)]^2 \\ &= (N-m+1)e^{-4\gamma t_m} [(N-m) + e^{2\gamma t_m}] \,. \end{aligned} \tag{D.49}$$

The final result for the expectation value of the entanglement witness is then given by

$$W(t) = \mathrm{Tr}[\hat{W}\hat{\rho}_{m-1}(t_m)] = 2 - \frac{4e^{-4\gamma t_m}(N-m+1)[(N+m-2)e^{2\gamma t_m}+m-N]}{N(N-1)}\,. \quad \text{(D.50)}$$

D.6 Separability of symmetric mixed states

Due to the sublinearity of entanglement, in the case of mixed states, it is hard to decide whether a state is entangled or not. However, in the case of an incoherent mixture of symmetric Dicke states, in Ref. [18] they developed a method to check for the separability of such states by solving $N+1$ polynomial equations. For this purpose, they constructed the so-called separable diagonally symmetric (SDS) states [18]

$$\hat{\rho}_{\mathrm{SDS}} = \frac{1}{2\pi}\int_0^{2\pi} d\phi \sum_{j=1}^{j_{\max}} x_j(\hat{\rho}[y_j,\phi])^{\otimes N}\,, \quad \text{(D.51)}$$

where the integral over ϕ cancels all single-atom coherences and the state is symmetric and separable by construction. Further, the single-atom states are parametrised as

$$\hat{\rho}[y,\phi] = \sqrt{y}\,|g\rangle + \sqrt{1-y}e^{i\phi}\,|e\rangle\,, \quad \text{(D.52)}$$

and the normalisation of the SDS state demands that the sum of the weighting factors x_j is equal to unity. Then, by rewriting the state $\hat{\rho}_{\mathrm{SDS}}$ in terms of symmetric Dicke states, they found the following set of polynomial equations [18]

$$\rho_{n_e} = N!\sum_{j=1}^{j_{\max}} \frac{x_j y_j^{N-n_e}(1-y_j)^{n_e}}{(N-n_e)!n_e!}\,,\ n_e \in \{0,...,N\}\,, \quad \text{(D.53)}$$

which needs to be solved to check whether the state

$$\hat{\rho} = \sum_{n_e=0}^{N} \rho_{n_e}\,|D_{n_e}^N\rangle\langle D_{n_e}^N| \quad \text{(D.54)}$$

is separable. Thereby, the solution needs to pass a "sanity check", i.e., the state $\hat{\rho}$ is only separable if one can find a solution of Eq. (D.53) that satisfies $0 \leq x_j, y_j \leq 1$ for all j. In Ref. [18], by numerically solving the set of equations for up to $N = 8$ atoms, they claim that in the case of Dicke superradiance the resulting mixed state is actually separable. For the discussion within this thesis, we extend these calculations to up to $N = 16$ atoms (see Chapter 5).

E Wigner-Eckart theorem and selection rules

In this appendix, we state the Wigner-Eckart theorem and show its application to the dipole operator to obtain selection rules for atomic dipole transitions.

E.1 Wigner-Eckart theorem

Let us consider two commuting angular momenta $\hat{\boldsymbol{L}}$ and $\hat{\boldsymbol{S}}$, which are added together to give the total angular momentum $\hat{\boldsymbol{J}} = \hat{\boldsymbol{L}} + \hat{\boldsymbol{S}}$. A natural basis is given by the tensor product basis defined as

$$|\ell, m_\ell; s, m_s\rangle \coloneqq |\ell, m_\ell\rangle \otimes |s, m_s\rangle \ . \tag{E.1}$$

However, it is often convenient to work in the common eigenbasis of $\hat{J}^2$ and $\hat{J}_z$. Since $[\hat{L}^2, \hat{J}_i] = [\hat{S}^2, \hat{J}_i] = 0$, $i \in \{x, y, z\}$, the new basis states can be characterised by four quantum numbers, so we write the states as $|j, m_j, (\ell, s)\rangle$. The matrix elements between the two introduced basis sets denoted as

$$\langle \ell, m_\ell; s, m_s | j, m_j\rangle \coloneqq \langle \ell, m_\ell; s, m_s | j, m_j, (\ell, s)\rangle \tag{E.2}$$

are the well-known Clebsch-Gordan coefficients.
Now, we continue by defining so-called tensor operators $\hat{T}_{k,m_k}$ by their transformation properties under rotations. These can be formulated via commutation relations with a given angular momentum operator $\hat{\boldsymbol{J}}$ as

$$[\hat{J}_z, \hat{T}_{k,m_k}] = \hbar m_k \hat{T}_{k,m_k} \ , \tag{E.3}$$

$$[\hat{J}_+, \hat{T}_{k,m_k}] = \hbar f_{k,m_k} \hat{T}_{k,m_k+1} \ , \tag{E.4}$$

$$[\hat{J}_-, \hat{T}_{k,m_k}] = \hbar f_{k,m_k-1} \hat{T}_{k,m_k-1} \ , \tag{E.5}$$

where $f_{k,m_k} \coloneqq \sqrt{k(k+1) - m_k(m_k+1)}$ and $\hat{J}_\pm \coloneqq \hat{J}_x \pm i\hat{J}_y$.
The Wigner-Eckart theorem now states that the matrix elements of such tensor operators

$\hat{T}_{k,m_k}$ can be related to Clebsch-Gordan coefficients via [113]

$$\langle j', m'_j|\hat{T}_{k,m_k}|j, m_j\rangle = (-1)^{2k}\frac{\langle j'\|\hat{T}_k\|j\rangle}{\sqrt{2j'+1}}\,\langle j, m_j; k, m_k|j', m'_j\rangle\ . \tag{E.6}$$

Here, $\langle j'\|\hat{T}_k\|j\rangle$ is the so-called reduced matrix element, which only depends on the angular momentum quantum numbers j', j, and k, but not on the corresponding magnetic quantum numbers.

E.2 Application to dipole transitions - selection rules

In the following, we apply the Wigner-Eckart theorem to the dipole moment operator. The dipole moment operator of a single atom can be written as $\hat{\boldsymbol{d}} = -e\hat{\boldsymbol{r}}$, where $\hat{\boldsymbol{r}} = \sum_\alpha \hat{\boldsymbol{r}}_\alpha$ is the sum over all position operators of the individual electrons. The eigenstates of an atomic system are, to a very good approximation, eigenstates of $\hat{J}^2$ and $\hat{J}_z$, where

$$\hat{\boldsymbol{J}} = \hat{\boldsymbol{L}} + \hat{\boldsymbol{S}} = \sum_\alpha(\hat{\boldsymbol{L}}_\alpha + \hat{\boldsymbol{S}}_\alpha) \tag{E.7}$$

is the total angular momentum. Thereby, $\hat{\boldsymbol{L}}_\alpha$ and $\hat{\boldsymbol{S}}_\alpha$ denote the orbital angular momentum and the spin of the αth electron. In this eigenbasis, the dipole matrix elements read

$$\boldsymbol{d}_{J,m_J;J',m'_J} \coloneqq \langle J, m_J|(-e\hat{\boldsymbol{r}})|J', m'_J\rangle\ . \tag{E.8}$$

Let us now consider a special case of tensor operators, the so-called vector operators, which are tensor operators of order 1, i.e., $k = 1$ in the previous notation. A vector operator is thus characterised by its three components $\hat{R}_q$, $q \in \{-1, 0, 1\}$, where $\hat{R}_q \coloneqq \hat{T}_{1,q}$. Such vector operators fulfil the commutation relations

$$[\hat{J}_\pm, \hat{R}_\pm] = 0\,, \tag{E.9}$$
$$[\hat{J}_\pm, \hat{R}_\mp] = \sqrt{2}\hbar\hat{R}_0\,, \tag{E.10}$$
$$[\hat{J}_z, \hat{R}_\pm] = \pm\hbar\hat{R}_\pm\,, \tag{E.11}$$
$$[\hat{J}_z, \hat{R}_0] = 0\,, \tag{E.12}$$
$$[\hat{J}_\pm, \hat{R}_0] = \sqrt{2}\hbar\hat{R}_\pm\,, \tag{E.13}$$

where we defined $\hat{R}_\pm \coloneqq \hat{R}_{\pm1}$. The vector operator $\hat{\boldsymbol{R}}$ is called a spherical vector operator and its components $\hat{R}_q$ are called spherical components if they are related to the cartesian components via

$$\hat{R}_+ = -\frac{1}{\sqrt{2}}(\hat{R}_x + i\hat{R}_y)\,, \tag{E.14}$$

$$\hat{R}_- = \frac{1}{\sqrt{2}}(\hat{R}_x - i\hat{R}_y)\,, \tag{E.15}$$

$$\hat{R}_0 = \hat{R}_z\,. \tag{E.16}$$

The commutation relations can then be summarised to a single commutation relation for the cartesian components reading

$$[\hat{J}_a, \hat{R}_b] = i\hbar\varepsilon_{abc}\hat{R}_c\,, \tag{E.17}$$

where ε_{abc} is the epsilon tensor.
In what follows, we show that the dipole moment operator is a spherical vector operator. Therefore, first note that

$$[\hat{L}_a, \hat{r}_b] = [\varepsilon_{acg}\hat{r}_c\hat{p}_g, \hat{r}_b] = \varepsilon_{acg}\hat{r}_c(-i\hbar)\delta_{gb} = \varepsilon_{acb}\hat{r}_c(-i\hbar) = i\hbar\varepsilon_{abc}\hat{r}_c\,. \tag{E.18}$$

Thus, we find that

$$\begin{aligned}[\hat{J}_a, \hat{d}_b] &= \left[\sum_\alpha (\hat{L}_\alpha)_a + (\hat{S}_\alpha)_a, -e\sum_\beta (\hat{r}_\beta)_b\right] = -e\sum_{\alpha,\beta}[(\hat{L}_\alpha)_a, (\hat{r}_\beta)_b] = -e\sum_{\alpha,\beta}\delta_{\alpha\beta}[(\hat{L}_\alpha)_a, (\hat{r}_\alpha)_b] \\ &= -e\sum_\alpha i\hbar\varepsilon_{abc}(\hat{r}_\alpha)_c = i\hbar\varepsilon_{abc}\hat{d}_c\,,\end{aligned} \tag{E.19}$$

which shows that $\hat{\boldsymbol{d}}$ is a spherical vector operator. Then, by applying the Wigner-Eckart theorem Eq. (E.6), we find for the matrix elements of the spherical components the following relation

$$\langle J, m_J|\hat{d}_\pm|J', m'_J\rangle \propto \langle J', m'_J; 1, \pm 1|J, m_J\rangle\ . \tag{E.20}$$

In addition, we generally have

$$\langle L, m_L; S, m_S|\hat{J}_z|J, m_J\rangle = \hbar m_J \langle L, m_L; S, m_S|J, m_J\rangle = \hbar(m_L + m_S)\langle L, m_L; S, m_S|J, m_J\rangle\ , \tag{E.21}$$

which implies that $\langle L, m_L; S, m_S|J, m_J\rangle = 0$ if $m_J \neq m_L + m_S$. Thus, the Clebsch-Gordan coefficients fulfil $\langle J', m'_J; 1, \pm 1|J, m_J\rangle \neq 0$ only if $m'_J \pm 1 = m_J$ and

$$\langle J, m_J|\hat{d}_+|J', m'_J\rangle \neq 0 \quad \text{only if} \quad m_J = m'_J + 1\,, \tag{E.22}$$

$$\langle J, m_J|\hat{d}_-|J', m'_J\rangle \neq 0 \quad \text{only if} \quad m_J = m'_J - 1\,, \tag{E.23}$$

$$\langle J, m_J|\hat{d}_0|J', m'_J\rangle \neq 0 \quad \text{only if} \quad m_J = m'_J\,. \tag{E.24}$$

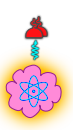

Finally, to find the dipole transition matrix elements $\boldsymbol{d}_m = \langle m|\hat{\boldsymbol{d}}|g\rangle$ introduced in Section 4.2.1, we have to write the dipole operator in its spherical components. Therefore, we define the polarisation vectors for left-circularly polarised, right-circularly polarised, and linear orthogonally polarised light as

$$\hat{\boldsymbol{\varepsilon}}_{\pm 1} = \hat{\boldsymbol{\varepsilon}}_{\pm} = \mp\frac{1}{\sqrt{2}}(\hat{\boldsymbol{e}}_x \pm i\hat{\boldsymbol{e}}_y)\,, \qquad \hat{\boldsymbol{\varepsilon}}_0 = \hat{\boldsymbol{e}}_z\,, \tag{E.25}$$

where the hat indicates normalisation to unity. Note that $\hat{\boldsymbol{\varepsilon}}_q^* \hat{\boldsymbol{\varepsilon}}_{q'} = \delta_{q,q'}$, i.e., the vectors are mutually orthogonal. Now, we can write the dipole operator as

$$\hat{\boldsymbol{d}} = \hat{d}_x\hat{\boldsymbol{e}}_x + \hat{d}_y\hat{\boldsymbol{e}}_y + \hat{d}_z\hat{\boldsymbol{e}}_z = \frac{1}{\sqrt{2}}(\hat{d}_x + i\hat{d}_y)\hat{\boldsymbol{\varepsilon}}_- - \frac{1}{\sqrt{2}}(\hat{d}_x - i\hat{d}_y)\hat{\boldsymbol{\varepsilon}}_+ + \hat{d}_z\hat{\boldsymbol{\varepsilon}}_0 \tag{E.26}$$

and since the dipole operator is Hermitian, we then find that

$$\hat{\boldsymbol{d}} = \hat{\boldsymbol{d}}^\dagger = \frac{1}{\sqrt{2}}(\hat{d}_x - i\hat{d}_y)\hat{\boldsymbol{\varepsilon}}_-^* - \frac{1}{\sqrt{2}}(\hat{d}_x + i\hat{d}_y)\hat{\boldsymbol{\varepsilon}}_+^* + \hat{d}_z\hat{\boldsymbol{\varepsilon}}_0^* = \hat{d}_-\hat{\boldsymbol{\varepsilon}}_-^* + \hat{d}_+\hat{\boldsymbol{\varepsilon}}_+^* + \hat{d}_0\hat{\boldsymbol{\varepsilon}}_0^*\,, \tag{E.27}$$

where we used Eqs. (E.14)-(E.16). Now, using Eqs. (E.22)-(E.24), we obtain for the dipole matrix element $\boldsymbol{d}_0$ introduced in Section 4.2.1

$$\begin{aligned}\boldsymbol{d}_0 = \langle 0|\hat{\boldsymbol{d}}|g\rangle = \langle 1,0|\hat{\boldsymbol{d}}|0,0\rangle &= \underbrace{\langle 1,0|\hat{d}_+|0,0\rangle}_{=0}\hat{\boldsymbol{\varepsilon}}_+^* + \underbrace{\langle 1,0|\hat{d}_-|0,0\rangle}_{=0}\hat{\boldsymbol{\varepsilon}}_-^* + \langle 1,0|\hat{d}_0|0,0\rangle\,\hat{\boldsymbol{\varepsilon}}_0^* \\ &= \langle 1,0|\hat{d}_0|0,0\rangle\,\hat{\boldsymbol{\varepsilon}}_0^* = \langle 1|\hat{d}_0|g\rangle\,\hat{\boldsymbol{\varepsilon}}_0^*\,.\end{aligned} \tag{E.28}$$

Analogously, we have

$$\boldsymbol{d}_1 = \langle 1|\hat{\boldsymbol{d}}|g\rangle = \langle 1|\hat{d}_+|g\rangle\,\hat{\boldsymbol{\varepsilon}}_+^*\,, \tag{E.29}$$

$$\boldsymbol{d}_{-1} = \langle -1|\hat{\boldsymbol{d}}|g\rangle = \langle -1|\hat{d}_-|g\rangle\,\hat{\boldsymbol{\varepsilon}}_-^*\,, \tag{E.30}$$

where we can assume with proper choice of phase that $\langle m|\hat{d}_m|g\rangle \in \mathbb{R}^+$ since we can generally write $\langle m|\hat{d}_m|g\rangle = r_m e^{i\phi_m}$ with $r_m \in \mathbb{R}^+$ and $\phi_m \in (-\pi, \pi]$. Now, by absorbing $e^{i\phi_m}$ in the definition of the excited states $|m\rangle$, one can achieve the claimed result.

F Quantum trajectory method

In the following procedure, which is based on Ref. [77], we decompose the time evolution governed by a master equation of the form

$$\frac{\partial}{\partial t}\hat{\rho} = \mathscr{L}\hat{\rho} \tag{F.1}$$

into so-called trajectories. The solution of Eq. (F.1) is formally given by

$$\hat{\rho}(t) = e^{\mathscr{L}t}\hat{\rho}(0)\,. \tag{F.2}$$

To rewrite Eq. (F.2), we first derive a general expansion for an exponential operator of the form $e^{t(\hat{A}+x\hat{B})}$. For this, we relate the expression to the physical problem of evolving a system that interacts with another system, described by a non-perturbed Hamiltonian $\hat{H}_0$ and some interaction term $\hat{V}$. The full time evolution in the Schrödinger picture is governed by the time evolution operator $\hat{U}(t,0) = e^{-\frac{i}{\hbar}t(\hat{H}_0+\hat{V})}$, where we assumed that the separate Hamiltonian parts are time-independent. We can decompose the time evolution operator in the interaction picture given by

$$\hat{U}_I(t,0) = \mathscr{T}\left(e^{-\frac{i}{\hbar}\int_0^t dt'\,\hat{V}_I(t')}\right) \tag{F.3}$$

as

$$\hat{U}_I(t,0) = \hat{U}_0(0,t)\hat{U}(t,0)\,, \tag{F.4}$$

where $\mathscr{T}$ is the time-ordering operator and $\hat{V}_I(t) = \hat{U}_0^\dagger(t,0)V\hat{U}_0(t,0)$. Furthermore, $\hat{U}_0(t,0)$ describes the time evolution initiated by the unperturbed Hamiltonian $\hat{H}_0$. Now, we make the identifications $\hat{A} = -\frac{i}{\hbar}\hat{H}_0$ and $x\hat{B} = -\frac{i}{\hbar}\hat{V}$ to find

$$\hat{U}_0(0,t) = \hat{U}_0^\dagger(t,0) = \hat{U}_0^{-1}(t,0) = e^{-t\hat{A}} \tag{F.5}$$

and

$$\hat{V}_I(t) = e^{-t\hat{A}}i\hbar x\hat{B}e^{t\hat{A}}\,. \tag{F.6}$$

Then, the full time evolution operator is

$$\hat{U}(t,0) = e^{t(\hat{A}+x\hat{B})} = \hat{U}_0^{-1}(0,t)\hat{U}_I(t,0) = e^{t\hat{A}}\mathscr{T}\left(e^{\int_0^t dt'\, e^{-t'\hat{A}}x\hat{B}e^{t'\hat{A}}}\right) = e^{t\hat{A}}\mathscr{T}\, e^{x\int_0^t ds\,\hat{B}(s)} \tag{F.7}$$

with $\hat{B}(s) = e^{-s\hat{A}}\hat{B}e^{s\hat{A}}$. Now, we write the last expression in a Dyson series to obtain

$$\begin{aligned} e^{t(\hat{A}+x\hat{B})} &= e^{t\hat{A}}\sum_{m=0}^{\infty} x^m \int_0^t dt_m \int_0^{t_m} dt_{m-1} \ldots \int_0^{t_2} dt_1\, \hat{B}(t_m)\hat{B}(t_{m-1})\ldots\hat{B}(t_1) \\ &= e^{t\hat{A}}\sum_{m=0}^{\infty} x^m \int_0^t dt_m \int_0^{t_m} dt_{m-1} \ldots \int_0^{t_2} dt_1\, e^{-t_m\hat{A}}\hat{B}e^{t_m\hat{A}}\ldots e^{-t_1\hat{A}}\hat{B}e^{t_1\hat{A}} \\ &= \sum_{m=0}^{\infty} x^m \int_0^t dt_m \int_0^{t_m} dt_{m-1} \ldots \int_0^{t_2} dt_1\, e^{\hat{A}(t-t_m)}\hat{B}e^{\hat{A}(t_m-t_{m-1})}\ldots e^{\hat{A}(t_2-t_1)}\hat{B}e^{\hat{A}t_1}\,. \end{aligned} \tag{F.8}$$

Using this expansion, we can write Eq. (F.2) as

$$\begin{aligned} \hat{\rho}(t) &= e^{\mathscr{L}t}\hat{\rho}(0) = e^{[(\mathscr{L}-\mathcal{S})+\mathcal{S}]t}\hat{\rho}(0) \\ &= \sum_{m=0}^{\infty}\int_0^t dt_m \int_0^{t_m} dt_{m-1} \ldots \int_0^{t_2} dt_1 \\ &\quad \times e^{(\mathscr{L}-\mathcal{S})(t-t_m)}\mathcal{S}e^{(\mathscr{L}-\mathcal{S})(t_m-t_{m-1})}\ldots e^{(\mathscr{L}-\mathcal{S})(t_2-t_1)}\mathcal{S}e^{(\mathscr{L}-\mathcal{S})t_1}\hat{\rho}(0)\,. \end{aligned} \tag{F.9}$$

This expression allows for an interpretation of the time evolution in terms of so-called *quantum trajectories* [77]. The total time evolution is given by the sum of all possible trajectories or paths that the system can take. In the case of an atom that spontaneously emits photons, the action of $\mathcal{S}$ could be the destruction of a photon in a direct photon measurement. Then, the trajectories consist of time spans, in which the system evolves without photon detections and of times at which photon detections take place (so-called quantum jumps). The *conditioned source density operator* at time t is [77]

$$\hat{\rho}_c(t) = \frac{\hat{\tilde{\rho}}_c(t)}{\mathrm{Tr}[\hat{\tilde{\rho}}_c(t)]}\,, \tag{F.10}$$

where $\hat{\tilde{\rho}}_c(t) = e^{(\mathscr{L}-\mathcal{S})(t-t_m)}\mathcal{S}e^{(\mathscr{L}-\mathcal{S})(t_m-t_{m-1})}\ldots e^{(\mathscr{L}-\mathcal{S})(t_2-t_1)}\mathcal{S}e^{(\mathscr{L}-\mathcal{S})t_1}\hat{\rho}(0)$ is the unnormalised conditioned density operator. Depending on the explicit form of $\mathscr{L}-\mathcal{S}$ and $\mathcal{S}$, one can often write the conditioned (unnormalised) density operator as a pure state reading

$$\hat{\rho}_c(t) = |\psi_c(t)\rangle\langle\psi_c(t)|\,, \quad \hat{\tilde{\rho}}_c(t) = |\bar{\psi}_c(t)\rangle\langle\bar{\psi}_c(t)|\,. \tag{F.11}$$

The time evolution without a quantum jump given by $\mathscr{L}-\mathcal{S}$ can then be replaced by the time evolution generated by a non-Hermitian Hamiltonian $\hat{H}$ and a quantum jump described by the action $\mathcal{S}\hat{\tilde{\rho}}_c(t) = \hat{C}\hat{\tilde{\rho}}_c(t)\hat{C}^\dagger$ is accounted for by applying the so-called collapse operator

$\hat{C}$ to the pure state. Thereby, each pure state trajectory is split into small time steps Δt and whether the state at time $t_n = n\Delta t$ is time-evolved without a collapse or undergoes a collapse is stochastically chosen depending on the collapse probability

$$p_c(t_n) = \langle \psi_c(t_n)|\hat{C}^\dagger \hat{C}|\psi_c(t_n)\rangle \, \Delta t \, . \tag{F.12}$$

Then, the time evolution of the density operator is obtained by the average over the stochastic trajectories of the pure states. We note that a single trajectory can be seen as a single physical realisation, whereas the density operator describes the ensemble average of all physical realisations. We further note that the choice of $\mathcal{S}$ is not unique, but rather that there exist multiple different so-called unravellings of the master equation with different physical interpretations.

Let us now describe the situation of post-selecting trajectories, e.g., due to conditional measurements. In Eq. (F.9), all possible quantum trajectories are included. However, we sometimes condition multi-photon measurements on the direction and time of previously measured photons, i.e., we select only specific quantum trajectories. Consider, for instance, only quantum trajectories, where one photon was measured at a specific time $\tilde{t}_1$. Then, we only have quantum trajectories with $m \geq 1$ and from Eq. (F.9) we get the unnormalised density operator

$$\begin{aligned}\hat{\tilde{\rho}}(t) = &\sum_{m=1}^{\infty}\sum_{n=1}^{m}\int_{\tilde{t}_1}^{t} dt_m \ldots \int_{\tilde{t}_1}^{t_{n+2}} dt_{n+1} \int_{0}^{t_{n+1}} dt_n \int_{0}^{\tilde{t}_1} dt_{n-1} \ldots \int_{0}^{t_2} dt_1 \\ &\times \delta(t_n - \tilde{t}_1) e^{(\mathscr{L}-\mathcal{S})(t-t_m)} \mathcal{S} \ldots \mathcal{S} e^{(\mathscr{L}-\mathcal{S})t_1} \hat{\rho}(0) \, .\end{aligned} \tag{F.13}$$

Here, we already changed the integral limits accordingly, i.e., all photon detections that occur after the photon detection at time $\tilde{t}_1$ can only occur in a time span beginning with the time $\tilde{t}_1$, while the last photon detection before the photon detection at time $\tilde{t}_1$ can only happen until the time $\tilde{t}_1$. Since n goes from 1 to m and m goes from 1 to infinity, every possible decomposition of numbers of photon detections before and after $\tilde{t}_1$ is accounted for. Therefore, we can do the replacement

$$\sum_{m=1}^{\infty}\sum_{n=1}^{m} \rightarrow \sum_{m=0}^{\infty}\sum_{n=0}^{\infty} \tag{F.14}$$

to have two new sums going from 0 to infinity, one for all photon detections after and one for all photon detections before the photon detection at time $\tilde{t}_1$. In addition, we can carry out the integral of the nth time t_n leading to

$$\hat{\tilde{\rho}}(t) = \sum_{m=0}^{\infty}\int_{\tilde{t}_1}^{t} dt_m \ldots \int_{\tilde{t}_1}^{t_2} dt_1 \, e^{(\mathscr{L}-\mathcal{S})(t-t_m)} \mathcal{S} \ldots \mathcal{S} e^{(\mathscr{L}-\mathcal{S})(t_1-\tilde{t}_1)} \mathcal{S}$$

$$\times \sum_{n=0}^{\infty} \int_0^{\tilde{t}_1} dt'_n \ldots \int_0^{t'_2} dt'_1 \, e^{(\mathscr{L}-\mathcal{S})(\tilde{t}_1-t'_n)} \mathcal{S} \ldots \mathcal{S} e^{(\mathscr{L}-\mathcal{S})t'_1} \hat{\rho}(0)$$

$$= e^{\mathscr{L}(t-\tilde{t}_1)} \mathcal{S} e^{\mathscr{L}\tilde{t}_1} \hat{\rho}(0) =: e^{\mathscr{L}(t-\tilde{t}_1)} \hat{\tilde{\rho}}_{\mathcal{S}}(\tilde{t}_1) \,, \tag{F.15}$$

where we can identify the density operator after the photon detection at time $\tilde{t}_1$ as

$$\hat{\rho}_{\mathcal{S}}(\tilde{t}_1) = \frac{\hat{\tilde{\rho}}_{\mathcal{S}}(\tilde{t}_1)}{\mathrm{Tr}[\hat{\tilde{\rho}}_{\mathcal{S}}(\tilde{t}_1)]} \,. \tag{F.16}$$

Eq. (F.15) means that the density operator evolves with the usual time evolution given by the master equation up to $\tilde{t}_1$, where the specified photon detection takes place, and afterwards evolves again with the time evolution given by the master equation.

G Dicke-like superradiance of distant non-interacting atoms - supporting calculations

In this appendix, we give some supporting calculations to Section 5.3.

G.1 Differential equations for the density matrix elements

In the first section, we explicitly carry out the projection of the master equation Eq. (5.36) onto the tensor product basis. A straightforward calculation yields

$$\begin{aligned}
\frac{\partial}{\partial t}\langle\alpha|\hat{\rho}(t)|\beta\rangle =& -\gamma\sum_{\mu=1}^{N}\Big(\langle\alpha|\hat{S}_+^{(\mu)}\hat{S}_-^{(\mu)}\hat{\rho}(t)|\beta\rangle + \langle\alpha|\hat{\rho}(t)\hat{S}_+^{(\mu)}\hat{S}_-^{(\mu)}|\beta\rangle - 2\langle\alpha|\hat{S}_-^{(\mu)}\hat{\rho}(t)\hat{S}_+^{(\mu)}|\beta\rangle\Big)\\
=& -\gamma\sum_{\mu=1}^{N}\Bigg(\sum_{\chi}\langle\alpha|\hat{S}_+^{(\mu)}|\chi\rangle\langle\chi|\hat{S}_-^{(\mu)}\hat{\rho}(t)|\beta\rangle + \sum_{\zeta}\langle\alpha|\hat{\rho}(t)\hat{S}_+^{(\mu)}|\zeta\rangle\langle\zeta|\hat{S}_-^{(\mu)}|\beta\rangle\\
&-2\sum_{\eta,\delta}\langle\alpha|\hat{S}_-^{(\mu)}|\eta\rangle\langle\eta|\hat{\rho}(t)|\delta\rangle\langle\delta|\hat{S}_+^{(\mu)}|\beta\rangle\Bigg)\\
\Leftrightarrow \frac{\partial}{\partial t}\rho_{\alpha,\beta}(t) \overset{(*)}{=}& 2\gamma\sum_{\mu=1}^{N}\rho_{\eta^{(\mu)},\delta^{(\mu)}}(t) - \gamma\sum_{\mu=1}^{N}\rho_{S_+^{(\mu)}\chi,\beta}(t) - \gamma\sum_{\mu=1}^{N}\rho_{\alpha,S_+^{(\mu)}\zeta}(t)\,,
\end{aligned}\tag{G.1}$$

whereby the last equal sign $(*)$ is restricted by the three conditions listed in Eqs. (5.38)-(5.40), which need to be fulfilled separately to obtain a contribution from the respective terms in the sums.

In general, this gives $2^{2N}-1$ real first-order differential equations for the density matrix elements. To reduce the number of differential equations, we assume specific initial density matrices. We only consider density matrices, which are block-diagonal with respect to the number of ground state atoms. Furthermore, we restrict ourselves to initial density matrices that provide the same initial conditions for the differential equations of the density matrix elements that are of the same form. If the initial state fulfils these two requirements, the state after the time evolution and consecutive conditional photon measurements at a particular position, for which the emitted photons accumulate the same phase for each atom, also meets the two requirements. The set of real first-order differential equations can then be

reduced to N^2 many equations, meaning that only particular differential equations need to be solved.
This leads to the following set of first-order differential equations for the diagonal elements

$$\frac{\partial}{\partial t}\begin{pmatrix} \rho_{g^{(0)},g^{(0)}}(t) \\ \rho_{g^{(1)}_\mu,g^{(1)}_\mu}(t) \\ \rho_{g^{(2)}_{\mu\nu},g^{(2)}_{\mu\nu}}(t) \\ \vdots \end{pmatrix} = \begin{pmatrix} -2\gamma N & 0 & 0 & \dots \\ 2\gamma & -2\gamma(N-1) & 0 & \\ 0 & 4\gamma & -2\gamma(N-2) & \\ \vdots & & & \ddots \end{pmatrix} \begin{pmatrix} \rho_{g^{(0)},g^{(0)}}(t) \\ \rho_{g^{(1)}_\mu,g^{(1)}_\mu}(t) \\ \rho_{g^{(2)}_{\mu\nu},g^{(2)}_{\mu\nu}}(t) \\ \vdots \end{pmatrix}, \tag{G.2}$$

while the set of first-order differential equations for the off-diagonal elements is given by

$$\frac{\partial}{\partial t}\begin{pmatrix} \rho_{g^{(1)}_\kappa,g^{(1)}_\lambda}(t) \\ \rho_{g^{(2)}_{\kappa\lambda},g^{(2)}_{\kappa\mu}}(t) \\ \rho_{g^{(2)}_{\kappa\lambda},g^{(2)}_{\mu\nu}}(t) \\ \rho_{g^{(3)}_{\kappa\lambda\mu},g^{(3)}_{\kappa\lambda\nu}}(t) \\ \rho_{g^{(3)}_{\kappa\lambda\mu},g^{(3)}_{\kappa\nu\xi}}(t) \\ \rho_{g^{(3)}_{\kappa\lambda\mu},g^{(3)}_{\nu\xi o}}(t) \\ \vdots \end{pmatrix} = \begin{pmatrix} -2\gamma(N-1) & 0 & 0 & 0 & 0 & 0 & \dots \\ 2\gamma & -2\gamma(N-2) & 0 & 0 & 0 & 0 & \\ 0 & 0 & -2\gamma(N-2) & 0 & 0 & 0 & \\ 0 & 4\gamma & 0 & -2\gamma(N-3) & 0 & 0 & \\ 0 & 0 & 2\gamma & 0 & -2\gamma(N-3) & 0 & \\ 0 & 0 & 0 & 0 & 0 & -2\gamma(N-3) & \\ \vdots & & & & & & \ddots \end{pmatrix} \begin{pmatrix} \rho_{g^{(1)}_\kappa,g^{(1)}_\lambda}(t) \\ \rho_{g^{(2)}_{\kappa\lambda},g^{(2)}_{\kappa\mu}}(t) \\ \rho_{g^{(2)}_{\kappa\lambda},g^{(2)}_{\mu\nu}}(t) \\ \rho_{g^{(3)}_{\kappa\lambda\mu},g^{(3)}_{\kappa\lambda\nu}}(t) \\ \rho_{g^{(3)}_{\kappa\lambda\mu},g^{(3)}_{\kappa\nu\xi}}(t) \\ \rho_{g^{(3)}_{\kappa\lambda\mu},g^{(3)}_{\nu\xi o}}(t) \\ \vdots \end{pmatrix}. \tag{G.3}$$

These two sets of first-order differential equations can then be solved analytically by either taking the matrix exponential or by a successive application of the Duhamel-principle.

G.2 Multi-time expectation values of pseudo-spin raising and lowering operators

To evaluate the higher-order photon correlation functions in Eq. (5.45), we need to find the multi-time pseudo-spin expectation values. This can be achieved by applying the quantum regression theorem of Appendix C. Therefore, we first need to compute the single-time expectation value $\langle \hat{S}_+(t)...\hat{S}_+(t)\hat{S}_-(t)...\hat{S}_-(t)\rangle$ consisting of m collective pseudo-spin raising and m collective pseudo-spin lowering operators. Expanding the collective operators leads to

$$\langle \hat{S}_+(t)...\hat{S}_+(t)\hat{S}_-(t)...\hat{S}_-(t)\rangle = \sum_{\mu_1=1}^{N}...\sum_{\mu_m=1}^{N}\sum_{\nu_1=1}^{N}...\sum_{\nu_m=1}^{N}\langle \hat{S}_+^{(\mu_1)}(t)...\hat{S}_+^{(\mu_m)}(t)\hat{S}_-^{(\nu_1)}(t)...\hat{S}_-^{(\nu_m)}(t)\rangle\ , \tag{G.4}$$

i.e., the evaluation of expectation values of the form $\langle \hat{S}_+^{(\mu_1)}(t)...\hat{S}_+^{(\mu_m)}(t)\hat{S}_-^{(\nu_1)}(t)...\hat{S}_-^{(\nu_m)}(t)\rangle$. First of all, we note that if $\mu_s = \mu_p$ or $\nu_s = \nu_p$ for some $s, p \in \{1, ..., N\}$, the expectation value is zero since $[\hat{S}_-^{(\mu)}]^2 = [\hat{S}_+^{(\mu)}]^2 = 0$ for all $\mu \in \{1, ..., N\}$. Further, remember that we consider density operators, which are block-diagonal with respect to the number of atoms in the ground state. Then, if any $\mu_s \neq \nu_p\ \forall p$ or $\nu_p \neq \mu_s\ \forall s$, the expectation value is also zero, such that

it is enough to examine expectation values of the form $\left\langle \prod_{s=1}^{m} \hat{S}_{+}^{(\mu_s)}(t) \prod_{p=1}^{m} \hat{S}_{-}^{(\mu_p)}(t) \right\rangle$ with $\mu_s \neq \mu_p$ for all $s \neq p$. This single-time expectation value can be calculated by using the master equation Eq. (5.36). To understand the structure, we first start with the expectation value $\langle \hat{S}_{+}^{(\mu)}(t) \hat{S}_{-}^{(\mu)}(t) \rangle$. To be able to apply the master equation, we build the time derivative reading

$$\begin{aligned}\frac{\partial}{\partial t} \langle \hat{S}_{+}^{(\mu)}(t) \hat{S}_{-}^{(\mu)}(t) \rangle &= \frac{\partial}{\partial t} \operatorname{Tr}[\hat{S}_{+}^{(\mu)} \hat{S}_{-}^{(\mu)} \hat{\rho}(t)] \\ &= -\gamma \sum_{\nu=1}^{N} \Big\{ \operatorname{Tr}[\hat{S}_{+}^{(\mu)} \hat{S}_{-}^{(\mu)} \hat{S}_{+}^{(\nu)} \hat{S}_{-}^{(\nu)} \hat{\rho}(t)] + \operatorname{Tr}[\hat{S}_{+}^{(\mu)} \hat{S}_{-}^{(\mu)} \hat{\rho}(t) \hat{S}_{+}^{(\nu)} \hat{S}_{-}^{(\nu)}] \\ &\quad -2 \operatorname{Tr}[\hat{S}_{+}^{(\mu)} \hat{S}_{-}^{(\mu)} \hat{S}_{-}^{(\nu)} \hat{\rho}(t) \hat{S}_{+}^{(\nu)}] \Big\} . \end{aligned} \tag{G.5}$$

We can simplify this differential equation by recognising that

$$\left.\begin{aligned} &\operatorname{Tr}[\hat{S}_{+}^{(\mu)} \hat{S}_{-}^{(\mu)} \hat{S}_{+}^{(\nu)} \hat{S}_{-}^{(\nu)} \hat{\rho}(t)] = \operatorname{Tr}[\hat{S}_{+}^{(\mu)} \hat{S}_{-}^{(\mu)} \hat{\rho}(t) \hat{S}_{+}^{(\nu)} \hat{S}_{-}^{(\nu)}] \\ &\operatorname{Tr}[\hat{S}_{+}^{(\mu)} \hat{S}_{-}^{(\mu)} \hat{S}_{+}^{(\nu)} \hat{S}_{-}^{(\nu)} \hat{\rho}(t)] = \operatorname{Tr}[\hat{S}_{+}^{(\mu)} \hat{S}_{-}^{(\mu)} \hat{\rho}(t) \hat{S}_{+}^{(\nu)} \hat{S}_{-}^{(\nu)}] \end{aligned}\right\} \text{for } \mu \neq \nu , \tag{G.6}$$

$$\left.\begin{aligned} &\operatorname{Tr}[\hat{S}_{+}^{(\mu)} \hat{S}_{-}^{(\mu)} \hat{S}_{+}^{(\nu)} \hat{S}_{-}^{(\nu)} \hat{\rho}(t)] = \operatorname{Tr}[\hat{S}_{+}^{(\mu)} \hat{S}_{-}^{(\mu)} \hat{\rho}(t) \hat{S}_{+}^{(\nu)} \hat{S}_{-}^{(\nu)}] = \operatorname{Tr}[\hat{S}_{+}^{(\mu)} \hat{S}_{-}^{(\mu)} \hat{\rho}(t)] \\ &\operatorname{Tr}[\hat{S}_{+}^{(\mu)} \hat{S}_{-}^{(\mu)} \hat{S}_{-}^{(\nu)} \hat{\rho}(t) \hat{S}_{+}^{(\nu)}] = 0 \end{aligned}\right\} \text{for } \mu = \nu . \tag{G.7}$$

Thus, if $\mu \neq \nu$, the term in the sum vanishes, so we only get a single contribution for $\mu = \nu$. Then, we obtain the differential equation

$$\frac{\partial}{\partial t} \langle \hat{S}_{+}^{(\mu)}(t) \hat{S}_{-}^{(\mu)}(t) \rangle = -2\gamma \langle \hat{S}_{+}^{(\mu)}(t) \hat{S}_{-}^{(\mu)}(t) \rangle \tag{G.8}$$

whose solution is an exponential decay $\langle \hat{S}_{+}^{(\mu)}(t) \hat{S}_{-}^{(\mu)}(t) \rangle = e^{-2\gamma t} \langle \hat{S}_{+}^{(\mu)}(0) \hat{S}_{-}^{(\mu)}(0) \rangle$. Next, we have a look at the single-time expectation value of two pseudo-spin raising and two pseudo-spin lowering operators $\langle \hat{S}_{+}^{(\mu_1)}(t) \hat{S}_{+}^{(\mu_2)}(t) \hat{S}_{-}^{(\mu_2)}(t) \hat{S}_{-}^{(\mu_1)}(t) \rangle$ with $\mu_1 \neq \mu_2$. In this case, we get two contributions from the sum, namely for $\mu_1 = \nu$ and for $\mu_2 = \nu$. The differential equation for the expectation value is therefore

$$\frac{\partial}{\partial t} \langle \hat{S}_{+}^{(\mu_1)}(t) \hat{S}_{+}^{(\mu_2)}(t) \hat{S}_{-}^{(\mu_2)}(t) \hat{S}_{-}^{(\mu_1)}(t) \rangle = -4\gamma \langle \hat{S}_{+}^{(\mu_1)}(t) \hat{S}_{+}^{(\mu_2)}(t) \hat{S}_{-}^{(\mu_2)}(t) \hat{S}_{-}^{(\mu_1)}(t) \rangle . \tag{G.9}$$

The generalisation to single-time expectation values of m pseudo-spin raising and m pseudo-spin lowering operators is then straightforward to obtain reading

$$\frac{\partial}{\partial t} \left\langle \prod_{s=1}^{m} \hat{S}_{+}^{(\mu_s)}(t) \prod_{p=1}^{m} \hat{S}_{-}^{(\mu_p)}(t) \right\rangle = -2m\gamma \left\langle \prod_{s=1}^{m} \hat{S}_{+}^{(\mu_s)}(t) \prod_{p=1}^{m} \hat{S}_{-}^{(\mu_p)}(t) \right\rangle \tag{G.10}$$

whose solution is again an exponential decay given by

$$\left\langle \prod_{s=1}^{m} \hat{S}_{+}^{(\mu_s)}(t) \prod_{p=1}^{m} \hat{S}_{-}^{(\mu_p)}(t) \right\rangle = e^{-2m\gamma t} \left\langle \prod_{s=1}^{m} \hat{S}_{+}^{(\mu_s)}(0) \prod_{p=1}^{m} \hat{S}_{-}^{(\mu_p)}(0) \right\rangle . \tag{G.11}$$

This calculation allows us to find the time evolution of the multi-time expectation values of pseudo-spin raising and lowering operators by applying the quantum regression theorem (see Appendix C). It implies that the differential equation for the two-time expectation value of two pseudo-spin raising and two pseudo-spin lowering operators is

$$\frac{\partial}{\partial \tau} \langle \hat{S}_{+}^{(\mu_1)}(t) \hat{S}_{+}^{(\mu_2)}(t+\tau) \hat{S}_{-}^{(\mu_2)}(t+\tau) \hat{S}_{-}^{(\mu_1)}(t) \rangle = -2\gamma \, \langle \hat{S}_{+}^{(\mu_1)}(t) \hat{S}_{+}^{(\mu_2)}(t+\tau) \hat{S}_{-}^{(\mu_2)}(t+\tau) \hat{S}_{-}^{(\mu_1)}(t) \rangle \ , \tag{G.12}$$

from which we obtain

$$\langle \hat{S}_{+}^{(\mu_1)}(t_1) \hat{S}_{+}^{(\mu_2)}(t_2) \hat{S}_{-}^{(\mu_2)}(t_2) \hat{S}_{-}^{(\mu_1)}(t_1) \rangle = e^{-2\gamma(t_2-t_1)} \, \langle \hat{S}_{+}^{(\mu_1)}(t_1) \hat{S}_{+}^{(\mu_2)}(t_1) \hat{S}_{-}^{(\mu_2)}(t_1) \hat{S}_{-}^{(\mu_1)}(t_1) \rangle \ , \tag{G.13}$$

where $t = t_1$ and $\tau = t_2 - t_1$. Since we solved the single-time expectation value appearing on the right of Eq. (G.13) beforehand, we already have the full solution of the two-time expectation value. Now, the multi-time expectation values can be found by a successive application of the quantum regression theorem, explicitly demonstrated for the two-time expectation values. This gives

$$\begin{aligned}
&\langle \hat{S}_{+}^{(\mu_1)}(t_1) ... \hat{S}_{+}^{(\mu_m)}(t_m) \hat{S}_{-}^{(\mu_m)}(t_m) ... \hat{S}_{-}^{(\mu_1)}(t_1) \rangle = \\
&= e^{-2\gamma(t_m - t_{m-1})} e^{-4\gamma(t_{m-1} - t_{m-2})} ... e^{-2m\gamma t_1} \, \langle \hat{S}_{+}^{(\mu_1)}(0) ... \hat{S}_{+}^{(\mu_m)}(0) \hat{S}_{-}^{(\mu_m)}(0) ... \hat{S}_{-}^{(\mu_1)}(0) \rangle \\
&= \left(\prod_{s=1}^{m} e^{-2\gamma t_s} \right) \langle \hat{S}_{+}^{(\mu_1)}(0) ... \hat{S}_{+}^{(\mu_m)}(0) \hat{S}_{-}^{(\mu_m)}(0) ... \hat{S}_{-}^{(\mu_1)}(0) \rangle \ .
\end{aligned} \tag{G.14}$$

G.3 Trace distance between the post-measurement states and the symmetric subspace

We want to calculate the trace distance between the time-evolved post-measurement states and the symmetric subspace spanned by the symmetric Dicke states. Therefore, we first note that the state after the measurement of m photons is block-diagonal with respect to the number of atoms in the ground state, i.e.,

$$\hat{\rho}_m = \bigoplus_{n_g} \hat{\rho}_{m,n_g} \, . \tag{G.15}$$

Since the symmetric Dicke states have a fixed number of ground state atoms, this implies that also the projected state is block-diagonal. So Eq. (5.66) simplifies to

$$\hat{\rho}_{m,\mathrm{proj}} = \sum_{n_g} \langle J,M|\hat{\rho}_{m,n_g}|J,M\rangle\,|J,M\rangle\langle J,M| = \bigoplus_{n_g} \langle J,M|\hat{\rho}_{m,n_g}|J,M\rangle\,|J,M\rangle\langle J,M| \ . \quad \text{(G.16)}$$

Now, an important property of the post-measurement states is that when all elements of a given row of $\hat{\rho}_{m,n_g}$ are summed up, the obtained value is independent of the row under consideration. This implies that the symmetric Dicke state $|J,M\rangle$ with n_g many atoms in the ground state is an eigenstate of the block matrix $\hat{\rho}_{m,n_g}$, so we can write

$$\hat{\rho}_{m,n_g} = \langle J,M|\hat{\rho}_{m,n_g}|J,M\rangle\,|J,M\rangle\langle J,M| \oplus \hat{\tilde{\rho}}_{m,n_g} \ . \quad \text{(G.17)}$$

Plugging Eq. (G.17) into Eq. (G.15), the state after m photon measurements reads

$$\hat{\rho}_m = \bigoplus_{n_g} \langle J,M|\hat{\rho}_{m,n_g}|J,M\rangle\,|J,M\rangle\langle J,M| \oplus \hat{\tilde{\rho}}_{m,n_g} \ , \quad \text{(G.18)}$$

such that the difference operator $\hat{\tilde{\rho}}_m \coloneqq \hat{\rho}_m - \hat{\rho}_{m,\mathrm{proj}}$ that is needed for the trace distance can be written as

$$\hat{\tilde{\rho}}_m = \bigoplus_{n_g} \hat{\tilde{\rho}}_{m,n_g} \ . \quad \text{(G.19)}$$

Since the Hermiticity of $\hat{\rho}_m$ and $\hat{\rho}_{m,\mathrm{proj}}$ implies that $\hat{\tilde{\rho}}_m$ is also Hermitian, the trace distance simplifies to

$$T(\hat{\rho}_m, \hat{\rho}_{m,\mathrm{proj}}) = \frac{1}{2}\,\mathrm{Tr}\left[\sqrt{\hat{\tilde{\rho}}_m^2}\right] = \frac{1}{2}\sum_i |\lambda_{m,i}| \ , \quad \text{(G.20)}$$

where the $\lambda_{m,i}$s are the eigenvalues of $\hat{\tilde{\rho}}_m$. Now, note that $\hat{\rho}_m$ is a density matrix and thus is positive semidefinite. This means that also the block matrices $\hat{\rho}_{m,n_g}$ and $\hat{\tilde{\rho}}_{m,n_g}$ are positive semidefinite implying that all eigenvalues $\lambda_{m,i}$ are either greater than zero or equal to zero. Therefore, the trace distance can be written as

$$T(\hat{\rho}_m, \hat{\rho}_{m,\mathrm{proj}}) = \frac{1}{2}\sum_i |\lambda_{m,i}| = \frac{1}{2}\sum_i \lambda_{m,i} = \frac{1}{2}\,\mathrm{Tr}[\hat{\tilde{\rho}}_m] \ , \quad \text{(G.21)}$$

i.e., we only need to determine the trace of the difference operator. This can be achieved by combinatorially calculating the diagonal entries of the matrices $\hat{\rho}_m$ and $\hat{\rho}_{m,\mathrm{proj}}$ and manually building the difference. Both matrices have the same normalisation $\binom{N}{m}^{-1}$ and follow the same time evolution accounted for by the function

$$\mathcal{T}(m,n_g) \coloneqq e^{-2(N-m)\gamma t_{m+1}}(e^{2\gamma t_{m+1}}-1)^{n_g-m} \ . \quad \text{(G.22)}$$

We note that this function is identical to the probabilities given in Eq. (5.58), but where $m = 1$ already belongs to the state after the first measurement. Now, it remains to count and calculate the entries on the diagonals of the two matrices. Let us consider the diagonal entry of a single tensor product state with n_g many atoms in the ground state. In the case of $\hat{\rho}_m$, we need to count how many times we obtain this state by successively applying the collective lowering operator. This number is given by the number of initial states leading to the considered tensor product state, which we define as

$$\mathcal{D}(m, n_g) \coloneqq \binom{n_g}{n_g - m} = \binom{n_g}{m}. \tag{G.23}$$

In the case of $\hat{\rho}_{m,\mathrm{proj}}$, we first need to count the number of incoherent terms in the block matrix $\hat{\rho}_{m,n_g}$, which is given by $\binom{N}{n_g - m}$. Second, we need the number of product states within a state in $\hat{\rho}_{m,n_g}$, which can be calculated as

$$\frac{1}{m!}\prod_{i=1}^{m}[N - (n_g - i)] = \binom{N - n_g + m}{m}, \tag{G.24}$$

where the factor $\frac{1}{m!}$ accounts for a multiple counting of the states. Third, taking also the projection onto the symmetric Dicke states into consideration, we define

$$\mathcal{D}_{\mathrm{proj}}(m, n_g) \coloneqq \binom{N}{n_g - m}\binom{N}{n_g}^{-2}\binom{N - n_g + m}{m}^2. \tag{G.25}$$

With these definitions, we can finally write the trace distance as

$$T(\hat{\rho}_m, \hat{\rho}_{m,\mathrm{proj}}) = \frac{1}{2}\binom{N}{m}^{-1}\sum_{n_g=0}^{N}\binom{N}{n_g}\mathcal{T}(m, n_g)[\mathcal{D}(m, n_g) - \mathcal{D}_{\mathrm{proj}}(m, n_g)], \tag{G.26}$$

where the factor $\binom{N}{n_g}$ accounts for the number of tensor product states within each block.

H Gaussian Moment Theorem - supporting calculations

Let us consider again the mth-order photon correlation function in the direction $\boldsymbol{k} = \mathbf{0}$, which is given by Eq. (6.31) reading

$$\begin{aligned} G^{(m)}(\mathbf{0}, ..., \mathbf{0}) &\approx \sum_{j=0}^{m} \binom{m}{j}^2 j!(2m-j)! \binom{N}{2m-j} (\overline{S_+ S_-})^j \left(\bar{S}_+ \bar{S}_-\right)^{m-j} \\ &= (N\overline{S_+ S_-})^m \sum_{j=0}^{m} \binom{m}{j}^2 j!(2m-j)! \frac{1}{N^{2m-j}} \binom{N}{2m-j} r^{m-j}\,, \end{aligned} \tag{H.1}$$

where we defined $r = \frac{N\bar{S}_+\bar{S}_-}{\overline{S_+S_-}}$. Similarly, we write the first-order photon correlation function in the direction $\boldsymbol{k} = \mathbf{0}$ as

$$G^{(1)}(\mathbf{0}) = N\overline{S_+ S_-}\left[1 + \left(1 - \frac{1}{N}\right) r\right]\,. \tag{H.2}$$

In what follows, we want to calculate the Taylor expansion of the normalised mth-order photon correlation function $g^{(m)}(\mathbf{0}, ..., \mathbf{0})$ around $r = 0$. From a pedagogical point of view, it is instructive to first consider the limit of a large atom number N. Therefore, we keep only the leading terms in both $G^{(m)}$ and $G^{(1)}$ by approximating

$$\begin{aligned} G^{(m)}(\mathbf{0}, ..., \mathbf{0}) &\approx (N\overline{S_+ S_-})^m \sum_{j=0}^{m} \binom{m}{j}^2 j! r^{m-j} \\ &= (N\overline{S_+ S_-})^m \left[\sum_{j=2}^{m} \binom{m}{j}^2 j! r^{m-j} + m!(mr+1)\right] \end{aligned} \tag{H.3}$$

and

$$G^{(1)}(\mathbf{0}) \approx N\overline{S_+ S_-}(1+r)\,. \tag{H.4}$$

Then,

$$[G^{(1)}(\mathbf{0})]^m \approx (N\overline{S_+S_-})^m(1+r)^m = (N\overline{S_+S_-})^m \sum_{j=0}^{m} \binom{m}{j} r^{m-j}$$
$$= (N\overline{S_+S_-})^m \left[\sum_{j=2}^{m} \binom{m}{j} r^{m-j} + mr + 1\right] \tag{H.5}$$

and thus we find that $G^{(m)}$ and $[G^{(1)}]^m$ are equal up to the linear order in r, except for a factor of $m!$. This implies that the linear order of the Taylor expansion of the approximated $g^{(m)}$ around $r = 0$ vanishes, so the leading correction is already of second order. We can also calculate this Taylor expansion in the large N limit explicitly, which is given by

$$g^{(m)}(\mathbf{0}, ..., \mathbf{0}) = m! - m!\frac{m(m-1)}{4} r^2 + \mathcal{O}(r^3)\,. \tag{H.6}$$

Thus, we would only require

$$\frac{m(m-1)}{4} r^2 \ll 1 \Leftrightarrow \left(\frac{\langle \hat{S}_+^{(\mu)} \rangle \langle \hat{S}_-^{(\mu)} \rangle}{\langle \hat{S}_+^{(\mu)} \hat{S}_-^{(\mu)} \rangle}\right)^2 \ll \frac{4}{N^2 m(m-1)}\,, \forall \mu \in \{1, ..., N\} \tag{H.7}$$

instead of the stronger condition given in Eq. (6.33), which can be obtained via a Taylor expansion of the unnormalised $G^{(m)}$ function up to the leading order in r. Therefore, the large N limit hints at a weaker condition, which is based on the second order in the Taylor expansion. We end this chapter by finally calculating the general Taylor expansion using the exact expressions given in Eq. (H.1) and (H.2). This leads to

$$g^{(m)}(\mathbf{0}, ..., \mathbf{0}) = \frac{(m!)^2 \binom{N}{m}}{N^m} - \frac{(m!)^2 \binom{N}{m} m(m-1)}{N^{m+1}} r$$
$$- \frac{1}{4} \frac{(m!)^2 \binom{N}{m} (N^2 - 3N - 2mN + 3m - m^2 + 2) m(m-1)}{N^{m+2}} r^2 + \mathcal{O}(r^3)\,. \tag{H.8}$$

We note that here we find a linear correction in r. However, this correction is independent of the number of atoms N and since we at least additionally require $\frac{1}{N} \ll \frac{1}{m^2}$ to obtain the Gaussian Moment Theorem, this first-order correction is negligible if we require that the second-order correction is much smaller than 1, expressed by

$$\left(\frac{\langle \hat{S}_+^{(\mu)} \rangle \langle \hat{S}_-^{(\mu)} \rangle}{\langle \hat{S}_+^{(\mu)} \hat{S}_-^{(\mu)} \rangle}\right)^2 \ll \frac{4}{(N^2 - 3N - 2mN + 3m - m^2 + 2) m(m-1)} \approx \frac{4}{N^2 m(m-1)}\,. \tag{H.9}$$

As a final remark, we note that from Eq. (H.8) we already find the $m!\binom{N}{m}$ factor calculated in Eq. (6.42). Therefore, we see that to obtain the Gaussian Moment Theorem, i.e.,

$g^{(m)}(\mathbf{0}, ..., \mathbf{0}) \approx m!$, we need

$$\frac{N(N-1)...(N-m+1)}{N^m} \approx 1 \Leftrightarrow \frac{1}{N} \ll \frac{1}{m^2}\,. \tag{H.10}$$

I Incoherent mth-order photon correlation function - Gaussian Moment Theorem

Motivated by the fact that thermal light sources are incoherent in first order, in this appendix, we investigate the conditions for which the incoherent higher-order photon correlation functions of the atomic ensemble exhibit thermal statistics, i.e., can be obtained via the Gaussian Moment Theorem. For this purpose, we split the atomic raising and lowering operators in a coherent and an incoherent part as [65, 114]

$$\hat{S}_{\pm}^{(\mu)} = \langle \hat{S}_{\pm}^{(\mu)} \rangle + \delta \hat{S}_{\pm}^{(\mu)} \,, \tag{I.1}$$

where $\langle \hat{S}_{\pm}^{(\mu)} \rangle$ describes the coherent radiation, whereas $\delta \hat{S}_{\pm}^{(\mu)}$ characterises the incoherent fluctuations. The object of interest is the normalised mth-order photon correlation function of the fluctuating part of the electric field operators, i.e.,

$$\delta g^{(m)}(\boldsymbol{k}_1, ..., \boldsymbol{k}_m) \coloneqq \frac{\delta G^{(m)}(\boldsymbol{k}_1, ..., \boldsymbol{k}_m)}{\delta G^{(1)}(\boldsymbol{k}_1) ... \delta G^{(1)}(\boldsymbol{k}_m)} \,, \tag{I.2}$$

whereby

$$\delta G^{(m)}(\boldsymbol{k}_1, ..., \boldsymbol{k}_m) = \langle \delta \hat{E}^{(-)}(\boldsymbol{k}_1) ... \delta \hat{E}^{(-)}(\boldsymbol{k}_m) \delta \hat{E}^{(+)}(\boldsymbol{k}_m) ... \delta \hat{E}^{(+)}(\boldsymbol{k}_1) \rangle \tag{I.3}$$

and

$$\delta \hat{E}^{(\pm)}(\boldsymbol{k}) = \sum_{\mu=1}^{N} e^{\mp i \boldsymbol{k} \boldsymbol{R}_\mu} \delta \hat{S}_{\mp}^{(\mu)} \,. \tag{I.4}$$

Let M be a set of n elements, then we denote by $P \sqsubset M$ an m-tuple of the n-set M if $|P| = m$ and $m < n$. With this notation, we can write

$$\begin{aligned} &\delta G^{(m)}(\boldsymbol{k}_1, ..., \boldsymbol{k}_m) \\ &= \sum_{\mu_1, ..., \mu_{2m}=1}^{N} e^{i \boldsymbol{k}_1 \boldsymbol{R}_{\mu_1}} ... e^{i \boldsymbol{k}_m \boldsymbol{R}_{\mu_m}} e^{-i \boldsymbol{k}_m \boldsymbol{R}_{\mu_{m+1}}} ... e^{-i \boldsymbol{k}_1 \boldsymbol{R}_{\mu_{2m}}} \langle \delta \hat{S}_{+}^{(\mu_1)} ... \delta \hat{S}_{+}^{(\mu_m)} \delta \hat{S}_{-}^{(\mu_{m+1})} ... \delta \hat{S}_{-}^{(\mu_{2m})} \rangle \end{aligned}$$

$$= \sum_{\substack{P,Q \sqsubset \{1,...,N\},\\ |P|=|Q|=m}} \prod_{\mu,\nu=1}^{m} e^{i\boldsymbol{k}_\mu \boldsymbol{R}_{P_\mu}} e^{-i\boldsymbol{k}_\nu \boldsymbol{R}_{Q_\nu}} \left\langle \prod_{\mu=1}^{m} \delta\hat{S}_+^{(P_\mu)} \prod_{\nu=1}^{m} \delta\hat{S}_-^{(Q_\nu)} \right\rangle . \tag{I.5}$$

The last equation may seem simple, but is not yet suitable for calculating the expectation values. Therefore, let us define

$$n_\mu^{(P)} \coloneqq \sum_{p\in P} \delta_{p,\mu} \, , \; \mu \in \{1, ..., N\} \, . \tag{I.6}$$

Then, we find

$$\left\langle \prod_{\mu=1}^{m} \delta\hat{S}_+^{(P_\mu)} \prod_{\nu=1}^{m} \delta\hat{S}_-^{(Q_\nu)} \right\rangle = \left\langle \prod_{\mu=1}^{N} [\delta\hat{S}_+^{(\mu)}]^{n_\mu^{(P)}} \prod_{\nu=1}^{N} [\delta\hat{S}_-^{(\nu)}]^{n_\nu^{(Q)}} \right\rangle = \prod_{\mu=1}^{N} \left\langle [\delta\hat{S}_+^{(\mu)}]^{n_\mu^{(P)}} [\delta\hat{S}_-^{(\mu)}]^{n_\mu^{(Q)}} \right\rangle \, , \tag{I.7}$$

where we used that $\hat{\rho} = \otimes_{\mu=1}^{N} \hat{\rho}_\mu$ in the second step. Instead of summing over the different m-tuples and accounting for the multiplicity of each element, we can also sum directly over the multiplicities of all the N elements. This gives

$$\begin{aligned} \delta G^{(m)}(\boldsymbol{k}_1, ..., \boldsymbol{k}_m) = & \sum_{\substack{i_1,...,i_N=0,\\ \sum_{\mu=1}^{N} i_\mu = m}}^{m} \sum_{\substack{j_1,...,j_N=0,\\ \sum_{\nu=1}^{N} j_\nu = m}}^{m} \prod_{\mu,\nu=1}^{N} \frac{1}{i_\mu! j_\nu!} \sum_{\sigma,\sigma' \in S_m} \prod_{p=1}^{i_1} \prod_{q=1}^{j_1} e^{i\left(\boldsymbol{k}_{\sigma(p)} - \boldsymbol{k}_{\sigma'(q)}\right)\boldsymbol{R}_1} \times ... \\ & \times \prod_{p=1}^{i_N} \prod_{q=1}^{j_N} e^{i\left(\boldsymbol{k}_{\sigma\left(p+\sum_{\mu=1}^{N-1} i_\mu\right)} - \boldsymbol{k}_{\sigma'\left(q+\sum_{\nu=1}^{N-1} j_\nu\right)}\right)\boldsymbol{R}_N} \prod_{\mu=1}^{N} \left\langle [\delta\hat{S}_+^{(\mu)}]^{i_\mu} [\delta\hat{S}_-^{(\mu)}]^{j_\mu} \right\rangle . \end{aligned} \tag{I.8}$$

Note that here $\prod_{s=1}^{0} ... \coloneqq 1$. Now, by using

$$\delta G^{(1)}(\boldsymbol{k}_1, \boldsymbol{k}_2) = \sum_{\mu,\nu=1}^{N} e^{i\boldsymbol{k}_1 \boldsymbol{R}_\mu} e^{-i\boldsymbol{k}_2 \boldsymbol{R}_\nu} \langle \delta\hat{S}_+^{(\mu)} \delta\hat{S}_-^{(\nu)} \rangle = \sum_{\mu=1}^{N} e^{i(\boldsymbol{k}_1 - \boldsymbol{k}_2)\boldsymbol{R}_\mu} \langle \delta\hat{S}_+^{(\mu)} \delta\hat{S}_-^{(\mu)} \rangle \, , \tag{I.9}$$

we obtain

$$\begin{aligned} \sum_{\sigma\in S_m} \prod_{p=1}^{m} \delta G^{(1)}(\boldsymbol{k}_p, \boldsymbol{k}_{\sigma(p)}) &= \sum_{\sigma\in S_m} \prod_{p=1}^{m} \sum_{\mu=1}^{N} e^{i(\boldsymbol{k}_p - \boldsymbol{k}_{\sigma(p)})\boldsymbol{R}_\mu} \langle \delta\hat{S}_+^{(\mu)} \delta\hat{S}_-^{(\mu)} \rangle \\ &= \sum_{\mu_1,...,\mu_m=1}^{N} \sum_{\sigma\in S_m} \prod_{p=1}^{m} e^{i(\boldsymbol{k}_p - \boldsymbol{k}_{\sigma(p)})\boldsymbol{R}_{\mu_p}} \langle \delta\hat{S}_+^{(\mu_p)} \delta\hat{S}_-^{(\mu_p)} \rangle \, . \end{aligned} \tag{I.10}$$

If we compare Eq. (I.8) to Eq. (I.10), we recognise that the incoherent photon correlation function of Eq. (I.8) can only be approximated by the Gaussian Moment Theorem if all terms with $i_\alpha, j_\beta \geq 2$ can be neglected. To find the explicit condition that must be satisfied, we

need to calculate the expectation values $\left\langle [\delta\hat{S}_+^{(\mu)}]^{i_\mu}[\delta\hat{S}_-^{(\mu)}]^{j_\mu}\right\rangle$. To evaluate these, we use

$$[\delta\hat{S}_\pm^{(\mu)}]^n = \left[\hat{S}_\pm^{(\mu)} - \langle\hat{S}_\pm^{(\mu)}\rangle\right]^n = \sum_{l=0}^{n}\binom{n}{l}(-1)^l[\hat{S}_\pm^{(\mu)}]^{n-l}\left[\langle\hat{S}_\pm^{(\mu)}\rangle\right]^l , \tag{I.11}$$

with which we find

$$\left\langle [\delta\hat{S}_+^{(\mu)}]^{i_\mu}[\delta\hat{S}_-^{(\mu)}]^{j_\mu}\right\rangle = \sum_{p=0}^{i_\mu}\sum_{q=0}^{j_\mu}\binom{i_\mu}{p}\binom{j_\mu}{q}(-1)^{p+q}\left[\langle\hat{S}_+^{(\mu)}\rangle\right]^p\left[\langle\hat{S}_-^{(\mu)}\rangle\right]^q\left\langle [\hat{S}_+^{(\mu)}]^{i_\mu-p}[\hat{S}_-^{(\mu)}]^{j_\mu-q}\right\rangle . \tag{I.12}$$

We note that $[\hat{S}_\pm^{(\mu)}]^n = 0$ for $n \geq 2$. Thus, we obtain

$$\begin{aligned}\left\langle [\delta\hat{S}_+^{(\mu)}]^{i_\mu}[\delta\hat{S}_-^{(\mu)}]^{j_\mu}\right\rangle = (-1)^{i_\mu+j_\mu}\left[\langle\hat{S}_+^{(\mu)}\rangle\right]^{i_\mu-1}\left[\langle\hat{S}_-^{(\mu)}\rangle\right]^{j_\mu-1}\times \\ \left[i_\mu j_\mu\langle\hat{S}_+^{(\mu)}\hat{S}_-^{(\mu)}\rangle + (1-i_\mu-j_\mu)\langle\hat{S}_+^{(\mu)}\rangle\langle\hat{S}_-^{(\mu)}\rangle\right] .\end{aligned} \tag{I.13}$$

Now, to obtain the condition for which all terms with $i_\alpha, j_\beta \geq 2$ in Eq. (I.8) can be neglected, we compare the term with m different $i_\mu = 1$ to the next higher term with $m-2$ different $i_\mu = 1$ and one $i_{\tilde{\mu}} = 2$. The ratio between the latter and the former needs to be much smaller than 1, expressed by

$$\frac{m(m-1)}{4}\left(\frac{\langle\hat{S}_+^{(\mu)}\rangle\langle\hat{S}_-^{(\mu)}\rangle}{\langle\delta\hat{S}_+^{(\mu)}\delta\hat{S}_-^{(\mu)}\rangle}\right)^2 \ll 1 \Leftrightarrow \left(\frac{\langle\hat{S}_+^{(\mu)}\rangle\langle\hat{S}_-^{(\mu)}\rangle}{\langle\delta\hat{S}_+^{(\mu)}\delta\hat{S}_-^{(\mu)}\rangle}\right)^2 \ll \frac{4}{m(m-1)} , \forall\mu\in\{1,...,N\} . \tag{I.14}$$

In the limit of Eq. (I.14), we can approximate the incoherent mth-order photon correlation function by

$$\begin{aligned}\delta G^{(m)}(\boldsymbol{k}_1,...,\boldsymbol{k}_m) \approx & \sum_{\substack{i_1,...,i_N=0,\\ \sum_{\mu=1}^N i_\mu = m}}^{1}\ \sum_{\substack{j_1,...,j_N=0,\\ \sum_{\nu=1}^N j_\nu = m}}^{1}\prod_{\mu,\nu=1}^{N}\frac{1}{i_\mu! j_\nu!}\sum_{\sigma,\sigma'\in S_m}\prod_{p=1}^{i_1}\prod_{q=1}^{j_1}e^{i\left(\boldsymbol{k}_{\sigma(p)}-\boldsymbol{k}_{\sigma'(q)}\right)\boldsymbol{R}_1}\times ... \\ \times\prod_{p=1}^{i_N}\prod_{q=1}^{j_N}e^{i\left(\boldsymbol{k}_{\sigma\left(p+\sum_{\mu=1}^{N-1}i_\mu\right)}-\boldsymbol{k}_{\sigma'\left(q+\sum_{\nu=1}^{N-1}j_\nu\right)}\right)\boldsymbol{R}_N}\prod_{\mu=1}^{N}\left\langle[\delta\hat{S}_+^{(\mu)}]^{i_\mu}[\delta\hat{S}_-^{(\mu)}]^{j_\mu}\right\rangle \\ = \sum_{\substack{P\subset\{1,...,N\},\\ |P|=m}}\ \sum_{\sigma\in S_m}\prod_{p=1}^{m}e^{i\boldsymbol{k}_p(\boldsymbol{R}_{P_p}-\boldsymbol{R}_{\sigma(P_p)})}\prod_{q=1}^{m}\langle\delta\hat{S}_+^{(P_q)}\delta\hat{S}_-^{(P_q)}\rangle \\ = \sum_{\substack{\mu_1,...,\mu_m=1,\\ \text{mutually different}}}^{N}\ \sum_{\sigma\in S_m}\prod_{p=1}^{m}e^{i(\boldsymbol{k}_p-\boldsymbol{k}_{\sigma(p)})\boldsymbol{R}_{\mu_p}}\langle\delta\hat{S}_+^{(\mu_p)}\delta\hat{S}_-^{(\mu_p)}\rangle .\end{aligned} \tag{I.15}$$

If we compare Eqs. (I.10) and (I.15), we notice that by applying Eq. (6.46) to the incoherent mth-order photon correlation function, we can approximate the last equation by the Gaussian Moment Theorem if $\frac{m!\,m^2}{N} \ll 1$. Let us finally end this appendix with the same remark that we did in the end of Section 6.2.1. If only $\tilde{N} = N - N_g$ many atoms are partially excited and N_g many atoms are in the ground state, we simply need to replace N by $\tilde{N}$ and all equations remain valid.

J Steady state of a plane wave laser driven atomic ensemble

Let us consider the general quantum master equation Eq. (2.74). If we assume that N identical two-level atoms are driven by a single plane wave laser field and that the atoms are separated far distant from each other, i.e., that their mutual separations are much larger than the transition wavelength, then dipole-dipole interactions between the atoms can be neglected and the master equation simplifies to

$$\frac{\partial}{\partial t}\hat{\rho}(t) = -\frac{i}{\hbar}[\hat{H}_A, \hat{\rho}(t)] - \frac{i}{\hbar}[\hat{H}_L, \hat{\rho}(t)] + \mathscr{L}_\gamma \hat{\rho}(t)\,. \tag{J.1}$$

Here,

$$\hat{H}_A = \hbar\omega_0 \sum_{\mu=1}^{N} \hat{S}_z^{(\mu)} \tag{J.2}$$

is the Hamilton operator of the atoms, whereas

$$\hat{H}_L = -i\hbar \sum_{\mu=1}^{N} [\Omega(\boldsymbol{R}_\mu)\hat{S}_+^{(\mu)} e^{-i\omega_L t} - \Omega^*(\boldsymbol{R}_\mu)\hat{S}_-^{(\mu)} e^{i\omega_L t}] \tag{J.3}$$

denotes the Hamiltonian describing the dynamics induced by the laser field. Thereby, ω_L is the laser frequency and

$$\Omega(\boldsymbol{R}_\mu) = \frac{\boldsymbol{dE}(\boldsymbol{R}_\mu)}{\hbar} = \sqrt{\frac{\hbar\omega_L}{2\varepsilon_0 V}}\frac{1}{\hbar}\boldsymbol{d}\boldsymbol{\varepsilon}\alpha e^{i\boldsymbol{k}_L\boldsymbol{R}_\mu} =: \tilde{\Omega} e^{i\boldsymbol{k}_L\boldsymbol{R}_\mu} \tag{J.4}$$

is the position-dependent Rabi frequency. In a last step, we separated the position-dependent phase that each atom sees, such that $\tilde{\Omega}$ is the same for each atom. Finally, the last term of Eq. (J.1) accounts for the spontaneous decay of each atom. To get rid off the oscillating phases in Eq. (J.3), we transform into a frame rotating with the laser frequency ω_L generated

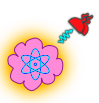

by the Hamiltonian [69]

$$\hat{H}_{\text{trafo}} = -\hbar\omega_L \sum_{\mu=1}^{N} \hat{S}_z^{(\mu)} \,. \tag{J.5}$$

The transformed density matrix reads

$$\hat{\tilde{\rho}}(t) = e^{-\frac{i}{\hbar}\hat{H}_{\text{trafo}}t}\hat{\rho}(t)e^{\frac{i}{\hbar}\hat{H}_{\text{trafo}}t} \,. \tag{J.6}$$

Further, we need to calculate the action of the rotation on the different terms in the master equation. We note that $[\hat{H}_A, \hat{H}_{\text{trafo}}] = 0$, such that $\hat{\tilde{H}}_A = \hat{H}_A$. Further,

$$\hat{\tilde{S}}_+^{(\mu)} = e^{-\frac{i}{\hbar}\hat{H}_{\text{trafo}}t}\hat{S}_+^{(\mu)}e^{\frac{i}{\hbar}\hat{H}_{\text{trafo}}t} = \hat{S}_+^{(\mu)}e^{i\omega_L t} \,, \tag{J.7}$$

$$\hat{\tilde{S}}_-^{(\mu)} = e^{-\frac{i}{\hbar}\hat{H}_{\text{trafo}}t}\hat{S}_-^{(\mu)}e^{\frac{i}{\hbar}\hat{H}_{\text{trafo}}t} = \hat{S}_-^{(\mu)}e^{-i\omega_L t} \,, \tag{J.8}$$

so $\mathscr{L}_\gamma$ is left unchanged under the transformation since products of $\hat{S}_+^{(\mu)}$ and $\hat{S}_-^{(\mu)}$ are left unchanged. However, the laser Hamiltonian becomes

$$\hat{\tilde{H}}_L = -i\hbar \sum_{\mu=1}^{N} [\Omega(\boldsymbol{R}_\mu)\hat{S}_+^{(\mu)} - \Omega^*(\boldsymbol{R}_\mu)\hat{S}_-^{(\mu)}] \,, \tag{J.9}$$

i.e., the oscillating phases are eliminated by the transformation. The master equation for the transformed density operator then reads

$$\begin{aligned} \frac{\partial}{\partial t}\hat{\tilde{\rho}}(t) &= -\frac{i}{\hbar}[\hat{H}_{\text{trafo}}, \hat{\tilde{\rho}}(t)] + e^{-\frac{i}{\hbar}\hat{H}_{\text{trafo}}t}\left[\frac{\partial}{\partial t}\hat{\rho}(t)\right]e^{\frac{i}{\hbar}\hat{H}_{\text{trafo}}t} \\ &= -\frac{i}{\hbar}[\hat{H}_A + \hat{H}_{\text{trafo}}, \hat{\tilde{\rho}}(t)] - \frac{i}{\hbar}[\hat{\tilde{H}}_L, \hat{\tilde{\rho}}(t)] + \mathscr{L}_\gamma\hat{\tilde{\rho}}(t) \,. \end{aligned} \tag{J.10}$$

We note that

$$\hat{H}_A + \hat{H}_{\text{trafo}} = -\hbar\Delta \sum_{\mu=1}^{N} \hat{S}_z^{(\mu)} \,, \tag{J.11}$$

where $\Delta = \omega_L - \omega_0$ is the detuning of the laser frequency with respect to the atomic transition frequency. Now, we consider the transformed laser Hamiltonian $\hat{\tilde{H}}_L$ more carefully. In what follows, we describe the situation relative to one of the atoms ν at position $\boldsymbol{R}_\nu$. We therefore write

$$\hat{\tilde{H}}_L = -i\hbar \sum_{\mu=1}^{N} [\Omega(\boldsymbol{R}_\mu)\hat{S}_+^{(\mu)} - \Omega^*(\boldsymbol{R}_\mu)\hat{S}_-^{(\mu)}] = -i\hbar \sum_{\mu=1}^{N} [\tilde{\Omega}\hat{S}_+^{(\mu)}e^{i\boldsymbol{k}_L\boldsymbol{R}_\mu} - \tilde{\Omega}^*\hat{S}_-^{(\mu)}e^{-i\boldsymbol{k}_L\boldsymbol{R}_\mu}]$$

$$= -i\hbar \sum_{\mu=1}^{N} [\tilde{\Omega} e^{i\boldsymbol{k}_L \boldsymbol{R}_\nu} \hat{S}_+^{(\mu)} e^{i\boldsymbol{k}_L(\boldsymbol{R}_\mu - \boldsymbol{R}_\nu)} - \tilde{\Omega}^* e^{-i\boldsymbol{k}_L \boldsymbol{R}_\nu} \hat{S}_-^{(\mu)} e^{-i\boldsymbol{k}_L(\boldsymbol{R}_\mu - \boldsymbol{R}_\nu)}]$$

$$= -i\hbar \sum_{\mu=1}^{N} [\Omega_R \hat{S}_+^{(\mu)} e^{i\eta_{\mu,\nu}} - \Omega_R^* \hat{S}_-^{(\mu)} e^{-i\eta_{\mu,\nu}}] , \tag{J.12}$$

where we defined $\Omega_R := \tilde{\Omega} e^{i\boldsymbol{k}_L \boldsymbol{R}_\nu}$ and $\eta_{\mu,\nu} := \boldsymbol{k}_L(\boldsymbol{R}_\mu - \boldsymbol{R}_\nu)$. Note that we can assume that $\tilde{\Omega}$ is real and that the νth atom is placed at the origin, i.e., $\boldsymbol{R}_\nu = \boldsymbol{0}$. Then, it follows that $\Omega_R = \Omega_R^* = \tilde{\Omega}$ and $\eta_{\mu,\nu} = \boldsymbol{k}_L(\boldsymbol{R}_\mu - \boldsymbol{R}_\nu) = \boldsymbol{k}_L \boldsymbol{R}_\mu =: \eta_\mu$ is independent of ν. So far, we were able to eliminate the oscillating phases, but we are still left with the position-dependent phases $e^{\pm i\eta_\mu}$. We can also eliminate these phases from the master equation if we do a basis transformation. Therefore, we define the new ground state and excited state of the μth atom as

$$|\tilde{g}_\mu\rangle := e^{-i\frac{\eta_\mu}{2}} |g_\mu\rangle , \tag{J.13}$$

$$|\tilde{e}_\mu\rangle := e^{i\frac{\eta_\mu}{2}} |e_\mu\rangle . \tag{J.14}$$

This corresponds to a basis transformation matrix in the subspace of the μth atom given by

$$T^{(\mu)} = \begin{pmatrix} \langle \tilde{e}_\mu | e_\mu \rangle & \langle \tilde{e}_\mu | g_\mu \rangle \\ \langle \tilde{g}_\mu | e_\mu \rangle & \langle \tilde{g}_\mu | g_\mu \rangle \end{pmatrix} = \begin{pmatrix} e^{-i\frac{\eta_\mu}{2}} & 0 \\ 0 & e^{i\frac{\eta_\mu}{2}} \end{pmatrix} . \tag{J.15}$$

Then, the operators $\hat{S}_+^{(\mu)} e^{i\eta_\mu}$ and $\hat{S}_-^{(\mu)} e^{-i\eta_\mu}$ act in this basis as usual raising and lowering operators since

$$T^{(\mu)} \left(\hat{S}_+^{(\mu)} e^{i\eta_\mu} \right) [T^{(\mu)}]^{-1} = \begin{pmatrix} 0 & 1 \\ 0 & 0 \end{pmatrix} , \tag{J.16}$$

$$T^{(\mu)} \left(\hat{S}_-^{(\mu)} e^{-i\eta_\mu} \right) [T^{(\mu)}]^{-1} = \begin{pmatrix} 0 & 0 \\ 1 & 0 \end{pmatrix} . \tag{J.17}$$

Therefore, we define the operators $\underline{\hat{S}}_+^{(\mu)} := \hat{S}_+^{(\mu)} e^{i\eta_\mu}$ and $\underline{\hat{S}}_-^{(\mu)} := \hat{S}_-^{(\mu)} e^{-i\eta_\mu}$, with which we find that

$$\hat{H}_A + \hat{H}_{\text{trafo}} = -\hbar\Delta \sum_{\mu=1}^{N} \underline{\hat{S}}_z^{(\mu)} \tag{J.18}$$

since $\underline{\hat{S}}_z^{(\mu)} = \frac{1}{2}(\underline{\hat{S}}_+^{(\mu)} \underline{\hat{S}}_-^{(\mu)} - \underline{\hat{S}}_-^{(\mu)} \underline{\hat{S}}_+^{(\mu)}) = \frac{1}{2}(\hat{S}_+^{(\mu)} \hat{S}_-^{(\mu)} - \hat{S}_-^{(\mu)} \hat{S}_+^{(\mu)}) = \hat{S}_z^{(\mu)}$. Further, $\mathscr{L}_\gamma$ can also be expressed in an unchanged functional shape in the new operators. So, we can write the

master equation as

$$\frac{\partial}{\partial t}\hat{\tilde{\rho}}(t) = i\Delta\sum_{\mu=1}^{N}[\hat{\underline{S}}_z^{(\mu)},\hat{\tilde{\rho}}(t)] - \Omega_R\sum_{\mu=1}^{N}[\hat{\underline{S}}_+^{(\mu)} - \hat{\underline{S}}_-^{(\mu)},\hat{\tilde{\rho}}(t)] \\ - \gamma\sum_{\mu=1}^{N}[\hat{\underline{S}}_+^{(\mu)}\hat{\underline{S}}_-^{(\mu)}\hat{\tilde{\rho}}(t) + \hat{\tilde{\rho}}(t)\hat{\underline{S}}_+^{(\mu)}\hat{\underline{S}}_-^{(\mu)} - 2\hat{\underline{S}}_-^{(\mu)}\hat{\tilde{\rho}}(t)\hat{\underline{S}}_+^{(\mu)}]\,, \tag{J.19}$$

where $\hat{\underline{S}}_\pm^{(\mu)}$ act like the usual raising and lowering operators in the new basis. However, we note that we then have to be somewhat careful when calculating the mth-order photon correlation function $g^{(m)}$ since the η_μ-phases arise in the electric field operators if we write $\hat{S}_-^{(\mu)}(t) = \hat{\underline{S}}_-^{(\mu)}(t)e^{i\eta_\mu}$.

Finally, let us find the steady state of the transformed quantum master equation. For this task, let us first consider a single atom at the origin. The master equation reduces to

$$\frac{\partial}{\partial t}\hat{\tilde{\rho}}(t) = i\Delta[\hat{\underline{S}}_z,\hat{\tilde{\rho}}(t)] - \Omega_R[\hat{\underline{S}}_+ - \hat{\underline{S}}_-,\hat{\tilde{\rho}}(t)] - \gamma[\hat{\underline{S}}_+\hat{\underline{S}}_-\hat{\tilde{\rho}}(t) + \hat{\tilde{\rho}}(t)\hat{\underline{S}}_+\hat{\underline{S}}_- - 2\hat{\underline{S}}_-\hat{\tilde{\rho}}(t)\hat{\underline{S}}_+]\,. \tag{J.20}$$

Here, the steady state solution, written in the basis $|\tilde{g}\rangle$, $|\tilde{e}\rangle$, is given by

$$\hat{\tilde{\rho}}_{\rm ss} = \begin{pmatrix} \frac{s}{2(1+s)} & -\frac{\sqrt{s(\gamma^2+\Delta^2)}}{\sqrt{2}(1+s)(\gamma-i\Delta)} \\ -\frac{\sqrt{s(\gamma^2+\Delta^2)}}{\sqrt{2}(1+s)(\gamma+i\Delta)} & \frac{2+s}{2(1+s)} \end{pmatrix}, \tag{J.21}$$

where we defined the saturation parameter

$$s = \frac{2\Omega_R^2}{\Delta^2+\gamma^2}\,. \tag{J.22}$$

If we now come back to the case of N identical independent two-level atoms, we find that Eq. (J.19) does not lead to a correlated time evolution of the atoms and that it has the same form as for a single atom, except for the summation over all atoms. This means that the steady state solution for N atoms is simply the Nth tensor product of the solution for a single atom, i.e.,

$$\hat{\tilde{\rho}}_{\rm ss}^{(N)} = \hat{\tilde{\rho}}_{\rm ss}^{\otimes N} = \bigotimes_{\mu=1}^{N}\hat{\tilde{\rho}}_{\rm ss}\,. \tag{J.23}$$

Bibliography

[1] T. Young. "I. The Bakerian Lecture. Experiments and calculations relative to physical optics". *Philosophical transactions of the Royal Society of London* (1804), 1–16.

[2] L. Mandel and E. Wolf. "Coherence Properties of Optical Fields". *Rev. Mod. Phys.* 37 (1965), 231–287.

[3] R. Hanbury Brown and R. Q. Twiss. "A Test of a New Type of Stellar Interferometer on Sirius". *Nature* 178 (1956), 1046–1048.

[4] P. A. M. Dirac. *The Principles of Quantum Mechanics*. Oxford University Press, 1981.

[5] R. J. Glauber. "Nobel Lecture: One hundred years of light quanta". *Rev. Mod. Phys.* 78 (2006), 1267–1278.

[6] R. J. Glauber. "The Quantum Theory of Optical Coherence". *Phys. Rev.* 130 (1963), 2529–2539.

[7] R. H. Dicke. "Coherence in Spontaneous Radiation Processes". *Phys. Rev.* 93 (1954), 99–110.

[8] R. H. Lehmberg. "Radiation from an N-Atom System. II. Spontaneous Emission from a Pair of Atoms". *Phys. Rev. A* 2 (1970), 889–896.

[9] N. E. Rehler and J. H. Eberly. "Superradiance". *Phys. Rev. A* 3 (1971), 1735–1751.

[10] R. Bonifacio and L. A. Lugiato. "Cooperative radiation processes in two-level systems: Superfluorescence". *Phys. Rev. A* 11 (1975), 1507–1521.

[11] M. Gross and S. Haroche. "Superradiance: An essay on the theory of collective spontaneous emission". *Physics Reports* 93 (1982), 301–396.

[12] J. P. Clemens, L. Horvath, B. C. Sanders, and H. J. Carmichael. "Collective spontaneous emission from a line of atoms". *Phys. Rev. A* 68 (2003), 023809.

[13] J. P. Clemens, L. Horvath, B. C. Sanders, and H. J. Carmichael. "Shot-to-shot fluctuations in the directed superradiant emission from extended atomic samples". *Journal of Optics B: Quantum and Semiclassical Optics* 6 (2004), S736.

[14] D. Porras and J. I. Cirac. "Collective generation of quantum states of light by entangled atoms". *Phys. Rev. A* 78 (2008), 053816.

[15] M. O. Scully and A. A. Svidzinsky. "The Super of Superradiance". *Science* 325 (2009), 1510–1511.

[16] A. A. Svidzinsky, J.-T. Chang, and M. O. Scully. "Cooperative spontaneous emission of N atoms: Many-body eigenstates, the effect of virtual Lamb shift processes, and analogy with radiation of N classical oscillators". *Phys. Rev. A* 81 (2010), 053821.

[17] R. Wiegner, J. von Zanthier, and G. S. Agarwal. "Quantum-interference-initiated superradiant and subradiant emission from entangled atoms". *Phys. Rev. A* 84 (2011), 023805.

[18] E. Wolfe and S. F. Yelin. "Certifying Separability in Symmetric Mixed States of N Qubits, and Superradiance". *Phys. Rev. Lett.* 112 (2014), 140402.

[19] R. Wiegner, S. Oppel, D. Bhatti, J. von Zanthier, and G. S. Agarwal. "Simulating superradiance from higher-order-intensity-correlation measurements: Single atoms". *Phys. Rev. A* 92 (2015), 033832.

[20] M. D. Lee, S. D. Jenkins, and J. Ruostekoski. "Stochastic methods for light propagation and recurrent scattering in saturated and nonsaturated atomic ensembles". *Phys. Rev. A* 93 (2016), 063803.

[21] R. T. Sutherland and F. Robicheaux. "Superradiance in inverted multilevel atomic clouds". *Phys. Rev. A* 95 (2017), 033839.

[22] Q.-u.-A. Gulfam and Z. Ficek. "Highly directional photon superbunching from a few-atom chain of emitters". *Phys. Rev. A* 98 (2018), 063824.

[23] I. Liberal, I. Ederra, and R. W. Ziolkowski. "Grating Lobes in Higher-Order Correlation Functions of Arrays of Quantum Emitters: Directional Photon Bunching Versus Correlated Directions". *Photonics* 6 (2019).

[24] S. J. Masson, I. Ferrier-Barbut, L. A. Orozco, A. Browaeys, and A. Asenjo-Garcia. "Many-Body Signatures of Collective Decay in Atomic Chains". *Phys. Rev. Lett.* 125 (2020), 263601.

[25] F. Robicheaux. "Theoretical study of early-time superradiance for atom clouds and arrays". *Phys. Rev. A* 104 (2021), 063706.

[26] S. J. Masson and A. Asenjo-Garcia. "Universality of Dicke superradiance in arrays of quantum emitters". *Nature Communications* 13 (2022), 2285.

[27] O. Somech and E. Shahmoon. "Quantum entangled states of a classically radiating macroscopic spin". *arXiv:2204.05455* (2022).

[28] H. Ma, O. Rubies-Bigorda, and S. F. Yelin. "Superradiance and subradiance in a gas of two-level atoms". *arXiv:2205.15255* (2022).

[29] E. Sierra, S. J. Masson, and A. Asenjo-Garcia. "Dicke Superradiance in Ordered Lattices: Dimensionality Matters". *Phys. Rev. Res.* 4 (2022), 023207.

[30] M. Bojer and J. von Zanthier. “Dicke-like superradiance of distant noninteracting atoms”. *Phys. Rev. A* 106 (2022), 053712.

[31] O. Rubies-Bigorda and S. F. Yelin. “Superradiance and subradiance in inverted atomic arrays”. *Phys. Rev. A* 106 (2022), 053717.

[32] S. J. Masson, J. P. Covey, S. Will, and A. Asenjo-Garcia. “Dicke superradiance in ordered arrays of multilevel atoms”. *arXiv:2304.00093* (2023).

[33] C. D. Mink and M. Fleischhauer. “Collective Radiative Interactions in the Discrete Truncated Wigner Approximation”. *arXiv:2305.19829* (2023).

[34] N. Piovella and S. Olivares. “Single-Photon Superradiance and Subradiance as Collective Emission from Symmetric and Anti-Symmetric States”. *Symmetry* 15 (2023).

[35] M. Cygorek, E. D. Scerri, T. S. Santana, Z. X. Koong, B. D. Gerardot, and E. M. Gauger. “Signatures of cooperative emission in photon coincidence: Superradiance versus measurement-induced cooperativity”. *Phys. Rev. A* 107 (2023), 023718.

[36] O. Rubies-Bigorda, S. Ostermann, and S. F. Yelin. “Characterizing superradiant dynamics in atomic arrays via a cumulant expansion approach”. *Phys. Rev. Res.* 5 (2023), 013091.

[37] W.-K. Mok, A. Asenjo-Garcia, T. C. Sum, and L.-C. Kwek. “Dicke Superradiance Requires Interactions beyond Nearest Neighbors”. *Phys. Rev. Lett.* 130 (2023), 213605.

[38] S. Cardenas-Lopez, S. J. Masson, Z. Zager, and A. Asenjo-Garcia. “Many-Body Superradiance and Dynamical Mirror Symmetry Breaking in Waveguide QED”. *Phys. Rev. Lett.* 131 (2023), 033605.

[39] F. Lohof, D. Schumayer, D. A. W. Hutchinson, and C. Gies. “Signatures of Superradiance as a Witness to Multipartite Entanglement”. *Phys. Rev. Lett.* 131 (2023), 063601.

[40] N. Skribanowitz, I. P. Herman, J. C. MacGillivray, and M. S. Feld. “Observation of Dicke Superradiance in Optically Pumped HF Gas”. *Phys. Rev. Lett.* 30 (1973), 309–312.

[41] M. S. Malcuit, J. J. Maki, D. J. Simkin, and R. W. Boyd. “Transition from superfluorescence to amplified spontaneous emission”. *Phys. Rev. Lett.* 59 (1987), 1189–1192.

[42] R. G. DeVoe and R. G. Brewer. “Observation of Superradiant and Subradiant Spontaneous Emission of Two Trapped Ions”. *Phys. Rev. Lett.* 76 (1996), 2049–2052.

[43] M. Scheibner, T. Schmidt, L. Worschech, A. Forchel, G. Bacher, T. Passow, and D. Hommel. “Superradiance of quantum dots”. *Nature Physics* 3 (2007), 106–110.

[44] J. A. Mlynek, A. A. Abdumalikov, C. Eichler, and A. Wallraff. “Observation of Dicke superradiance for two artificial atoms in a cavity with high decay rate”. *Nature Communications* 5 (2014), 5186.

[45] T. Laurent, Y. Todorov, A. Vasanelli, A. Delteil, C. Sirtori, I. Sagnes, and G. Beaudoin. "Superradiant Emission from a Collective Excitation in a Semiconductor". *Phys. Rev. Lett.* 115 (2015), 187402.

[46] M. O. Araújo, I. Krešić, R. Kaiser, and W. Guerin. "Superradiance in a Large and Dilute Cloud of Cold Atoms in the Linear-Optics Regime". *Phys. Rev. Lett.* 117 (2016), 073002.

[47] A. Angerer, K. Streltsov, T. Astner, S. Putz, H. Sumiya, S. Onoda, J. Isoya, W. J. Munro, K. Nemoto, J. Schmiedmayer, and J. Majer. "Superradiant emission from colour centres in diamond". *Nature Physics* 14 (2018), 1168–1172.

[48] S. Okaba, D. Yu, L. Vincetti, F. Benabid, and H. Katori. "Superradiance from lattice-confined atoms inside hollow core fibre". *Communications Physics* 2 (2019), 136.

[49] G. Ferioli, A. Glicenstein, F. Robicheaux, R. T. Sutherland, A. Browaeys, and I. Ferrier-Barbut. "Laser-Driven Superradiant Ensembles of Two-Level Atoms near Dicke Regime". *Phys. Rev. Lett.* 127 (2021), 243602.

[50] A. Rastogi, E. Saglamyurek, T. Hrushevskyi, and L. J. LeBlanc. "Superradiance-Mediated Photon Storage for Broadband Quantum Memory". *Phys. Rev. Lett.* 129 (2022), 120502.

[51] W. Kersten, N. de Zordo, O. Diekmann, T. Reiter, M. Zens, A. N. Kanagin, S. Rotter, J. Schmiedmayer, and A. Angerer. "Triggered Superradiance and Spin Inversion Storage in a Hybrid Quantum System". *Phys. Rev. Lett.* 131 (2023), 043601.

[52] G. Facchinetti, S. D. Jenkins, and J. Ruostekoski. "Storing Light with Subradiant Correlations in Arrays of Atoms". *Phys. Rev. Lett.* 117 (2016), 243601.

[53] A. Asenjo-Garcia, M. Moreno-Cardoner, A. Albrecht, H. J. Kimble, and D. E. Chang. "Exponential Improvement in Photon Storage Fidelities Using Subradiance and "Selective Radiance" in Atomic Arrays". *Phys. Rev. X* 7 (2017), 031024.

[54] Y.-X. Zhang and K. Mølmer. "Theory of Subradiant States of a One-Dimensional Two-Level Atom Chain". *Phys. Rev. Lett.* 122 (2019), 203605.

[55] K. E. Ballantine and J. Ruostekoski. "Subradiance-protected excitation spreading in the generation of collimated photon emission from an atomic array". *Phys. Rev. Res.* 2 (2020), 023086.

[56] A. Cipris, N. A. Moreira, T. S. do Espirito Santo, P. Weiss, C. J. Villas-Boas, R. Kaiser, W. Guerin, and R. Bachelard. "Subradiance with Saturated Atoms: Population Enhancement of the Long-Lived States". *Phys. Rev. Lett.* 126 (2021), 103604.

[57] V. Weisskopf and E. Wigner. "Berechnung der natürlichen Linienbreite auf Grund der Diracschen Lichttheorie". *Zeitschrift für Physik* 63 (1930), 54–73.

[58] W. Heitler and S. Ma. "Quantum theory of radiation damping for discrete states". *Proceedings of the Royal Irish Academy. Section A: Mathematical and Physical Sciences*. Vol. 52. JSTOR. 1948, 109–125.

[59] W. Heitler. *The Quantum Theory of Radiation*. Courier Corporation, 1984.

[60] M. Goldberger and K. Watson. *Collision Theory*. Structure of matter series. Wiley, 1964.

[61] G. S. Agarwal. *Quantum Optics: Quantum Statistical Theories of Spontaneous Emission and their Relation to Other Approaches*. Springer tracts in modern physics. Springer, 1974.

[62] H.-P. Breuer and F. Petruccione. *The Theory of Open Quantum Systems*. Oxford University Press, 2002.

[63] M. Kiffner, M. Macovei, J. Evers, and C. Keitel. "Chapter 3 - Vacuum-Induced Processes in Multilevel Atoms". Ed. by E. Wolf. Vol. 55. Progress in Optics. Elsevier, 2010, 85–197.

[64] R. Zwanzig. "Memory Effects in Irreversible Thermodynamics". *Phys. Rev.* 124 (1961), 983–992.

[65] C. Cohen-Tannoudji, J. Dupont-Roc, and G. Grynberg. *Atom-Photon Interactions: Basic Processes and Applications*. John Wiley & Sons, 1998.

[66] J. D. Jackson. *Classical Electrodynamics*. John Wiley & Sons, 2021.

[67] L. Novotny and B. Hecht. *Principles of Nano-Optics*. Cambridge University Press, 2006.

[68] M. Bojer, L. Götzendörfer, R. Bachelard, and J. von Zanthier. "Engineering of spontaneous emission in free space via conditional measurements". *Phys. Rev. Res.* 4 (2022), 043022.

[69] Z. Ficek and S. Swain. *Quantum Interference and Coherence: Theory and Experiments*. Vol. 100. Springer Science & Business Media, 2005.

[70] S. Mährlein, L. Götzendörfer, K. Günthner, J. Evers, and J. von Zanthier. "Birth, death, and revival of spontaneous emission in a three-atom system". *Phys. Rev. Res.* 2 (2020), 013278.

[71] S. Wolf, S. Richter, J. von Zanthier, and F. Schmidt-Kaler. "Light of Two Atoms in Free Space: Bunching or Antibunching?" *Phys. Rev. Lett.* 124 (2020), 063603.

[72] S. Richter, S. Wolf, J. von Zanthier, and F. Schmidt-Kaler. "Imaging Trapped Ion Structures via Fluorescence Cross-Correlation Detection". *Phys. Rev. Lett.* 126 (2021), 173602.

[73] S. Richter, S. Wolf, J. von Zanthier, and F. Schmidt-Kaler. "Collective photon emission of two correlated atoms in free space". *Phys. Rev. Res.* 5 (2023), 013163.

[74] J.-T. Chang, J. Evers, M. O. Scully, and M. Suhail Zubairy. "Measurement of the separation between atoms beyond diffraction limit". *Phys. Rev. A* 73 (2006), 031803.

[75] J.-T. Chang, J. Evers, and M. Suhail Zubairy. "Distilling two-atom distance information from intensity-intensity correlation functions". *Phys. Rev. A* 74 (2006), 043820.

[76] D. Bhatti, M. Bojer, and J. von Zanthier. "Different types of coherence: Young-type interference versus Dicke superradiance". *Phys. Rev. A* 104 (2021), 052401.

[77] H. Carmichael. *An Open Systems Approach to Quantum Optics: Lectures Presented at the Université Libre de Bruxelles, October 28 to November 4, 1991.* Vol. 18. Springer Science & Business Media, 2009.

[78] C. Thiel, J. von Zanthier, T. Bastin, E. Solano, and G. S. Agarwal. "Generation of Symmetric Dicke States of Remote Qubits with Linear Optics". *Phys. Rev. Lett.* 99 (2007), 193602.

[79] M. Ali, A. R. P. Rau, and G. Alber. "Quantum discord for two-qubit X states". *Phys. Rev. A* 81 (2010), 042105.

[80] X.-M. Lu, J. Ma, Z. Xi, and X. Wang. "Optimal measurements to access classical correlations of two-qubit states". *Phys. Rev. A* 83 (2011), 012327.

[81] Y. Huang. "Quantum discord for two-qubit X states: Analytical formula with very small worst-case error". *Phys. Rev. A* 88 (2013), 014302.

[82] M. Namkung, J. Chang, J. Shin, and Y. Kwon. "Revisiting Quantum Discord for Two-Qubit X States: The Error Bound to an Analytical Formula". *International Journal of Theoretical Physics* 54 (2015), 3340–3349.

[83] Q. Chen, C. Zhang, S. Yu, X. X. Yi, and C. H. Oh. "Quantum discord of two-qubit X states". *Phys. Rev. A* 84 (2011), 042313.

[84] P. Kok, W. J. Munro, K. Nemoto, T. C. Ralph, J. P. Dowling, and G. J. Milburn. "Linear optical quantum computing with photonic qubits". *Rev. Mod. Phys.* 79 (2007), 135–174.

[85] P. Kok and B. W. Lovett. *Introduction to Optical Quantum Information Processing.* Cambridge University Press, 2010.

[86] F. Flamini, N. Spagnolo, and F. Sciarrino. "Photonic quantum information processing: a review". *Reports on Progress in Physics* 82 (2018), 016001.

[87] L. Mandel and E. Wolf. *Optical Coherence and Quantum Optics.* Cambridge University Press, 1995.

[88] C. Gerry and P. L. Knight. *Introductory Quantum Optics.* Cambridge University Press, 2005.

[89] R. P. Stanley. *Enumerative Combinatorics.* 2nd ed. Cambridge Studies in Advanced Mathematics. Cambridge University Press, 2011.

[90] J. Ruostekoski and J. Javanainen. "Quantum field theory of cooperative atom response: Low light intensity". *Phys. Rev. A* 55 (1997), 513–526.

[91] S. D. Jenkins and J. Ruostekoski. "Controlled manipulation of light by cooperative response of atoms in an optical lattice". *Phys. Rev. A* 86 (2012), 031602.

[92] S. D. Jenkins, J. Ruostekoski, J. Javanainen, S. Jennewein, R. Bourgain, J. Pellegrino, Y. R. P. Sortais, and A. Browaeys. "Collective resonance fluorescence in small and dense atom clouds: Comparison between theory and experiment". *Phys. Rev. A* 94 (2016), 023842.

[93] E. Shahmoon, D. S. Wild, M. D. Lukin, and S. F. Yelin. "Cooperative Resonances in Light Scattering from Two-Dimensional Atomic Arrays". *Phys. Rev. Lett.* 118 (2017), 113601.

[94] L. A. Williamson and J. Ruostekoski. "Optical response of atom chains beyond the limit of low light intensity: The validity of the linear classical oscillator model". *Phys. Rev. Res.* 2 (2020), 023273.

[95] L. A. Williamson, M. O. Borgh, and J. Ruostekoski. "Superatom Picture of Collective Nonclassical Light Emission and Dipole Blockade in Atom Arrays". *Phys. Rev. Lett.* 125 (2020), 073602.

[96] M. Reitz, C. Sommer, and C. Genes. "Cooperative Quantum Phenomena in Light-Matter Platforms". *PRX Quantum* 3 (2022), 010201.

[97] N. S. Baßler, M. Reitz, K. P. Schmidt, and C. Genes. "Linear optical elements based on cooperative subwavelength emitter arrays". *Opt. Express* 31 (2023), 6003–6026.

[98] S. L. Bromley, B. Zhu, M. Bishof, X. Zhang, T. Bothwell, J. Schachenmayer, T. L. Nicholson, R. Kaiser, S. F. Yelin, M. D. Lukin, A. M. Rey, and J. Ye. "Collective atomic scattering and motional effects in a dense coherent medium". *Nature Communications* 7 (2016), 11039.

[99] J. Rui, D. Wei, A. Rubio-Abadal, S. Hollerith, J. Zeiher, D. M. Stamper-Kurn, C. Gross, and I. Bloch. "A subradiant optical mirror formed by a single structured atomic layer". *Nature* 583 (2020), 369–374.

[100] C. Cohen-Tannoudji, J. Dupont-Roc, and G. Grynberg. *Photons and Atoms: Introduction to Quantum Electrodynamics*. John Wiley & Sons, 1997.

[101] S. Swain. "Master equation derivation of quantum regression theorem". *Journal of Physics A: Mathematical and General* 14 (1981), 2577–2580.

[102] A. Streltsov, G. Adesso, and M. B. Plenio. "Colloquium: Quantum coherence as a resource". *Rev. Mod. Phys.* 89 (2017), 041003.

[103] K. Modi, A. Brodutch, H. Cable, T. Paterek, and V. Vedral. "The classical-quantum boundary for correlations: Discord and related measures". *Rev. Mod. Phys.* 84 (2012), 1655–1707.

[104] G. Adesso, T. R. Bromley, and M. Cianciaruso. "Measures and applications of quantum correlations". *Journal of Physics A: Mathematical and Theoretical* 49 (2016), 473001.

[105] R. Horodecki, P. Horodecki, M. Horodecki, and K. Horodecki. "Quantum entanglement". *Rev. Mod. Phys.* 81 (2009), 865–942.

[106] Y. Yao, X. Xiao, L. Ge, and C. P. Sun. "Quantum coherence in multipartite systems". *Phys. Rev. A* 92 (2015), 022112.

[107] W. K. Wootters. "Entanglement of Formation of an Arbitrary State of Two Qubits". *Phys. Rev. Lett.* 80 (1998), 2245–2248.

[108] D. A. Meyer and N. R. Wallach. "Global entanglement in multiparticle systems". *Journal of Mathematical Physics* 43 (2002), 4273–4278.

[109] G. K. Brennen. "An Observable Measure of Entanglement for Pure States of Multi-Qubit Systems". *Quantum Info. Comput.* 3 (2003), 619–626.

[110] A. J. Scott. "Multipartite entanglement, quantum-error-correcting codes, and entangling power of quantum evolutions". *Phys. Rev. A* 69 (2004), 052330.

[111] P. J. Love, A. M. van den Brink, A. Y. Smirnov, M. H. S. Amin, M. Grajcar, E. Il'ichev, A. Izmalkov, and A. M. Zagoskin. "A Characterization of Global Entanglement". *Quantum Information Processing* 6 (2007), 187–195.

[112] P. Krammer, H. Kampermann, D. Bruß, R. A. Bertlmann, L. C. Kwek, and C. Macchiavello. "Multipartite Entanglement Detection via Structure Factors". *Phys. Rev. Lett.* 103 (2009), 100502.

[113] A. Messiah. *Quantum Mechanics*. Courier Corporation, 2014.

[114] H. Carmichael. *Statistical Methods in Quantum Optics 1: Master Equations and Fokker-Planck Equations*. Vol. 1. Springer Science & Business Media, 1999.

Chapter quotes

The quotes at the beginning of the chapters have been taken from the following resources: Chapter 1 from Roy J. Glauber's Nobel Lecture *One hundred years of light quanta* (2006) [5], Chapter 2 from Ref. [61], Chapter 3&4 from Ref. [6], Chapter 5 from Ref. [7], Chapter 6 from Ref. [88], and Chapter 7 from W. Pauli's letter to N. Bohr (1955).

List of publications

[1] **M. Bojer**, J. von Zanthier
Dicke-like superradiance of distant noninteracting atoms
Physical Review A **106**, 053712 (2022)

J.v.Z. conceived the original idea. M.B. developed the theory and drafted the manuscript. Both authors discussed the theoretical results and contributed to the final manuscript.

[2] **M. Bojer**, L. Götzendörfer, R. Bachelard, J. von Zanthier
Engineering of spontaneous emission in free space via conditional measurements
Physical Review Research **4**, 043022 (2022)

J.v.Z. conceived the original idea. L.G. performed preliminary calculations. M.B. developed the theory and drafted the manuscript. R.B. placed the research into a wider theoretical context and helped, in particular, with the theoretical interpretation. All authors discussed the theoretical results and contributed to the final manuscript.

[3] **M. Bojer**, Z. Huang, S. Karl, S. Richter, P. Kok, J. von Zanthier
A quantitative comparison of amplitude versus intensity interferometry for astronomy
New Journal of Physics **24** 043026 (2022)

[4] D. Bhatti, **M. Bojer**, J. von Zanthier
Different types of coherence: Young-type interference versus Dicke superradiance
Physical Review A **104**, 052401 (2021)

[5] **M. Bojer**, A. Friedenberger, E. Lutz
Quantum witness of a damped qubit with generalized measurements
Journal of Physics Communications **3** 065003 (2019)

In preparation

[6] **M. Bojer**, J. Eckert, S. Karl, S. Richter, J. von Zanthier
Phase Retrieval in Incoherent Diffractive Imaging using higher-order photon correlation functions

[7] **M. Bojer**, J. Evers, J. von Zanthier
Remote sensing using an auxiliary quantum system

[8] **M. Bojer**, A. Cidrim, R. Bachelard, J. von Zanthier
Light statistics from ensembles of two-level emitters